Molekulare Dynamik in binären Glasbildnern studiert mittels ^{31}P- und ^{2}H-NMR

Von der Universität Bayreuth
zur Erlangung des Grades eines
Doktors der Naturwissenschaften (Dr. rer. nat.)
genehmigte Abhandlung

von
Daniel Bock
geboren am 20. März 1980 in Kronach

Erster Gutachter: Prof. Dr. Ernst Rößler
Zweiter Gutachter: Prof. Dr. Michael Vogel

Tag der Einreichung: 15.06.2015
Tag des Kolloquiums: 06.11.2015

Inhaltsverzeichnis

1 Abstract **5**

2 Kurzdarstellung **7**

3 Ausführliche Zusammenfassung **11**

3.1 Einführung 11
3.2 Phänomenologie reiner Glasbildner 11
3.3 Primäre Relaxation in binären Glasbildnern 17
3.3.1 Stand des Wissens 17
3.3.2 Eigene Ergebnisse 25
3.4 Der β-Prozess im Mischsystem 40
3.4.1 Stand des Wissens 40
3.4.2 Eigene Ergebnisse 42
3.5 Interpretation der NMR-Relaxationsdaten 46
3.6 Grundlagen der NMR und verwendete Methoden 51
3.6.1 Der Kernspin und seine Wechselwirkungen 51
3.6.2 Linienformanalyse 53
3.6.3 Spin-Relaxation 54
3.6.4 Stimuliertes Echo 54
3.6.5 2D-Spektren 55

4 Publikationen **57**

Publikation 1:
On the cooperative nature of the ß-process in neat and binary glasses: A dielectric and nuclear magnetic resonance spectroscopy study 61
Publikation 2:
Dynamics of asymmetric binary glass formers. I. A dielectric and nuclear magnetic resonance spectroscopy study 75
Publikation 3:
Dynamics of asymmetric binary glass formers. II. Results from nuclear magnetic resonance spectroscopy 89
Publikation 4:
Dynamic heterogeneities in glass-forming systems 103

Literaturverzeichnis **115**

Danksagung **131**

1 Abstract

The subject of this thesis is the investigation of molecular reorientation dynamics of binary mixtures of organic glass formers. Utilizing various nuclear magnetic resonance (NMR) spectroscopic techniques including line-shape analysis, measurement of stimulated echo decay, of two-dimensional (2D) spectra and of spin relaxation allows for selective observation of both components over the full concentration range. Systems are studied which show a high „dynamic asymmetry“, i.e. a large difference of the glass transition temperatures of the neat components. The focus is on the primary structural relaxation (α-process) as well as on the slow β-process, a secondary relaxation generically found in many glass formers at $T \lessapprox T_g$.

After preliminary studies on different polymer-plasticizer systems had revealed pronounced dynamic heterogeneities especially for the low-T_g component, systematic investigations over a wide composition range ($0.1 \leq c_TPP \leq 0.9$) on tripropyl phosphate (TPP, $T_g = 135K$) / polystyrene (PS, $T_g = 335K$) were realized. Measurements were performed by means of ^{31}P and ^{2}H NMR as well as differential scanning calorimetry (DSC), results from dielectric spectroscopy (DS) and depolarized dynamic light scattering (DLS) were contributed from further PhD theses. The work is described in three publications (Publikationen 1-3). A fourth summarizes further examinations including those of a mixture of low-molecular liquids (Publikation 4).

Publikationen 2 and 3 treat the investigation of the primary relaxation in the mixtures of TPP/PS. In the dielectric spectra solely governed by TPP, two relaxations (α_1 and α_2) can be identified. Making use of NMR experiments these can be assigned to the dynamics of PS (α_1) and TPP (α_2). Consequently a fraction of TPP molecules participates in the slow dynamics of PS. Accordingly two distinct glass transition temperatures $T_{g1}(c_{TPP}) > T_{g2}(c_{TPP})$ are determined for the first time over the whole concentration range. While $T_{g1}(c_{TPP})$ monotonously decreases starting from neat PS , $T_{g2}(c_{TPP})$ passes through a maximum at $c_{TPP} \approx 0.35$, which can be explained by the time constants described in the current thesis. The dynamics of PS in the mixtures maintaining time-temperature superposition (TTS) with only slight stretching of correlation functions as revealed by ^{2}H NMR stimulated echo decays complies to a great extent with those of neat glass formers. Therefore at $T < T_{g1}$ for TPP an isotropic motion in an essentially immobilized matrix of PS is proven. Thereby ^{31}P NMR stimulated echo decays reveal extremely stretched, quasilogarithmic correlation functions reflecting pronounced dynamic

heterogeneities; TTS is not fulfilled.

Although the time window of the stimulated echo technique covers more than five decades it is not sufficient for an observation of the complete correlation loss. However, it can be shown that DS results give a quantitative interpolation of the NMR correlation functions. Thereby the fraction of TPP involved in the dynamics of PS is taken into account. In accordance with DS results this fraction gradually disappears with rising temperature. By means of 2D ^{31}P NMR spectra dynamic exchange within the correlation time distribution of the α_2-process is proven which gives evidence of the transient nature of an essential part of the dynamic heterogeneities. ^{2}H NMR experiments moreover disclose that the PS matrix, rigid at $T < T_{g1}$, reflects the isotropic motion of TPP in an restricted motion on the same time scale. The remarkable similarities of the observed phenomenons in mixtures with that observed in confinement lead to the conclusion, that dynamics of the low-T_g component in an essentially immobile matrix of the high-T_g component might be ruled by an „intrinsic confinement“.

In Publikation 1 the secondary relaxation, that shows correlation times practically independent of concentration in all mixtures of TPP and PS albeit not present in neat PS, is studied. By means of NMR investigations it is shown that a spatially restricted motion is underlying this β-relaxation, as is in neat glass formers. This is demonstrated for the first time using also ^{31}P NMR by adapting the well-known techniques of ^{2}H NMR. Corresponding experiments by means of ^{2}H NMR on PS in the mixtures show that PS reflects the motion of TPP by performing a similar motion on the same time scale. While in neat glass formers essentially all molecules take part in the β-process, this is not the case in the mixtures. For TPP as well as PS a fraction growing with decreasing TPP concentration turns out to be immobile on the time scale of the β-process. Both findings are taken as evidence for a cooperative nature of the β-process.

Hitherto not published is the analysis of relaxation times $T_1(T)$ und $T_2(T)$ likewise measured in various mixed systems. On the basis of TPP/PS it is shown, that a semiquantitative interpolation of the ^{31}P NMR relaxation times by extrapolation of the dielectric spectral density is possible.

By hands of 2-methyltetrahydrofuran-d_3 (MTHF, $T_g = 96K$) / m-tricresyl phosphate (m-TCP, $T_g = 206K$) the component dynamics of a dynamically asymmetric binary mixture of two low-molecular weight glass former can be studied (Publikation 4). Two distinct time constants are related to the decoupled dynamics of both components. According to the smaller T_g-contrast the essential phenomenons known from polymer-plasticizer systems are found in less severe form and therefore demonstrate that it is not the polymer-nature that rules the dynamics in the mixed system.

2 Kurzdarstellung

Gegenstand dieser Arbeit ist die Untersuchung der molekularen Reorientierungsdynamik binärer Mischungen organischer Glasbildner. Die Anwendung der Kernspinresonanz-Spektroskopie (NMR) mit Methoden wie der Linienformanalyse, Messung des Stimulierte-Echo-Zerfalls, der zweidimensionalen (2D-) Spektren und der Spinrelaxation ermöglicht eine selektive Betrachtung der beiden Komponenten. Es werden Systeme untersucht, welche sich durch eine hohe „dynamische Asymmetrie“, d.h. durch einen großen Unterschied in der Glasübergangstemperatur der reinen Spezies auszeichnen. Typische Beispiele sind Polymer-Weichmacher-Systeme, die hier im Vordergrund stehen. Das Interesse gilt hierbei sowohl der primären Strukturrelaxation (α-Prozess) als auch dem langsamen β-Prozess (einer Sekundärrelaxation, die generisch in vielen Glasbildnern bei $T \lessapprox T_g$ beobachtet wird).

Nachdem Vorarbeiten an verschiedenen Polymer-Weichmacher-Systemen ausgeprägte dynamische Heterogenitäten v.a. für die Nieder-T_g-Komponente nachgewiesen hatten, werden systematische Untersuchungen über einen großen Konzentrationsbereich am System Tripropylphosphat (TPP, $T_g = 135K$) / Poly(styrol) (PS, $T_g = 335K$) vorgestellt. Messungen wurden mittels ^{31}P- und ^{2}H-NMR sowie Differenzkalorimetrie (DSC) ausgeführt, Ergebnisse der dielektrischen Spektroskopie (DS) sowie der depolarisierten dynamischen Lichtstreuung (DLS) wurden aus anderen Doktorarbeiten eingebracht. Die Arbeiten sind in drei Veröffentlichungen beschrieben (Publikationen 1-3). Eine Vierte fasst weitere Untersuchungen u.a. von niedermolekularen Mischungen zusammen (Publikation 4).

Publikationen 2 und 3 widmen sich der Untersuchung der Primärrelaxation in den Mischungen von TPP/PS. In den dielektrischen Spektren, die alleine durch TPP bestimmt sind, treten zwei Relaxationen (α_1 und α_2) auf. Durch NMR-Experimente können diese der Dynamik des TPP (α_2) und der des PS (α_1) zugeordnet werden. Danach partizipiert ein Teil der TPP-Moleküle an der langsamen Dynamik des PS, während ein anderer Teil eine entkoppelte schnellere Bewegung vollführt. Entsprechend können zwei getrennte Glasübergangstemperaturen $T_{g1}(c_{TPP}) > T_{g2}(c_{TPP})$ erstmalig über den gesamten Konzentrationsbereich identifiziert werden. Während $T_{g1}(c_{TPP})$ ausgehend vom reinen PS monoton abfällt, zeigt der Verlauf von $T_{g2}(c_{TPP})$ ein Maximum. Dies findet seine Erklärung in einer charakteristischen Veränderung des Temperaturverlaufs der Zeitkonstanten bei niedrigen TPP-Konzentrationen. Die Dynamik des PS in der Mischung

entspricht, wie insbesondere ^{2}H-NMR Stimulierte-Echo-Experimente zeigen, unter Erhalt von Zeit-Temperatur-Superposition (TTS) und nur leichter Streckung der Korrelationsfunktion weitgehend der eines reinen Glasbildners. Für $T < T_{g1}$ wird eine isotrope Bewegung von TPP in einer im Wesentlichen immobilisierten Matrix von PS nachgewiesen. Dabei finden sich in ^{31}P-NMR Stimulierte-Echo-Zerfällen extrem verbreiterte, quasilogarithmische Korrelationsfunktionen. Diese spiegeln ausgeprägte dynamische Heterogenitäten wider, deren Ausmaß mit niedrigeren TPP-Konzentrationen zunimmt; TTS ist hierbei nicht erfüllt.

Obwohl das Zeitfenster der Stimulierte-Echo-Methode mehr als fünf Dekaden umfasst, genügt dieses nicht, um den kompletten Korrelationsverlust zu beobachten. Es kann jedoch gezeigt werden, dass die dielektrischen Ergebnisse eine quantitative Interpolation der NMR-Korrelationsfunktionen ermöglichen, wobei der Anteil von an der PS-Dynamik teilnehmendem TPP berücksichtigt werden muss. Dieser Anteil verschwindet mit steigender Temperatur sukzessive. Mittels 2D-^{31}P-NMR-Spektroskopie kann innerhalb der breiten Korrelationszeitenverteilung des α_2-Prozesses dynamischer Austausch nachgewiesen und somit gezeigt werden, dass ein wesentlicher Anteil der dynamischen Heterogenitäten transienter Natur ist. Der isotrope Charakter des α_2-Prozesses wird bestätigt. ^{2}H-NMR Experimente offenbaren darüberhinaus, dass die bei $T < T_{g1}$ feste PS-Matrix auf der Zeitskala der schnellen isotrope Bewegung des TPP eine eingeschränkte Bewegung ausführt. Die auffallenden Ähnlichkeiten der beobachteten Phänomene in der Mischung mit jenen von Glasbildnern in einschränkender Geometrie führen zur Vermutung, dass die Dynamik der Nieder-T_g-Komponente in einer weitgehend immobilisierten Matrix der Hoch-T_g-Komponente durch ein „intrinsisches Confinement“ bestimmt sein könnte.

In Publikation 1 wird die Sekundärrelaxation untersucht, die in allen Mischungen von TPP und PS praktisch konzentrationsunabhängige Korrelationszeiten $\tau_\beta(T)$ zeigt, jedoch im reinen PS nicht vorhanden ist. Mittels Untersuchungen der NMR wird gezeigt, dass dieser β-Relaxation, wie in reinen Gläsern, eine räumlich stark eingeschränkte Bewegung zu Grunde liegt. Dieser Nachweis geschah erstmalig auch mit Hilfe der ^{31}P-NMR, in dem die bekannten Methoden der ^{2}H-NMR auf jene übertragen wurden. Entsprechende ^{2}H-NMR-Experimente an PS in der Mischung zeigen, dass PS an der Bewegung von TPP mit einer ähnlichen Bewegung auf gleicher Zeitskala teilnimmt. Während in reinen Glasbildnern praktisch alle Moleküle am β-Prozess teilhaben, ist dies in den Mischungen jedoch nicht der Fall. Sowohl für TPP als auch für PS erweist sich ein mit abnehmender TPP-Konzentration wachsender Anteil als immobil auf der Zeitskala des β-Prozesses. Beide Befunde werden als Hinweis auf einen kooperativen Charakter des β-Prozesses gewertet.

Bislang nicht veröffentlicht ist die Analyse der ebenfalls gemessenen Relaxationszeiten $T_1(T)$ und $T_2(T)$ in verschiedenen Mischsystemen, in denen sich ebenfalls die breiter werdenden Korrelationszeitenverteilungen offenbaren. Anhand von

TPP/PS wird gezeigt, dass eine semiquantitative Interpolation der ^{31}P-NMR-Relaxationszeiten durch Extrapolation der dielektrischen Spektraldichte zur entsprechenden Larmorfrequenz möglich ist.

Mit 2-Methyltetrahydrofuran-d_3 (MTHF, T_g = 96K) / m-Trikresylphosphat (m-TCP, T_g = 206K) kann erstmals mittels NMR die Komponentendynamik einer dynamisch asymmetrischen binären Mischung zweier niedermolekularer Glasbildner verfolgt werden (Publikation 4). Zwei getrennte Zeitkonstanten werden der entkoppelten Dynamik der beiden Komponenten zugeordnet. Entsprechend dem kleineren T_g-Kontrast finden sich in schwächerer Ausprägung wesentliche Phänomene aus den Polymer-Weichmacher-Systemen wieder und zeigen, dass im Wesentlichen der T_g-Kontrast die entscheidende Größe für die Etablierung von dynamischen Heterogenitäten im Mischsystem ist.

3 Ausführliche Zusammenfassung

3.1 Einführung

Bei Temperaturen unterhalb des Schmelzpunktes T_m stellt der Kristall den thermodynamisch stabilen Zustand einer Substanz dar. Der Kristall zeichnet sich durch eine regelmäßige Anordnung der Bausteine aus. Er ist jedoch nicht die einzige Erscheinungsform des Festkörpers. Für nahezu alle Flüssigkeiten kann die Kristallisation, d.h. die Ausbildung einer Fernordnung, z. B. durch Abkühlung mittels ausreichend hoher Kühlraten verhindert werden. Die Struktur der Flüssigkeit bleibt dann erhalten und ein Glas entsteht. Daneben besteht eine Vielzahl weiterer Verfahren amorphe Festkörper, die sich durch fehlende Translationssymmetrie auszeichnen, herzustellen. Glasartige Materialien sind in unserem täglichen Leben allgegenwärtig, vom Silikat-Netzwerkglas bis hin zu metallischen Gläsern. Molekulare Gläser begegnen uns auch in Form von Pharmazeutika und Produkten der Lebensmittelindustrie. Polymere sind eine weitere wichtige Klasse von Glasbildnern. Wenngleich eine theoretische Beschreibung des Übergangs von der Flüssigkeit zum Glas noch aussteht, so ist doch dessen Phänomenologie im Wesentlichen bekannt. In Mischsystemen, dem Gegenstand der vorliegenden Arbeit, hingegen existiert bislang noch keine allgemein anerkannte Beschreibung der Dynamik.

3.2 Phänomenologie reiner Glasbildner

Die Viskosität η und ebenso die Korrelationszeit τ der Strukturrelaxation eines Glasbildners steigen während des Abkühlens bei $T < T_m$ kontinuierlich um mehr als zwölf Größenordnungen an (siehe Abb. 3.1(a)) und erreichen bei der Glasübergangstemperatur T_g festkörpertypische Werte von $\eta \approx 10^{12} Pas$ bzw. $\tau \approx 100s$.

Charakteristisch für die sog „Glasdynamik“ ist das Auftreten einer zweistufigen Korrelationsfunktion (siehe Abb. 3.1(b)). Ausgehend von einer monoexponentiellen Dynamik der einfachen Flüssigkeit spaltet sich bei Abkühlung von der schnellen Dynamik („fast dynamics“ oder „mikroskopische Dynamik“) die langsame strukturelle Dynamik (α-Prozess) ab.

Letztere ist, wie hier am Beispiel der molekularen Reorientierungsdynamik gezeigt wird, gekennzeichnet durch nicht-exponentielle (gestreckte) Korrelationsfunktionen und ein super-Arrhenius-Temperaturverhalten der Zeitkonstanten (siehe

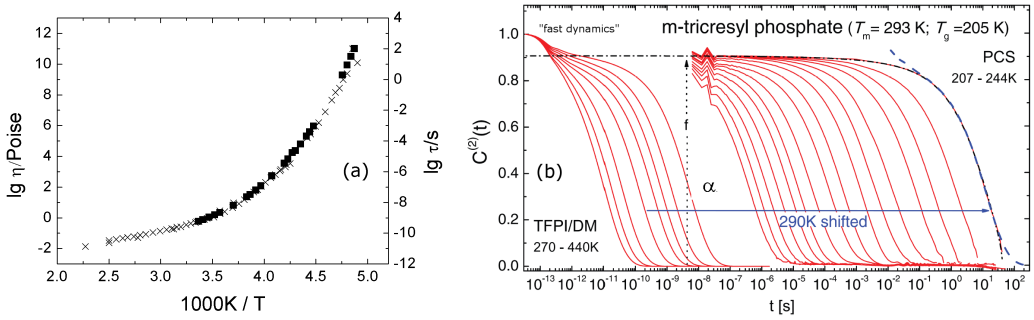

Abbildung 3.1: *(a) m-Trikresylphosphat (TCP): Viskosität η (■, [1]) und strukturelle Relaxationszeit τ (✕, aus Messungen der dielektrischen Spektroskopie, der dynamischen Lichtstreuung sowie der NMR, [2]), als Funktion der reziproken Temperatur. (b) TCP: Reorientierungskorrelationsfunktion $C_2(t)$ aus Lichtstreuexperimenten, gewonnen mittels Doppelmonochromator (DM), Tandem-Fabry-Perot-Interferometrie (TFPI) und Photonen-Korrelations-Spektroskopie (PCS); aus [3].*

Abb. 3.1(a)). Die α-Relaxation in reinen Glasbildnern erfüllt über weite Temperaturbereiche das Zeit-Temperatur-Superpositionsprinzip (TTS) [4], d.h. die Korrelationsfunktionen zu verschiedenen Temperaturen lassen sich durch Verschiebung auf der logarithmischen Zeitachse zur Deckung bringen, wie Abb. 3.1(b) verdeutlicht. Bei Temperaturen $T \leq T_g$ besteht eine Nichtlinearität der Relaxation, die sich insbesondere in einer Abhängigkeit der Relaxationszeit von der thermischen Vorgeschichte äußert [5, 6].

Für die Ursache der gestreckten Relaxation kann man sich grundsätzlich zwei Szenarien vorstellen [7]. Denkbar ist, dass die gestreckt exponentielle Form eine intrinsische Eigenschaft ungeordneter Systeme ist. Man spricht in diesem Fall von dynamischer Homogenität. Zum anderen ist denkbar, dass in ungeordneten Systemen eine Vielzahl unterschiedlicher Relaxationszeiten vorliegt. Bei geeigneter Verteilung dieser Relaxationszeiten erhält man ebenfalls ein nichtexponentielles Verhalten der Korrelationsfunktion des Gesamtsystems. In diesem Fall spricht man von dynamischer Heterogenität. Mehrere experimentelle Techniken wurden entwickelt, um zwischen dynamisch heterogener und homogener Relaxation zu unterscheiden [8], darunter ein vierdimensionales NMR-Experiment [9], ein „deep-bleach“-Experiment [10] und nichtresonantes dielektrisches Lochbrennen [11]. Dynamische Heterogenitäten, d.h. verschiedene Subensemble besitzen unterschiedliche Mobilität, wurde praktisch immer nachgewiesen [7, 9–16]. Von besonderem Interesse ist die Lebensdauer der dynamischen Heterogenitäten. Im Allgemeinen geht man davon aus, dass diese von der Größenordnung der α-Relaxationszeit ist. Diese Annahme resultiert vor allem aus NMR-Untersuchungen [17, 18], und wird auch durch Simulationen gestützt [19]. Rückschlüsse aufgrund der Einzelmolekül-

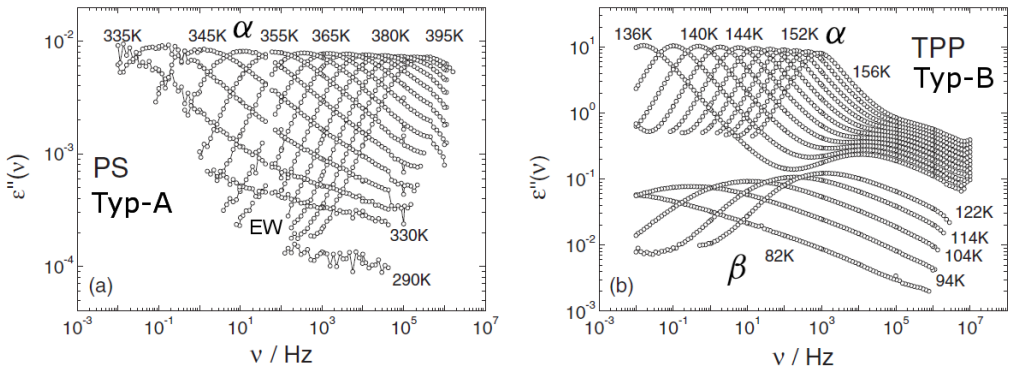

Abbildung 3.2: *Dielektrische Verlustspektren, (a) Typ-A-Glasbildner Polystyrol (PS); (b) Typ-B-Glasbildner Tripropylphosphat (TPP); aus Publikation 1.*

spektroskopie an Polymerfilmen, dass die Lebensdauer von Heterogenitäten ein Vielfaches der α-Relaxationszeit betragen kann [20, 21] erwiesen sich als nicht reproduzierbar [22].

Kennzeichnend für den Glaszustand ist auch das Auftreten von Sekundärrelaxationen. Abbildung 3.2 zeigt dielektrische Verlustspektren, wie sie im Rahmen dieser Arbeit diskutiert werden. Für viele Glasbildner (sog. Typ-B-Glasbildner [23]) findet sich im dielektrischen Spektrum bei höheren Frequenzen bzw. niedrigeren Temperaturen als der α-Peak ein weiteres Relaxationsmaximum: Der langsame β-Prozess, vgl. Abb. 3.2(b) am Beispiel Tripropylphosphat. Für andere (sog. Typ-A-Glasbildner) erscheint im Spektrum eine Abflachung der Hochfrequenzflanke des α-Prozesses, der sog. Excess-Wing (EW, siehe Abb. 3.2(a) am Beispiel Polystyrol). Abbildung 3.3(a) zeigt einen schematischen Überblick über die relevanten Relaxationsprozesse. Die Sekundärprozesse zeigen sich zwischen α-Prozess und mikroskopischer Dynamik (u.a. sog. Bosonenpeak). Diese Sekundärprozesse werden auch bei kleinen starren Molekülen beobachtet [24–26] und müssen daher intermolekularen Ursprungs sein. Da sich β-Prozesse darüber hinaus auch in metallischen [27] sowie ionischen Gläsern [28, 29] finden, kann man diese als intrinsisch für den glasartigen Zustand betrachten.

Der β-Prozess manifestiert sich in der dielektrischen Spektroskopie unterhalb von T_g als breiter, häufig näherungsweise symmetrischer Peak (vgl. Abb. 3.2(b)) [31, 32]. Oft kann für die Beschreibung eine temperaturunabhängige Verteilung von Aktivierungsenergien zu Grunde gelegt werden [31, 33–35]. Die Temperaturabhängigkeit der Peak-Maxima zeigt folglich Arrhenius-Verhalten (siehe Inset in Abb. 3.3(b)), wobei die Breite des Peaks mit der inversen Temperatur skaliert. Ein Befund der dielektrischen Spektroskopie ist, dass die Relaxationsstärke als

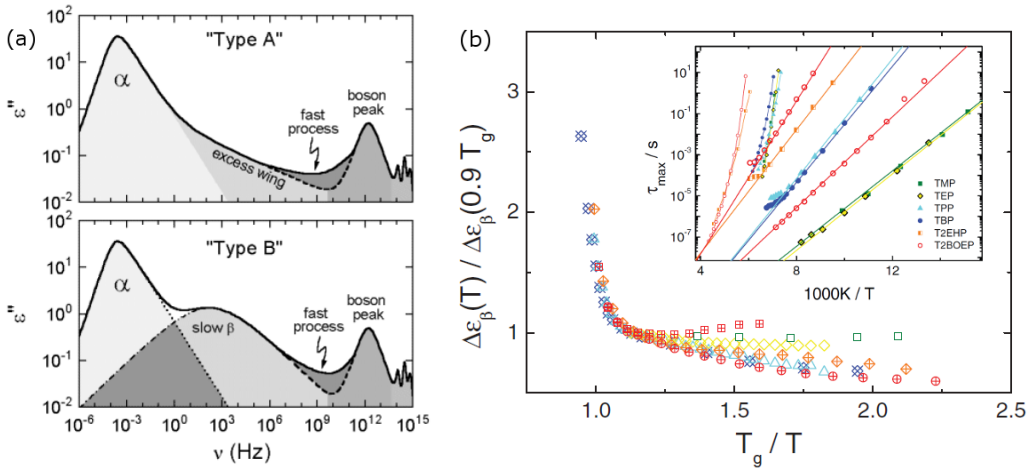

Abbildung 3.3: *(a) Dielektrisches Verlustspektrum, schematisch, für Typ-A-Glasbildner (oben) und Typ-B-Glasbildner (unten); nach [30]. (b) Relative dielektrische Relaxationsstärke des β-Prozesses verschiedener Phosphat-Glasbildner. Inset: Zeitkonstanten der entsprechenden α- (kleine Symbole) und β-Prozesse. Durchgezogene Linien sind Berechnungen aufgrund Aktivierungenergieverteilung; nach [31].*

universelle Eigenschaft unterhalb von T_g nahezu konstant bleibt und in der Nähe von T_g stark ansteigt (siehe Abb. 3.3(b)) [31].

Es ist per se nicht klar, ob am β-Prozess alle Moleküle teilnehmen, oder nur ein Teil. Von Johari und Goldstein stammt das "islands of mobility"-Konzept [26], bei dem ein Subensemble von Molekülen auch für $T < T_g$ eine erhöhte Beweglichkeit behält. Von Williams und Watts stammt dagegen die These, dass alle Moleküle am β-Prozess teilnehmen, und demzufolge durch den β-Prozess für alle Subensemble die Korrelation zu einem Teil verloren geht [36].

Der β-Prozess ist auch mittels ^{2}H-NMR zugänglich. Hier manifestiert sich ein β-Prozess in der Spin-Gitter-Relaxation $T_1(T)$, die bei T_g ihre Temperaturabhängigkeit ändert (siehe Abb. 3.4(a)). Typ-A-Glasbildner weisen in der ^{2}H-NMR für $T < T_g$ eine absolut höhere Spin-Gitter-Relaxationszeit und eine weniger starke Temperaturabhängigkeit von $T_1(T)$ auf als Typ-B-Systeme. In Echo-Pulsfolgen zur Messung der Festkörperspektren kann durch eine Verlängerung des Pulsabstandes eine erhöhte Empfindlichkeit auf Kleinwinkelbewegungen erzielt werden, für Details sei auf Kap. 3.4 verwiesen. Bezüglich des Bewegungsprozesses wurde der β-Prozess struktureller Gläser [37–39] wie auch plastischer Kristalle [40, 41] ausgiebig mittels derartiger ^{2}H-NMR-Techniken untersucht. Demzufolge ist der β-Prozess eine räumlich stark eingeschränkte Kleinwinkelbewegung, an der im reinen Glasbildner nahezu alle Moleküle teilnehmen [42–44]. Das Konzept der „islands of mobility" hat sich für reine Glasbildner bislang immer ausschliessen lassen. Die Bewegung

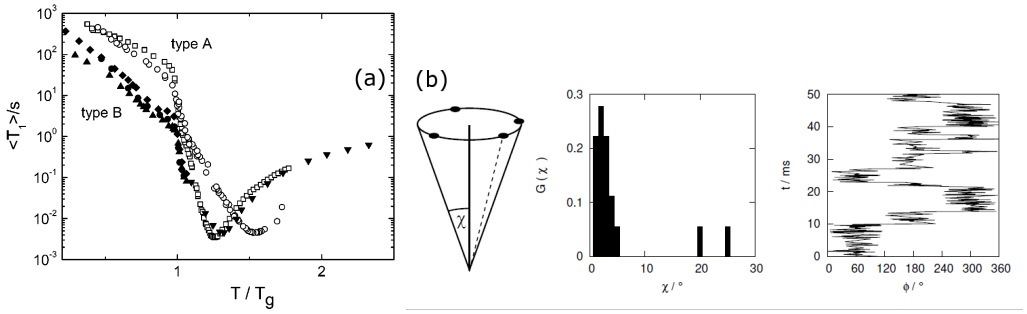

Abbildung 3.4: *(a) Mittlere ^2H-NMR Spin-Gitter-Relaxationszeit $\langle T_1(T)\rangle$ als Funktion der Temperatur für Typ-A- und Typ-B-Glasbildner. Typ-A-Systeme: o-Terphenyl-d_{14} ($\omega_L/2\pi$ = 55MHz, offene Quadrate) und Glyzerin-d_5 ($\omega_L/2\pi$ = 55MHz, offene Kreise). Typ-B-Systeme: Toluol-d_5 $\omega_L/2\pi$ = 46MHz, Dreieck Spitze oben, $\omega_L/2\pi$ = 46MHz, Dreieck spitze unten), 45% Chlorbenzol-d_5/Dekalin ($\omega_L/2\pi$ = 46MHz, volle Kreise), and 45% Chlorbenzol/Dekalin-d_{18} ($\omega_L/2\pi$ = 46MHz, Prismen); aus [48]. (b) „wobbling-on-a-cone"-Modell [49], Schema, angenommene Sprungwinkelverteilung $G(\chi)$, Trajektorie der Molekülorientierung (Bsp.); aus [50].*

lässt sich im Rahmen des „wobbling-on-a-cone"-Modells (siehe Abb. 3.4(b)) als Bewegung auf einer Konusfläche beschreiben [45]. Entsprechend der ansteigenden Relaxationsstärke in der DS vergrößert sich der Öffnungswinkel χ des Konus für $T \gtrsim T_g$ [40, 41, 46, 47].

Eine Vielzahl phänomenologischer Modelle will das Nicht-Arrhenius-Verhalten des α-Prozesses beim Glasübergang erklären und verknüpft jeweils die Relaxationszeit mit makroskopischen Eigenschaften der Flüssigkeit, etwa der Konfigurationsentropie [51, 52], dem freien Volumen [53–55], der freien Energie [56, 57], oder den Elastizitätskonstanten [58]. Ergänzt werden die Modelle durch Theorien auf einer allgemeineren Basis, z.B. der Modenkopplungstheorie [4, 59, 60], der „random-first-order-transition"-Theorie (RFOT) [61, 62], Energielandschafts-Modellen [63, 64], Frustrationsmodellen [65], der „entropic barrier hopping theory" [66] und „kinetically constrained models" [67].

Die Modenkopplungstheorie (MCT) beschreibt den Glasübergang als rein kinetisches Phänomen [59, 70]. Bei einer kritischen Temperatur T_c tritt ein dynamischer Phasenübergang auf, d.h. unterhalb von T_c ist die Bewegung zum Erliegen gekommen, ohne dass sich die Struktur der Flüssigkeit wesentlich ändert [60, 71]. Die Teilchen sind hierbei in einem „Käfig", gebildet durch ihre Nachbarteilchen, gefangen („cage effect"). Molekulardynamik-Simulationen (MD) [72–74] und Experimente an kolloidalen Systemen [69] deuten darauf hin, dass die MCT den Übergang der Dynamik von der einfachen Flüssigkeit zum Glas zutreffend beschreibt. Abbildung 3.5(a) zeigt Simulationen des mittleren Verschiebungsquadrats

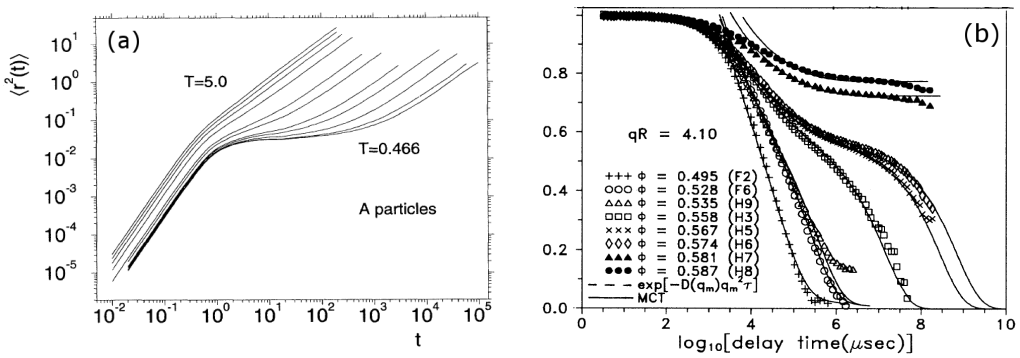

Abbildung 3.5: *(a) Mittleres Verschiebungsquadrat $< r^2(t) >$ als Funktion der Zeit für verschiedene Simulationstemperaturen T für eine Komponente einer binären Mischung von Lennard-Jones-Teilchen; aus [68]. (b) Intermediäre Streufunktionen kolloidaler Flüssigkeiten für verschiedene Volumenfraktionen Φ. Symbole sind experimentelle Ergebnisse der dynamischen Lichtstreuung, durchgezogene Linien Interpolationen der MCT; aus [69].*

$\langle r^2(t)\rangle$ als Funktion der Zeit für verschiedene Temperaturen für eine Komponente einer binären Mischung von Lennard-Jones-Teilchen [68]. Bei kurzen Zeiten (ballistisches Regime) erkennt man eine Proportionalität zu t^2, bei langen Zeiten gilt $\langle r^2\rangle \propto t$ (normale Diffusion). Zwischen den beiden Regimes entsteht bei tieferen Temperaturen ein Plateau aufgrund des Käfigeffekts. Abbildung 3.5(b) zeigt Messungen der intermediären Streufunktion an kolloidalen Flüssigkeiten und Interpolationen entsprechend der MCT [69]. Für Volumenfraktionen $\Phi < 0.574$ zerfallen die Dichtefluktuationen; die Suspension verhält sich wie eine Flüssigkeit. Für $\Phi \geq 0.581$ zerfallen die Störungen nicht mehr; es liegt ein glasartiger Zustand vor.

Reine Glasbildner sind experimentell weitgehend charakterisiert, die Entwicklung der dynamischen Suszeptibilität ist für einige „gute Glasbildner“ im gesamten Temperaturbereich vom Siedepunkt bis in die Nähe von T_g bekannt [3, 72, 73, 77–80]. Für den experimentell anspruchsvollen Zugang zum Glasübergang, bei dem sich die relevanten Größen um viele Dekaden verändern, hilft eine Reihe verschiedener Methoden. Abbildung 3.6(a) zeigt den jeweils zugänglichen Korrelationszeitenbereich der Neutronenstreuung (NS), der depolarisierten Lichtstreuung mit Hilfe von Doppelmonochromator (DM), Tandem-Fabry-Perot-Interferometer (TFPI) sowie Photonen-Korrelationsspektroskopie (PCS), des optischen Kerr-Effekts (OKE), der dielektrischen Spektroskopie (DS), sowie der Kernspinresonanz (NMR) mit Field-Cycling-Relaxometrie (FC), welche die Spin-Gitter-Relaxation in Abhängigkeit des Magnetfeldes misst. Daneben stehen in der NMR die Messung von stimuliertem Echo und 2D-Spektren, die Linienformanalyse (1D-NMR), sowie die

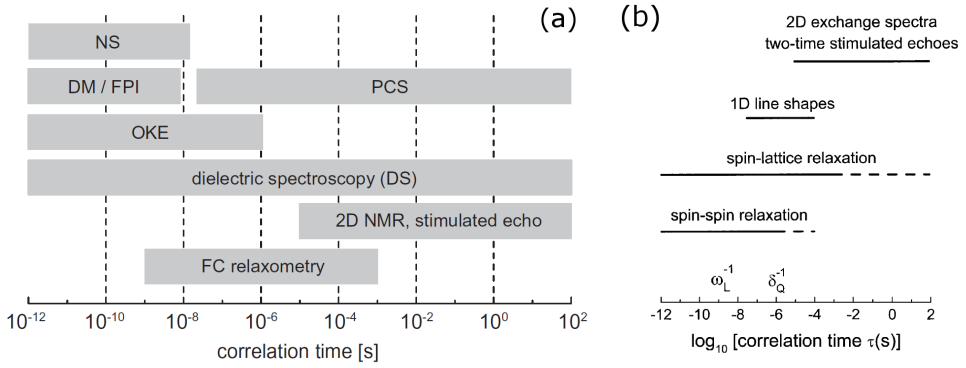

Abbildung 3.6: *(a) Zeitfenster verschiedener Methoden zur Untersuchung der molekularen Dynamik; aus [75]. (b) Zeitfenster verschiedener NMR-Techniken; aus [76].*

Messung der Spin-Spin-Relaxation zur Verfügung (Abb. 3.6(b)). Letztere kommen in dieser Arbeit zum Einsatz.

3.3 Primäre Relaxation in binären Glasbildnern

3.3.1 Stand des Wissens

In binären Mischungen ist die Dynamik wesentlich komplexer als in reinen Glasbildnern, und es gibt bislang keine allgemein anerkannte Beschreibung. Von besonderem Interesse sind dynamisch asymmetrische Mischungen, die sich durch einen großen Unterschied im T_g der reinen Komponenten auszeichnen. Zu diesen gehören Polymer-Blends [81, 82], Polymer-Weichmacher-Systeme [83–90], sowie Mischungen zweier niedermolekularer Glasbildner [91–95].

Ein experimentelles Faktum ist, dass in binären Mischungen kalorimetrisch zwei getrennte T_g nachgewiesen werden (in Abb. 3.7(a) exemplarisch gezeigt für Mischungen der Weichmacher DMP, DBP, DOP mit Polystyrol) [96–102]. Während die Existenz eines gemeinsamen T_g lange Zeit als Kriterium für die Mischbarkeit eines binären Systems angesehen wurde [103], gilt die Existenz von zwei getrennten T_g in gewissen Konzentrationsbereichen als gesichert und wurde beobachtet in Polymerblends [104], Polymer-Weichmacher-Systemen [97, 105] und auch in Mischungen eines niedermolekularen Glasbildners mit Tristyrol [94]. Unklar ist bislang jedoch, inwiefern die beiden T_g jeweils zu niedrigen und hohen Konzentrationen extrapoliert werden dürfen. Die Fragestellung nach dem weiteren Verlauf des oberen T_g führt zum Punkt, wie sich Moleküle eines Glasbildners mit hohem T_g isoliert in einem Glasbildner mit niedrigem T_g verhalten. Das Problem, wie sich die untere Glasübergangstemperatur (vgl. Abb. 3.7(a)) bei abnehmender

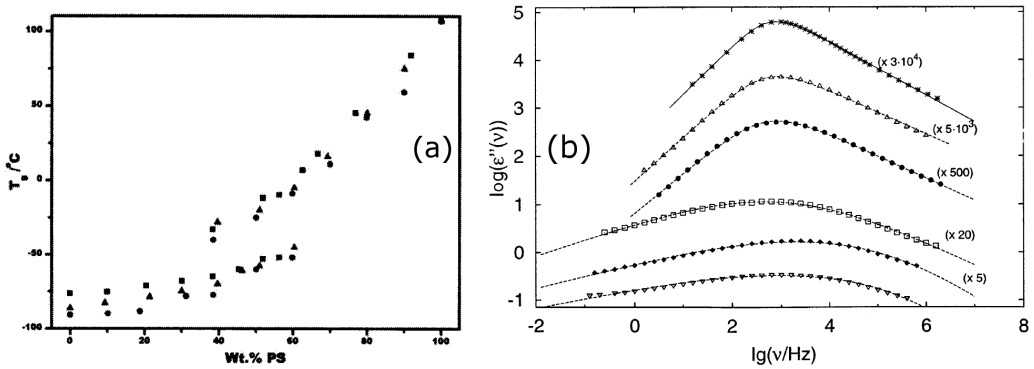

Abbildung 3.7: *(a) Glasübergangstemperaturen T_g als Funktion der Konzentration von PS in Mischung mit Dimethylphthalat (DMP, ●), Di-n-butylphthalat (DBP, ■), Bis(2-ethylhexyl)phthalate (DOP, ▲); aus [98]. (b) Dielektrische Verlustspektren von reinem TCP (oberste Kurve) sowie von TCP in OS und PS mit von oben nach unten zunehmender Molmasse; aus [96].*

Additivkonzentration entwickelt ist letztlich gleichbedeutend mit der Frage, wie sich isolierte Additivmoleküle in der festen Matrix eines Polymers verhalten.

Ein besonders markanter Befund in binären Glasbildner ist das Auftreten stark verbreiterter dielektrischer Verlustspektren. Von Blochowicz et al. [96] werden binäre Mischungen des niedermolekularen Glasbildners TCP (Nieder-T_g-Komponente) mit Oligo- und Polystyrolen (OS/PS, Hoch-T_g-Komponente) verschiedener Molmassen studiert. Die dielektrischen Spektren der Mischungen werden hierbei aufgrund des geringen Dipolmoments von OS/PS allein von der Nieder-T_g-Komponente bestimmt. Abbildung 3.7(b) zeigt dielektrische Verlustspektren etwa 50%iger Mischungen (bezogen auf die Masse) von TCP mit OS/PS verschiedener Molmassen verglichen mit denen des reinen TCP. Augenfällig ist die Verbreiterung vor allem auf der Niederfrequenzseite, die desto ausgeprägter ist, je höher die Molmasse des OS/PS und damit der T_g-Kontrast ist. Weiterhin wurde festgestellt, dass die Verbreiterung zunimmt mit abnehmender Konzentration der Nieder-T_g-Komponente. Wie später noch gezeigt wird, spiegeln die stark verbreiterten Spektren ausgeprägte dynamische Heterogenitäten wider. Auffällig ist eine zunehmende Verbreiterung der Spektren mit fallender Temperatur und damit eine Verletzung des Frequenz-Temperatur-Superpositionsprinzip (FTS) [96].

Erst durch Ergebnisse der NMR-Spektroskopie ist dynamische Heterogenität belegt und die dielektrischen Spektren ergeben sich als Folge breiter Korrelationszeitenverteilungen $G(\ln\tau)$. Ein Beweis für die ausgeprägten dynamischen Heterogenitäten der Nieder-T_g-Komponente ist das Auftreten von Zweiphasen-NMR-Spektren [76, 107]. Bei einer breiten Verteilung von Korrelationszeiten,

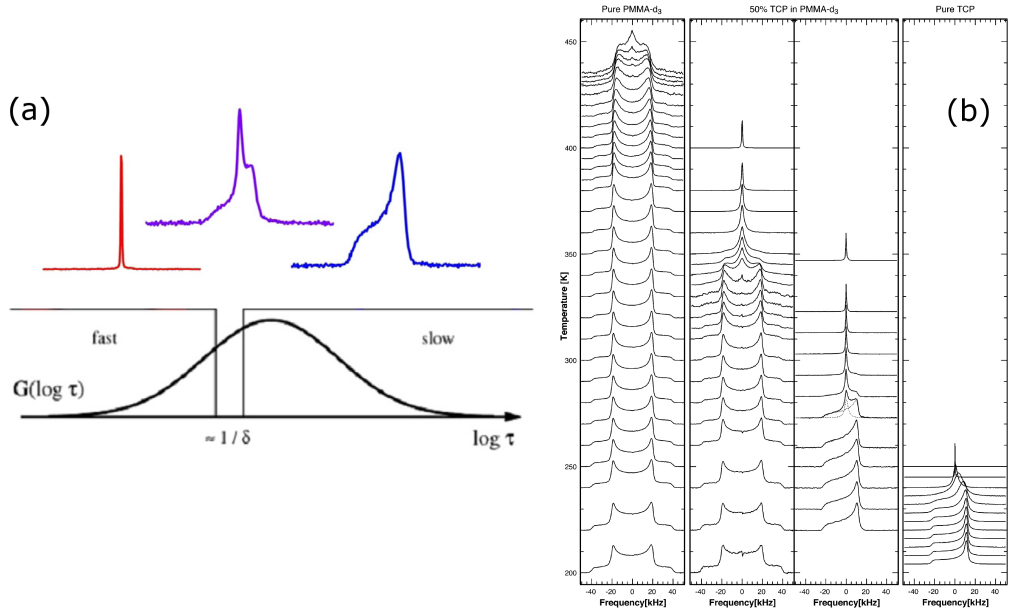

Abbildung 3.8: *(a) Zweiphasen-NMR-Spektren als Resultat einer breiten Verteilung von Korrelationszeiten $G(\log\tau)$; aus Publikation 4. (b) ^{2}H-NMR-Spektren (links) reines PMMA, 50% PMMA in TCP; ^{31}P-NMR-Spektren (rechts) 50% in PMMA, reines TCP; die Grundlinie der Spektren zeigt jeweils die Temperatur, gestrichelte Linien zeigen Anteile von Lorentz- und Festkörperspektrum entsprechende einer Anpassung mittels Zweiphasenspektrum, aus [106].*

skizziert in Abb. 3.8(a), ist der Übergangsbereich $\tau \approx 1/\delta$, in dem sich spektrale Änderungen zeigen, schmal im Vergleich zur gesamten Verteilung $G(\log\tau)$, und eine Superposition der beiden Grenzfallspektren schneller isotroper Rotation und des (ungeordneten) Festkörpers genügt zur Beschreibung. Der temperaturabhängige Wichtungsfaktor $W(T)$ gibt den Anteil der Flüssigkeitslinie an. Abbildung 3.8(b) zeigt ^{2}H-NMR-Spektren (links) von reinem PMMA-d$_3$ und PMMA-d$_3$ in Mischung mit TCP, sowie ^{31}P-NMR-Spektren (rechts) von TCP in Mischung mit PMMA und von reinem TCP. In der Mischung ist der Linienformkollaps des PMMA zu niedrigen Temperaturen verschoben, ähnelt in seiner Qualität jedoch dem des Reinen. Für TCP lässt sich der Linienformübergang mittels oben eingeführter Zweiphasenspektren beschreiben. Weiterhin ist auch eine Entkopplung der Komponentendynamik erkennbar: Während die ^{31}P-NMR-Spektren bei $T \approx 320K$ zeigen, dass alle TCP-Moleküle schnell ($\tau < 1/\delta_{CSA} \approx 10^{-5}s$) reorientieren, liegt bei der gleichen Temperatur für PMMA ein ^{2}H-NMR-Festkörperspektrum vor, das heißt im Wesentlichen reorientieren alle PMMA-Segmente langsam ($\tau > 1/\delta_Q \approx 10^{-5}s$). Wie in dieser Arbeit noch gezeigt wird, kann die Entkopplung der Komponenten-

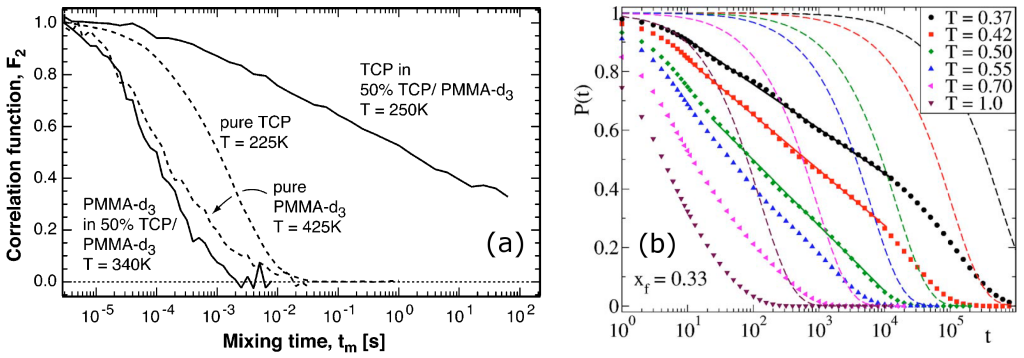

Abbildung 3.9: *(a) Orientierungskorrelationsfunktionen $F_2(t)$ aus NMR-Stimulierte-Echo-Zerfall; aus [106]. (b) Korrelationsfunktionen aus Monte-Carlo-Simulationen für verschiedene Temperaturen. Symbole: Komponente hoher Mobilität, gestrichelte Linien: Komponente niedriger Mobilität; aus [112].*

dynamik zwei getrennte T_g in der Mischung erklären.

Verschiedene phänomenologische Ansätze, bei denen eine lokal unterschiedliche Konzentration den beobachteten dynamischen Heterogenitäten zu Grunde liegt, werden zur Erklärung besagter Phänomene diskutiert. Zu unterscheiden sind thermisch induzierte Gleichgewichtsfluktuationen der Konzentration (concentration fluctuations, CF) [108] und Selbstkonzentrationseffekte [109]. Letztere basieren auf der relativ lokalen Natur der strukturellen Relaxation, so dass die lokal maßgebliche Konzentration einer Komponente immer höher ist als die Makroskopische. Auch Kombinationen beider Effekte werden diskutiert [110].

Interessant ist der Vergleich der Phänomene mit jenen im „harten“ Confinement. Tatsächlich finden sich für Glasbildner in einschränkenden Geometrien sehr ähnliche Phänomene. Auch in realen dynamisch asymmetrischen binären Systemen ist in gewissen Konzentrations- und Temperaturbereichen ($T_{g2} < T < T_{g1}$) die Bewegung der Nieder-T_g-Komponente in einer weitgehend immobilen Matrix der Hoch-T_g-Komponente und somit die Existenz eines „intrinsischen Confinement“ denkbar. Die Beobachtung von Zweiphasenspektren zeugt auch in diesem Fall von einer heterogenen Verbreiterung der α-Relaxation [48]. In beiden Situationen finden sich über weite Temperaturbereiche Zweiphasenspektren. Ähnlich wie die Ausprägung dieser im Mischsystem mit abnehmender Konzentration oder aber mit zunehmendem T_g-Kontrast zunimmt, beobachtet man die gleiche Tendenz in Silica-Matrices mit abnehmender Porengröße [111].

Die NMR-Stimulierte-Echo-Technik ermöglicht die Detektion von langsamer Dynamik $1/\delta < \tau < T_1$ bis hin zur Zeitskala der Spin-Gitter Relaxation T_1. Mittels ^{31}P-NMR Stimulierte-Echo-Technik wurde quasilogarithmischer Korrelationsver-

lust [106] für den Weichmacher TCP (Abb. 3.9(a)) nachgewiesen, während mittels ^{2}H-NMR gezeigt wurde, dass die Relaxation für die Hoch-T_g-Komponente PMMA im Vergleich zum Reinen nur moderat verbreitert ist. Die Beobachtungen decken sich mit den Resultaten von Monte-Carlo-Simulationen eines „coarse-grained"-Modells binärer Mischungen [112] (siehe Abb. 3.9(b)). Auch hier ergeben sich für die Komponente geringer Mobilität (Hoch-T_g) nur moderat verbreiterte Korrelationsfunktionen, die Komponente hoher Mobilität (Nieder-T_g) zeigt quasilogarithmischen Zerfall, der bis zum Korrelationsverlust der langsamen Komponente bestehen bleibt.

Bei der Studie eines Polymer-Blends aus Polymethylvinylether (PVME) und PS [113] zeigt sich bei niedrigen PVME-Konzentrationen im dielektrischen Spektrum eine stark verbreiterte Doppelpeakstruktur, sowie eine Arrhenius-Temperaturabhängigkeit der Relaxationspeaks. Die Beobachtung wird mit dem segmentalen α-Prozess des PVME, unter dem beschleunigenden Einfluss eines Confinement durch die PS-Ketten in Verbindung gebracht. Auch quasielastische Neutronenstreuung an Polyethylenoxid (PEO)/PMMA und atomistische MD-Simulationen zeigen für PEO heterogene „confined" Dynamik [114].

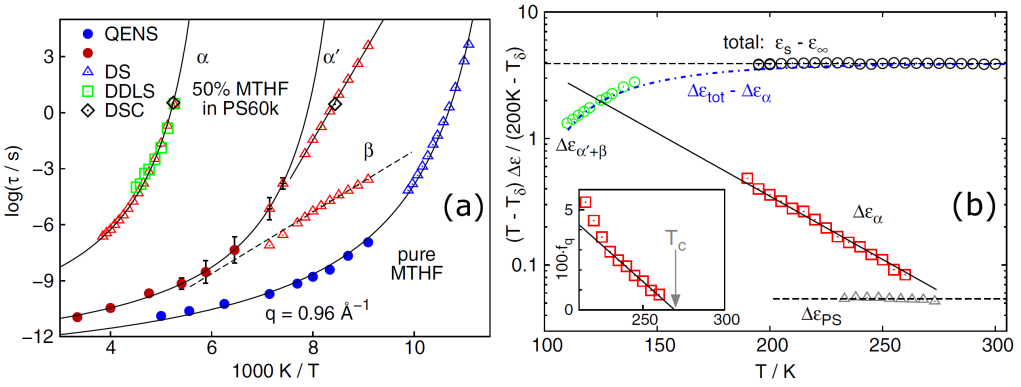

Abbildung 3.10: *(a) Korrelationszeiten τ für reines MTHF, sowie 50% MTHF in PS; aus [90]. (b) Dielektrische Relaxationsstärken $\Delta\epsilon$ der verschiedenen Prozesse, korrigiert um die Temperaturabhängigkeit der Gesamtrelaxationsstärke. Inset: Fraktion der Moleküle f_q, die am langsamen α-Prozess teilhaben; aus [90].*

Die Auswertung von Experimenten der DS und der quasielastischen Neutronenstreuung (QENS) am Mischsystems 2-Methyltetrahydrofuran (MTHF) in PS [90] führte zu einer neuen Interpretation der Dynamik, die schließlich auch wegweisend für die hier vorgelegten Arbeiten war. Kalorimetrisch werden zwei T_g gefunden. Die dielektrischen Spektren der Mischungen werden aufgrund des schwachen Dipolmoments von PS allein durch die MTHF-Komponente bestimmt. Für diese werden drei Prozesse nachgewiesen: Ein langsamer α-Prozess, ein schneller

α'-Prozess und ein β-Prozess (siehe Abb. 3.10(a)). Erstmals wurden die Relaxationsstärken genauer betrachtet. Die Relaxationsstärke $\Delta\epsilon_\alpha$ in der Mischung ist bei genügend tiefen Temperaturen weitaus höher als der Beitrag, der vom PS zu erwarten wäre - d.h. eine MTHF-Fraktion nimmt am α-Prozess der Matrix teil. Die Temperaturabhängigkeit der Relaxationsstärken (siehe Abb. 3.10(b)) zeigt bei Temperaturerhöhung ein Ansteigen für den α'-Prozess, während der α-Prozess in der Relaxationsstärke abnimmt bis bei $T = T_c$ nur noch das Signal der PS-Matrix übrig bleibt. Inkohärente Streufunktionen der quasielastischen Neutronenstreuung bei $T < T_g^\alpha$, also bei Temperaturen, bei denen in der Mischung eine starre PS-Matrix existiert, lassen sich unter Zuhilfenahme der dielektrischen Relaxationsstärken als Abfälle auf von Null verschiedene Langzeitplateauwerte beschreiben. Dieses Verhalten der Nieder-T_g-Komponente wird mit einem Typ-A-Glasübergang, wie ihn die Modenkopplungstheorie voraussagt (siehe unten), in Zusammenhang gebracht. Bei $T_{g\alpha} > T > T_{g\alpha'}$ findet sich für die Zeitkonstanten des α'-Prozess ein Übergang von Vogel-Fulcher-Tammann- zu Arrhenius-Verhalten. Als Ursache wird wiederum ein „intrinsisches Confinement“ benannt. Die Arbeit zeigt eines der wenigen Experimente an binären Systemen, die im Rahmen der MCT analysiert wurden.

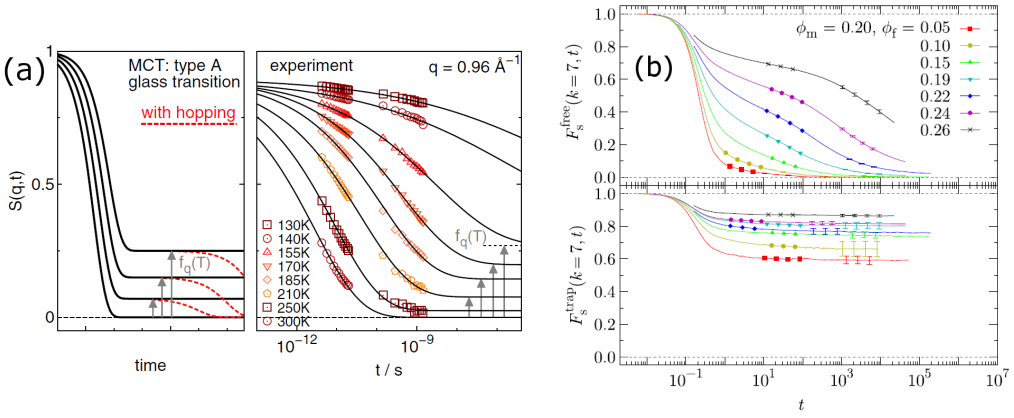

Abbildung 3.11: *(a) Inkohärente Streufunktionen $S(q,t)$; links: MCT-Typ-A-Glasübergang (schematisch); rechts: Experimente der quasielastischen Neutronenstreuung von 50% MTHF in PS-60k-d_8. Fit mittels KWW und Plateauwert f_q aus dielektrischen Daten; aus [90]. (b) MD-Simulationen der „Single-particle“ intermediären Streufunktion $F_S(k,t)$ als Funktion der Zeit t bei festem $k = 7$ (nahe des ersten Maximums des statischen Strukturfaktors), und festem Volumenanteil der Matrix $\phi_m = 0.20$ für verschiedene Volumenanteile der Flüssigkeit Φ_f, oben für die freien, unten die „gefangenen“ Teilchen; aus [115]*

Binäre Mischungen wechselwirkender Partikel können als Modellsystem für

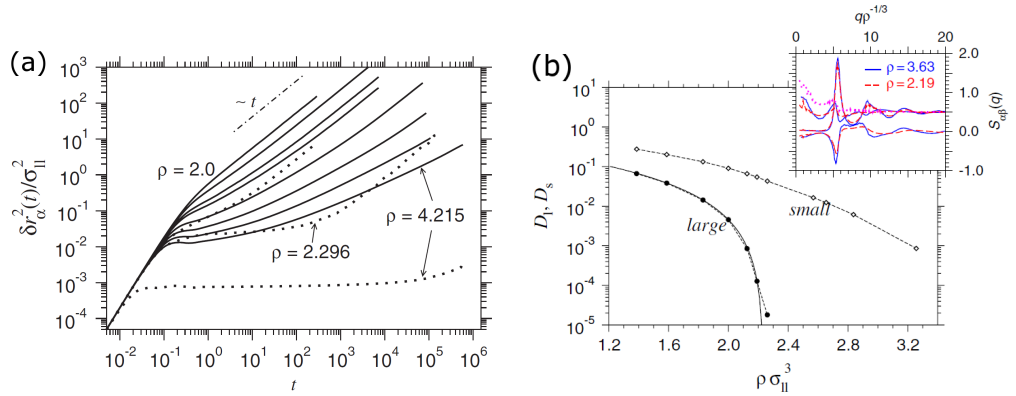

Abbildung 3.12: *(a) Mittleres Verschiebungsquadrat (MSD) aus Molekulardynamik-Simulationen equimolarer Mischungen großer (gepunktete Linien) und kleiner (durchgezogene Linien) „weicher Kugeln“, für verschiedene Anzahldichten ρ; aus [116]. (a) Selbstdiffusionskonstante D für kleine (small) und große (large) Teilchen als Funktion der dimensionslosen Dichte $\rho\sigma_{ll}^3$; Inset: Partieller statischer Strukturfaktor $S_{\alpha\beta}(q)$, als Funktion von $q\rho^{1/3}$, für hohe (blau) und niedrige (rot) Anzahldichten ρ; aus [116].*

binäre Gläser angesehen werden. Abbildung 3.12(a) zeigt das mittlere Verschiebungsquadrat (MSD) aus Molekulardynamik-Simulationen equimolarer Mischungen großer und kleiner „weicher Kugeln“ (soft spheres) [116]. Erkennbar sind deutliche Unterschiede in der Langzeitdynamik der beiden Spezies. Die Simulationen zeigen ein Szenario mit zwei getrennten Übergängen: Ein Glasübergang der großen Kugeln, und eine separate Lokalisierung der kleinen Kugeln. Für die kleinen Kugeln (durchgezogene Linien) findet sich anomale Diffusion, die sich in einem Potenzgesetz der Zeitabhängigkeit des mittleren Verschiebungsquadrats $\langle r^2(t)\rangle \propto t^p$ mit $p < 1$ ausdrückt.

In diesen Modellen wird also eine dynamische Entkopplung kleiner und großer Teilchen erwartet, und die kleinen Teilchen behalten auch unterhalb des Glasübergangs der größeren eine signifikante Beweglichkeit, die sich in einer größeren Diffusionskonstante äußert (siehe Abb. 3.12(b)) [117–119]. Man kann daher die Dynamik der kleinen Komponente als Bewegung in einer starren porösen Matrix interpretieren. In dieser Matrix findet ein sogenannter Lokalisierungs-Übergang der kleinen Teilchen statt. Dieser äußert sich darin, dass das mittlere Verschiebungsquadrat (MSD) der Teilchen mit steigender Dichte (analog mit sinkender Temperatur) besagte subdiffusive Zeitabhängigkeit zeigt und unterhalb einer charakteristischen Temperatur einen für lange Zeiten t-unabhängigen Wert annimmt, der der Lokalisierungslänge entspricht. Der partielle statische Strukturfaktor (siehe Inset in Abb. 3.12(b)) zeigt, dass die Effekte dynamischer Natur sind da die statische

Struktur bei Variation der Dichte keine wesentliche Änderung erfährt. Ein einfaches Modell für den Teilchentransport durch ein Medium zufälliger Hindernisse ist das Lorentz-Gas-Modell [120, 121]. Auch in diesem einfachen Modell findet sich subdiffusives Verhalten und ein Lokalisierungsübergang bei einer kritischen Dichte [122]. Numerische Simulationen [115] harter Kugeln in einer ungeordneten Matrix von Hindernissen („quenched annealed mixture“, siehe auch [123]) zeigen ebenfalls ein Langzeit-Plateau in der intermediären Streufunktion (siehe Abb. 3.11(b)). In den Simulationen wurden die Teilchen, die in abgeschlossenen Hohlräumen „gefangen“ („trapped“) sind, getrennt von den Teilchen in miteinander verbundenen („percolating“) Hohlräumen berechnet, wobei sich qualitative Unterschiede zeigten. Während die „single-particle“ intermediäre Streufunktion der freien Teilchen für $t \to \infty$ immer komplett auf Null abfällt, ist dies für die „gefangenen“ nie der Fall. Das MSD der freien Teilchen nimmt immer diffusives Verhalten an, während das für die „gefangenen“ Teilchen immer in Sättigung geht, wobei der Grenzwert die mittlere Porengröße reflektiert. Das Langzeitplateau rührt also in in diesem Fall von in abgetrennten Hohlräumen der Matrix „gefangenen“ Teilchen her.

Im Rahmen der Modenkopplungstheorie (MCT) des Glasübergangs ergeben sich ebenfalls Voraussagen der Dynamik in binären Glasbildnern. Für reine Glasbildner sagt die Theorie die Existenz einer kritischen Temperatur $T_c > T_g$ voraus, bei der die strukturelle α-Relaxationszeit divergiert und das Langzeitlimit f der Dichteautokorrelationsfunktion, der sogenannte Nichtergodizitätsparameter, diskontinuierlich von 0 auf $f_c > 0$ springt. Dieses Szenario wird als Typ-B-Glasübergang bezeichnet und findet sich in reinen Systemen. Für binäre Mischungen deren Komponenten sich hinreichend in der Größe unterscheiden dagegen sagt die MCT unterschiedliche Szenarien für die beiden Spezies voraus [119]. Für die kleinen mobilen Partikel in der immobilen Matrix der großen Teilchen tritt ein sogenannter Typ-A-Glasübergang auf: Hierbei wächst der Nichtergodizitätsparameter unter Abkühlung unter T_c kontinuierlich von Null an, näherungsweise gilt $f \propto T_c - T$. Auch wenn die Theorie wie auch Simulationsarbeiten sich meist auf wechselwirkende Partikel ohne Orientierungsfreiheitsgrade beschränken und damit die Translation mobiler Teilchen in einer langsamen Matrix beschreiben [119, 124], wird die Existenz eines Typ-A-Glasübergangs auch für Rotation zweiatomiger Moleküle vorausgesagt [125] und wurde auch in Simulationen gefunden [126].

Wie erwähnt wurden von Blochowicz und Mitarbeitern [90, 94] experimentelle Resultate in binären molekularen Systemen erstmals im Sinne eines Typ-A-Glasübergangs interpretiert und damit neue Fragestellungen aufgeworfen. Dies war, wie gesagt, in gewisser Hinsicht wegweisend für die vorliegende Arbeit, in der unter anderem folgenden Fragen nachgegangen wird:

- Wie entwickeln sich die Dynamik und die beiden T_g über den gesamten Konzentrationsbereich?

- Kann der langsame (α-) Prozess der Matrix für das Additiv nachgewiesen werden?
- Kann die von Blochowicz und Mitarbeitern eingeführte Interpretation vor allem mit komponentenspezifischer NMR überprüft werden?
- Welcher Natur ist der schnelle (α'-) Prozess des Additivs?
- Kann mittels NMR geklärt werden, ob alle Moleküle am Austausch innerhalb der Verteilung $G(\ln\tau)$ teilnehmen?
- Wie verhält sich der β-Prozess unter Variation der Konzentration?
- Ergeben sich in niedermolekularen (nichtpolymeren) Mischsystemen grundsätzlich ähnliche Phänomene?

3.3.2 Eigene Ergebnisse

Aufbauend auf den Studien von Blochowicz und Mitarbeitern [90, 94] wurde nach einem geeigneten Modellsystem gesucht, um die genannten Fragen beantworten zu können. Das Augenmerk lag vor allem darauf, zwei Fraktionen von Nieder-T_g-Molekülen, entsprechend dem schnellen α'- und dem langsamen α-Prozess nachzuweisen sowie die Temperaturabhängigkeit der Relaxationsstärken $\Delta\epsilon(T)$, die mit dem Typ-A-Glasübergang erklärt wurde, wiederzufinden. In Voruntersuchungen an den Systemen m-TCP in PMMA war dies nicht eindeutig möglich. Abbildung 3.13(a) zeigt die aus dem Stimulierte-Echo-Zerfall bestimmten Reorientierungskorrelationsfunktionen von m-TCP für verschiedene Konzentrationen. Man beobachtet den Übergang von Kohlrausch-Zerfall im reinen TCP hin zu quasilogarithmischem Zerfall bei mittleren und niedrigen Konzentrationen der Mischung. Ein bimodales Verhalten kann z.B. bei $c_{TCP} = 95\%$ oder $c_{TCP} = 86\%$ erahnt werden, eine quantitative Beschreibung gelang jedoch nicht. Interessant ist wieder der Vergleich mit Ergebnissen für m-TCP in porösen Silica-Matrizen (Abb. 3.13(b)) [111]. Dort ist die Bimodalität schärfer ausgeprägt, und der Verlauf der Abfälle lässt sich mit einem Modell beschreiben, bei dem die Korrelationszeit vom Abstand des Moleküls von der Porenwand abhängt (durchgezogene Linien). Ein Zweiphasenmodell, bestehend aus einem Anteil entsprechend der Bulk-Dynamik, die den in der Abbildung sichtbaren Abfall bei $t < 10^{-3}s$ erklärt, und einem Anteil, der von der Porenwand dominiert ist (verbleibende Korrelation bei $t > 10^{-2}s$) liefert vergleichbare Ergebnisse (gestrichelte Linien).

In der Erwartung, ausgeprägtere Effekte zu finden, wurde in der Folge eine Erhöhung des dynamischen Kontrasts angestrebt. Nachdem Versuche mit Trimethylphosphat durch die schlechten Mischungseigenschaften erschwert wurden, konnten unter Verwendung des Nieder-T_g-Glasbildners Triethylphosphat (TEP,

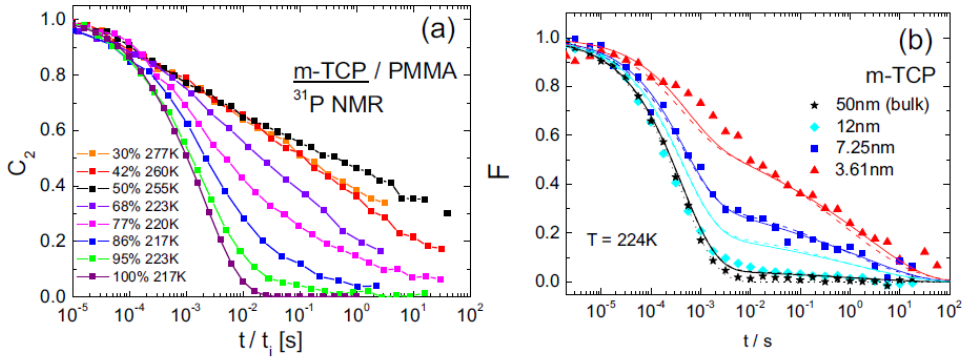

Abbildung 3.13: *Reorientierungskorrelationsfunktionen von m-TCP, bestimmt aus ^{31}P-NMR Stimulierte-Echo-Zerfall. (a) Mischsystem TCP/PMMA; aus Publikation 4. (b) m-TCP in porösen Silica-Matrizen angegebener Porengrößen; aus Publikation 4.*

T_g = 137K) in der Tat alle bereits bekannten Phänomene in verstärkter Form wiedergefunden werden. In Abb. 3.14(a) lässt sich anhand einiger ^{2}H- und ^{31}P-NMR-Spektren noch einmal die dynamische Entkopplung der beiden Komponenten erkennen. Der Wichtungsfaktor $W(T)$ (Abb. 3.14(b)) gibt den Anteil der Flüssigkeitslinie an. Während für TEP $W(T)$ mit sinkender Konzentration immer breiter wird, ähnelt der NMR-Glasübergang von PMMA in der Mischung dem des Reinen und zeugt von einer allenfalls moderaten Verbreiterung für die Hoch-T_g-Komponente PMMA. Bemerkenswert ist an dieser Stelle eine Besonderheit des PMMA, das schon im Reinen dynamische Heterogenitäten aufweist, die sich in Zweiphasenspektren widerspiegeln (vgl. Abb. 3.8(b)). Daneben sei noch erwähnt, dass der ^{2}H-NMR-Linienformübergang (entspricht $\tau \approx 10^{-5}s$) für PMMA in 75% TEP bei $T \approx 245K$ und somit ungewohnt weit oberhalb des kalorimetrisch bestimmten T_{g1} = 160K beobachtet wird. Die große Temperaturdifferenz zeugt von einer geringen Fragilität des PMMA in Lösung. Der Stimulierte-Echo-Zerfall (Abb. 3.14(c)) offenbart für die Mischungen extrem verbreiterte Korrelationsfunktionen, die im vorhandenen Zeitfenster nicht vollständig aufgenommen werden können. Weder der Wichtungsfaktor $W(T)$ noch der Stimulierte-Echo-Zerfall lieferten jedoch hinreichende Anzeichen für eine bimodale Korrelationszeitenverteilung, die dem Szenario zweier TEP-Fraktionen Rechnung trägt.

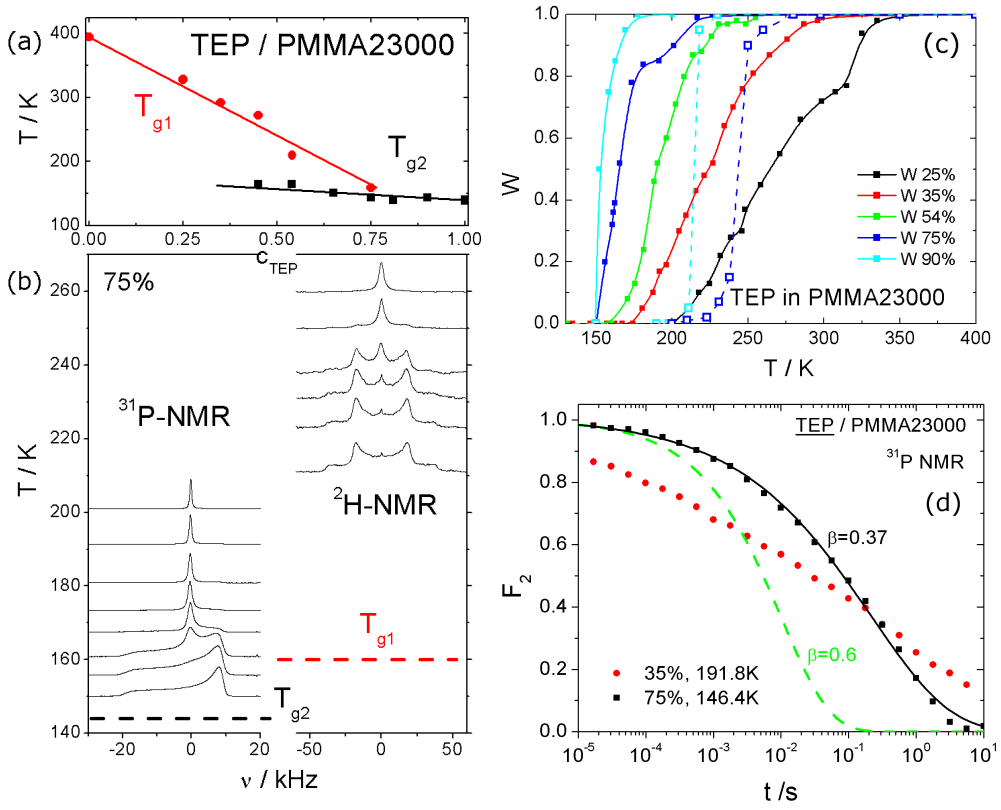

Abbildung 3.14: *Mischsystem Triethylphosphat (TEP)/PMMA. (a) Glasübergangstemperaturen T_{g1} und T_{g2} aus DSC-Messungen als Funktion der Konzentration c_{TEP}. (b) ^{31}P-NMR-Spektren (links), ^{2}H-NMR-Spektren (rechts) für 75% TEP in PMMA-d_3; Grundlinie der Spektren zeigt jeweils die Temperatur, horizontale gestrichelte Linien zeigen T_{g1} und T_{g2} aus DSC; unveröffentlicht. (c) Wichtungsfaktor der Flüssigkeitslinie $W(T)$ für den Bereich der Zweiphasen-Spektren für verschiedene Konzentrationen von TEP in PMMA-d_3: volle Symbole, durchgezogene Linien: aus ^{31}P-NMR; offene Symbole, gestrichelte Linien: $W(T)$ aus ^{2}H-NMR (aufgrund des engen Temperaturbereichs liegen nur wenige Punkte vor). (d) Reorientierungskorrelationsfunktion $F_2(t)$ aus ^{31}P-NMR Stimulierte-Echo-Messungen für 75% und 35% TEP in PMMA; durchgezogene Linie: Anpassung einer Kohlrauschfunktion, zum Vergleich Kohlrausch-Abfall entsprechend dem typischen Verhalten reiner Glasbildner (gestrichelte Linie).*

TPP in Polystyrol (Publikationen 2 und 3)

Eine umfassende, quantitative Beschreibung ausschließlich auf Basis der NMR-Ergebnisse war damit aufgrund der komplexen Dynamik im Mischsystem nicht möglich. Ein künftiges Modellsystem sollte leicht interpretierbare dielektrische Spektren zeigen, um mittels dieser einen Überblick über die Dynamik gewinnen zu können. Bei dem System TEP/PMMA war dies nicht der Fall, da sowohl TEP als auch PMMA ein vergleichbares Dipolmoment tragen und somit beide zu den dielektrischen Spektren beitragen. Darüberhinaus zeigt PMMA starke Sekundärrelaxation, die eine Analyse weiter erschwert. Erst mit Tripropylphosphat (TPP) in Polystyrol war ein geeignetes System gefunden. Nur geringe Kristallisationsneigung auch im reinen TPP und gute Mischbarkeit über den gesamten Konzentrationsbereich sind gegeben. Durch die Wahl dieser Komponenten lassen sich mittels NMR beide Komponenten selektiv untersuchen. ^{31}P-NMR-Messungen geben Aufschluss über die Dynamik des TPP, ^{2}H-NMR reflektiert die des (Ketten-deuterierten) PS-d_3. Durch den ausgeprägten Unterschied in den Dipolmomenten der beiden Komponenten sind die Messungen der dielektrischen Spektroskopie in allen untersuchten Mischungen praktisch ausschließlich durch das Signal von TPP bestimmt. Der ausgeprägte T_g-Kontrast (TPP: T_g = 136K, PS (M_w = 2440g/mol): T_g = 335K) lässt starke dynamische Heterogenitäten erwarten, während durch die Wahl des kurzkettigen PS alle relevanten Effekte in den NMR-Observablen im zugänglichen Temperaturbereich liegen. Für die beiden reinen Komponenten ist FTS erfüllt, d.h. die Bildung einer Masterkurve für die Spektren ist möglich. Während man mittels DS für reines TPP eine β-Relaxation gut beobachten kann (siehe Abb. 3.2(a)), wird PS als Typ-A-Glasbildner identifiziert: In der Nähe von T_g ändert sich der Exponent des Potenzgesetzes für die Hochfrequenzflanke des α-Prozesses, typisch für den sog. Excess-Wing. Es finden sich unterhalb von T_g keine Anzeichen eines β-Prozesses. Unter diesen Voraussetzungen erlaubt das gewählte System auch die Analyse des β-Prozess in den Mischungen. Die Ergebnisse bzgl. des β-Prozesses sind in Publikation 1 zusammengestellt und werden in Kapitel 3.4 beschrieben. Publikationen 2 und 3 zeigen die Ergebnisse für $T > T_{g2}$. Im Folgenden seien die Ergebnisse an diesem System für $T > T_{g2}$ etwas genauer vorgestellt.

Abbildung 3.15 zeigt ^{31}P-Hahn-Echo- (TPP) sowie ^{2}H-Solid-Echo-Spektren (PS) für verschiedene Temperaturen und Konzentrationen. Die Dynamik von TPP und PS ist entkoppelt. Für PS verschiebt sich unter Erhöhung der TPP-Konzentration der Linienformübergang von einer zentralen Lorentzlinie zum Festkörperspektrum zu niedrigeren Temperaturen und reflektiert somit eine Beschleunigung der Dynamik. Die Qualität des Linienformübergangs bleibt dabei weitgehend erhalten, es finden sich keine Zweiphasen-Spektren. Für TPP hingegen verschiebt sich der Linienformübergang unter Zugabe von PS nicht nur zu höheren Temperaturen, sondern es können in den Mischungen Zweiphasenspektren beobachtet werden.

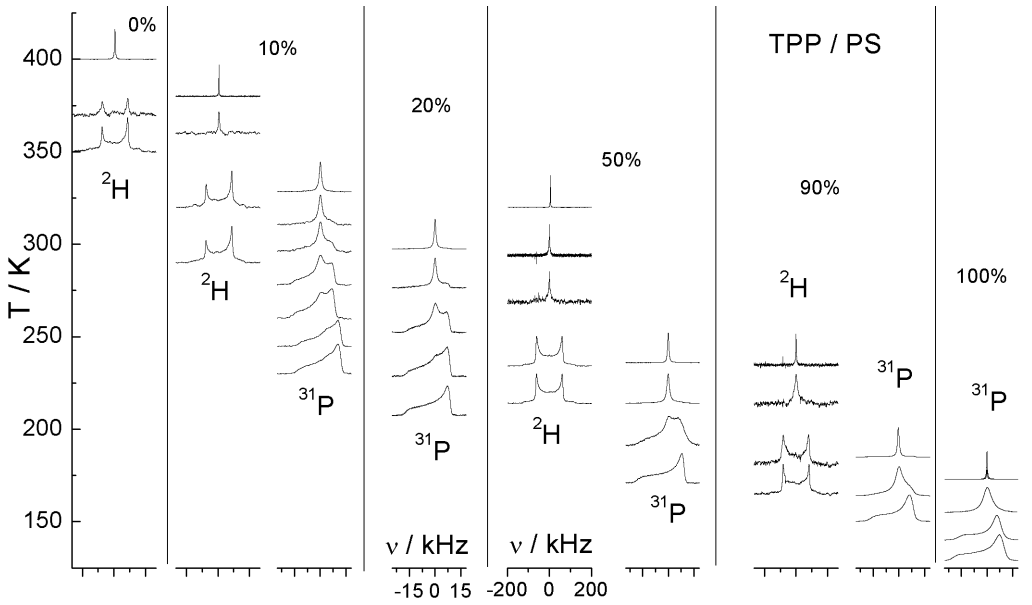

Abbildung 3.15: *^{2}H- und ^{31}P-NMR-Spektren für verschiedene Temperaturen und verschiedene c_{TPP} des Mischsystems TPP / PS-d_3; aus Publikation 3.*

Analoge Ergebnisse liefert die DS [127]: Unter Zugabe von PS (c_{TPP} = 90%, Abb. 3.16(a)) findet sich eine auffällige Verbreiterung auf der Niederfrequenzseite der Hauptrelaxation von TPP. FTS ist hierbei nicht erfüllt - die Verbreiterung auf der Niederfrequenzseite ist umso ausgeprägter, je tiefer die Temperatur ist. Die Dynamik von TPP verlangsamt sich als Folge des Antiweichmachereffekts von PS. Der zweite Peak in Abb. 3.16(a) reflektiert den nahezu unveränderten β-Prozess (vgl. Kap. 3.4).

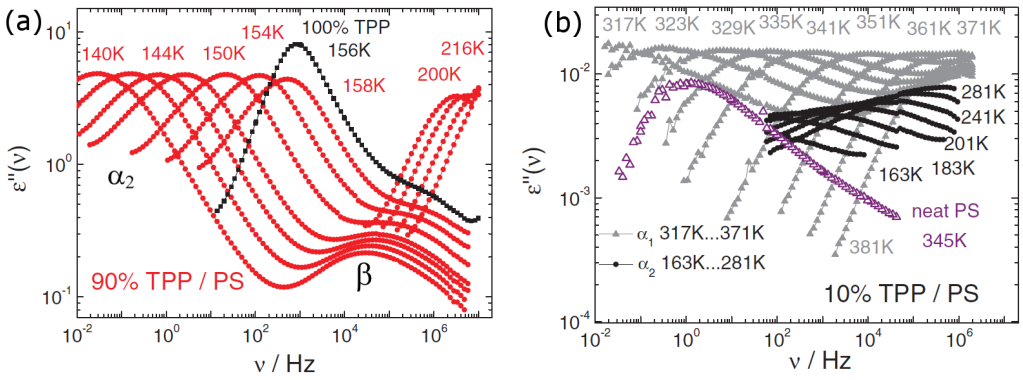

Abbildung 3.16: *Dielektrische Verlustspektren im Mischsystem TPP/PS. (a) Hohe TPP-Konzentration c_{TPP} = 90% (rote Kreise), zum Vergleich: reines TPP (schwarze Quadrate); aus Publikation 2. (b) Niedrige TPP-Konzentration c_{TPP} = 10%; volle Dreiecke, hohe Temperaturen: α_1-Relaxation; volle Kreise, niedrige Temperaturen: α_2-Relaxation; offene Dreiecke: Reines PS bei 345 K; aus Publikation 2.*

Abbildung 3.16(b) zeigt am Beispiel der 10% TPP/PS-Mischung die Situation bei niedrigen Konzentrationen. Im Gegensatz zu c_{TPP} = 90% werden neben dem β-Prozess (nicht in der Abbildung gezeigt) zwei Relaxationsphänomene beobachtet, die in Analogie zur Nomenklatur von Blochowicz et al. (dort α- und α'-) [90, 94] hier α_1- (hohe Temperaturen, Dreiecke) und α_2-Prozess (niedrige Temperaturen, Kreise) genannt werden. Zeitkonstanten beider Prozesse sind für c_{TPP} = 20% in Abb. 3.17 eingetragen. Das NMR-Ergebnis vorwegnehmend sei hier schon gesagt, dass beide Prozesse von TPP isotropen, d.h. Flüssigkeitscharakter aufweisen.

Während die α_1-Relaxation eine Nicht-Arrhenius-Temperaturabhängigkeit aufweist, ähnlich der von reinem PS, jedoch zu niedrigeren Temperaturen verschoben, zeigt die α_2-Relaxation Arrhenius-Verhalten. ^{2}H-NMR-Experimente zeigen für die PS-Dynamik Korrelationszeiten, die mit denen des dielektrisch sondierten α_1-Prozesses übereinstimmen. Die dielektrische Relaxationsstärke des α_1-Prozesses übersteigt die von reinem PS. Daher muss geschlossen werden, dass ein Anteil der TPP-Moleküle an der α-Relaxation des PS teilnimmt (hier α_1-Prozess genannt). Der α_1-Prozess zeigt Debye-Verhalten auf der Niederfreuquenzseite (d.h. $\epsilon \propto \nu$) und FTS ist erfüllt.

Der α_2-Prozess zeigt eine starke Abflachung der Niederfrequenzflanke, FTS ist nicht erfüllt. Die zugehörigen Zeitkonstanten zeigen für höhere TPP-Konzentrationen ebenfalls Nicht-Arrhenius-Temperaturabhängigkeit (wird später gezeigt) und er entwickelt sich für $c_{TPP} \to 1$ stetig in den α-Prozess von reinem TPP. Die Entwicklung des α_2-Prozesses mit abnehmender TPP-Konzentration sei zunächst anhand der DS-Spektren diskutiert. In Abb. 3.18 sind Spektren für verschiedene Konzentrationen bei jeweils ähnlichem $\tau_{\alpha 2}$ dargestellt. In Übereinstim-

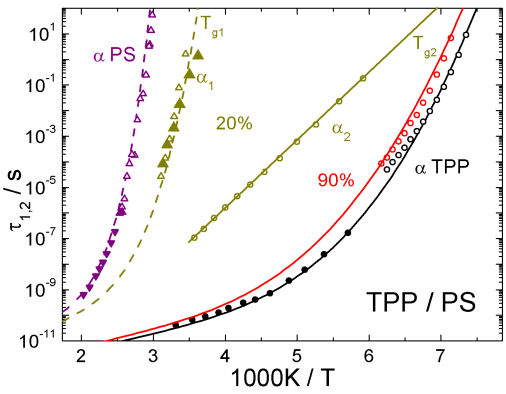

Abbildung 3.17: *Zeitkonstanten des α-Prozesses von reinem PS (c_{TPP} = 0), reinem TPP, des α_2-Prozesses der Mischung mit c_{TPP} = 90% sowie des α_1- und α_2-Prozesses der Mischung mit c_{TPP} = 20%; offene Symbole: DS; gefüllte Symbole: NMR (reines PS: [128], reines TPP: [2]); T_{g1} und T_{g2} sind durch die Schnittpunkte der Extrapolationen mit der oberen Achse (τ = 100s) gegeben.*

mung mit den NMR-Spektren ist eine systematisch zunehmende Verbreiterung der Relaxation mit sinkender Konzentration zu erkennen. Während für $1 > c_{TPP} > 0.2$ eine Interpolation der α_2-Spektren mittels der Havriliak-Negami (HN-) Funktion möglich ist, lässt sich für geringe $c_{TPP} \leq 0.2$ das Verlustspektrum für $T < T_{g1}$ durch die Annahme einer temperaturunabhängigen Aktivierungsenergieverteilung $g(E)$ beschreiben. Die Zeitkonstanten zeigen dann Arrhenius-Verhalten. Wie eine Analyse (Publikation 2) und auch direkte Inspektion von Abb. 3.16(b) zeigt, sinkt die Relaxationsstärke des langsamen α_1-Prozess mit steigender Temperatur, während die des α_2-Prozesses ansteigt (siehe Abb. 3.16(b)). Dies legt die Vermutung nahe, dass die α_2-Fraktion mit steigender Temperatur auf Kosten der α_1-Fraktion wächst und der Anteil der Letzteren für hohe Temperaturen gegen Null strebt, wie schon von Blochowicz et al. gefunden [90].

Stimulierte-Echo-Experimente erlauben der NMR einen direkten Zugang zur Reorientierungskorrelationsfunktion $C_2(t)$ (siehe Kap. 3.6.4). Solche Messungen wurden systematisch für PS und TPP durchgeführt. Erstmals war es möglich, beide Komponenten mit Hilfe des Stimulierten Echos zu vermessen und $C_2(t)$ zu bestimmen. In Abbildung 3.19 sind beispielhaft einige Korrelationsfunktionen von PS-d_3 und TPP dargestellt. Die Ergebnisse der ^{2}H-NMR (linke Spalte) zeigen Zerfälle, die sich durch Kohlrausch-Funktionen beschreiben lassen (durchgezogene Linien). Zeit-Temperatur-Superposition (TTS) ist jeweils erfüllt, mit abnehmender Konzentration nimmt die Streckung leicht zu. Die Zeitkonstanten τ_{α_1} entsprechen denen der DS, der die Verbreiterung beschreibende Parameter β_K ist ähnlich

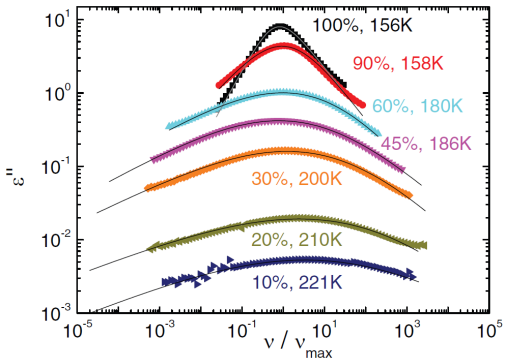

Abbildung 3.18: *Dielektrische Spektren des α_2-Prozesses bei ungefähr gleichem $\tau_{\alpha 2}$.*

dem von der DS gefundenen. Somit wird endgültig klar, dass der α_1-Prozess aus TPP-Molekülen resultiert, welche am α-Prozess des PS teilnehmen.

^{31}P-NMR (rechte Spalte in Abb. 3.19) findet in der Mischung für hohe TPP-Konzentrationen Zerfälle, deren Streckung zu langen Zeiten nicht durch Kohlrauschfunktionen (gepunktete Linie für c_{TPP} = 90%) reproduziert werden kann. Eine Zeitdomänendarstellung der HN-Verteilung mit den in der DS für α_2 gefundenen Parametern (durchgezogene Linie für c_{TPP} = 90%) kann die Abfälle gut beschreiben. Bei c_{TPP} = 50% finden sich allerdings wesentlich stärker verbreiterte Korrelationsfunktionen. Die quantitative Analyse in der Zeitdomäne ist schwierig, jedoch können mittels der Ergebnisse der DS die NMR-Korrelationsfunktionen erklärt werden. Die in der DS für die α_2-Relaxation gefundenen HN-Verteilungen genügen zur Beschreibung zunächst nicht und liefern im Vergleich zu schnelle Abfälle (gestrichelte Linien). Die NMR-Korrelationsfunktionen lassen sich durch die in der DS gefundenen HN-Verteilungen jedoch dann reproduzieren (durchgezogene Linien), wenn ein nicht relaxierender Sockel angenommen wird. Dieser Sockel wird mit dem α_1-Prozess zugeordneten TPP-Molekülen begründet und sein Anteil entspricht in etwa dem in der DS gefundenen Anteil. Er ist somit ein indirekter Nachweis des α_1-Prozesses. Bei niedrigen Konzentrationen (in Abb. 3.19 gezeigt für c_{TPP} = 20%) gelingt wiederum nur unter Annahme eines nicht relaxierenden Sockels die Interpolation der Stimulierte-Echo-Zerfallskurven konsistent zu den DS-Ergebnissen. Die gestrichelten Linien zeigen den entsprechenden Abfall ohne Annahme eines Anteils von α_1. Für TPP ist in den Mischungen in allen Fällen TTS nicht erfüllt. Durch Kombination von NMR, DS und DLS konnten schließlich Zeitkonstanten über große Temperatur- und Konzentrationsbereiche bestimmt werden (Diskussion s.u.).

Durch Vorliegen einer temperaturunabhängigen Aktivierungsenergieverteilung

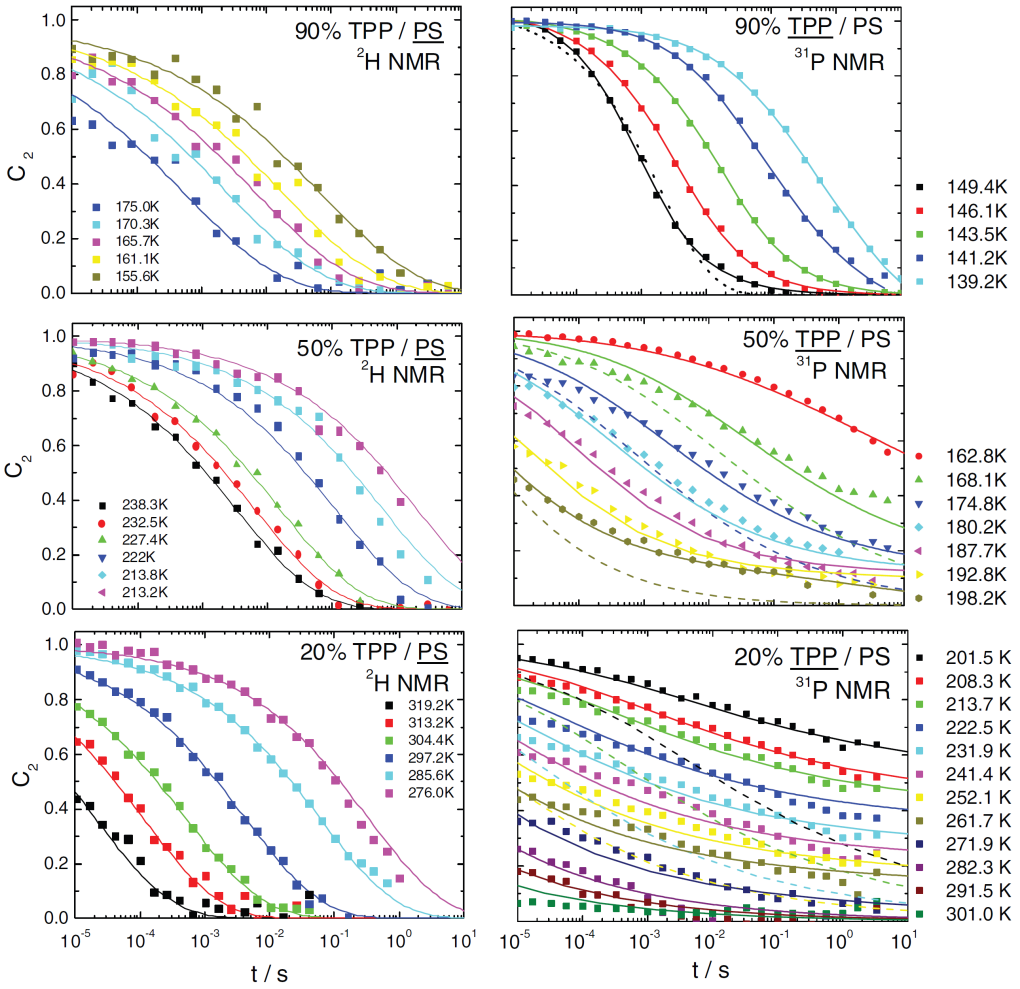

Abbildung 3.19: *Reorientierungskorrelationsfunktionen im Mischsystem TPP/PS, bestimmt aus Stimulierte-Echo-Zerfall der ^{2}H-NMR (links, Linien sind Kohlrausch-Fits) sowie der ^{31}P-NMR (rechts, Linien: 90%: Kohlrausch-Zerfall(punktiert), HN (durchgezogen); 50%: HN mit (durchgezogen) und ohne (strichliert) nichtrelaxierendem Sockel; 20%: Zerfall entsprechend temperaturunabhängiger Aktivierungsenergieverteilung mit (durchgezogen) und ohne (strichliert) nichtrelaxierendem Sockel).*

ähnelt der α_2-Prozess in der dielektrischen Phänomenologie einem β-Prozess. Das Vorliegen von Zweiphasen-NMR-Spektren mit einem Anteil einer zentralen Lorentzlinie (siehe Abb. 3.15, $c_{TPP} = 20\%$, $T = 250K$) zeigt jedoch eindeutig, dass der entsprechende Anteil an TPP-Molekülen isotrop (d. h. flüssigkeitsähnlich) reorientiert - im Gegensatz zu einem β-Prozess, der in der hier verwendeten Nomenklatur auf einer räumlich stark eingeschränkten Bewegung beruht. 2D-NMR-Spektren

geben Aufschluss über die Geometrie langsamer ($1/\delta < \tau < T_1$) Reorientierungen. Bei c_{TPP} = 20% und T = 200K gemessene 2D-NMR-Spektren (siehe Abb. 3.20(a)) zeigen für den α_2-Prozess isotrope Reorientierung . Die gemesssenen 2D-Spektren lassen sich mittels einer Superposition der beiden Subspektren für isotrope Reorientierung und keine Bewegung (siehe Kap. 3.6.5) beschreiben. Es zeigen sich keinerlei Anzeichen, dass sich der Charakter der α_2-Relaxation hin zu einer eingeschränkten Bewegung ändert (vgl. [90]). Andererseits ist jedoch klar, dass dem α_1-Prozess zugeordneten TPP-Moleküle am α_2-Prozess in Form einer eingeschränkten Bewegung teilnehmen können (wie für die PS-Matrix selbst in Kap. 3.4 gezeigt).

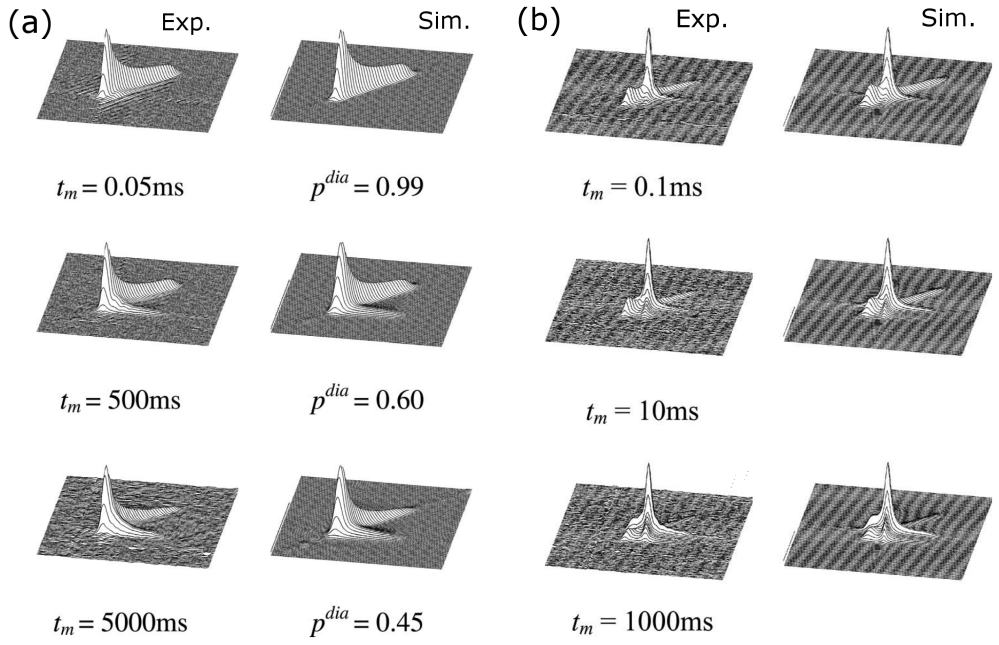

Abbildung 3.20: ^{31}*P-NMR 2D-Spektren, 20% TPP in PS. (a)* T = 200K*; Links: Experiment, Mischzeit angegeben; rechts: Simulation, Anteil des Diagonal-Subspektrums angegeben; (b)* T = 269.5K*; links: Experiment, Mischzeit angegeben; rechts: Simulation. Aus Publikation 3.*

Neben dem Charakter der α_2-Relaxation, der als isotrope Bewegung identifiziert wurde, lassen sich mittels 2D-NMR-Spektren auch die dynamischen Heterogenitäten von TPP untersuchen (Abbildung 3.20(b)). Ein Austausch-Pattern (vgl. Abb. 3.36) weist für den wesentlichen Anteil der dynamischen Heterogenitäten eine transiente Natur nach. Der Austausch findet wiederum auf vergleichbaren Zeitskalen wie die α_2-Relaxation statt. Die Wichtungen der vier Subspektren sind im Limes

kurzer bzw. langer Mischzeit unter der Annahme vollständigen Austauschs durch den 1D-Wichtungsfaktors bei entsprechender Temperatur gegeben (siehe Kap. 3.6.5, [106, 129]). Bei einem Vergleich der gefundenen Wichtungen mit den erwarteten Werten finden sich in Übereinstimmung mit den Stimulierte-Echo-Zerfällen (vgl. Abb. 3.19) Anzeichen, dass nicht alle Moleküle am Austausch teilhaben. Hier ist davon auszugehen, dass die dem α_1-Subensemble zuzuordnenden Moleküle auch nicht am Austausch auf der Zeitskala von $\tau_{\alpha 2}$ teilnehmen.

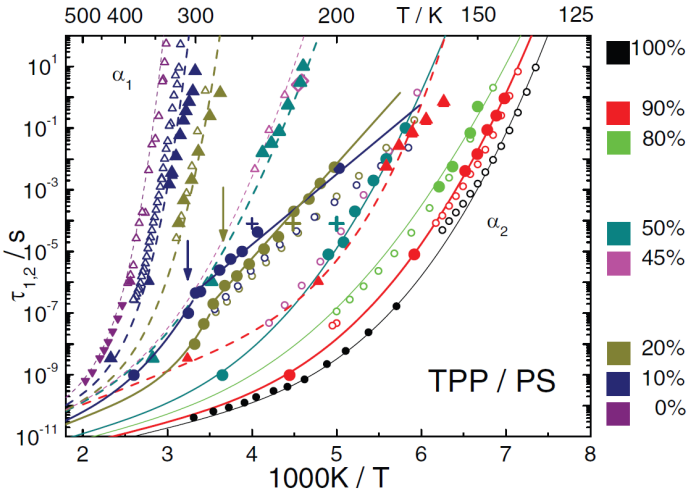

Abbildung 3.21: *Zeitkonstanten aus der DS (△: α_1; ○: α_2), ^{2}H-NMR (▼; ▲: reines PS, [128]; +: solid-echo, siehe Kap. 3.4), ^{31}P-NMR (●, reines TPP: Ref. [2]), für Konzentration laut Farbcode. Linien dienen der Blickführung (gestrichelt: α_1-Relaxation; durchgezogen: α_2-Relaxation). Pfeile markieren T_{g1}; aus Publikation 3.*

Zusammenfassend sind in Abb. 3.21 die Zeitkonstanten der NMR-Messungen mit einigen Ergebnissen der DS für verschiedene Konzentrationen dargestellt. Erkennbar ist, wie sich die Zeitkonstanten des α_2-Prozesses bei Erniedrigung der Konzentration zu höheren Temperaturen verschieben und bei niedrigen Konzentrationen zu einem Arrhenius-Verhalten übergehen. Die Aktivierungsenergie nimmt bei weiterer Konzentrationserniedrigung ab. Für c_{TPP} = 10% und c_{TPP} = 20% ist in den Zeitkonstanten aus dem ^{31}P-NMR Stimulierte-Echo-Zerfall jeweils ein stark-zu-fragil-Übergang erkennbar (siehe Abb. 3.21). Hierbei geht die Temperaturabhängigkeit von Nicht-Arrhenius ($T > T_{g1}$) zu Arrhenius ($T < T_{g1}$) über.

Zwei Glasübergangstemperaturen T_{g1} und T_{g2} können über annähernd den gesamten Konzentrationsbereich bestimmt werden (siehe Abb. 3.22) – übereinstimmend mittels DS, thermischer Analyse (DSC) sowie NMR. $T_{g1}(c_{TPP})$ verringert sich monoton ausgehend vom reinen PS zu hoch verdünntem PS, $T_{g2}(c_{TPP})$ ist

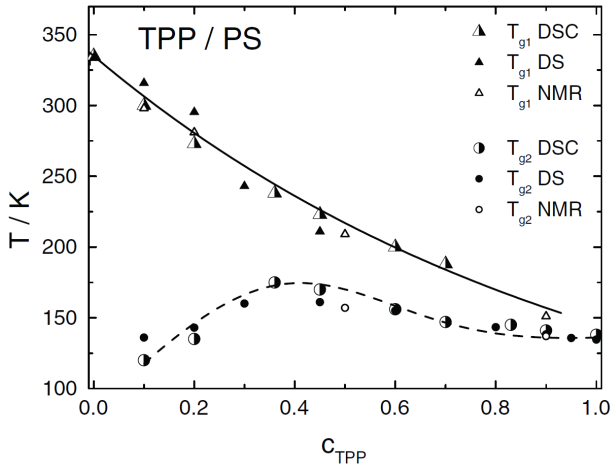

Abbildung 3.22: *Glasübergangstemperaturen T_{g1} und T_{g2} als Funktion der TPP-Konzentration, bestimmt mittels DS, DSC und NMR; aus Publikation 3.*

deutlich geringer und der Verlauf von T_{g2} zeigt bei $c_{TPP} = 0.35$ ein Maximum. Die Ursache dieses erstmals gefundenen Verhaltens ist das Zusammenspiel aus dem Anti-Weichmachereffekt, durch den sich $T_{g2}(c_{TPP})$ bei Zugabe von PS erhöht, und einer abnehmenden Aktivierungsenergie des Arrhenius-förmigen α_2-Prozesses bei geringen c_{TPP}, wie anhand von Abb. 3.21 zu erkennen ist.

Somit ist erstmals eine konsistente Beschreibung der Dynamik mit Hilfe der DS und NMR gelungen und bestätigt in großen Teilen die Resultate der Arbeiten von Blochowicz et al. [90, 94]. Unterschiede bestehen im Verlauf von $T_g(c)$. Während Blochowicz et al. betonen, dass für MTHF-Konzentrationen $c_{MTHF} \geq 0.6$ beide Prozesse komplett vereinigt sind und damit nur ein gemeinsamer Glasübergang vorliegt, werden hier für TPP/PS bei allen untersuchten Konzentrationen getrennte Prozesse und zwei T_g gefunden.

Nicht-polymeres Mischsystem MTHF / m-TCP (Publikation 4)

Mit dem Mischsystem 2-Methyltetrahydrofuran (MTHF, $T_g = 96K$)/m-Trikresylphosphat (m-TCP, $T_g = 206K$) wurde eine niedermolekulare (nicht-polymere) Mischung analysiert. Der T_g-Kontrast ist hierbei unvermeidlich kleiner als beim System TPP/PS. ^{2}H-NMR ermöglicht Zugang zur Dynamik des methylgruppendeuterierten MTHF-d_3, ^{31}P-NMR zu der von m-TCP. Da beide Substanzen vergleichbares Dipolmoment besitzen, sind die dielektrischen Spektren durch beide Komponenten bestimmt. Zusätzlich zu den Messungen mittels NMR, DSC und DS wurden im Rahmen weiterer Doktorarbeiten Lichtstreuexperimente mittels Photo-

nenkorrelationsspektroskopie (PCS), Tandem-Fabry-Perot-Interferometer (TFPI) und Doppelmonochromator (DM) durchgeführt [130, 131]. Die Streuintensität ist im Wesentlichen durch m-TCP gegeben, das sich aufgrund der konjugierten Doppelbindungen durch eine ausgeprägte Anisotropie der Polarisierbarkeit auszeichnet. Lediglich im Falle hoher MTHF-Konzentrationen ist deshalb von einem Beitrag durch MTHF auszugehen.

In DSC-Experimenten gelingt es nicht, zwei getrennte T_g nachzuweisen. Wie unten gezeigt, lassen sich die kalorimetrischen $T_g(c_{MTHF})$ durch Vergleich mit NMR- und DS-Zeitkonstanten der Dynamik der Komponenten TCP (dann als T_{g1} bezeichnet) und MTHF (T_{g2}) zuordnen und sind in Abb. 3.23 markiert. Weiterhin fällt auf, dass die Breite der kalorimetrischen Glasstufe keine ausgeprägte Konzentrationsabhängigkeit zeigt, im Gegensatz zu TPP/PS. An dieser Stelle sei auf die Arbeiten von Savin et al. [98] hingewiesen.

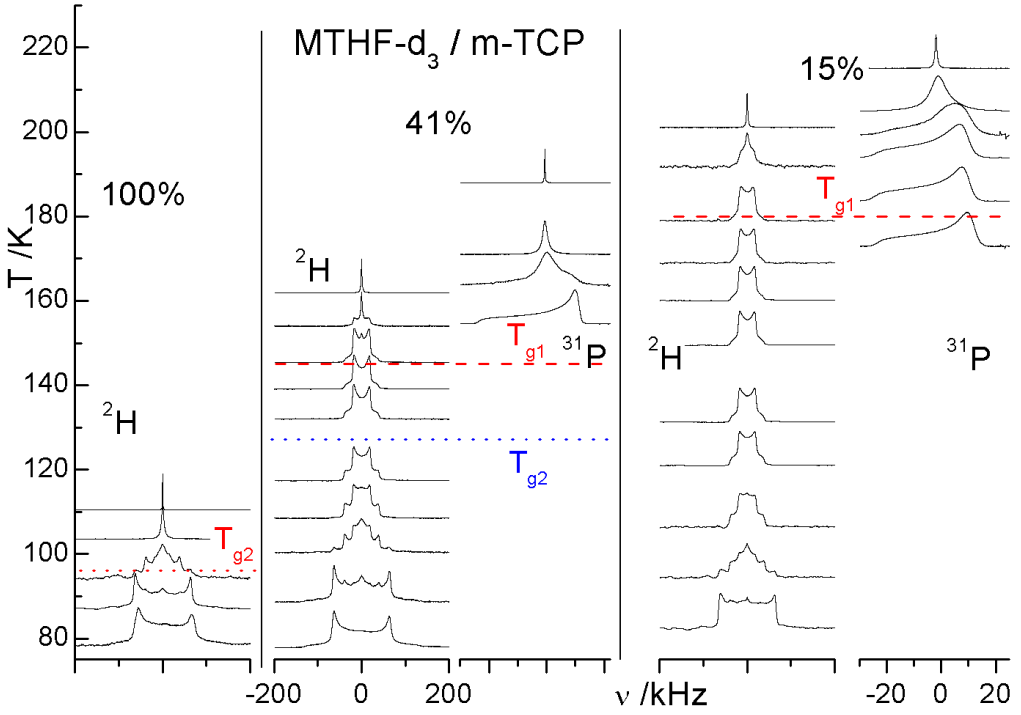

Abbildung 3.23: *^{2}H- und ^{31}P-NMR-Spektren für MTHF / TCP; gestrichelte Linien zeigen kalorimetrische T_{g1}, punktierte Linien T_{g2} (rot: DSC, blau: DS); Publikation 4.*

Abbildung 3.23 zeigt einige ^{2}H- und ^{31}P-NMR-Spektren von reinem MTHF und Mischungen mit m-TCP. Im reinen MTHF beobachtet man bei $T \approx 80K$ ein Spektrum immobiler C-^{2}H-Bindungen, d.h. auch die CH_3- Rotation ist langsam ($\tau_{CH_3} > 1/\delta$). Unter Temperaturerhöhung vollzieht sich ein Linienformübergang, bis

bei $T \approx 105K$ nur noch eine zentrale lorentzförmige Flüssigkeitslinie vorliegt. Für c_{MTHF} = 41% gehen die bei tiefen Temperaturen beobachteten Festkörperspektren bei $80K < T < 120K$ in ein durch schnelle ($\tau_{CH_3} < 1/\delta$) Methylgruppenrotation um den Faktor ≈ 3 verschmälertes Pake-Spektrum über. Bei $T \approx 150K$ sind Zweiphasenspektren zu beobachten, die eine Korrelationszeitenverteilung für den α_2-Prozess bzw. MTHF nachweisen. Verglichen mit den Resultaten im System TPP/PS ist der Temperaturbereich, in dem Zweiphasenspektren beobachtet werden, schmal. Bei $T = 165K$ liegt schließlich nur noch eine zentrale Lorentzlinie vor, während sich in den ^{31}P-NMR-Spektren bei gleicher Temperatur noch ein durch einen CSA-Tensor bestimmtes Festkörperspektrum findet, d.h. es werden langsame TCP-Moleküle detektiert. Somit zeigt sich wiederum eine Entkopplung der Komponentendynamik. Für c_{MTHF} = 15% bleibt der durch Methylgruppenrotation bedingte Übergang zu bewegungsverschmälerten Spektren weitgehend unverändert im Vergleich zu c_{MTHF} = 41%, während der vom α_2-Prozess verursachte Übergang in eine zentrale Lorentzlinie weiter zu höheren Temperaturen verschoben ist. Für $120K < T < 170K$ liegen Festkörperspektren vor, deren unscharfe Form von einer räumlich eingeschränkten schnellen Bewegung zeugt. Eine mögliche Erklärung liefert die DS: Der mittels DS beobachtete α-Peak des reinen MTHF weist einen Excess-Wing auf. In den Mischungen jedoch findet sich eine β-Relaxation (Kreuze in Abb. 3.25(b)), deren Aktivierungsenergie kaum konzentrationsabhängig ist, deren absolute Zeitkonstanten sich jedoch mit geringerer Konzentration verkleinern. Für $T > 120K$ wird dieser im schnellen Grenzfall ($\tau_\beta << 1/\delta$) beobachtet und kommt somit als Ursache der in den Spektren beobachteten Bewegungseffekte in Frage.

Die Beschleunigung der Dynamik von m-TCP unter Zugabe von MTHF lässt sich direkt in den ^{31}P-NMR-Spektren ablesen (siehe Abb. 3.24). Bei c_{TPP} = 41% lassen sich die ^{31}P-NMR-Spektren als Zweiphasenspektren interpretieren. Noch deutlicher ausgeprägt ist der Zweiphasencharakter der Spektren bei c_{TPP} = 70%. Damit liegen auch für die Hoch-T_g-Komponente Anzeichen einer heterogen verbreiterten Dynamik vor, wohingegen im System TPP/PS dies in den ^{2}H-Spektren für PS nicht beobachtet werden konnte.

Die mit Kohlrauschfunktionen beschreibbaren Korrelationszerfälle aus ^{31}P-NMR Stimulierte-Echo-Messungen erfahren mit steigender MTHF-Konzentration eine zunehmende Verbreiterung (siehe Abb. 3.25(a)). Das Ergebnis ist konsistent mit der Linienformanalyse, die eine heterogene Dynamik nachweist. Der Parameter β_K zeigt sich als nicht temperaturabhängig, FTS ist somit erfüllt. Experimente der PCS liefern übereinstimmende Ergebnisse [131].

Abbildung 3.25(b) zeigt eine Auswahl von mittels der genannten Methoden gewonnenen Zeitkonstanten. In den Mischungen lassen sich zwei Prozesse nachweisen. In den dielektrischen Verlustspektren werden für den α-Prozess Doppelpeakstrukturen nachgewiesen. Die Zeitkonstanten des niederfrequenten Peaks stimmen mit den

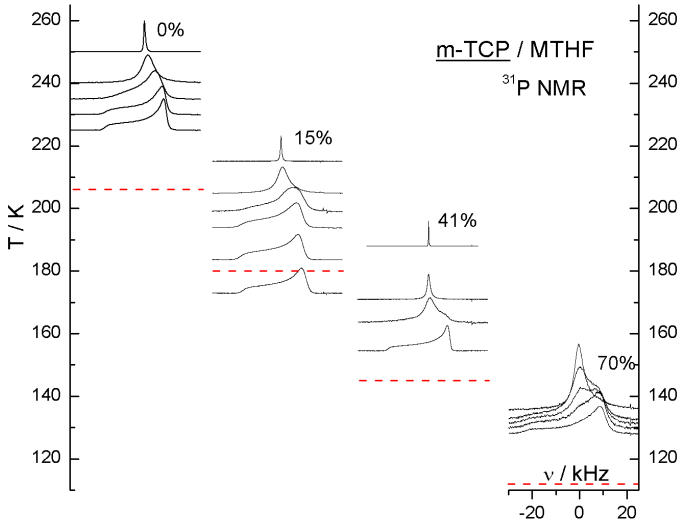

Abbildung 3.24: *^{31}P-NMR-Spektren für MTHF / TCP. Gestrichelte rote Linien zeigen kalorimetrische T_{g1}.*

Resultaten der ^{31}P-NMR für den α-Prozess des m-TCP in der Mischung überein (in Analogie zum System TPP/PS hier α_1-Prozess genannt), repräsentieren also die Matrix-Dynamik. Die Zeitkonstanten des hochfrequenten Peaks entsprechen den ^{2}H-NMR-Resultaten für MTHF in der Mischung, diese werden demzufolge der Dynamik des MTHF zugeordnet (α_2-Prozess). Auch aus den Spektren der dynamischen Lichstreuung (DM und TFPI) lassen sich bei hohen MTHF-Konzentrationen zwei getrennte Zeitkonstanten bestimmen (vgl. c_{MTHF} = 95%).

Auch in diesem niedermolekularen System ist daher die Komponentendynamik entkoppelt. Es lassen sich mittels DS, DLS und NMR zwei Prozesse (α_1 und α_2) nachweisen, obwohl mittels DSC keine zwei getrennten T_g aufgelöst werden konnten. Die beiden Prozesse α_1 und α_2 beschreiben im Wesentlichen die Dynamik des TCP und des MTHF. Die dynamische Heterogenität der Nieder-T_g-Komponente sowie das Maß der Entkopplung der Dynamik sind jedoch weniger stark ausgeprägt als im Fall TPP/PS, entsprechend dem geringeren dynamischen Kontrast. Da beide Komponenten vergleichbares Dipolmoment tragen, lässt sich im Rahmen dieser Arbeit ohne eine eingehende Analyse der dielektrischen Daten nicht klären, ob eine MTHF-Fraktion zum α_1-Prozess beiträgt.

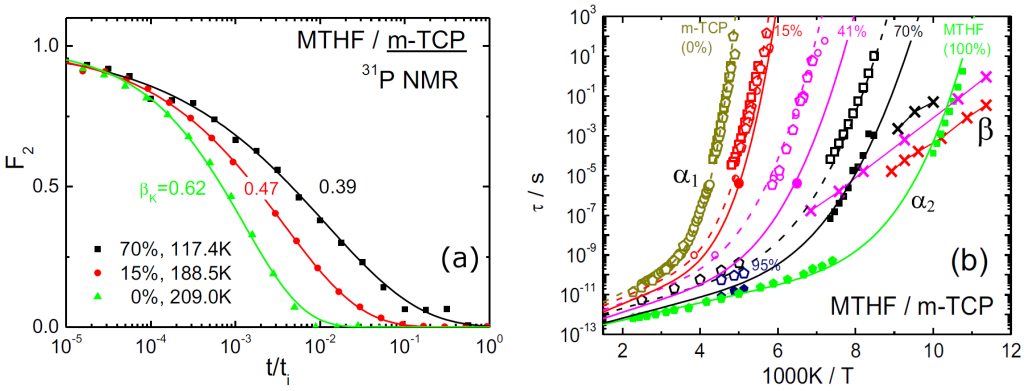

Abbildung 3.25: *Niedermolekulares Mischsystem MTHF/m-TCP. (a) Korrelationsfunktionen der Hoch-T_g-Komponente TCP aus ^{31}P-NMR Stimulierte-Echo-Zerfall zu angegebenen MTHF-Konzentrationen, auf Anfangszerfall normiert; aus Publikation 4. (b) Strukturrelaxationszeiten τ_α aus DS (Quadrate, Kreuze), NMR (Kreise), und Lichtstreuung (PCS und TFPI, Pentagons); Linien dienen der Blickführung (gestrichelt: α_1-Relaxation; durchgezogen: α_2-Relaxation, β-Prozess). Offene Symbole zeigen α_1-, gefüllte α_2-Prozess, Kreuze: β-Prozess; aus Publikation 4.*

3.4 Der β-Prozess im Mischsystem

3.4.1 Stand des Wissens

Mischsysteme eignen sich auch für die Untersuchung des β-Prozesses [91, 132–135]. Im Folgenden seien zunächst die NMR-Szenarien für den β-Prozess bei $T \leq T_g$ geschildert, wie sie bislang für reine Systeme belegt sind. Für $T < T_g$ ändern sich die Solid-Echo-Spektren der ^{2}H-NMR mit der Temperatur nicht merklich, insbesondere bleibt die quadrupolare Kopplungskonstante δ_Q (siehe Gl. (3.13)) weitgehend erhalten. Erhöht man jedoch den Interpulsabstand t_p der Echopulsfolge und erhöht damit die Empfindlichkeit auf Kleinwinkelbewegungen, so findet sich bei Glasbildnern, bei denen dielektrisch eine β-Relaxation nachgewiesen wird, eine verringerte Intensität bei $\nu = 0$.

Abbildung 3.26(a) zeigt bei $T \approx 0.83T_g$ aufgenommene ^{2}H-NMR Solid-Echo-Spektren der Typ-B-Glasbildner Toluol und Polybutadien (PB) sowie der Typ-A-Glasbildner Polystyrol (PS) und Glyzerin, für die dielektrisch kein β-Prozess gefunden wird und bei denen sich die Linienform bei $T < T_g$ mit t_p praktisch nicht ändert. Der phänomenologische Linienformparameter R beschreibt die Intensität des auf die Höhe der Singularitäten normierten Spektrums bei $\nu = 0$. Für lange t_p fällt $R(t_p)$ im reinen Typ-B-Glasbildner auf 0 ab und zeigt, dass im Wesentlichen alle Moleküle am β-Prozess teilnehmen. Die Temperaturabhängigkeit von $R(T)$ für

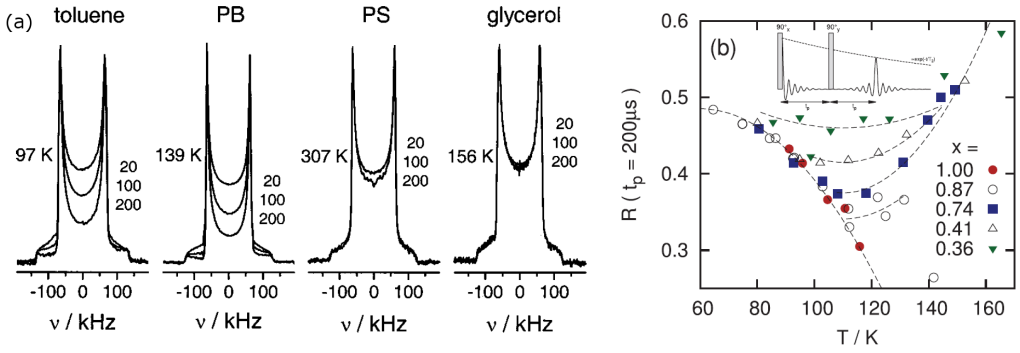

Abbildung 3.26: *(a) ^{2}H-NMR Solid-Echo-Spektren jeweils aufgenommen bei $T \approx 0.83T_g$ mit angegebenen Pulsabständen in µs für die Typ-B-Glasbildner Toluol und Polybutadien sowie die Typ-A-Glasbildner Polystyrol und Glyzerin [39]. (b) ^{2}H-NMR-Linienformparameter $R(T)$ bei Pulsabstand $t_p = 200\mu s$ für Toluol ($x = 1$) und Toluol in PCB54 bei angegebener Toluol-Konzentration x [46].*

Toluol bei langem Pulsabstand t_p ist in Abb. 3.26(b) eingetragen (rote Punkte). Bei $T > 120K$ wird die Linienform im reinen Toluol durch die α-Relaxation bestimmt.

Gleichartige Untersuchungen wurden auch bereits für Glasbildner in Mischungen durchgeführt. In Abb. 3.26(b) ist $R(T)$ für langes t_p für verschiedene Konzentrationen von Toluol in dem polychlorierten Biphenyl PCB54 (Typ-A-Glasbildner) gezeigt [46]. Die DS zeigt für alle untersuchten Mischungen Zeitkonstanten τ_β identisch zur β-Relaxation des reinen Toluol [50, 95]. Der Einfluss der α-Relaxtion verschiebt sich dagegen in den Mischungen zu höheren Temperaturen. In $R(T)$ wird daher ein Minimum beobachtet, die β-Relaxation läuft hier durch das Zeitfenster der NMR, das durch $\tau \approx 1/\delta$ gegeben ist. Für niedrige Konzentrationen wird das Minimum flacher und wie gezeigt wurde fällt $R(t_p)$ für lange t_p dann nicht mehr auf 0 ab. Es wurde daraus geschlossen, dass in den binären Gläsern unterhalb eines Schwellwertes der Toluol-Konzentration nicht mehr alle Toluol-Moleküle zum β-Prozess beitragen [46].

Bei einer dielektrischen Studie des Mischsystems Toluol (Typ-B-Glasbildner, schwächeres Dipolmoment) in Picolin (Typ-A, stärkeres Dipolmoment) [50] wurde die Relaxationsstärke des β-Prozesses untersucht. Bei einer mittleren Konzentration lag diese über der für Toluol zu erwartenden Gesamtrelaxationsstärke. Dies wurde als Hinweis gewertet, dass Picolin zum β-Prozess des Toluols beiträgt. Eine ähnliche Situation wurde für Mischungen von Toluol mit PCB54 präsentiert [50, 95].

Die beiden Phänomene, dass zum einen PCB54 zur durch das Toluol verursachten dielektrischen β-Relaxation beiträgt, zum anderen die β-Relaxation unterhalb einer gewissen Konzentration nicht mehr alle Toluol-Moleküle umfasst, lassen den

Schluss auf eine gewisse Kooperativität des β-Prozesses zu. Als Hinweis auf Kooperativität wird auch vielfach die hohe Aktivierungsenergie angeführt [136, 137]. Auch aus MD-Simulationen wird für den β-Peak im mechanischen Verlustmodul auf eine kooperative Natur des zugrundeliegenden Prozesses geschlossen [138]. Hierzu wurde ein kleiner Anteil Teilchen in den Simulationen fixiert. Während für einen lokalen Prozess eine Fixierung eines kleinen Anteils Teilchen kaum Auswirkungen haben sollte, so war der β-Prozess bei 2.5% festgehaltener Teilchen kaum noch vorhanden. Andererseits gibt es auch Studien, die für den β-Prozess einen lokalen Charakter zeigen. So können etwa MD-Simulationen von hantelförmigen Molekülen [139] unterhalb einer bestimmten Temperatur die Aufspaltung in α- und β-Prozess zeigen. Für beide Prozesse finden sich dynamische Heterogenitäten, d.h. Verteilungen von Korrelationszeiten. Während für den α-Prozess starke dynamische Korrelationen auffallen, d.h. eine größere Zahl räumlich benachbarter Moleküle zeigt ähnliche Mobilität, sind diese für den β-Prozess nur schwach ausgeprägt. Daneben ist ein auffälliges Merkmal von experimenteller Seite auch die nur schwache Konzentrationsabhängigkeit der β-Zeitkonstanten in Mischungen (z.B. festgestellt in MTHF/Oligostyrol [94]).

Bestandteil der vorliegenden Arbeit ist es, die Methoden der ^{2}H-NMR zur Untersuchung des β-Prozesses erstmals auf die ^{31}P-NMR zu übertragen. Mithilfe derer soll anhand einer binären Mischung der Frage nachgegangen werden, ob der β-Prozess als lokaler oder als kooperativer Prozess zu betrachten ist, und ob das Konzept der „islands of mobility“, wenn es auch in reinen Systemen bislang immer widerlegt werden konnte, in binären Mischungen dennoch allgemein zum Tragen kommen kann [46].

3.4.2 Eigene Ergebnisse

Das in Kap. 3.3.2 beschriebene System TPP/PS zeigt sich auch geeignet, den β-Prozess zu studieren. TPP zeigt wie bereits diskutiert (Abb. 3.2(b)) als Typ-B-Glasbildner in den dielektrischen Verlustspektren einen ausgeprägten β-Prozess. Die Spektren für $T < T_g$ können durch eine temperaturunabhängige Aktivierungsenergieverteilung beschrieben werden, entsprechende Zeitkonstanten τ_β sind Abb. 3.27 zu entnehmen. Für Polystyrol hingegen findet sich, typisch für einen Typ-A-Glasbildner, kein β-Prozess, sondern lediglich ein Excess-Wing (Abb. 3.2(a)). In den Mischungen mit $c_{TPP} > 45\%$ bleibt die Temperaturabhängigkeit der β-Relaxation praktisch unverändert erhalten, bei niedrigen Konzentrationen nehmen Aktivierungsenergie und Zeitkonstanten leicht ab (siehe Abb. 3.27).

In reinem TPP wurde erstmals die ^{31}P-NMR-Hahn-Echo Folge zur Untersuchung der β-Relaxation angewandt. Die Spektren für $T < T_g$ in Abb. 3.28 zeigen ganz analog zu den ^{2}H-NMR Solid-Echo-Spektren von Toluol (vgl. Abb. 3.26(a)) mit längerem t_p ein Absinken der Intensität. Mit steigender Temperatur nimmt $R(T)$

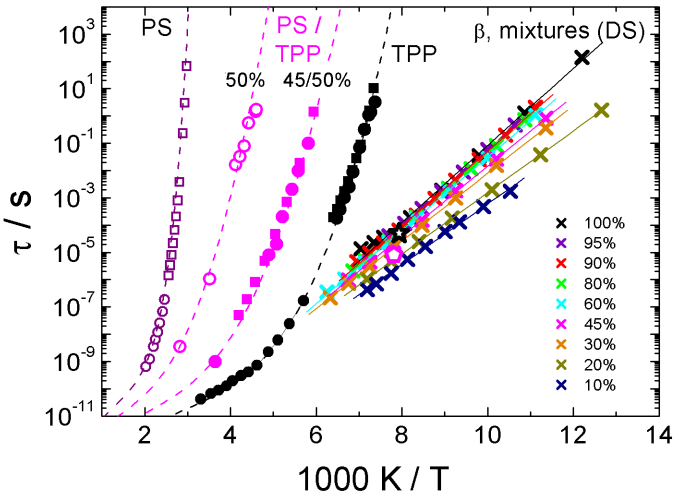

Abbildung 3.27: *Strukturrelaxationszeiten τ_α reines PS (DS: offene Quadrate [128], NMR: offene Kreise), reines TPP (DS: gefüllte Quadrate, NMR: gefüllte Kreise [2]) und in Mischung (c_{TPP} = 45%, DS (dominiert von TPP): volle Quadrate; c_{TPP} = 50%, ^{2}H-NMR: offene Kreise, ^{31}P-NMR: volle Kreise); Zeitkonstanten τ_β des β-Prozesses in reinem TPP und in Mischungen (DS: Kreuze) , τ_β von TPP aus ^{31}P-NMR Hahn-Echo (offener Stern) and von PS in Mischungen aus ^{2}H-NMR Solid-Echo (offenes Pentagon); Publikation 1.*

ab (siehe Abb. 3.30 oben, 100%). Der Verlauf von $R(T)$ ist wiederum sehr ähnlich zu den Ergebnissen von Toluol (vgl. Abb. 3.26(b)).

In den Mischungen mit PS zeigt sich in den ^{31}P-NMR-Spektren (siehe Abb. 3.29(b)), wie bei $T \approx 120K$ die Linienform auf t_p-Änderung reagiert. Bei $T \approx 148K$ ist die t_p-Abhängigkeit dagegen wieder nahezu verschwunden. Folglich beobachtet man in $R(T)$ ein Minimum bei $T \approx 120K$ (siehe Abb. 3.30 oben, 10, 20, 50%). Die Zeitkonstante, die sich aus dem Minimum ableiten lässt, ist in Abb. 3.27 eingetragen und stimmt mit jenen des für TPP mittels DS sondierten β-Prozesses überein.

Die Linienform der ^{2}H-NMR Solid-Echo-Spektren von reinem PS-d$_3$, gemessen mit langem Interpulsdelay t_p, zeigt für $T < T_{g1}$ keine ausgeprägte Temperaturabhängigkeit. $R(T)$ bleibt hier nahezu konstant (siehe Abb. 3.30 unten), dieses Resultat entspricht dem erwarteten Verhalten eines Typ-A-Glasbildners. In den Mischungen mit TPP hingegen zeigen die Spektren (in Abb. 3.29(a) dargestellt für c_{TPP} = 50%) bei $T \approx 87K$ nur schwache Empfindlichkeit auf t_p-Variation, die unter Temperaturerhöhung zunimmt, bei $T \approx 121K$ maximal wird, um bei höheren Temperaturen wieder abzunehmen. Entsprechend ergibt sich bei $T \approx 120K$ ($<< T_{g1}$) in $R(T)$ ein Minimum (Abb. 3.30 unten). Dieses ist um so stärker ausgeprägt, je

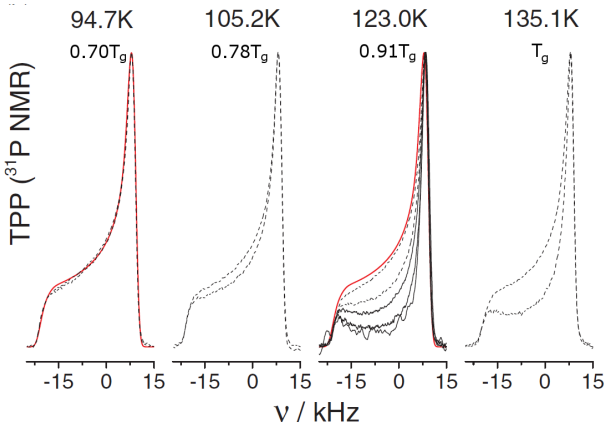

Abbildung 3.28: *^{31}P-NMR Hahn-Echo-Spektren von TPP bei angegebenen Temperaturen ($T \leq T_g$) mit Pulsabständen t_p = 20μs und 200μs, bei T = 123K zusätzlich 400μs, 800μs und 1600μs; rote Linien sind Anpassungen eines Festkörperspektrums an die Daten.*

höher die TPP-Konzentration ist und tritt jeweils bei der gleichen Temperatur auf, bei der auch in der ^{31}P-NMR-Messung an TPP ein Minimum zu beobachten ist. Dieses Ergebnis zeigt klar, dass die PS-Segmente in der Mischung unterhalb von T_{g2} ebenfalls eine räumlich stark eingeschränkte Bewegung auf der Zeitskala des β-Prozesses ausführen.

Als einen weiteren Effekt zeigen die aus den ^{2}H-NMR-Spektren bestimmten $R(T)$-Werte bei höheren Temperaturen eine Schulter bzw. für c_{TPP} = 20% und 10% ein zweites Minimum. Die diesen Minima zugeordneten Zeitkonstanten stimmen mit denen des isotropen α_2-Prozesses von TPP überein (siehe Abb. 3.21). Die PS-Segmente in der Mischung werden also durch die isotrope Bewegung von TPP zu einer (neben dem β-Prozess) weiteren räumlich eingeschränkten Bewegung angeregt.

Auch die Spin-Gitter-Relaxation (siehe Abb. 3.31) gibt dieses Szenario wieder . Allgemein ist die Spin-Gitter-Relaxation für $T < T_g$ durch Sekundärrelaxationen bestimmt. In reinem TPP zeigt $T_1(T)$ eine relativ starke Temperaturabhängigkeit (siehe Abb. 3.31(a)), deren apparente Steigung $\frac{\partial}{\partial T} \log T_1(T) \propto mE$ durch den Exponenten in der Hochfrequenzflanke im Spektrum des β-Prozesses sowie dessen mittlere Aktivierungsenegie gegeben ist. Ein Vergleich mit Ergebnissen der DS extrapoliert zur NMR-Larmorfrequenz ω_L (schwarze Linie in Abb. 3.31(a), $T < 135K$) zeigt gute Übereinstimmung. Für reines PS hingegen findet man unterhalb von T_g eine schwächere Temperaturabhängigkeit, die typisch für den Excess-Wing ist [140]. In der Mischung hingegen (Abb. 3.31(b)) zeigen beide Komponenten die gleiche starke Temperaturabhängigkeit, die auch mit den Resultaten der DS für den in

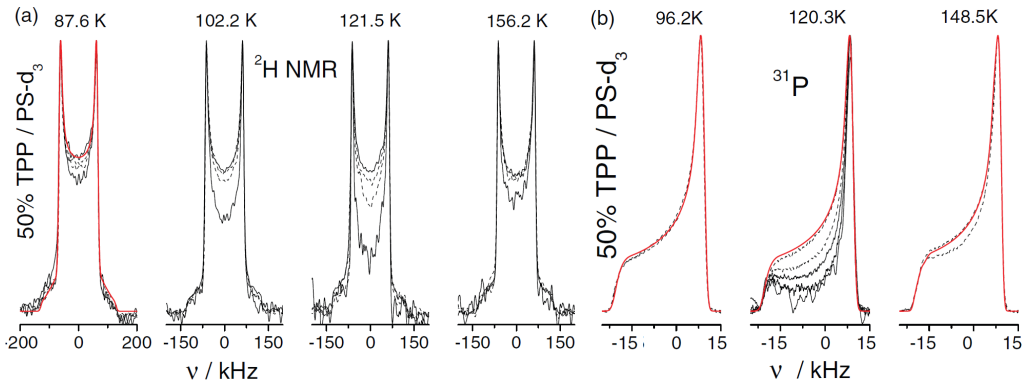

Abbildung 3.29: *(a) ^{2}H-NMR Solid-Echo-Spektren von 50% PS-d_3 in TPP, jeweils mit t_p = 40μs, 80μs, 200μs; rote Linie ist eine Anpassung mittels ^{2}H-Festkörperspektrum für kurze t_p; aus Publikation 1. (b) ^{31}P-NMR Hahn-Echo-Spektren von 50% TPP in PS-d_3, jeweils mit t_p = 20μs und 200μs, für T = 120.3K zusätzlich t_p = 400μs, 800μs, 1600μs (durchgezogene schwarze Linien); Rote Linien sind Anpassungen mittels CSA-Pulverspektrum für kurze t_p; aus Publikation 1.*

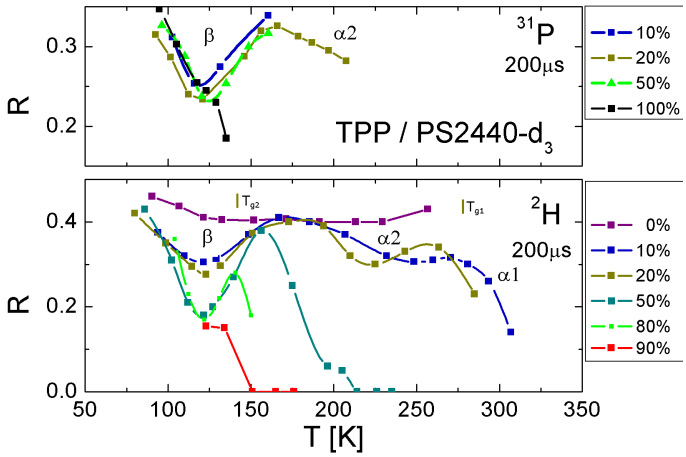

Abbildung 3.30: *Linienform-Parameter $R(T)$ der ^{31}P-NMR Hahn-Echo- (oben) und ^{2}H-NMR Solid-Echo-Spektren (unten), gemessen mit t_p = 200μs für reines PS und TPP sowie Mischungen von PS mit TPP; für c_{TPP} = 20% sind T_{g1} und T_{g2} markiert; aus Publikation 3.*

der Mischung unveränderten β-Prozess übereinstimmt. Der Befund ist ein Hinweis auf übereinstimmende Aktivierungenergieverteilungen für die im β-Prozess involvierten TPP-Moleküle und PS-Segmente. Nicht klar ist hingegen, ob die Relaxationsstärken bzw. Konuswinkel im „wobbling-on-a-cone“-Modell für beide

Komponenten gleich sind. Diese drücken sich durch den absoluten Wert der Relaxationszeit aus. Vergleicht man die ^{2}H- mit den ^{31}P-Spin-Gitter-Relaxationszeiten unterhalb von T_g, so fällt auf, dass T_1 für PS länger ist als man aufgrund des Unterschieds der Kopplungskonstanten für TPP und PS ($\left(\frac{\delta_Q(PS)}{\delta_{CSA}(TPP)}\right)^2 \approx 35 \pm 5$) erwarten könnte. Dies könnte ein Hinweis auf eine geringere Bewegungsintensität der PS-Komponente sein.

Als ein weiteres Detail kann man in der ^{2}H-NMR Spin-Gitter-Relaxationszeit von PS in TPP (Abb. 3.31) bei $T \approx 260K$ eine Andeutung eines Minimums erkennen, die mit dem Relaxationszeitminimum in der entsprechenden ^{31}P-NMR $T_1(T)$–Kurve zusammenfällt. Wie auch in $R(T)$ spiegelt sich hier die isotrope Bewegung von TPP in einer eingeschränkten Bewegung des PS wider. Bei $c_{TPP} = 90\%$ zeigt sich der Effekt entsprechend der beschleunigten Dynamik von TPP bei $T \approx 225K$.

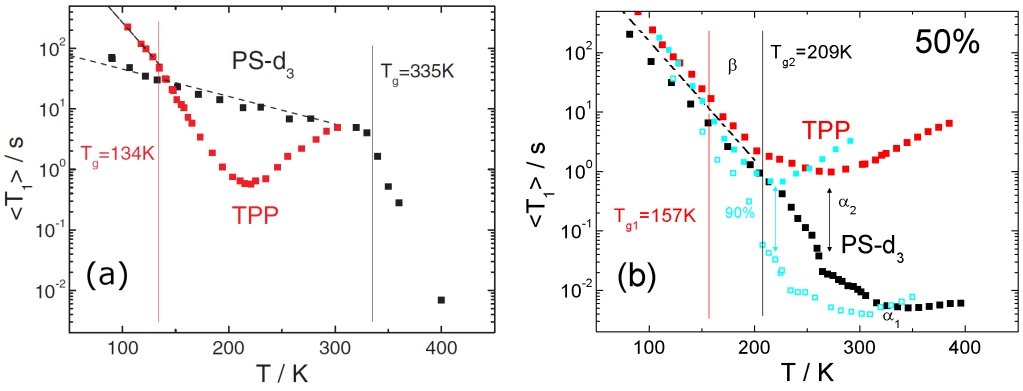

Abbildung 3.31: *(a) Spin-Gitter-Relaxationszeiten für reines TPP (^{31}P-NMR) und für reines PS-d$_3$ (^{2}H-NMR). Die ^{2}H-Relaxation ist unterhalb T_g nichtexponentiell, deshalb ist die mittlere Relaxationszeit $\langle T_1 \rangle$ angegeben. Vertikale Linien zeigen T_g; gestrichelte Linie: Interpolation durch ein exponentielles Relaxationsgesetz für PS-d$_3$; gestrichelte Linie bei $T < 135K$: Abschätzung von T_1 für TPP aus der dielektrischen Spektraldichte. (b) Spin-Gitter-Relaxationszeiten für 50% TPP/PS-d$_3$, ^{31}P-NMR und ^{2}H-NMR; gestrichelte Linie: Abschätzung aus der dielektrischen Spektraldichte, konzentrationsunabhängig, skaliert; vertikale Linien zeigen T_g; aus Publikation 1. Zusätzlich: $c_{TPP} = 90\%$ (cyan).*

3.5 Interpretation der NMR-Relaxationsdaten

In einigen Mischsystemen wurde die Spin-Gitter-Relaxation $T_1(T, c)$ vor allem oberhalb von T_g gemessen. Die komplexe Dynamik der mobileren Komponente in binären Systemen, unter anderem das Versagen des FTS-Prinzips, machen eine quantitative Beschreibung der bei nur einer Frequenz gemessenen Relaxationszei-

ten fast unmöglich. Für das System TPP/PS wird aufgrund der vorausgehenden Erkenntnisse insbesondere aus DS-Messungen eine semiquantitative Interpolation jedoch erstmals möglich. Abbildung 3.32(a) zeigt die ^{31}P-NMR Spin-Gitter-

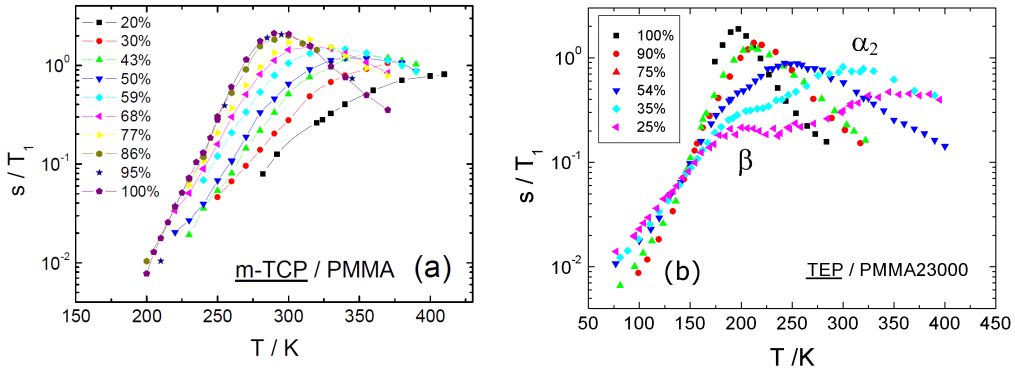

Abbildung 3.32: *^{31}P-NMR-Spin-Gitter-Relaxationsrate als Funktion der Temperatur für (a) TCP in PMMA; aus Publikation 4. (b) TEP in PMMA; unveröffentlicht.*

Relaxationsrate als Funktion der Temperatur für die Mischungen m-TCP/PMMA verschiedener Konzentrationen. Für reines m-TCP beobachtet man ein hohes, scharfes Relaxationsmaximum. Unter der Zugabe von PMMA verbreitert es sich und nimmt an Amplitude ab. Ausserdem verschiebt sich das Maximum zu höheren Temperaturen, eine Folge der durch den Antiweichmachereffekt verlangsamten Dynamik. Die Verbreiterung der Relaxationskurve ist eine direkte Konsequenz der Verbreiterung von $G(\ln\tau)$ mit der Abnahme der Konzentration, wie sie in den DS-Spektren und im Stimulierten Echo beobachtet wird (vgl. Kap. 3.3.2).

In den entsprechenden Relaxationsdaten des Systems Triethylphosphat (TEP) / Poly(methylmethacrylat) (PMMA, siehe Abb. 3.32(b)) findet sich ein anderes Szenario. Hier erscheinen bei niedrigen TEP-Konzentrationen zwei Relaxationsmaxima. Das Maximum bei hohen Temperaturen wird dem α_2-Prozess zugeordnet, jenes bei tiefen Temperaturen ist dem β-Prozess des TEP geschuldet, der bei niedrigen Konzentrationen gut getrennt vom α_2-Prozess ist. Im reinen TEP dagegen sind die Prozesse nicht klar getrennt; weiterhin erschwert dort die hohe Kristallisationsneigung eine Messung für $T_g < T < 170K$.

Abbildung 3.33(a) zeigt ^{2}H-NMR Spin-Gitter-Relaxationszeiten für reines MTHF-d_3 und für MTHF-d_3 in der Mischung mit m-TCP. Zum Vergleich sind Ergebnisse für MTHF-d_7 [141] eingefügt. Bemerkenswert ist, dass die mittleren Spin-Gitter-Relaxationszeiten von ring(d_7)- und methyl(d_3)-deuteriertem MTHF praktisch identisch sind. Im Gegensatz dazu findet sich etwa für Toluol ein durch schnelle Methylgruppenrotation verursachtes zweites Minimum in $T_1(T)$ bei tiefen

Temperaturen [142]. Zum Vergleich sei auch noch auf Arbeiten an Propylencarbonat (PC) verwiesen. Für PC ist ein einziges, verbreitertes Minimum zu beobachten. Dieses wird beschrieben durch eine schwache Entkopplung zwischen Methylgruppenrotation und Molekülreorientierung [142]. Dennoch unterscheiden sich die Relaxationszeiten von methyl- und ringdeuteriertem PC bei tiefen Temperaturen erheblich. Im Fall des MTHF ist das durch den α-Prozess bestimmte Minimum in $T_1(T)$ bei ring- und methylgruppendeuteriertem Molekül praktisch identisch, und selbst bei $T = T_g$ stimmen die Werte überein. Mutmaßlich ist die Methylgruppenrotation unterhalb von T_g zum Erliegen gekommen, und bei höheren Temperaturen langsam verglichen mit dem α-Prozess, so dass sich reines MTHF-d_3 wie ein starres Molekül verhält. In den Mischungen wird die isotrope Molekülbewegung im Gegensatz zur Methylgruppenrotation verlangsamt (vgl. Solid-Echo-Spektren in Abb. 3.23). Für eine quantitative Analyse der T_1-Relaxation müsste deshalb das komplexe Wechselspiel zwischen Methylgruppen- und Rumpfbewegung berücksichtigt werden. Qualitativ lässt sich jedoch wieder eine Zunahme des Relaxationsminimums und eine Verbreiterung der Relaxation nachweisen. In der ^{31}P-NMR T_1-Relaxation von m-TCP, hier der Komponente niedriger Mobilität, fehlt diese Verbreiterung (siehe Abb. 3.33(b)). Man beobachtet unter Zugabe von MTHF eine Verschiebung zu niedrigen Temperaturen entsprechend dem Weichmachereffekt, während die qualitative Temperaturabhängigkeit für alle untersuchten Konzentrationen erhalten bleibt.

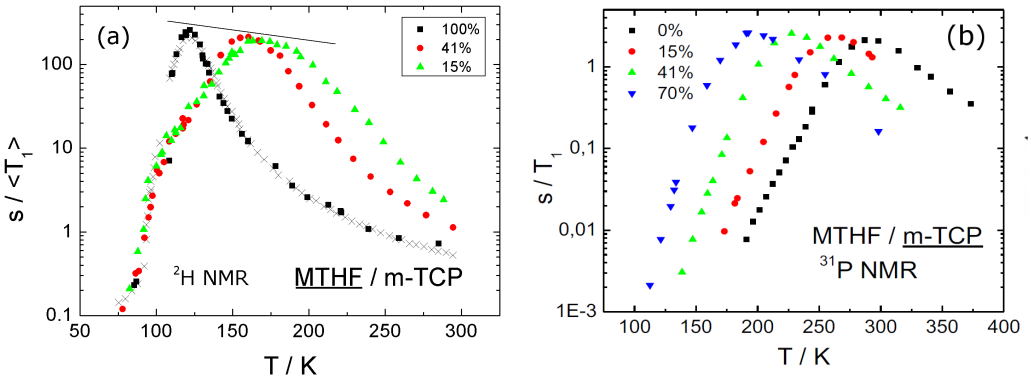

Abbildung 3.33: *(a) Kehrwert der mittleren ^{2}H-NMR Spin-Gitter-Relaxationszeiten für reines MTHF-d_3, MTHF-d_3 in m-TCP, unveröffentlicht; zum Vergleich reines MTHF-d_7 [141] (Kreuze). (b) ^{31}P-NMR Spin-Gitter-Relaxationsrate reines TCP (0% MTHF) und TCP in MTHF (Massenanteil MTHF angegeben); aus Publikation 4.*

In der Spin-Gitter-Relaxation sind wie auch bei den anderen Methoden die beobachteten Phänomene für dynamisch asymmetrische Mischungen und Glasbildner im

Confinement ähnlich. In beiden Fällen zeigt das Maximum der Relaxationsrate eine auffallende Verbreiterung zu hohen Temperaturen und nimmt an Stärke ab, jeweils eine direkte Folge einer kontinuierlich verbreiterten Korrelationszeitenverteilung; eine quantitative Beschreibung fehlt allerdings bislang.

Um die NMR-Relaxationsdaten $T_1(T)$ und die ebenfalls gemessenen $T_2(T)$ des Systems TPP/PS quantitativ zu beschreiben, werden die vorliegenden Ergebnisse der DS (Publikation 2) benutzt. Die Analyse ist bislang unveröffentlicht und wird deshalb hier ausführlicher dargestellt.

Die Spin-Gitter- $(1/T_1)$ und die Spin-Spin-Relaxationsrate $(1/T_2)$ sind unter den gegebenen Bedingungen durch die Anisotropie der chemischen Verschiebung bestimmt, und es gilt für ^{31}P-NMR:

$$\begin{aligned} \frac{1}{T_1} &= KJ(\omega_L) \\ \frac{1}{T_2} &= K/6(3J(\omega_L) + 4J(0)) \end{aligned} \tag{3.1}$$

wobei die Konstante $K = \frac{2}{15}(\omega_L \Delta\sigma)^2$ durch die Anisotropie $\Delta\sigma$ des Tensors der chemischen Verschiebung und die Larmorfrequenz ω_L gegeben ist.

Aus dem Festkörperspektrum bei tiefen Temperaturen erhält man $\Delta\sigma = 189ppm$ (entsprechend $\delta = 2\pi 20.4kHz$, vgl. Kap. 3.6). Die zur Berechnung der Relaxationszeiten benötigte Spektraldichte bei der Larmorfrequenz $J(\omega_L)$ wird anhand der DS-Daten berechnet und für $\omega = \omega_L$ extrapoliert. $J(\omega)$ ist gegeben durch

$$J(\omega) = \int_0^\infty \cos(\omega t)\Phi(t)dt \tag{3.2}$$

und bei $\omega = 0$

$$J(0) = \langle\tau\rangle = \int_0^\infty \Phi(t)dt \tag{3.3}$$

Für die Korrelationsfunktion $\Phi(t)$ folgt mit Hilfe des Williams-Watts-Ansatzes [36]:

$$\Phi(t) = \left[(1 - S(T))\,\Phi_\beta(t) + S(t)\right]\Phi_\alpha(t) = \Phi_\beta(t)\Phi_\alpha(t) \tag{3.4}$$

Der letztlich einzige freie Fit-Parameter $1 - S(T)$ entspricht der relativen Relaxationsstärke des β-Prozesses.

Für jede Konzentration wurde für den β-Prozess von der entsprechenden temperaturunabhängigen Verteilung von Aktivierungsenergien $g(E)$, wie sie die DS liefert, ausgegangen. Unter der Annahme, dass $g(E)$ auch für $T > T_{g2}$ gültig ist, kann für jede vorgegebene Temperatur $g(E)$ auf eine Korrelationszeitenverteilung $G_\beta(\ln\tau)$ abgebildet werden. Für die Korrelationsfunktion des β-Prozesses $\Phi_\beta(t)$ ergibt sich somit:

$$\Phi_\beta(t) = \int_{-\infty}^\infty \exp(-t/\tau)G_\beta(\ln\tau)d\ln\tau \tag{3.5}$$

Für den α_2-Prozess wird im Falle des reinen TPP gemäß DS eine Cole-Davidson-Verteilung mit $\beta = 0.77$ gefordert. Die leichte Abweichung des hier verwendeten Parameters β aus der DS im Vergleich zu einer früheren Analyse der NMR-Relaxation [2] ist auf den dort nicht berücksichtigten β-Prozess zurückzuführen.

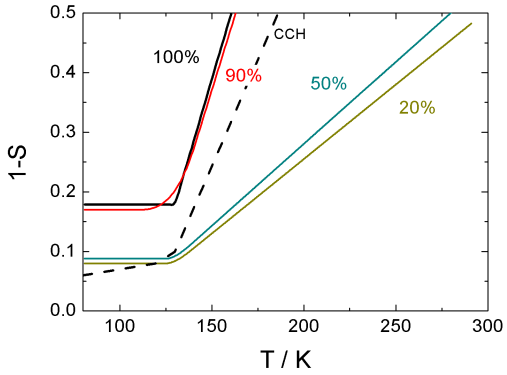

Abbildung 3.34: *Relative Relaxationsstärke des β-Prozesses $1 - S(T)$ für TPP und TPP in PS als Ergebnis des Fits; zum Vergleich Cyanocyclohexan (CCH) [41].*

Für die Mischungen $c_{TPP} = 90\%, 80\%, 50\%$ wurde die dielektrische Suszeptibilität des α_2-Prozesses durch die Havriliak-Negami (HN)-Funktion beschrieben. Die Korrelationsfunktion $\Phi_\alpha(t)$ in den Mischungen ist analog zu Gleichung (3.5) gegeben durch die HN-Korrelationszeitenverteilung [143, 144]. In die Berechnung der Spin-Spin-Relaxation T_2 geht $\langle\tau\rangle = J(0)$ ein. Für HN ist dies nicht definiert, es muss daher eine zusätzliche Annahme getroffen werden. Naheliegend erscheint die Bedingung, dass die langsamsten TPP-Moleküle in der Mischung mit der Korrelationszeit der PS-Matrix reorientieren. Für die HN-Korrelationszeitenverteilung des α_2-Prozesses von TPP wird deshalb ein Abschneidepunkt eingeführt, so dass $G(\ln\tau)$=0 für $\tau > \tau_{PS}$. Aufgrund dessen ist eine Renormierung von $G(\ln\tau)$ nötig. Anschliessend folgt der Ansatz nach Gleichung (3.4). Der α_1-Prozess wird vernachlässigt: Ein bestimmender Einfluss auf $T_1(T)$ wird nur bei hohen Temperaturen erwartet, wie die Ergebnisse aus DS und Stimulierte-Echo-Zerfall zeigten, verschwindet dort jedoch der Anteil von am α_1-Prozess involviertem TPP. Bei niedrigen Temperaturen ist T_1 durch den β-Prozess bestimmt.

Im Fall niedriger Konzentrationen ($c_{TPP} \leq 20\%$) wird für den α_2-Prozess gemäß DS eine temperaturunabhängige Aktivierungsenergieverteilung statt HN verwendet.

Für die relative Relaxationsstärke $1 - S(T)$ des β-Prozesses als einzigen Fitparameter ergibt sich für $T < T_g$ ein konstanter Wert, bei $T \approx T_g$ wird ein Anstieg mit der Temperatur angenommen. Diese Annahmen sind im Einklang mit den üblichen

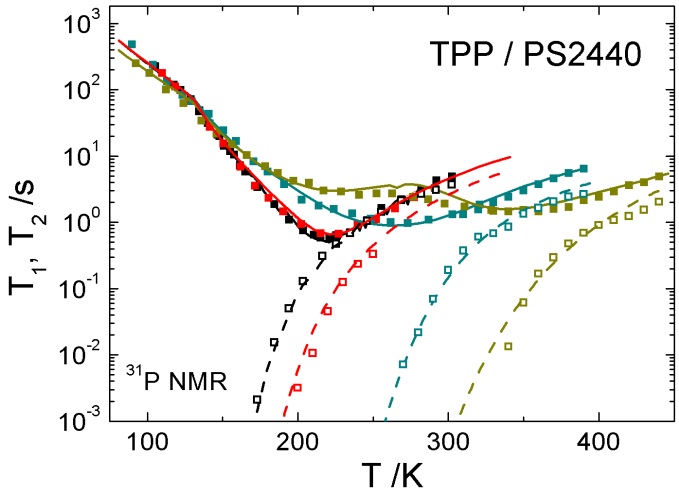

Abbildung 3.35: *^{31}P-NMR Spin-Gitter- (gefüllte Symbole) sowie Spin-Spin-Relaxationszeiten (offene Symbole), TPP in PS, für die Konzentrationen c_{TPP} = 1 (schwarz), 0.9 (rot), 0.5 (cyan dunkel) und 0.2 (gelb dunkel). Linien siehe Text; Spin-Spin-Relaxation unveröffentlicht.*

Befunden für das qualitative Verhalten von $1 - S(T)$ in der DS (siehe Abb. 3.3(b)). Temperaturabhängigkeit und absolute Werte von $1 - S(T)$ sind vergleichbar mit denen einer entsprechenden Analyse der ^{2}H-NMR Spin-Gitter-Relaxation für den β-Prozess des plastischen Kristalls Cyanocyclohexan [41] (siehe Abb. 3.34). Wie Abb. 3.35 zeigt, werden $T_1(T)$ und $T_2(T)$ für alle betrachteten Konzentrationen simultan angenähert und die wesentlichen Merkmale semi-quantitativ wiedergegeben.

3.6 Grundlagen der NMR und verwendete Methoden

Im Rahmen dieser Arbeit finden verschiedene ^{2}H- sowie ^{31}P-NMR Methoden Anwendung. Eine vollständige Beschreibung der NMR-Grundlagen findet sich in der Standard-Literatur [145–148]. Im Folgenden seien die verwendeten NMR-Methoden kurz dargestellt.

3.6.1 Der Kernspin und seine Wechselwirkungen

Der Kernspin bezeichnet den Gesamtdrehimpuls eines Atomkerns. Bei Kernen, die nicht aus einer geraden Protonenzahl und gleichzeitig einer geraden Neutronenzahl bestehen, ist der Kernspin verschieden von Null. An den Kernspin I ist über das

gyromagnetische Verhältnis γ ein magnetisches Moment μ gekoppelt:

$$\vec{\mu} = \gamma \vec{I} \tag{3.6}$$

Die Wechselwirkung zwischen diesem magnetischen Moment und einem äußeren statischen Magnetfeld B_0 bewirkt eine Zeeman-Aufspaltung eines ohne Feld entarteten Niveaus in 2I+1 Niveaus mit der Energie

$$\hat{H}_Z = -\hat{\vec{\mu}} \cdot \vec{B}_0 = \gamma B_0 \hat{I}_z \tag{3.7}$$

Die Besetzung dieser Niveaus ist durch die Boltzmann-Verteilung gegeben. Durch die Besetzungsdifferenz unterscheiden sich Absorption und Emission und deshalb werden Absorptionsexperimente möglich. Zu dem Hamiltonoperator der Zeeman-Wechselwirkung addieren sich die Operatoren der lokalen Wechselwirkungen:

$$\hat{H} = \hat{H}_Z + \hat{H}_{local} \tag{3.8}$$

Zwei Arten lokaler Felder sind für diese Arbeit von besonderer Relevanz, zum einen der anisotrope Anteil der chemischen Verschiebung im Fall der ^{31}P-NMR (Spin $I = 1/2$), zum anderen die quadrupolare Wechselwirkung im Fall der ^{2}H-NMR (Spin $I = 1$).

Die chemiche Verschiebung ist die Wechselwirkung des Kerns mit seiner elektronischen Umgebung. Die Elektronenhülle schirmt das Feld B_0 ab, am Kernort wirkt ein lokales Feld

$$\vec{B}_S = \tilde{\sigma} \vec{B}_0 \tag{3.9}$$

wobei der chemische Verschiebungstensor $\tilde{\sigma}$ die richtungsabhängige Stärke der Abschirmung angibt. In seinem Hauptachsensystem ist der chemische Verschiebungstensor diagonal und lässt sich in einen isotropen und einen anisotropen Teil zerlegen. Während der isotrope Anteil der Wechselwirkung die Resonanzfrequenz nur verschiebt, bewirkt der anisotrope Anteil eine Abhängigkeit der Resonanzfrequenz von der molekularen Orientierung. Für einen axialsymmetrischen Tensor erhält man für die Verschiebung der Frequenz im rotierenden Koordinatensystem [148]

$$\Delta\omega_{CSA} = \frac{1}{2}\delta_{CSA}(3\cos^2\Theta - 1) \tag{3.10}$$

wobei für δ_{CSA} zusammen mit der Larmorfrequenz $\omega_L = \gamma B_0$ gilt:

$$\delta_{CSA} = \frac{2}{3}\omega_L \Delta\sigma_{CSA} \tag{3.11}$$

Kerne mit einem Spin $I > 1/2$ können neben dem magnetischen Dipolmoment auch ein elektrisches Quadrupolmoment tragen. Sie wechselwirken dann mit

dem elektrischen Feldgradienten (EFG) am Kernort. Der Hamiltonoperator der Quadrupol-Wechselwirkung ist [147]

$$\hat{H}_Q = \frac{eQ}{2I(2I-1)\hbar^2}\vec{I}\tilde{V}\vec{I} \tag{3.12}$$

Mit der quadrupolaren Kopplungskonstanten

$$\delta_Q = \frac{3eQ}{4\hbar}V_{ZZ}^{HAS} \tag{3.13}$$

ergibt sich für die Orientierungsabhängigkeit der Resonanzfrequenz für Spin I=1 und im Falle eines symmetrischen Tensors des EFG ist die Verschiebung der Frequenz im rotierenden Koordinatensystem [148]

$$\Delta\omega_Q = \pm\frac{\delta_Q}{2}(3\cos^2\Theta - 1) \tag{3.14}$$

3.6.2 Linienformanalyse

Für die Messungen aller gezeigten eindimensionalen NMR-Spektren wurde im Falle der ^{31}P-NMR die Hahn-Echo- [149], im Falle der ^{2}H-NMR die Solid-Echo-Pulsfolge [150] verwendet.

Für eine statische, isotrope Verteilung von Molekülorientierungen erhält man das Festkörperspektrum [148], für $I = 1/2$

$$S_{slow}(\omega) \propto \frac{1}{\sqrt{1+\frac{\omega}{\delta_{CSA}}}} \tag{3.15}$$

und für I=1

$$S_{slow}(\omega) \propto \frac{1}{\sqrt{1+\frac{\omega}{\delta_Q}}} + \frac{1}{\sqrt{1-\frac{\omega}{\delta_Q}}} \tag{3.16}$$

Falls die Moleküle frei und schnell verglichen mit der Zeitskala $1/\delta_{CSA}$ rotieren können wird die Anisotropie vollständig ausgemittelt, und man erhält eine lorentzförmige Flüssigkeitslinie

$$S_{fast}(\omega) \propto \frac{1}{1+(T_2\omega)^2} \tag{3.17}$$

T_2 bezeichnet die Spin-Spin-Relaxationszeit.

3.6.3 Spin-Relaxation

Bloembergen, Purcell und Pound stellten 1948 erstmals eine Theorie auf, die die Relaxationseffekte auf statistische Fluktuationen der lokalen Felder, die z.B. durch regellose Bewegung der Moleküle in der Flüssigkeit erzeugt werden[151]. Ihre Herleitungen beziehen sich auf die Dipol-Dipol-Kopplung als dominierende Wechselwirkung. Analog gelten für die CSA-Wechselwirkung und die quadrupolare Kopplung Proportionalitäten zur Spektraldichte bei der Larmorfrequenz $J(\omega_L)$, siehe auch Kap. 3.5:

$$1/T_1^{CSA} \propto J(\omega_L) \tag{3.18}$$

$$1/T_1^{Q} \propto J(\omega_L) + 4J(2\omega_L) \tag{3.19}$$

Die Spin-Gitter-Relaxationszeit T_1 wurde bei hinreichend tiefen Temperaturen mittels Saturation-Recovery-, bei hohen Temperaturen mit Hilfe der Inversion-Recovery-Folge bestimmt. Für Messungen der Spin-Spin-Relaxationszeit T_2 kam die CPMG-Sequenz (nach Carr, Purcell, Meiboom, Gill) [152, 153] zum Einsatz.

3.6.4 Stimuliertes Echo

Der Zerfall der stimulierte-Echo-Amplitude liefert einen quantitativen Zugang zur Orientierungskorrelationsfunktion des zweiten Legendrepolynoms. Im Experiment werden Pulsfolgen mit fester Evolutionszeit t_p zur Aufzeichnung des Zerfalls als Funktion der Mischzeit t_m angewendet: Im Fall der ^{31}P-NMR die Dreipulsfolge $(\pi/2)$ - t_p - $(\pi/2)$ - t_m - $(\pi/2)$, für die ^{2}H-NMR die Vierpulsfolge $(\pi/2)$ - t_p - $(\pi/4)$ - t_m - $(\pi/4)$ (Spin-Alignment). Durch eine jeweils geeignete Phasenzyklisierung wird der Sinus-Anteil des stimulierten Echos detektiert [9, 76, 154].

Für die Echo-Amplitude gilt

$$I(t_p, t_m) \propto \langle \sin(\omega_{local}(0)t_p) \sin(\omega_{local}(t_m)t_p) \rangle \exp(-(t_m/T_1)^{\beta_K}) \tag{3.20}$$

Der Term in spitzen Klammern ist hierbei die Orientierungskorrelationsfunktion $F_{t_p}^{sin}(t_m)$ im Ensemblemittel, der gestreckt exponentielle Term ist ein Dämpfungsfaktor, der NMR-Relaxationseffekte berücksichtigt. Für die ^{31}P-NMR ist die Größe T_1 durch die Spin-Gitter-Relaxationszeit (mit $\beta_K = 1$) gegeben, bei der ^{2}H-NMR steht an deren Stelle die quadrupolare Relaxationszeitkonstante T_{1Q} (mit $\beta_K < 1$). Die normierte Korrelationsfunktion $F_{t_p}^{sin}(t_m)$ lässt sich zerlegen [155]

$$F_{t_p}^{sin}(t_m) = [1 - F_\infty]\phi_{t_p}(t_m) + F_\infty \tag{3.21}$$

wobei die Funktion $\phi_{t_p}(t_m)$ den Korrelationsverlust aufgrund der Bewegung beschreibt, während $F_\infty = F_\infty(t_p)$ für die nicht relaxierende Restkorrelation steht. Deren Wert hängt von der Geometrie der Reorientierung ab und ist u.a. für

isotrope Bewegung bekannt [76, 155]. Im Grenzfall $t_p \to 0$ verschwindet die Restkorrrelation und $\phi_{t_p}(t_m)$ nähert die Korrelationsfunktion $\langle\omega_{local}(0)\omega_{local}(t_m))\rangle$ an, die proportional zur Orientierungskorrelationsfunktion $C_2(t_m)$ des zweiten Legendre-Polynoms ist [76]:

$$\lim_{t_p \to 0} \phi_{t_p}(t_m) \propto \langle\omega_{local}(0)\omega_{local}(t_m))\rangle \propto C_2(t_m) \tag{3.22}$$

3.6.5 2D-Spektren

2D-Spektren $S(\omega_1, \omega_2; t_m)$ lassen sich interpretieren als die Wahrscheinlichkeit $P_{2,0}(\omega_1, \omega_2; t_m)$, zum Zeitpunkt $t = t_m$ die Frequenz ω_2 zu finden, wenn diese ω_1 zum Zeitpunkt $t = 0$ war [148]. Dies ist analog zu dem Produkt aus der a-priori Wahrscheinlichkeit $P_{1,0}(\omega_1)$ für das Vorliegen einer Frequenz ω_1 vor der Mischzeit und der bedingten Wahrscheinlichkeit $P_{1,1}(\omega_2; t_m|\omega_1; 0)$, dass nach der Mischzeit ω_2 gemessen wird, wenn vor der Mischzeit ω_1 vorlag. Zur Messung der ^{31}P-NMR 2D-Spektren wurde eine 4-Puls-Folge unter Verwendung der TPPI-Technik (time-proportional phase incrementation, [148]) genutzt. Im Falle isotroper Bewegung und Vorliegen einer breiten Korrelationszeitenverteilung lassen sich die 2D-Spektren als Superposition von vier Subspektren (Abb. 3.36) darstellen: Keine Reorientierung während der Mischzeit führt zu einem Festkörperspektrum S_{Solid} auf der Diagonale

$$S^{dia}(\omega_1, \omega 2) \propto S_{Solid}(\omega_1)\delta(\omega_2 - \omega_1), \tag{3.23}$$

das relative Gewicht $p^{dia}(t_m)$ stimmt mit dem Wert der Korrelationsfunktion $F(t_m)$ überein. Für langsame, uneingeschränkte, isotrope Reorientierung erhält man

$$S^{reo}(\omega_1, \omega_2) \propto S_{Solid}(\omega_1)S_{Solid}(\omega_2), \tag{3.24}$$

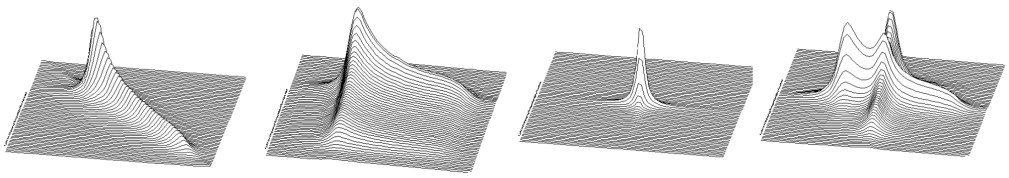

Abbildung 3.36: *Simulierte ^{31}P-NMR 2D-Grenzfallspektren, von links: Diagonale $S^{dia}(\omega_1, \omega_2)$, isotrope Reorientierung $S^{reo}(\omega_1, \omega_2)$, Lorentzlinie $S^{lor}(\omega_1, \omega_2)$, Austausch $S^{ex}(\omega_1, \omega_2)$*

für schnelle Reorientierung eine Lorentzlinie bei $\omega_1 = \omega_2 = 0$:

$$S^{lor}(\omega_1, \omega_2) \propto S_{lor}(\omega_1) S_{lor}(\omega_2), \tag{3.25}$$

und für Austausch zwischen schnellen und langsamen Molekülen

$$S^{ex}(\omega_1, \omega_2) \propto S_{lor}(\omega_1) S_{Solid}(\omega_2) + S_{lor}(\omega_2) S_{Solid}(\omega_1). \tag{3.26}$$

Die Analyse wurde bereits erfolgreich auf Ergebnisse asymmetrischer binärer Glasbildner angewendet [47, 76, 96, 106, 129].

4 Publikationen

Liste der einbezogenen Publikationen

Pub. 1 On the cooperative nature of the ß-process in neat and binary glasses: A dielectric and nuclear magnetic resonance spectroscopy study
D. Bock, R. Kahlau, B. Micko, B. Pötzschner, G. J. Schneider, and E. A. Rössler
THE JOURNAL OF CHEMICAL PHYSICS 139, 064508 (2013).

Pub. 2 Dynamics of asymmetric binary glass formers. I. A dielectric and nuclear magnetic resonance spectroscopy study
R. Kahlau, D. Bock, B. Schmidtke, and E. A. Rössler
THE JOURNAL OF CHEMICAL PHYSICS 140, 044509 (2014).

Pub. 3 Dynamics of asymmetric binary glass formers. II. Results from nuclear magnetic resonance spectroscopy
D. Bock, R. Kahlau, B. Pötzschner, T. Körber, E. Wagner, and E. A. Rössler
THE JOURNAL OF CHEMICAL PHYSICS 140, 094505 (2014).

Pub. 4 Dynamic heterogeneities in glass-forming systems
D. Bock, N. Petzold, R. Kahlau, S. Gradmann, B. Schmidtke, N. Benoit, and E.A. Rössler
JOURNAL OF NON-CRYSTALLINE SOLIDS 407, 88 (2015).

Individuelle Beiträge zu gemeinsamen Publikationen

Pub. 1 Von mir wurden alle NMR-Messungen an TPP und PS ausgeführt, mit Ausnahme der Spin-Gitter-Relaxationsmessungen am reinen TPP für $T > 120K$ (ausgeführt von B. Pötzschner). NMR-Experimente an Ethanol wurden von G. J. Schneider durchgeführt, alle Experimente der dielektrischen Spektroskopie von R. Kahlau. Sämtliche Analysen der NMR-Ergebnisse wurden von mir während meiner Promotion erstellt.

Pub. 2 Von mir wurden alle DSC- and NMR-Messungen ausgeführt. Experimente der dielektrischen Spektroskopie wurden von R. Kahlau, Lichtstreu-Experimente von B. Schmidtke durchgeführt. Sämtliche Analysen der DSC- und NMR-Ergebnisse wurden von mir während meiner Promotion erstellt.

Pub. 3 Von mir wurden alle NMR-Messungen durchgeführt, mit Ausnahmen der ^{31}P-NMR stimulierte-Echo-Zerfallsmessungen der 20%-Probe sowie der 2D-Spektren der 20%-Probe bei $T = 200K$ (E. Wagner), der ^{31}P-NMR stimulierte-Echo-Zerfallsmessungen der 80%-Probe (T. Körber). Experimente der dielektrischen Spektroskopie wurden von R. Kahlau, Lichtstreu-Experimente von B. Schmidtke durchgeführt. Sämtliche Analysen der DSC- und NMR-Ergebnisse wurden von mir während meiner Promotion erstellt.

Pub. 4 Von mir wurden alle DSC- and NMR-Messungen am System MTHF/m-TCP und, soweit nicht vorher veröffentlicht, am System TPP/PS durchgeführt. Sämtliche Analysen dieser Ergebnisse wurden von mir während meiner Promotion erstellt. Die Studie des Systems m-TCP/PMMA war Teil meiner Diplomarbeit, Messungen wurden zum Teil von N. Wirth und D. Bingemann durchgeführt. NMR-Experimente an m-TCP in Silika-Matrizen stammen von S. Gradmann. Experimente der dielektrischen Spektroskopie wurden von R. Kahlau, TFPI-Experimente von B. Schmidtke, und PCS-Experimente von N. Petzold ausgeführt.

Weitere Publikationen

- Reorientational Dynamics of Organophosphate Glass Formers - a joint Study by ^{31}P NMR, Dielectric Spectroscopy and Light Scattering
  S. Adishchev, D. Bock, C. Gainaru, R. Kahlau, B. Micko, N. Petzold, B. Pötzschner, and E. A. Rössler,
  Z. Phys. Chem. 226, 1149 (2012).

- Evolution of the dynamic susceptibility in molecular glass formers: Results from light scattering, dielectric spectroscopy, and NMR
  N. Petzold, B. Schmidtke, R. Kahlau, D. Bock, R. Meier, B. Micko, D. Kruk, and E. A. Rössler,
  J. Chem. Phys. 138, 12A510 (2013).

Publikation 1

On the cooperative nature of the ß-process in neat and binary glasses: A dielectric and nuclear magnetic resonance spectroscopy study

D. Bock, R. Kahlau, B. Micko, B. Pötzschner, G. J. Schneider, and E. A. Rössler
The Journal of Chemical Physics 139, 064508 (2013).

© 2013 AIP Publishing LLC
doi:10.1063/1.4816374

THE JOURNAL OF CHEMICAL PHYSICS **139**, 064508 (2013)

On the cooperative nature of the β-process in neat and binary glasses: A dielectric and nuclear magnetic resonance spectroscopy study

D. Bock,[1] R. Kahlau,[1] B. Micko,[1] B. Pötzschner,[1] G. J. Schneider,[2] and E. A. Rössler[1]
[1]*Experimentalphysik II, Universität Bayreuth, 95440 Bayreuth, Germany*
[2]*Jülich Centre for Neutron Science JCNS, Outstation at FRM2, Forschungszentrum Jülich GmbH, 85747 Garching, Germany*

(Received 28 May 2013; accepted 9 July 2013; published online 14 August 2013)

By means of dielectric as well as ^{2}H and ^{31}P nuclear magnetic resonance spectroscopy (NMR) the component dynamics of the binary glass tripropyl phosphate (TPP)/polystyrene (PS/PS-d_3) is selectively investigated for concentrations distributed over the full range. We study the secondary (β-) relaxation below T_g, which is found in all investigated samples containing TPP, but not in neat polystyrene. The dielectric spectrum of the β-process is described by an asymmetric distribution of activation energies, essentially not changing in the entire concentration regime; its most probable value is $E/k \cong 24\ T_g$. Persistence of the β-process is confirmed by ^{31}P NMR Hahn-echo and spin-lattice relaxation experiments on TPP, which identify the nature of the β-process as being highly spatially hindered as found for other (neat) glasses studied previously, or re-investigated within this work. The corresponding ^{2}H NMR experiments on PS-d_3 confirm the absence of a β-process in neat PS-d_3, but reveal a clear signature of a β-process in the mixture, i.e., polystyrene monomers perform essentially the same type of secondary relaxation as the TPP molecules. Yet, there are indications that some fractions of PS-d_3 as well as TPP molecules become immobilized in the mixture in contrast to the case of neat glasses. We conclude that in a binary glass the β-process introduced by one component induces a highly similar motion in the second component, and this may be taken as an indication of its cooperative nature. © *2013 AIP Publishing LLC*. [http://dx.doi.org/10.1063/1.4816374]

I. INTRODUCTION

Since the works of Johari and Goldstein (JG)[1] a second (or β-) relaxation peak is a well documented relaxation feature observed in many liquids at frequencies higher than those of the primary α–relaxation upon (super-) cooling.[2–7] In some cases, for type-A glass formers[8] (in contrast to type-B systems with a well resolved secondary process), such a β-peak is missing and only an "excess wing" appears on the high-frequency flank of the α-peak. Even two resolved secondary relaxation peaks may be found.[9,10] Photon correlation spectroscopy (PCS) studies of type-B glass formers have identified only an excess wing, which is masked by a strong β-peak in the dielectric spectrum.[10–12] Why PCS does not probe the β-process while it is clearly detected in dielectric and mechanical relaxation as well as in nuclear magnetic resonance (NMR) experiments remains a challenge to be understood. Thus, the situation is quite puzzling since there exists no final conclusion concerning the nature of these processes and their relevance with regard to the glass transition phenomenon.

As a β-process is also observed for molecules without internal degrees of freedom, it is assumed to be generic to the glassy state. In contrast to the α-process the β-process is often loosely called a "local" process. This classification may suggest that the extent of cooperativity of the dynamics typical of the α-process is not found for secondary relaxations. Actually, however, all correlation lengths discussed for the α-process are, if at all present, on the order of a few nanometers which still is rather local. A prominent feature which might point to a local character of the dynamics is the fact that below T_g the most probable relaxation time τ_β of the β-process follows an Arrhenius temperature dependence, the peak width increases with reciprocal temperature as expected for a temperature independent distribution of activation energies, and the relaxation strength changes only weakly.[8,13] Yet, the mean activation energies are quite high, usually in the range $E/k \cong 11$–$26\ T_g$.[5,7] Its generic nature is also signaled by the fact that the relaxation strength strongly increases above T_g, i.e., the β-process probes the "softening" of the glass above T_g. Important to note is that a β-process is also observed in super-cooled plastic crystals (glassy crystals) with activation energies almost not altered with respect to that of the corresponding structural glass.[13,14]

Systematic ^{2}H NMR solid-echo studies on structural glass formers such as toluene, decalin, and polybutadiene[15–18] as well as on glassy crystals like ethanol[19] or cyano cyclohexane[20,21] have been carried out in the past. Due to its high sensitivity on small-angle reorientations, the solid-echo technique yields a clear picture of the nature of the β-process in terms of its single-particle dynamics.[22,23] Spatially highly restricted reorientation of essentially all molecules prevails in the glassy state of neat systems. As suggested by random walk simulations,[22,24] the β-process is a multi-step process (like the α-process), so that the overall loss of correlation is not achieved before a number of elementary steps with a jump time $\tau_J \ll \tau_\beta$ are performed. The wobbling-on-a-cone model allows to reproduce the salient features of the NMR spectra as well as to quantify the extent of spatial

 © 2013 AIP Publishing LLC

This article is copyrighted as indicated in the article. Reuse of AIP content is subject to the terms at: http://scitation.aip.org/termsconditions. Downloaded to IP: 132.180.21.130 On: Wed, 11 Dec 2013 14:55:21

restriction with a full opening cone angle $\chi < 10°$.[22,23] The NMR manifestation of the β-process in plastic crystals is essentially indistinguishable from that in canonical glasses.[19–21] Investigating the β-process in binary glass formers has shown that in a certain concentration range both components exhibit the same highly hindered (slow) wobbling of their molecular axis independent of size and shape of the molecules.[17] These experimental findings may allow to speculate that the β-process displays some extent of cooperativity, too.

In the present study the binary glass tripropyl phosphate (TPP)/(deuterated) polystyrene (PS/PS-d_3, $M_w \approx 2 \times 10^3$ g/mol) is investigated well below T_g by means of dielectric spectroscopy, ^{2}H and ^{31}P NMR. Nine concentrations spread over the complete range are chosen. The system is characterized by a large T_g contrast of the pure components ($\Delta T_g \cong 200$ K). Caused by the choice of this system the application of ^{31}P and ^{2}H NMR allows to probe selectively the dynamics of TPP and PS-d_3, respectively. Beyond that, dielectric spectroscopy (DS) provides information on the evolution of the distribution of activation energies when changing concentration. For comparison we included unpublished ^{2}H NMR results on ethanol for which a β-process is well identified by DS[14] (cf. also Ref. 17). As the molecular dipole moment of TPP is significantly higher than that of PS, the DS experiment of the mixture probes, in reasonable approximation, solely the TPP dynamics. For the first time we probe the characteristics of the β-process also by a ^{31}P NMR Hahn-echo sequence. As will be demonstrated, in binary glasses the type-B component causes the other component to participate in a common β-process. Yet, a fraction of both components becomes immobilized, i.e., in binary glasses – in contrast to neat systems – islands of rigidity appear, as already reported previously.[25] Our results clearly favor the interpretation that the β-process is a cooperative process – as is the α-process.

II. EXPERIMENTAL DETAILS AND DATA ANALYSIS

A. Systems

A polystyrene sample with the molecular mass $M_w = 2250$ g/mol (PS) and another polystyrene sample, partially deuterated at the backbone, with very similar mass $M_w = 2440$ g/mol (PS-d_3) were purchased from Polymer Standards Service (Mainz, Germany) and used without further treatment. Since the chains consist of more than 20 monomer units, we assume that any specific end group of the polymer chains will not have a considerable effect on the investigation of the segmental dynamics. For the dielectric experiments PS was used for the preparation of the mixtures, while PS-d_3 was used for the NMR measurements. Tripropyl phosphate (TPP, 99%) was bought from Sigma Aldrich and used as received, too (cf. also Ref. 26). A list of mass concentrations $c = m_{TPP}/(m_{TPP} + m_{PS/PS\text{-}d3})$ of the mixtures measured by DS and/or NMR is given by Table I. Ethanol-d_2 (deuterated at the methylene group) was purchased from Aldrich. We do not find any indication that phase separation or crystallization occurs in the binary glasses. Among other tests, light scattering experiments show a homogeneous sample.

TABLE I. Mass concentrations of systems measured by DS and/or NMR.

c	0	0.1	0.2	0.3	0.45	0.5	0.6	0.8	0.9	0.95	1
DS	x	x	x	x	x	…	x	x	x	x	x
^{2}H NMR	x	x	x	…	…	x	…	x	x	…	…
^{31}P NMR	…	x	x	…	…	x	…	…	…	…	x

B. Dielectric spectroscopy

Dielectric measurements were carried out with the Alpha-A analyzer by Novocontrol while temperature was kept constant within ±0.2 K by using the Quatro-H temperature controller by Novocontrol. The absolute accuracy is assumed to be better than ±1 K. The sample cell has the design published by Wagner and Richert and assures a constant sample volume.[27] All β-relaxation peaks have an asymmetric shape and can be interpolated with the $G_\beta(\ln \tau)$ distribution introduced in Ref. 28. Actually, the time constant is the only parameter discussed in this article, which can also be obtained in good approximation via $\tau_\beta = 1/(2\pi \nu_{max})$ by determining the maximum positions ν_{max}. In order to obtain the time constants of the α-relaxation of neat PS a Kohlrausch function is used for the data interpolation. In the case of neat TPP a Cole-Davidson model is preferred. Time constants of the α-process in the mixtures, where the primary relaxation peak is significantly broadened in relation to neat TPP, were defined by the peak positions like $\tau_\alpha = 1/(2\pi \nu_{max})$. A more detailed analysis of the structural relaxation peaks of all investigated mixtures will be presented in a forthcoming publication.

C. NMR

The ^{31}P NMR experiments were carried out using a Bruker Avance III console and a Spectrospin 400 MHz cryomagnet. The field strength of 9.4 T corresponds to a Larmor frequency $\nu_L = 161.98$ MHz for ^{31}P. The length of the $\pi/2$-pulse was 2.2 μs. A home-built (in cooperation with Bruker Biospin GmbH) double resonance probe was cooled by liquid nitrogen using an Oxford CF1200 cryostat, controlled by an Oxford ITC-503. Temperature accuracy was ±2 K, stability was better than ±0.2 K. The ^{2}H NMR experiments were carried out on a Bruker Avance DSX spectrometer and an Oxford 300 MHz cryomagnet. The field strength of 7 Tesla corresponds to a ^{2}H Larmor frequency of $\nu_L = 46.067$ MHz; the length of the $\pi/2$-pulse was 2.8 μs. A home-built probe was cooled by liquid nitrogen using a CryoVac Konti cryostat and an Oxford ITC-503 temperature controller. Temperature accuracy was better than ±1 K, stability was better than ±0.2 K.

At temperatures below its minimum the spin-lattice relaxation time $T_1(T)$ was measured via a saturation recovery sequence. Above the T_1 minimum temperature the inversion recovery sequence was applied. In the case of ^{31}P the spin-lattice relaxation was found to be in non-exponential, as in this ^{2}H NMR the relaxation below T_g is non-exponential as in this case spin-diffusion can be neglected at least at short relaxation times. Therefore the mean value $\langle T_1 \rangle$ is given, which is obtained by interpolating the relaxation function by

This article is copyrighted as indicated in the article. Reuse of AIP content is subject to the terms at: http://scitation.aip.org/termsconditions. Downloaded to IP: 132.180.21.130 On: Wed, 11 Dec 2013 14:55:21

a Kohlrausch decay (stretched exponential). This decay function is also used to interpolate the decay of the solid-echo (cf. below and Eq. (3)).

The NMR frequency depends on the angle θ between the principal interaction tensor axis and the magnetic field direction:

$$\nu_{local}(\theta) = (\pm)(3\cos^2\theta - 1) \cdot \delta_{CSA/Q}/2, \qquad (1)$$

where ν_{local} is the shift of the resonance frequency with respect to the Larmor frequency ν_L. The parameter $\delta_{CSA/Q}$ (in kHz) specifies the anisotropy of the interaction tensor, which is given by the interaction of the nuclear quadrupolar moment (Q) with the electrical field gradient in the case of ^{2}H NMR. In the case of PS-d$_3$, the orientation of the ^{2}H-C bonds at the chain backbone is probed. Due to the spin $I = 1$ two transitions occur and positive as well as negative signs are valid. In the case of ^{31}P NMR (spin $I = 1/2$) the rigid lattice spectrum is determined by the chemical shift anisotropy (CSA), and in Eq. (1) δ_{CSA} is used and only the negative sign is found. Both interaction tensors CSA and Q are axially symmetric in the present case. In the case of an isotropic distribution of tensor orientations (e.g., in glasses) characteristic powder spectra are observed, a (symmetric) Pake spectrum in the case of ^{2}H NMR whereas the CSA spectrum is asymmetric.

The solid-state spectra were collected by applying a Hahn-echo (^{31}P NMR) or a solid-echo sequence (^{2}H NMR) preceded by a saturation sequence of five $\pi/2$ pulses; the buildup time was chosen to be 2.5 T_1 or 1 s at least. In the case of ^{31}P NMR ^{1}H decoupling was applied during the echo sequence. Appropriate 8-fold (^{2}H) and 16-fold (^{31}P) phase cycling was applied.[29] Fits to the solid-echo Pake spectra were corrected for finite pulse excitation.[30,31] Simulations have shown that in the case of small angle reorientations as typically found for the β-process the largest effect in the solid-echo spectrum is found for the condition $\tau_\beta \delta_{local} \cong 1$.[32]

III. RESULTS

A. Neat components—Dielectric spectra

The susceptibility spectra of PS ($T_g = 335$ K) are shown in Fig. 1(a). Above T_g a pronounced peak is visible, which is identified as the structural or α-relaxation. The low amplitude reflects the rather non-polar nature of the PS monomer. Close to T_g, the high-frequency side of the α-peak is made up of a crossover from one power-law behavior to another one usually called excess wing. This spectral shape is typical for a type-A glass former, where no explicit secondary relaxation peak is resolvable. While temperature is increased the main relaxation peak shifts to higher frequencies. When the sample is cooled below T_g the α-peak moves out of the frequency window and the signal, now consisting only of the excess wing contribution, drops close to the resolution limit of the spectrometer. No indications for a secondary (β-) relaxation peak are observed.

The dielectric spectra of neat TPP ($T_g = 134$ K) are displayed in Fig. 1(b). As in the case of PS above T_g an α-relaxation peak can be identified, the amplitude of which exceeds the one of PS by a factor of about 1000, i.e., the TPP molecule carries a strong dipole moment. At frequencies several decades above the maximum position of the α-peak a secondary relaxation is well resolved (type-B glass former). This secondary peak survives at temperatures below T_g when the α-peak has already left the frequency window. Its spectrum broadens significantly when temperature is lowered. When temperature is increased above, say, $T = 150$ K, both peaks approach each other until above $T = 156$ K the measurement of the super-cooled liquid cannot be continued due to the crystallization of the sample.

The time constants of both α- and β-process are shown in Fig. 2. In the case of neat PS we added the results of Ediger and co-workers,[33] and for TPP we included the ^{31}P NMR results obtained by applying the stimulated echo technique as well as the data from an analysis of the spin-lattice and spin-spin relaxation.[26] Good agreement is found between the NMR and DS results. While the τ_α show the typical super-Arrhenius temperature dependence, the β-process in TPP exhibits an Arrhenius behavior. The mean activation energy is found to be $E/k = 3240$ K $= 24\ T_g$.

B. Neat components—^{31}P and ^{2}H NMR results

As seen in Fig. 3(a), below T_g the spin-lattice relaxation time $T_1(T)$ of PS-d$_3$ displays a rather weak temperature

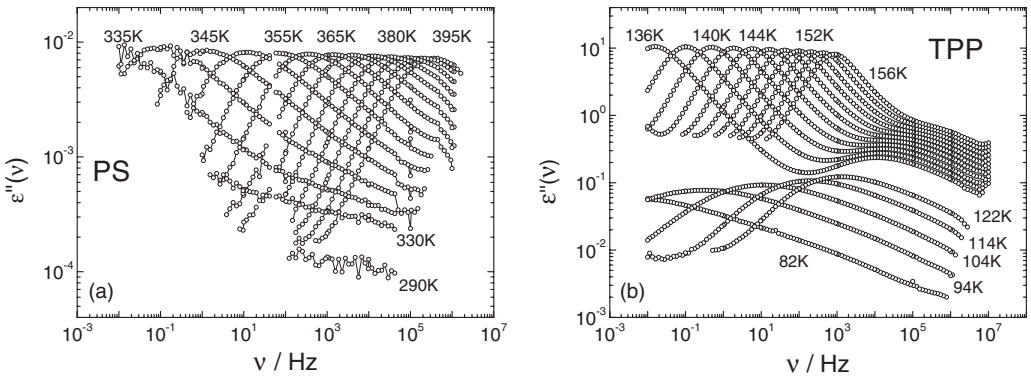

FIG. 1. (a) Dielectric spectra of neat PS; $T = 290$K and $T = 330$ – 395 K in 5 K steps (some temperatures indicated). (b) Susceptibility spectra of neat TPP revealing a well resolved β-process (some temperatures indicated; data above T_g partially taken from Ref. 26).

This article is copyrighted as indicated in the article. Reuse of AIP content is subject to the terms at: http://scitation.aip.org/termsconditions. Downloaded to IP: 132.180.21.130 On: Wed, 11 Dec 2013 14:55:21

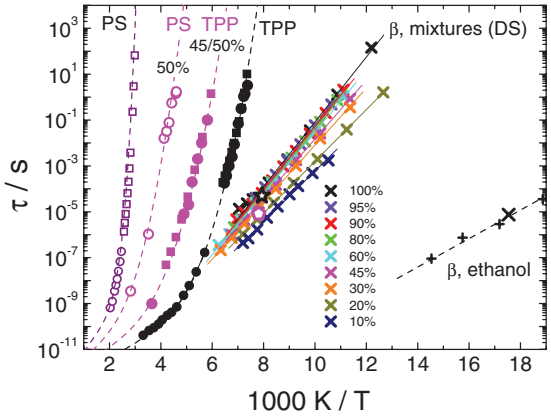

FIG. 2. Structural relaxation times τ_α in neat PS (DS: open squares, NMR: open circles[33]), and neat TPP (DS: full squares, NMR: full circles[26]) and in the mixtures $c = 45\%$ (DS probing TPP, full squares) and $c = 50\%$ (^{31}P NMR probing TPP, full circles; and ^{2}H NMR probing PS dynamics, open circles); time constant τ_β of the β-process in neat TPP and in the mixtures as revealed by DS (crosses, color code for the concentrations given in legend), τ_β of TPP yielded by ^{31}P Hahn-echo (open star) and of PS in the mixture by ^{2}H solid-echo (open pentagon). For comparison, time constants of the β-process of ethanol as given by DS (plus signs)[14] and NMR (cross). Solid lines: Arrhenius-fits (see Fig. 7), dashed lines: guides for the eye.

dependence typical of an excess wing determining the relaxation in the glass as indicated by the dielectric spectra (cf. Fig. 1(a)). Approximately an exponential temperature dependence $\langle T_1 \rangle \propto e^{-T/To} \propto 1/J(\omega = const.)$ with $T_o = 96$ K is observed (dashed line), as also found for the spectral density $J(\omega)$ of many type-A glasses by dielectric spectroscopy.[7,8,34,35] We note that dynamic mechanical analysis appears to show a β-process in high molecular mass polystyrene,[36] yet, we do not see any indication of this in our NMR as well as dielectric experiments on our sample. Despite of the low molecular dipole moments of polystyrene samples dielectric spectroscopy is principally able to detect a β-relaxation in polystyrene.[37] Above T_g the α-process dominates and T_1 decreases, yet a relaxation minimum is not observed as it occurs at even higher temperatures.

In the case of ^{31}P NMR on TPP, a well resolved T_1-minimum is found and attributed to the α-process. The corresponding time constant $\tau_\alpha(T) = 1/(2\pi\nu_L)$ agrees with the results from a full T_1/T_2 analysis.[26] Below T_g the temperature dependence of T_1 becomes weaker, yet, it is much stronger than in the case of PS-d$_3$ due to the β-process controlling the relaxation. As the ^{31}P relaxation is controlled by the chemical shift anisotropy (CSA; cf. Sec. II C) the relation $1/T_1 \propto \varepsilon''(\omega_L)$[26,38,39] is expected to hold and one can check this relationship by inserting the intensity of the dielectric spectra of the respective temperatures (cf. Fig. 1(b)) extrapolated to the Larmor frequency ($\nu_L = 161.98$ MHz) of the ^{31}P NMR experiment. As indicated by the dashed line in Fig. 3(a), indeed, the temperature dependence of $T_1(T)$ is well reproduced by that of ε''. A different situation is found for the comparison of the ^{2}H and ^{31}P T_1 data of the mixtures (Fig. 3(b)), which will be discussed in detail in Sec. III D.

The β-process can also be accessed by analyzing the NMR spectra via the application of a two-pulse echo sequence, namely the Hahn-echo (^{31}P) or the solid-echo (^{2}H) sequence. The majority of former NMR studies on the β-process in molecular glasses are based on ^{2}H solid-echo experiments.[15–22] There, subtle spectral changes characteristic of a highly hindered molecular reorientation have been identified by varying the inter-pulse delay t_p. In Fig. 4(a) this is first documented for the structural glass of neat ethanol-d$_2$ for which DS has identified a comparatively fast β-process with $E/k = 15\ T_g$ (cf. also Fig. 2).[14] While at low as well as high temperatures (yet below $T_g = 92$ K) rather weak spectral changes are recognized and the spectra display more or less the typical solid-state ^{2}H NMR powder (Pake) shape, at intermediate temperatures ($T_g - 30$ K) a strong decrease of the spectral intensity around zero frequency is observed for long delay time t_p, yet the singularities prevail. We conclude that well in the glassy state of ethanol the β-process passes through the NMR time window.

Fig. 4(b) shows the results of an analogue experiment on TPP. Due to the different spin dynamics for the $I = 1/2$ nucleus ^{31}P, in contrast to the $I = 1$ spin systems in the case

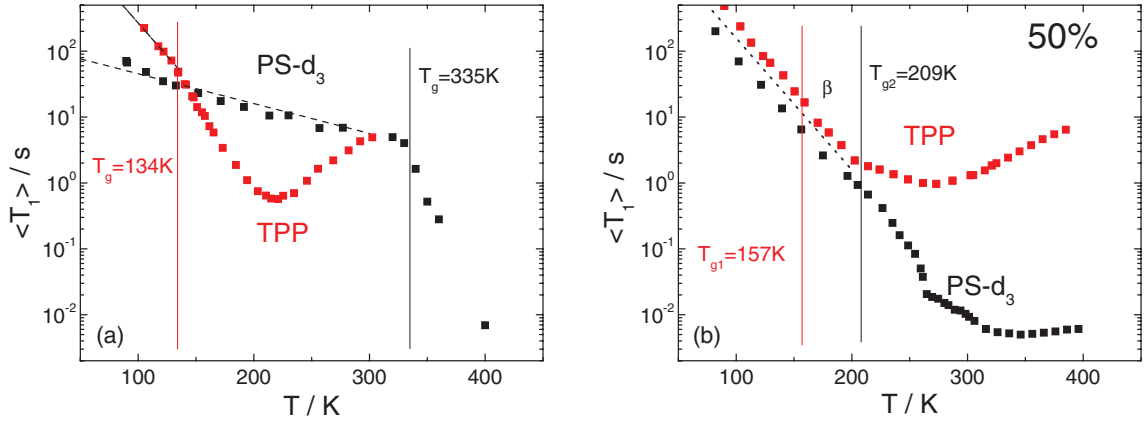

FIG. 3. (a) Spin-lattice relaxation times of neat TPP (^{31}P NMR) and neat PS-d$_3$ (^{2}H NMR). ^{2}H relaxation is non-exponential below T_g and therefore the mean relaxation time $\langle T_1 \rangle$ is given. Glass transition temperatures T_g are indicated by vertical lines; dashed line: interpolation by an exponential relaxation law for PS-d$_3$; dashed line below T_g of TPP: estimate of T_1 of TPP from the dielectric spectral density. (b) Spin lattice relaxation times of 50% TPP/PS-d$_3$ (^{31}P NMR and ^{2}H NMR; dashed line: estimate from the dielectric spectral density; vertical solid lines indicate T_g (for a detailed assessment cf. Sec. III D).

This article is copyrighted as indicated in the article. Reuse of AIP content is subject to the terms at: http://scitation.aip.org/termsconditions. Downloaded to IP: 132.180.21.130 On: Wed, 11 Dec 2013 14:55:21

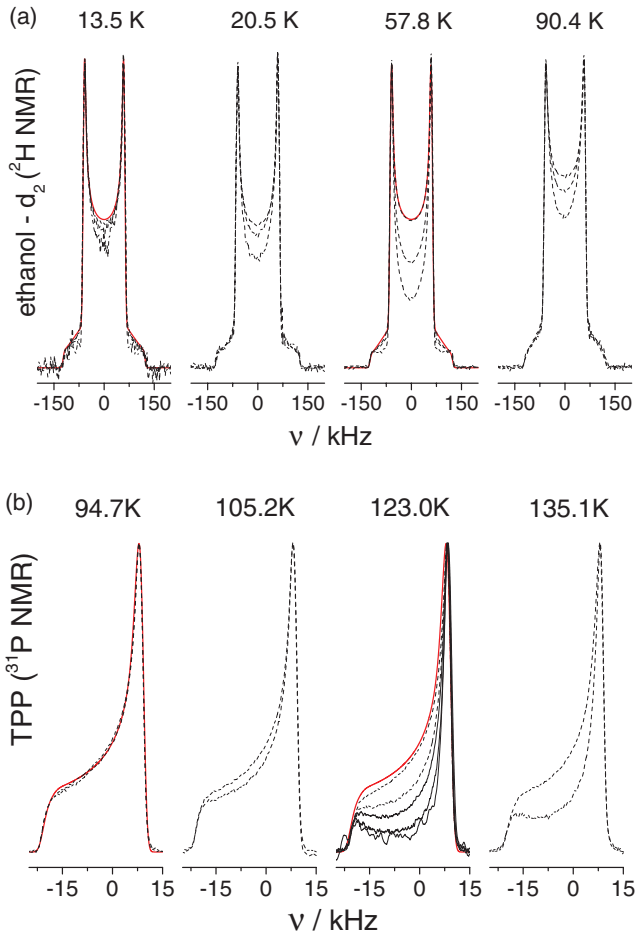

FIG. 4. (a) Solid-echo spectra of ethanol-d_2 at indicated temperatures, each set representing inter-pulse delays of 20 μs, 100 μs, and 200 μs; for shortest inter-pulse delay t_p a fit with a Pake model is shown as solid line ($\delta_Q = 123$ kHz); (b) Hahn-echo spectra of neat TPP, each set with inter-pulse delays of 20 μs and 200 μs, at 123 K additionally 400 μs, 800 μs, and 1600 μs (solid lines). A fit to the powder spectrum is included for shortest t_p as solid line ($\delta_{CSA} = 20.5$ kHz). All datasets are normalized to their maximum values.

of ^{2}H, a Hahn-echo sequence was applied. Like in Fig. 4(a), all spectra are normalized to their maximum values. As mentioned the relevant spin interaction in TPP is given by the CSA, which leads to an intrinsically asymmetric solid-state powder spectrum. The heteronuclear ^{1}H-^{31}P coupling was removed by ^{1}H decoupling, and the homonuclear ^{31}P-^{31}P coupling can be ignored safely due to the large distance between the nuclei in different molecules. Again, spectral intensity is lost mainly at the center of the spectra. In contrast to ethanol the effect is most prominent close to $T_g = 134$ K. Qualitatively, this is understood as the β-process in TPP is much slower than the one in ethanol (cf. Fig. 2). At $T = 123$ K extremely large inter-pulse delays (spectra marked by solid line) were applied. Here the intensity around $\nu = -5$ kHz almost vanishes, indicating that essentially all molecules participate in the β-process.

The spectral changes observed for neat ethanol ($T < T_g$) as well as TPP are very similar to those reported previously for pure toluene, decalin or polybutadiene or a decalin/chlorobenzene mixture;[17,23] even for the glassy crystalline phases of ethanol[19] or cyano cyclohexane.[20] The NMR spectrum looses intensity in the center of the spectrum, as said, a characteristic of a highly hindered motion. Assuming a wobbling-on-a-cone model, one finds for all examples that the angular displacement does not exceed 10°, which is therefore a rather generic feature of the β-process.[21,22] The second Legendre polynomial, determining the NMR frequency shift in the solid state, exhibits the highest sensitivity on a small angle reorientation at $\theta = 45°$ or $\nu = \delta_{CSA/Q}/4$, respectively, because here the derivative $|d\nu_{local}/d\theta|$ is maximal. This is seen directly in the case of ^{31}P NMR. Since in ^{2}H NMR the contributions of both signs in Eq. (1) are combined (two NMR transitions are involved), due to reasons of symmetry the highest sensitivity is found at $\nu = 0$.

The spectral effect can be quantified by measuring the intensity at the center of the spectrum with respect to that at the singularity,[18] explicitly a quantity R is defined by

$$\begin{aligned} R &= I(\nu = 0)/I(\nu = \delta_Q/2) && {}^2\text{H NMR}, \\ R &= I(\nu = -\delta_{CSA}/4)/I(\nu = \delta_{CSA}/2) && {}^{31}\text{P NMR}. \end{aligned} \tag{2}$$

In Fig. 5(a) the R values for long t_p (200 μs) (solid symbols) measured in ethanol (^{2}H NMR) and TPP (^{31}P NMR) are displayed as a function of the reduced temperature T/T_g. As expected a minimum is observed for ethanol at which the condition $\tau_\beta \delta_Q \cong 1$ applies with δ_Q specifying the quadrupolar interaction (cf. Sec. II C).[20] We note that in the case of short t_p values (e.g. $t_p = 20$ μs) no such minima are found in $R(T)$ as essentially no dephasing of the NMR frequencies (due to molecular reorientation involved in the β-process) is monitored; i.e., the spectrum has the undistorted powder shape (cf. Fig. 4). An analysis of the undisturbed low-temperature Pake spectrum (cf. Fig. 4) yields $\delta_Q = 123$ kHz for ethanol-d_2. From this an estimate of the time constant of the β-process can be given. The resulting τ_β is included in Fig. 2 and fits well into the DS findings.

In Fig. 5(a) we also included the ^{2}H NMR results on the glassy crystalline phase of cyano cyclohexane.[20] Again a minimum is observed in $R(T)$, however, at higher reduced temperature, which correlates well with the fact that $E/k = 19\ T_g$ is larger than in ethanol (15 T_g). In the case of TPP, with its much slower β-process, i.e., with higher activation energy $E/k = 24\ T_g$, a minimum can only be anticipated at highest temperatures, as above T_g the α-process interferes. Still, the time constant extracted via $\tau_\beta \delta_{CSA} \cong 1$ with $\delta_{CSA} = 20.5$ kHz is compatible with those from DS (cf. Fig. 2). The results for TPP are very similar to those of toluene (cf. again Fig. 5(a)), the paradigmatic glass former without internal (DS active) degrees of freedom, the β-process of which has been systematically investigated by ^{2}H NMR.[15–17] It turns out that the mean activation energy is the same as for TPP.[5] Finally, the result for PS-d_3 is included in Fig. 5(a). Here, essentially no temperature dependence is observed in agreement with the results from DS where no β-process is resolvable. In conclusion, the NMR spectra clearly reflect the β-process in the different glasses. Depending on the value of the mean activation energy E the quantity R reveals a minimum more or less below T_g.

This article is copyrighted as indicated in the article. Reuse of AIP content is subject to the terms at: http://scitation.aip.org/termsconditions. Downloaded to IP: 132.180.21.130 On: Wed, 11 Dec 2013 14:55:21

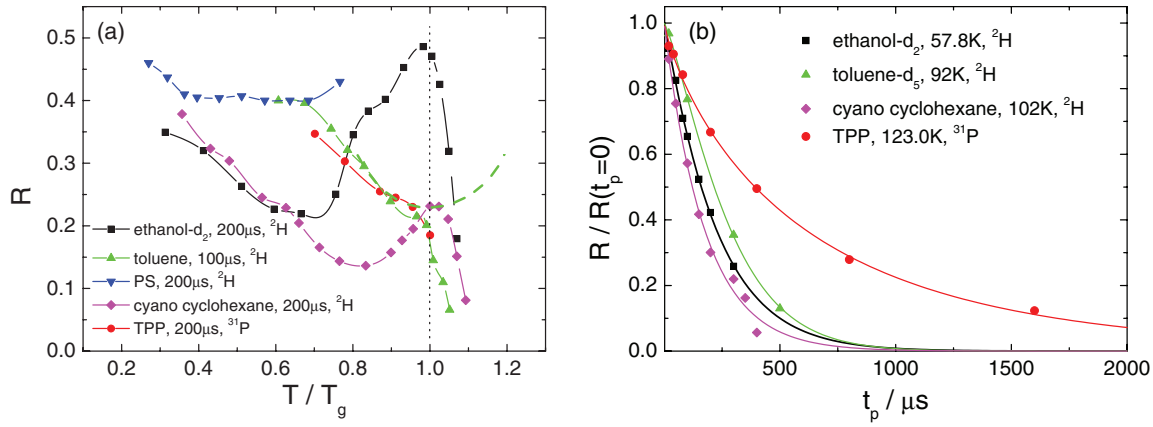

FIG. 5. (a) The parameter $R(T)$ at (high) $t_p = 200$ μs quantifying the spectral changes occurring in the solid-state NMR spectra for glassy ethanol, PS and plastically crystalline cyano cyclohexane (CNC),[20] TPP, as well as toluene-d5[15] at $t_p = 100$ μs. Lines are guides for the eye. For toluene (as well as TPP) a minimum above T_g, as would be expected without the influence of the α-process, is anticipated (dashed line). (b) Parameter R normalized to $R(t_p = 0)$ characterizing the spectral changes of the NMR spectra of ethanol, toluene, CNC, and TPP as a function of the inter-pulse delay t_p for temperatures as indicated; lines: Kohlrausch fits.

Figure 5(b) displays the dependence $R(t_p)$, normalized by $R(t_p = 0)$, for the temperatures of the minima found in Fig. 5(a). For ethanol, toluene[15] and cyano cyclohexane[20] $R(t_p)$ reaches almost zero at longest time t_p, which signals that essentially all molecules participate in the β-process. Again, $R(t_p)$ completely decays to zero. In the case of TPP, $R(t_p)$ shows a very similar behavior, yet, on somewhat longer inter-pulse times which are not accessible by ^{2}H NMR due to its faster spin-spin relaxation. We can conclude that essentially all TPP molecules participate in the β-process of neat TPP glass.

C. Characterizing the β-process in the TPP/PS mixtures by dielectric spectroscopy

In order to gain information about the β-relaxation in the mixture, PS molecules are now added stepwise to the TPP. By producing mixtures with $c = 0\%, 10\%, 20\%, 30\%, 45\%, 60\%, 80\%, 90\%, 95\%, 100\%$ mass fraction of TPP (cf. Table I), the entire concentration range is covered by DS experiments (as well as by NMR, cf. below). As the dielectric signal of PS is significantly smaller than that of TPP, we can safely assume that in the mixtures only the TPP dipoles are probed by DS.

For the concentration $c = 45\%$ dielectric spectra are compiled in Fig. 6. At temperatures above $T = 160$ K a peak is observed, which shifts to higher frequencies when temperature is increased. This peak is caused by the α-relaxation of TPP in the mixture. The corresponding time constants lie between those of the two neat systems as is seen in Fig. 2. Adding PS to TPP always ends up in a slowing down of the structural relaxation of the TPP ensemble due to the anti-plasticizer effect. The α-peak is strongly broadened; especially the low-frequency power-law exponent is reduced to values much smaller than 1, which is not found in the neat systems. In Fig. 2 we included the results of ^{2}H and ^{31}P NMR obtained from analyzing stimulated echo decays, for $c = 50\%$, which probe the structural relaxations of PS and TPP, respectively. Clearly, the time constant τ_α of PS is significantly longer than that of TPP, i.e., the dynamics of the two components are decoupled and two T_g can be defined, T_{g1} (PS) and T_{g2} (TPP). As stated before, a detailed assessment of the structural relaxations of the TPP/PS mixtures is given in a forthcoming publication; here we focus on the β-relaxation.

Below 160 K, when the α-peak has left the low-frequency limit of the spectrometer (Fig. 6), a β-relaxation is found like in the case of neat TPP. In particular, no essential change of the time constant is observed. This rather weak concentration dependence of the β-process is reflected in the Arrhenius plot of the time constants extracted from the maximum positions of the β-relaxation (Fig. 2). As in neat TPP the time constants τ_β follow Arrhenius laws for any concentration. For all TPP concentrations higher than $c \cong 60\%$ the $\tau_\beta(T)$ curves are essentially the same, yielding a mean activation energy $E/k = 24\, T_g$. At lower concentrations a slight reduction of E is observed, and the attempt frequency ν_0 is reduced, too. This is best seen in Fig. 7 where ν_0 and E are plotted as a function of concentration. Below $c = 60\%$ both E and ν_0 show a weak linear decrease. The slight extent of the concentration dependence of E is rather surprising, and one could argue that it points to the interpretation of the β-relaxation to be an intramolecular process due to some particularity of the TPP

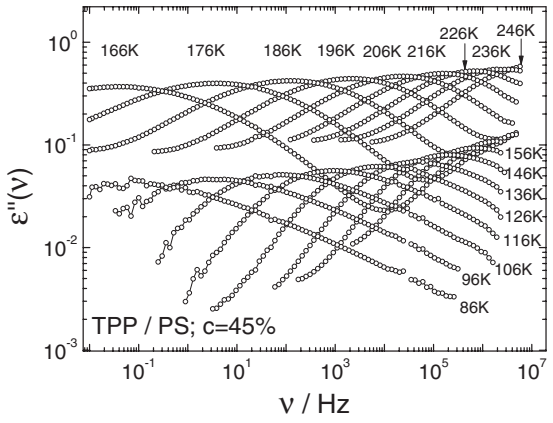

FIG. 6. Dielectric spectra of 45% TPP in PS at indicated temperatures.

This article is copyrighted as indicated in the article. Reuse of AIP content is subject to the terms at: http://scitation.aip.org/termsconditions. Downloaded to IP: 132.180.21.130 On: Wed, 11 Dec 2013 14:55:21

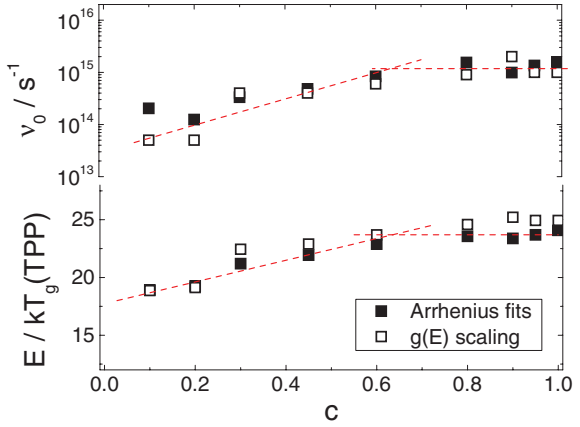

FIG. 7. Attempt rates ν_0 (upper panel) and activation energies (lower panel) for the whole concentration range of TPP. Full symbols: yielded by Arrhenius fits of $\tau_\beta(T)$ data in Fig. 2. Open symbols: yielded by $g(E)$ scaling (cf. text).

molecule. As we will demonstrate, however, this interpretation is misleading. Comparing the time constants of the β- and α-process in the mixtures one recognizes that their separation grows when PS is added (cf. Fig. 2). In other words, as the β-process essentially does not change but T_g of the mixture grows with the amount of PS, no structural relaxation of any considered mixture interferes with the analysis of the secondary relaxation carried out here.

The concentration dependence of the τ_β shown in Fig. 2 is also seen directly from the peak positions: comparing the β-peak of different mixtures, its spectral position shifts only weakly when PS molecules are added (cf. Fig. 8(a)). The only obvious change is a decrease of its amplitude. Next we consider the spectral shape of the β-peaks. As a first attempt, in Fig. 8(a) a symmetric log-Gaussian function, as usually found for β-processes,[5] is fitted to the data set for $c = 45\%$. However, the fit is not fully successful; the spectra do not appear symmetric. The asymmetric shape becomes even more obvious in Fig. 8(b), where data of the $c = 45\%$ sample at different temperatures are scaled onto their maximum height and position. Here, a temperature dependent broadening of the peak is observed, which is typical of a thermally activated process.

If a relaxation process is governed by a temperature independent distribution of activation energies $g(E)$ (which is actually a characteristic of a thermally activated process) the resulting distribution of correlation times $G(\ln\tau/\tau_o)$ can be calculated via the Arrhenius law $\ln\tau/\tau_o = E/kT$, leading to $G(\ln\tau/\tau_o) = kT\, g(kT \ln\tau/\tau_o)$. Here, a constant attempt time τ_o is assumed. In the case of a broad function $g(E)$, the shape of the resulting distribution $G(\ln\tau/\tau_o)$ is reproduced by the corresponding susceptibility in good approximation, $G(\ln\nu_o/\nu) \cong \chi''(\ln\nu_o/\nu)$. As a consequence, the susceptibility peak must increase with temperature, while it shifts to higher frequencies and decreases its width, exactly as it is observed experimentally in the case of most β-processes.[7] Thus, a re-scaling of the susceptibility spectra can be applied to yield a master curve representing the distribution $g(E)$.[35,40,41] Plotting $\varepsilon''/T\Delta\varepsilon_\beta$ as a function of $T\ln\nu_0/\nu$ is expected to yield master curves, provided that the $g(E)$ is indeed temperature independent. The only free parameter of this scaling is the attempt rate ν_0 of the relaxation, which is assumed to be constant for all spectra, i.e., temperature independent.

The results of the scaling procedure applied to the data of the TPP/PS mixtures are shown in Fig. 9. In all samples a broad but asymmetric $g(E)$ is revealed, justifying to identify the β-relaxation in all mixtures as thermally activated. This is in accord with the time constants τ_β following Arrhenius laws (Fig. 2). While $g(E)$ in Fig. 9 are very similar for all concentrations, the peak position (most probable energy barrier) is only constant for concentrations $c > 60\%$. For $c \leq 60\%$ a trend to lower activation energies becomes obvious. This corresponds to the above findings, where activation energies of the Arrhenius laws (Fig. 2) and peak positions at a fixed temperature (Fig. 8(a)) became concentration dependent below $c = 60\%$. This is once again demonstrated in Fig. 7, where activation energies and attempt rates ν_o gained from the $g(E)$ scaling (Fig. 9) as well as from the Arrhenius fits (Fig. 2) are compared. Both analyses yield comparable results and the same concentration dependences. Summarizing, we can state that the β-relaxation of all investigated mixtures is

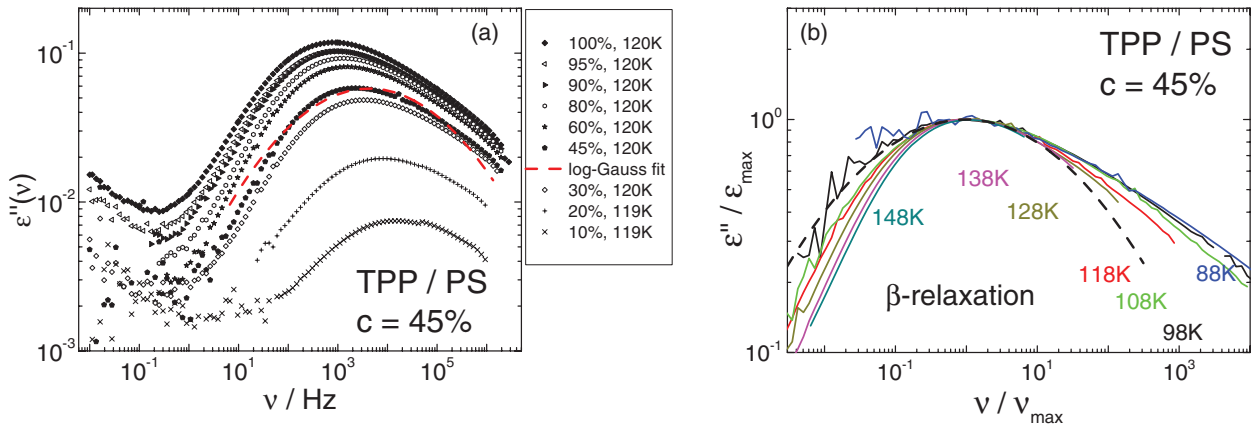

FIG. 8. (a) Susceptibility data of several mixtures of TPP in PS at similar temperature (119–120 K; mass fractions and temperatures indicated). Dashed line: Symmetric model function (log-Gauss) fit to the $c = 45\%$ data. (b) Data of the 45% sample at indicated temperatures, scaled to match maximum height and position. Dashed line: Fit from Fig. 5(a) scaled to maximum.

This article is copyrighted as indicated in the article. Reuse of AIP content is subject to the terms at: http://scitation.aip.org/termsconditions. Downloaded to IP: 132.180.21.130 On: Wed, 11 Dec 2013 14:55:21

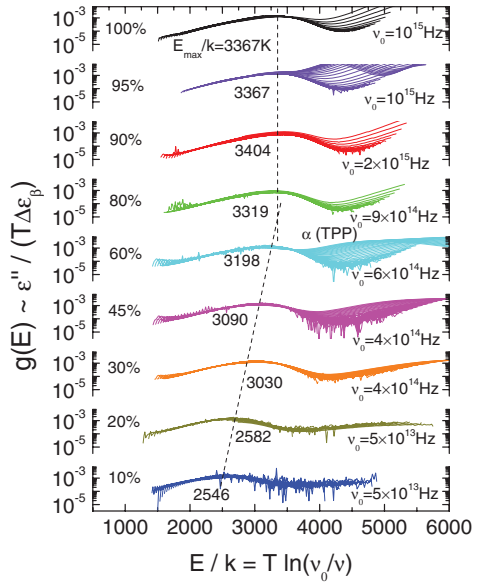

FIG. 9. Distribution of activation energies $g(E)$ obtained from scaling the susceptibility (cf. text) of the sub-T_g measurements of all investigated mixtures (concentrations, attempt rates, and most probable activation energies indicated). Dashed lines: Guides to the eye. Note: At high E/k deviations are observed due to the α-process of TPP.

governed by asymmetric but temperature independent distributions of activation energies $g(E)$. As a consequence, all time constants τ_β follow Arrhenius laws. All susceptibility data can be collapsed in order to reveal $g(E)$, making a detailed discussion of shape parameters, as obtainable by data fitting, needless in the context of this work.

D. Characterizing the β-process in the TPP/PS-d$_3$ mixtures by NMR experiments

As documented by the dielectric spectra, the β-process in the TPP/PS mixtures is well separated from the α-process. This is an important prerequisite for probing it by NMR, in particular, by applying a Hahn-echo (^{31}P) or a solid-echo (^{2}H) two-pulse sequence. The concentration selection of TPP/PS-d$_3$ mixtures investigated with these techniques can be inferred from Table I. Figure 10(a) shows the Hahn-echo spectra of TPP of the $c = 20\%$ mixture. A series of spectra, again normalized to their maximum values, is collected at three selected temperatures with a pulse delay $t_p = 40\ \mu$s, 80 μs, and 200 μs. While at high as well as low temperature no spectral changes are recognized, a weak but well discernible decrease of intensity around $\nu = -\delta_{CSA}/4$ is recognized at the intermediate temperature $T = 121.0$ K. Again, the characteristic spectral changes associated with a β-process are well identified. In the case of the $c = 50\%$ sample a similar evolution of the ^{31}P spectra is observed (cf. Fig. 10(b)), here, even longer t_p values have been applied at $T = 120.3$ K (solid lines) and the intensity around $\nu = -\delta_{CSA}/4$ almost vanishes at longest time t_p as in the case of neat TPP (cf. Figs. 4(b) and 5(b)).

As before for the neat components the spectral effect can be quantified by measuring the intensity close to the center of the spectrum with respect to the singularity, i.e., the quantity $R(t_p)$ (cf. Eq. (2)). In Fig. 11(a) the R values for long t_p (200 μs) (solid symbols) measured for three TPP concentrations ($c = 10\%$, 20%, 50%, and for comparison 100%) are plotted versus temperature. Except for $c = 100\%$ (as discussed before) a distinct minimum, essentially not shifting, is displayed. This signals immediately that the time constant of the process does not significantly change in the mixtures, a result already known from our DS study (cf. Fig. 2). In contrast to the $c = 100\%$ sample the minimum in $R(t_p)$ is well resolved due to the larger separation of α- and β-process in the mixtures. Also the depth of the minimum is very similar, at lowest concentration $c = 10\%$ it is somewhat less deep.

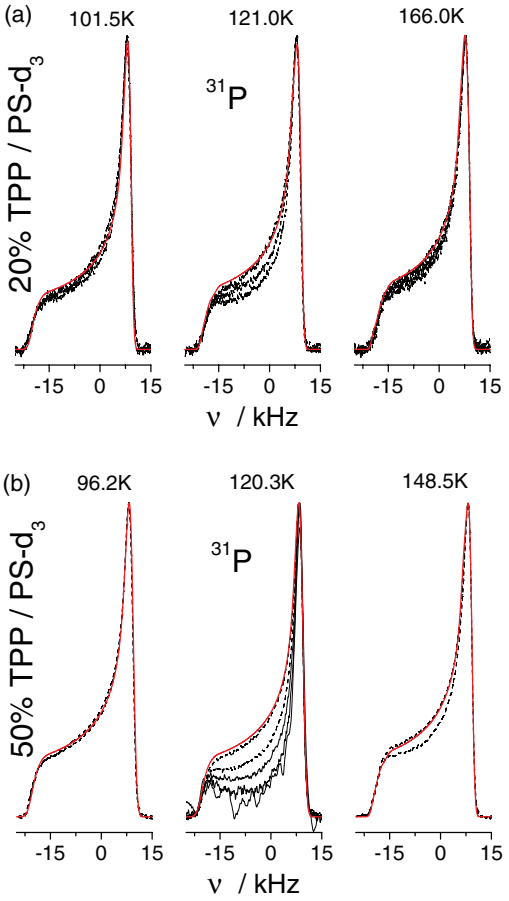

FIG. 10. ^{31}P Hahn-echo spectra of TPP/PS-d$_3$ glass at indicated temperatures, (a) $c = 20\%$, each set with $t_p = 40\ \mu$s, 80 μs, and 200 μs (b) $c = 50\%$, 20 μs and 200 μs each, at $T = 120.3$ K very long interpulse delays were applied additionally (solid lines, $t_p = 400\ \mu$s, 800 μs, and 1600 μs) and the intensity at $\nu = -\delta_{CSA}/4$ almost vanishes. For shortest t_p a fit by a CSA powder spectrum is included (solid line).

The decays of $R(t_p)$ for the different TPP concentrations at very similar temperatures are displayed in Fig. 11(c) and compared to the data of neat TPP. While for the $c = 50\%$ sample the decay of $R(t_p)$ is similar to that of $c = 100\%$, the situation for $c = 20\%$ is different. The $R(t_p)$ appears not to relax completely down to zero, indicating that at low TPP concentrations only a fraction of TPP molecules participates in the β-process, i.e., some molecules have become immobilized. Yet, in all cases the decay is described by a Kohlrausch function (cf. Eq. (3), below) with $\beta = 0.95$, and the apparent

This article is copyrighted as indicated in the article. Reuse of AIP content is subject to the terms at: http://scitation.aip.org/termsconditions. Downloaded to IP: 132.180.21.130 On: Wed, 11 Dec 2013 14:55:21

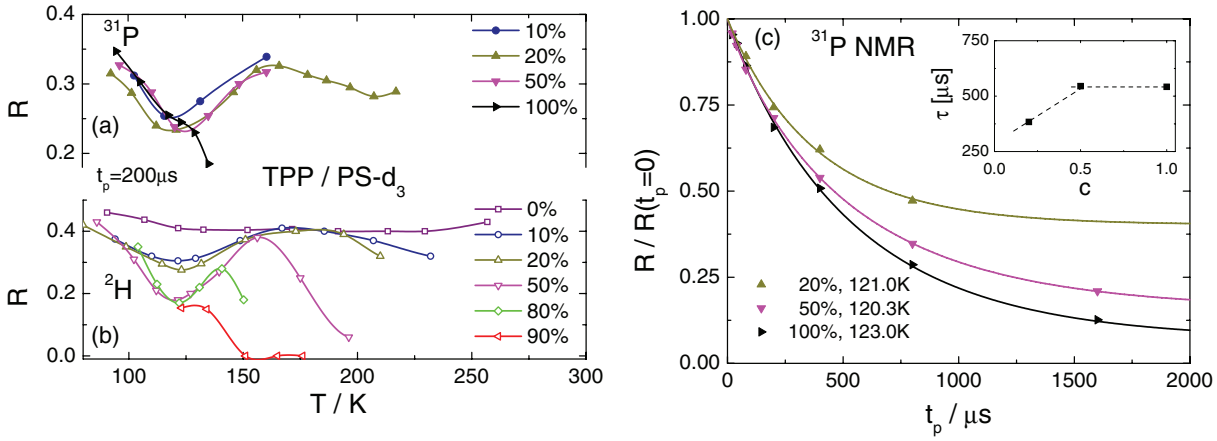

FIG. 11. Temperature dependence of line-shape parameter R at $t_p = 200\ \mu$s for (a) TPP and (b) PS-d$_3$; mass fractions as indicated. Lines serve as guides for the eye. (c) Dependence of $R(t_p)$, normalized to short t_p values, on the inter-pulse delay t_p as revealed by ^{31}P Hahn-echo; mass fractions, and temperatures as indicated; inset: time constant as a function of concentration, dashed lines: a possible interpretation.

time constant (Fig. 11(b), inset) becomes somewhat shorter as also observed in the dielectric spectra (cf. Fig. 2).

Neat PS is a type-A glass former not showing any spectrally resolved β-process in the DS spectra. This is also confirmed by ^{2}H spin-lattice relaxation measurements, which display only a weak temperature dependence in the glassy state as discussed before (cf. Fig. 3). Here, the question arises whether polystyrene in the mixture exhibits a β-process. Due to the selectivity of ^{2}H NMR probing solely the dynamics of the PS-d$_3$ molecules ^{2}H solid-echo spectra can give a clear-cut answer. Figure 12 shows a series of solid-echo spectra of TPP/PS-d$_3$ with $c = 50\%$ taken at different t_p values for three temperatures. A pronounced spectral change is observed at intermediate temperature $T = 121.5$ K. Similar results are observed for the $c = 20\%$ sample, in particular, the largest spectral change is again observed at 123.0 K. Moreover, the effect is found at similar temperatures as in the case of TPP studied by ^{31}P NMR. It seems that PS in the mixture shows some secondary relaxation, too, which passes through the solid-echo time window well below T_g at similar temperatures as in the case of TPP. The corresponding $R(T)$ values (at long inter-pulse delay $t_p = 200\ \mu$s) are included in Fig. 11(b). While no distinct temperature dependence is observed in neat PS-d$_3$ ($c = 0\%$), a minimum emerges when TPP molecules are added. Up to $c = 50\%$ the minimum depth increases monotonously. Remarkably, the minima do not shift with concentration and they are positioned roughly at the same temperature as the minima resulting from the ^{31}P Hahn-echo experiment on TPP (Fig. 11(a)). Actually, the minimum of $R(T)$ is slightly shifted to higher temperatures in the case of the ^{2}H spectra of PS-d$_3$, which is expected due to the higher coupling constant δ_Q. Taking $\delta_Q = 122.4$ kHz from an analysis of the low-temperature ^{2}H solid-state spectra of PS-d$_3$, the extracted time constant τ_β agrees well with those determined by DS as well as by ^{31}P Hahn-echo experiment (cf. Fig. 2). These findings strongly suggest that in the mixtures polystyrene monomers participate in the highly hindered reorientation of the β-process introduced by the TPP molecules. In other words, the β-process is not solely an intramolecular process. It appears that the TPP molecules cause the monomer units of polystyrene to wobble in a rather similar way and on the same time scale as the TPP molecules do.

In order to further investigate the t_p dependence of the ^{2}H solid-echo spectra, Fig. 13(a) shows the solid-echo spectra at very similar temperatures for the different investigated

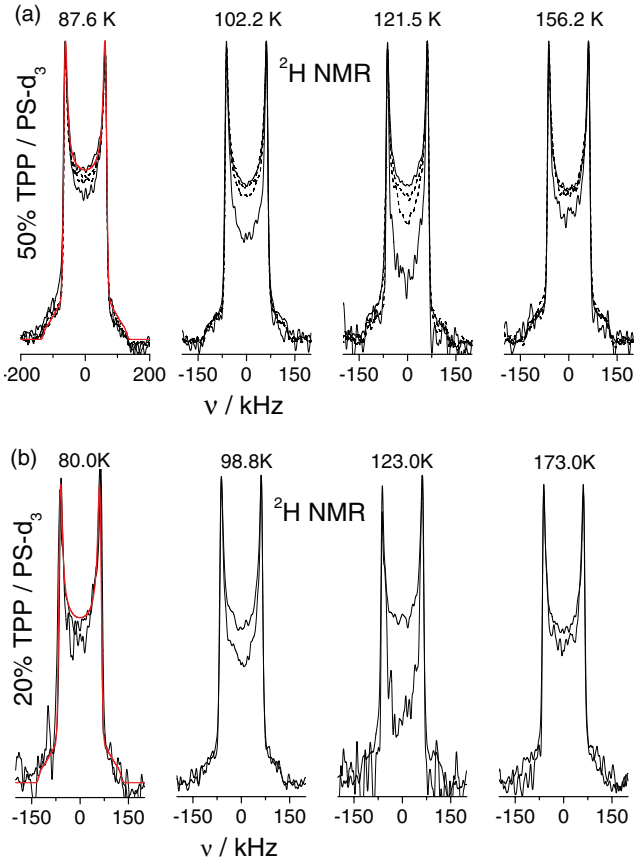

FIG. 12. ^{2}H NMR spectra of TPP/PS-d$_3$, normalized to maxima, at indicated temperatures. (a) c = 50%; each set with $t_p = 20\ \mu$s, 200 μs (solid lines), 40 μs and 80 μs (dashed lines), (b) $c = 20\%$, $t_p = 20\ \mu$s and 200 μs. For lowest temperatures fits with Pake spectral shape are included (solid red line, $\delta_Q = 122.4$ kHz).

This article is copyrighted as indicated in the article. Reuse of AIP content is subject to the terms at: http://scitation.aip.org/termsconditions. Downloaded to IP: 132.180.21.130 On: Wed, 11 Dec 2013 14:55:21

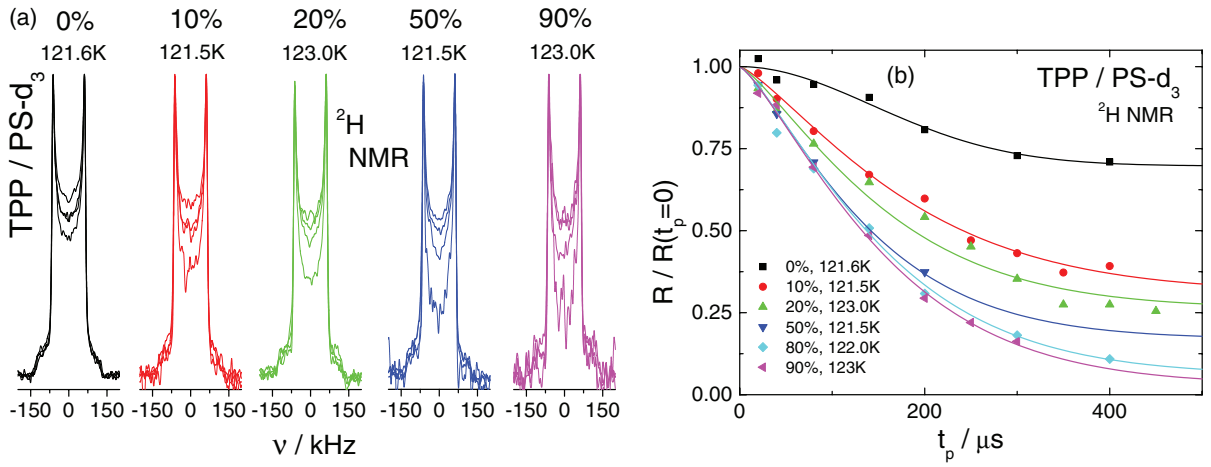

FIG. 13. (a) ^{2}H NMR spectra of TPP/PS-d$_3$ for various concentrations of TPP at indicated temperatures; each set with $t_p = 20$ μs, 40 μs, 80 μs, and 200 μs. (b) R values as a function of inter-pulse delay, normalized to short t_p value. Lines are fits according to Eq. (3).

concentrations. For neat PS-d$_3$ one recognizes only weak spectral changes, which is actually due to some other relaxation mechanism, while the spectral changes induced by large t_p values significantly grow with increasing TPP concentration. Explicitly, at $t_p = 200$ μs the spectral intensity at zero frequency is the lower, the higher c is. It seems as if the fraction of PS molecules participating in the β-process grows with the fraction of TPP molecules present in the mixture. Figure 13(b) displays the corresponding evolution of $R(t_p)$. For all concentrations c > 0 $R(t_p)$ decays on similar t_p time scale ($\tau = (170 \pm 20)$ ms and $\beta = 1.28$), while for $c = 0$ (neat PS-d$_3$) a qualitatively different, slower decay is observed. The latter finding is in accordance with the fact that actually neat PS does not exhibit a β-process and another relaxation process may be active. For $c = 90\%$ and $c = 80\%$ $R(t_p)$ decays down to very low values at long delay times, while for $c \leq 50\%$ $R(t_p)$ appears to level off at different plateaus at longest t_p. In particular, a systematic trend of the final plateau to increase with decreasing concentration is recognized.

To access quantitatively the decay $R(t_p)$ and in particular the plateau at longest times t_p we describe the normalized decay by the following expression[25]

$$R_n(t_p, c) = f_\beta(c) \cdot \exp\left(-\left(\frac{t_p}{\tau}\right)^\beta\right) + (1 - f_\beta(c)), \qquad (3)$$

where $f_\beta(c)$ is interpreted as a fraction of molecules which contributes to the β-process, and τ and β are parameters describing the effective time evolution of the echo spectra. We note that the latter time constant is not identical with τ_β as determined from the DS spectra. In the case of TPP, a free fit by Eq. (3) to $R(t_p)$ (cf. Fig. 11) provides similar relaxation times τ (and similar $\beta = 0.95 \pm 0.05$) with a small trend to become somewhat shorter at low $c = 20\%$. Since a correlation between τ and τ_β is expectable, this is in accordance with the DS result where a weak trend to shorter τ_β is revealed for $c < 60\%$ (cf. Fig. 3). The long-time value $1 - f_\beta$ is not any longer zero but increases with decreasing TPP concentration. The corresponding value $f_\beta(c)$ reflecting the fraction of TPP molecules participating in the β-process is found in Fig. 14. The higher is the TPP concentration, the higher is the fraction of TPP molecules participating in the β-process. We note that in the case of ethanol, cyano cyclohexane, and toluene (Fig. 5(a)) we find a plateau value $1 - f_\beta = 0.0 \pm 0.04$ while in the case of neat TPP we find $f_\beta = 0.93$, i.e., $1 - f_\beta = 0.07 \pm 0.04$ putting our above given statement on a quantitative basis: in neat glasses essentially all molecules take part in the β-process while this is no longer the case in a binary system.

In the case of PS-d$_3$ a corresponding analysis of $R(t_p)$ along Eq. (3) (solid lines in Fig. 13(b)) provides essentially the same time constants, but, nevertheless, varying fractions of PS molecules participating in the β-process. The result is included in Fig. 14. With increasing TPP concentration also the fraction of PS molecules participating in the β-process grows quickly. It even appears that the fraction f_β of PS is higher than that of TPP. This excess fraction becomes most conspicuous at $c = 0$, where a plateu value of $f_\beta(c = 0) = 0.25$ is found. This is somewhat unreasonable, since, due to the absence of TPP molecules, no contribution to the β-relaxation is expected at all. One can argue that, due to some further

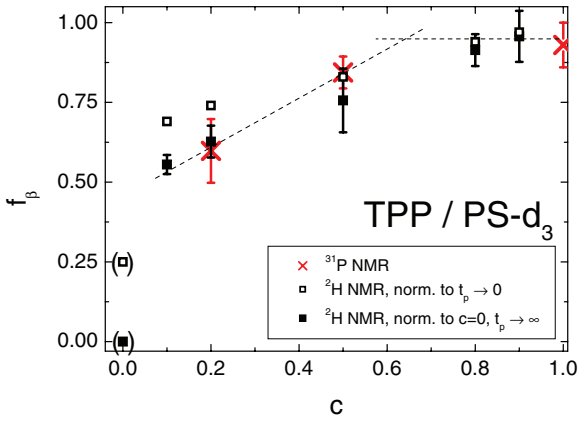

FIG. 14. Fraction of molecules of TPP (crosses) and PS-d$_3$ (full squares: normalized to behavior of neat PS-d$_3$; open squares: normalized to short t_p value) participating in the β-process as estimated by the Hahn-echo and solid-echo experiments. Dashed straight lines: A possible interpretation.

This article is copyrighted as indicated in the article. Reuse of AIP content is subject to the terms at: http://scitation.aip.org/termsconditions. Downloaded to IP: 132.180.21.130 On: Wed, 11 Dec 2013 14:55:21

relaxation process in neat PS, $R(t_p)$ decays to some plateau which has to be taken into account also in the mixture. Thus renormalizing $1 - f_\beta$ by $1 - f_\beta(neat\ PS)$, the fraction f_β decreases and becomes similar to that of TPP. Thus the fractions of TPP and PS molecules participating in the β-process coincide for each concentration.

As discussed above, the dynamics of neat PS-d_3 and TPP have also been characterized by the spin-lattice relaxation monitored as a function of temperature (cf. Fig. 3(a)). No indication of a β-process shows up for PS-d_3 while below T_g in TPP the ^{31}P relaxation is clearly controlled by the β-process. The findings for the TPP/PS mixture with $c = 50\%$ are shown in Fig. 3(b). With respect to the neat components, the results are now quite different. Below T_g the temperature dependences $T_1(T)$ of TPP and PS-d_3 run parallel, i.e., the same strong temperature dependence is observed in both methods. Above T_g a minimum is found for TPP which reflects the isotropic reorientation of the TPP molecules in the mixture. A similar minimum occurring yet at higher temperatures is found for PS-d_3. This difference directly reflects the decoupling of the primary (isotropic) dynamics of the components: in the mixture PS reorients much slower than TPP, a fact well known from results on asymmetric binary glass formers.[42,43] There is a further feature the detailed discussion of which is postponed to a forthcoming publication: At temperatures for which the T_1 minimum of TPP occurs, particularities are also observed in the ^{2}H relaxation of PS-d_3. This shows that the fast isotropic dynamics of TPP affects the polystyrene monomers leading to a highly hindered (i.e., non-isotropic) dynamics, however, occurring at similar time scale as the TPP molecules. These findings demonstrate that a plasticizer molecule does not only change the T_g but also induces additional dynamics on the polymer.

As in the case of neat TPP the temperature dependence of the spin-lattice relaxation can be understood on a quantitative level by taking the dielectric results into account. These provide the dynamic susceptibility determined by a temperature independent distribution of activation energies, which actually does not change significantly in the mixture. Analogously to the case of ^{31}P dielectric susceptibility data can be compared to $T_1(T)$ of ^{2}H NMR after extrapolating it to higher frequencies. As can be seen in Fig. 3(b) (dashed line) the slope of $T_1(T)$ of TPP as well as PS-d_3 is reproduced.

IV. DISCUSSION AND CONCLUSION

We have studied the secondary (β-) relaxation process in the binary glass mixture TPP/PS by dielectric spectroscopy as well as TPP/PS-d_3 by ^{31}P and ^{2}H NMR. While neat TPP exhibits a β-process (type-B glass former) and neat polystyrene shows none (type-A), in the mixture also PS-d_3 molecules clearly participate in the β-relaxation. Here, for both TPP and PS-d_3, NMR spectra reveal a spatially highly restricted motion as identified by NMR in other type-B systems, like toluene[16,22] or ethanol.[17,23] Up to our knowledge a Hahn-echo sequence (here for ^{31}P) has been applied for the first time to monitor the subtle spectral changes deep in the glass characteristic of the β-process. The dielectric spectra reflect a distribution of activation energies which is temperature independent; yet, its asymmetric shape is rather unusual for β-processes and does not change with concentration, a phenomenon observed also in other binary glass formers.[25,43,44] Even at a TPP concentration of $c = 10\%$ the mean activation energy is still similar to that of neat TPP. The β-process introduced by the type-B component survives in the mixture and induces the type-A molecule to participate in the relaxation process. Yet, in contrast to neat systems not all molecules participate in the β-process; islands of rigidity or immobility appear. The higher the concentration of the type-B component the higher is the fraction of both components which participate. We emphasize, as we do not find any indication for the mixed glasses to decompose, the immobilized molecules are not part of crystalline regions. Instead the mixtures become glasses with inhomogeneously distributed dynamics. In a recent ^{2}H NMR study of another binary system (toluene/aroclor) an indication of a threshold concentration has been found below which immobile type-B molecules appear.[25] Although not sufficient NMR data at various concentrations has been collected in the present study a similar behavior can be anticipated also for TPP/PS-d_3. Only below, say, $c = 60\%$ some relevant fraction of TPP or PS-d_3 appear to become immobilized. This corresponds with the (slight) change of the mean activation energy below 60% (cf. Figs. 7 and 9).

All together the presented experimental findings point into the direction that also the β-process exhibits some cooperative nature. When mixed with type-B molecules, type-A molecules do react to the highly hindered motion introduced by the β-process, actually a behavior expected in (dense) condensed matter. A similar phenomenon is observed for the decoupled isotropic reorientation of the TPP molecules in the vitrified matrix of polystyrene. Whether the extent of spatial hindrance is the same for the two molecules is yet to be investigated. In any case both components show dynamics on the same time scale.

ACKNOWLEDGMENTS

The authors acknowledge financial support by Deutsche Forschungsgemeinschaft (DFG) under Grant No. RO 907/10.

[1] G. Johari and M. Goldstein, J. Chem. Phys **53**, 2372 (1970).
[2] G. Williams and D. C. Watts, Trans. Faraday Soc. **67**, 1971 (1971).
[3] L. Wu, Phys. Rev. B **43**, 9906 (1991).
[4] A. Arbe, D. Richter, J. Colmenero, and B. Farago, Phys. Rev. E **54**, 3853 (1996).
[5] A. Kudlik, C. Tschirwitz, S. Benkhof, T. Blochowicz, and E. Rössler, Europhys. Lett. **40**, 649 (1997).
[6] K. L. Ngai and M. Paluch, J. Chem. Phys. **120**, 857 (2004).
[7] C. Gainaru, R. Kahlau, E. A. Rössler, and R. Böhmer, J. Chem. Phys. **131**, 184510 (2009).
[8] A. Kudlik, S. Benkhof, T. Blochowicz, C. Tschirwitz, and E. Rössler, J. Mol. Struct. **479**, 201 (1999).
[9] M. Paluch, S. Pawlus, S. Hensel-Bielowka, E. Kaminska, D. Prevosto, S. Cappacioli, P. A. Rolla, and K. L. Ngai, J. Chem. Phys. **122**, 234506 (2005).
[10] N. Petzold, B. Schmidtke, R. Kahlau, D. Bock, R. Meier, B. Micko, D. Kruk, and E. A. Rössler, J. Chem. Phys. **138**, 12A510 (2013).
[11] L. Comez, D. Fioretto, L. Palmieri, L. Verdini, P. A. Rolla, J. Gapinski, T. Pakula, A. Patkowski, W. Steffen, and E. W. Fischer, Phys. Rev. E **60**, 3086 (1999).
[12] A. Brodin, E. A. Rössler, R. Bergman, and J. Mattsson, Eur. Phys. J. B **36**, 349 (2003).

This article is copyrighted as indicated in the article. Reuse of AIP content is subject to the terms at: http://scitation.aip.org/termsconditions. Downloaded to IP: 132.180.21.130 On: Wed, 11 Dec 2013 14:55:21

[13]C. Tschirwitz, S. Benkhof, T. Blochowicz, and E. Rössler, J. Chem. Phys. **117**, 6281 (2002).
[14]S. Benkhof, A. Kudlik, T. Blochowicz, and E. Rössler, J. Phys.: Condens. Matter **10**, 8155 (1998).
[15]M. Vogel and E. Rössler, J. Phys. Chem. B **104**, 4285 (2000).
[16]M. Vogel and E. Rössler, J. Chem. Phys. **114**, 5802 (2001).
[17]M. Vogel, C. Tschirwitz, G. Schneider, C. Koplin, P. Medick, and E. Rössler, J. Non-Cryst. Solids **307–310**, 326 (2002).
[18]S. A. Lusceac, C. Gainaru, M. Vogel, C. Koplin, P. Medick, and E. A. Rössler, Macromolecules **38**, 5625 (2005).
[19]G. Schneider, Diploma thesis, Universität Bayreuth, 2001.
[20]B. Micko, S. A. Lusceac, H. Zimmermann, and E. A. Rössler, J. Chem. Phys **138**, 074503 (2013).
[21]B. Micko, D. Kruk, and E. A. Rössler, J. Chem. Phys. **138**, 074504 (2013).
[22]M. Vogel and E. Rössler, J. Chem. Phys. **115**, 10883 (2001).
[23]M. Vogel, P. Medick, and E. A. Rössler, Annu. Rep. NMR Spectrosc. **56**, 231 (2005).
[24]M. Vogel and E. Rössler, J. Magn. Reson. **147**, 43 (2000).
[25]B. Micko, C. Tschirwitz, and E. A. Rössler, J. Chem. Phys. **138**, 154501 (2013).
[26]S. Adishchev, D. Bock, C. Gainaru, R. Kahlau, B. Micko, N. Petzold, B. Pötzschner, and E. A. Rössler, Z. Phys. Chem. **226**, 1149 (2012).
[27]H. Wagner and R. Richert, J. Phys. Chem. B **103**, 4071 (1999).
[28]T. Blochowicz, C. Tschirwitz, S. Benkhof, and E. A. Rössler, J. Chem. Phys. **118**, 7544 (2003).
[29]D. Schaefer, J. Leisen, and H. W. Spiess, J. Magn. Reson., Ser. A **115**, 60 (1995).
[30]M. Bloom, J. H. Davis, and M. I. Valic, Can. J. Phys. **58**, 1510 (1980).
[31]K. Schmidt-Rohr and H. W. Spiess, *Multidimensional Solid-State NMR and Polymers* (Academic Press, New York, 1994) p. 66.
[32]S. A. Lusceac, Ph.D. thesis, Universität Bayreuth, 2005.
[33]Y. He, T. R. Lutz, and M. D. Ediger, Macromolecules **37**, 5032 (2004).
[34]C. Gainaru, A. Rivera, S. Putselyk, G. Eska, and E. A. Rössler, Phys. Rev. B **72**, 174203 (2005).
[35]C. Gainaru, R. Böhmer, R. Kahlau, and E. Rössler, Phys. Rev. B **82**, 104205 (2010).
[36]N. G. McCrum, B. E. Read, and G. Williams, *Anelastic and Dielectric Effects in Polymer Solids* (Wiley, London, 1967).
[37]J. Hintermeyer, A. Herrmann, R. Kahlau, C. Goiceanu, and E. A. Rössler, Macromolecules **41**, 9335 (2008).
[38]E. Rössler and P. Eiermann, J. Chem. Phys. **100**, 5237 (1994).
[39]T. Blochowicz, A. Kudlik, S. Benkhof, J. Senker, and E. A. Rössler, J. Chem. Phys **110**, 12011 (1999).
[40]L. Wu and S. Nagel, Phys. Rev. B **46**, 11198 (1992).
[41]J. Wiedersich, S. V. Adichtchev, and E. Rössler, Phys. Rev. Lett. **84**, 2718 (2000).
[42]D. Bingemann, N. Wirth, J. Gmeiner, and E. A. Rössler, Macromolecules **40**, 5379 (2007).
[43]T. Blochowicz, S. A. Lusceac, P. Gutfreund, S. Schramm, and B. Stühn, J. Phys. Chem. B **115**, 1623 (2011).
[44]D. Cangialosi, A. Alegría, and J. Colmenero, J. Chem. Phys. **128**, 224508 (2008).

This article is copyrighted as indicated in the article. Reuse of AIP content is subject to the terms at: http://scitation.aip.org/termsconditions. Downloaded to IP: 132.180.21.130 On: Wed, 11 Dec 2013 14:55:21

Publikation 2

Dynamics of asymmetric binary glass formers. I. A dielectric and nuclear magnetic resonance spectroscopy study

R. Kahlau, D. Bock, B. Schmidtke, and E. A. Rössler
The Journal of Chemical Physics 140, 044509 (2014).

© 2014 AIP Publishing LLC
doi:10.1063/1.4861428

THE JOURNAL OF CHEMICAL PHYSICS **140**, 044509 (2014)

Dynamics of asymmetric binary glass formers. I. A dielectric and nuclear magnetic resonance spectroscopy study

R. Kahlau, D. Bock, B. Schmidtke, and E. A. Rössler[a)]
Experimentalphysik II, Universität Bayreuth, 95440 Bayreuth, Germany

(Received 30 October 2013; accepted 20 December 2013; published online 29 January 2014)

Dielectric spectroscopy as well as ^{2}H and ^{31}P nuclear magnetic resonance spectroscopy (NMR) are applied to probe the component dynamics of the binary glass former tripropyl phosphate (TPP)/polystyrene (PS/PS-d$_3$) in the full concentration (c_{TPP}) range. In addition, depolarized light scattering and differential scanning calorimetry experiments are performed. Two glass transition temperatures are found: $T_{g1}(c_{TPP})$ reflects PS dynamics and shows a monotonic plasticizer effect, while the lower $T_{g2}(c_{TPP})$ exhibits a maximum and is attributed to (faster) TPP dynamics, occurring in a slowly moving or immobilized PS matrix. Dielectric spectroscopy probing solely TPP identifies two different time scales, which are attributed to two sub-ensembles. One of them, again, shows fast TPP dynamics (α_2-process), the other (α_1-process) displays time constants identical with those of the slow PS matrix. Upon heating the α_1-fraction of TPP decreases until above some temperature T_c only a single α_2-population exists. Inversely, below T_c a fraction of the TPP molecules is trapped by the PS matrix. At low c_{TPP} the α_2-relaxation does not follow frequency-temperature superposition (FTS), instead it is governed by a temperature independent distribution of activation energies leading to correlation times which follow Arrhenius laws, i.e., the α_2-relaxation resembles a secondary process. Yet, ^{31}P NMR demonstrates that it involves isotropic reorientations of TPP molecules within a slowly moving or rigid matrix of PS. At high c_{TPP} the super-Arrhenius temperature dependence of $\tau_2(T)$, as well as FTS are recovered, known as typical of the glass transition in neat systems. © *2014 AIP Publishing LLC*. [http://dx.doi.org/10.1063/1.4861428]

I. INTRODUCTION

The evolution of the dynamic susceptibility in neat glass formers is well documented starting at temperatures close to the boiling point and reaching the glass transition temperature T_g, where the liquid becomes an amorphous solid.[1–7] In particular, light scattering, dielectric, and NMR spectroscopy have provided a wealth of information. In contrast, binary glass formers are less studied, and no broadly accepted picture of the rather complex dynamics has established so far. Of special interest are so-called asymmetric glass formers, which are characterized by a large difference of the T_g values of the components. They are most conveniently prepared by blending a polymer with a low-molecular mass additive,[8–13] yet also purely low-molecular weight mixtures have been studied.[14–18] It is well established that such systems exhibit two glass transition temperatures albeit they are fully miscible.[19–25] In other words, such binary liquids display pronounced dynamic heterogeneities,[5,26,27] which are in particular well documented by NMR.[28–30] For example, intrinsic confinement effects are expected when the mobile (low-T_g) component still relaxes in a matrix of an arrested (high-T_g) component. Indeed, the NMR phenomenology is similar to that of neat glass formers embedded in porous systems.[31–34]

Binary systems consisting of soft or hard spheres have also been investigated by simulations[35–37] as well as by mode coupling theory (MCT).[38–41] In contrast to neat systems, for which a type-B glass transition scenario is expected by MCT, which is triggered by cage formation and characterized by a discontinuous change of the non-ergodicity parameter f from zero to $f > 0$ at a critical temperature T_c, the mobile molecules in binary liquids are expected to exhibit a type-A transition, and f should increase continuously from zero upon cooling below T_c. Here, the mobile (small) particles undergo a localization transition, while the less mobile (large) ones are still arrested due to the cage effect. In a recent paper by Blochowicz *et al.*[13] experimental hints have been given that indeed such type-A transitions might be observed in mixed molecular liquids. We note that such dynamic heterogeneities have also been explained either by concentration fluctuations[42,43] or so-called self-concentration effects.[44] It is the aim of the present contribution to dwell on this issue by applying several experimental methods to study selectively the dynamics of each component on a (short-chain) polymer-additve system.

The binary glass tripropyl phosphate (TPP)/(deuterated) polystyrene (PS/PS-d$_3$, $M_w \approx 2 \times 10^3$ g/mol) is characterized by means of dielectric spectroscopy (DS), ^{2}H and ^{31}P NMR as well as by dynamic depolarized light scattering (DLS) and differential scanning calorimetry (DSC). Thirteen concentrations equally spread over the full concentration range are investigated. The system is characterized by a large T_g contrast of the pure components ($\Delta T_g \cong 200$ K).[45,46] Due to the choice of this system the application of ^{31}P and ^{2}H NMR allows for probing selectively the dynamics of TPP

a)Author to whom correspondence should be addressed. Electronic mail: ernst.roessler@uni-bayreuth.de.

 © 2014 AIP Publishing LLC

This article is copyrighted as indicated in the article. Reuse of AIP content is subject to the terms at: http://scitation.aip.org/termsconditions. Downloaded to IP: 132.180.21.93 On: Wed, 29 Jan 2014 15:49:49

TABLE I. TPP mass concentrations c_{TPP} of mixtures studied by the different methods, including the assumed errors (see text). NMR data of 80% will be discussed in Paper II.[47]

c_{TPP} [%] nom.	0	10	20	30	36	45	50	60	70	80	90	95	100
DS	0	8 ± 3	18 ± 3	29 ± 2	…	45 ± 1	…	60 ± 1	…	80 ± 1	90 ± 1	95 ± 1	100
DSC	0	10 ± 1	20 ± 1	…	36 ± 1	45 ± 1	…	60 ± 1	70 ± 1	83 ± 1	90 ± 1	…	100
DLS	…	…	…	…	…	…	…	…	…	80 ± 1	90 ± 1	…	100
^{2}H NMR	0	10 ± 1	20 ± 1	…	…	…	50 ± 1	…	…	80 ± 1 (Paper II)[47]	90 ± 1	…	…
^{31}P NMR	…	10 ± 1	20 ± 1	…	…	…	50 ± 1	…	…	80 ± 1 (Paper II)[47]	90 ± 1	…	100

and PS-d_3, while dielectric spectroscopy provides essentially information on the dynamics of the mobile component TPP, since its molecular dipole moment is significantly higher than that of PS. Regarding the pronounced β-process present in the mixed system, it has been studied thoroughly by our group.[45] Its time constant shows the typical Arrhenius behavior with an activation energy $\langle E \rangle / k \cong 24\ T_g$, which virtually does not vary due to mixing, and which is associated with a spatially highly hindered dynamics as found in other glasses. Actually, throughout this work, only a spatially highly restricted process shall be understood as a β-process. Although introduced by TPP, in the mixture both components participate in the β-process. This has been taken as an indication of its cooperative nature.

In the present contribution we focus on the dynamics of both components above T_g, more precisely above T_{g2} of the mobile component. By performing DSC experiments we can identify two glass transition temperatures. We will demonstrate that the high-T_g component PS shows liquid dynamics similar to that of neat systems while TPP displays rather complex heterogeneous dynamics. For example, the temperature dependence of the correlation time changes from super-Arrhenius at high c_{TPP} to Arrhenius behavior at low concentrations. Thus, the additive process may be confused with a β-process, and it is up to NMR to proof whether the process is still liquid-like (isotropic) or β-process-like.

This contribution consists of two parts, the present one essentially deals with the results collected by dielectric spectroscopy, complemented by time constants provided by NMR and DLS as well as DSC. In Paper II[47] continuative NMR experiments are reported and analyzed in accordance with the dielectric results.

II. EXPERIMENTAL DETAILS AND DATA ANALYSIS

A. Systems

A polystyrene sample with the molecular mass $M_w = 2250$ g/mol (PS), and another polystyrene sample, partially deuterated at the backbone, with very similar mass $M_w = 2440$ g/mol (PS-d_3) were purchased from Polymer Standards Service (Mainz, Germany) and used without further treatment. For the DS experiments PS was used for the preparation of the mixtures, while PS-d_3 was used for the NMR measurements. Tripropyl phosphate (TPP, 99%) was bought from Sigma Aldrich and used as received, too. We do not find any indication that phase separation or crystallization occurs in the mixtures. Among other tests, light scattering experiments show a homogeneous sample. NMR and DLS samples were prepared in the measurement tubes and cells, while the DSC and DS samples had to be prepared in separate test tubes (exact concentrations valid for different methods are listed in Table I). Generally a concentration error of $\pm 1\%$ is assumed for the sample preparation. After the preparation all sample vessels were left at elevated temperatures for one or two days in order to guarantee a maximum possible spatial homogeneity. In the case of DSC and DS the sample had to be transferred afterwards from the preparation vessel to the measurement cell. In the case of DS the samples of low concentrations had to be heated carefully during the transfer, because they are highly viscous at room temperature. Since some fraction of the TPP content may have evaporated during this process, the assumed actual error for the $c_{TPP} = 10\%$–30% samples is somewhat higher (Table I). In contrast, the DSC samples could be transferred to the measurement cells without heating. For the sake of clarity the nominal (nom.) concentrations are discussed throughout the paper.

B. Dielectric spectroscopy

Dielectric measurements were carried out with the Alpha-A Analyzer by Novocontrol while temperature was kept constant within ± 0.2 K by using the Quatro-H temperature controller by Novocontrol. The absolute accuracy is assumed to be better than ± 1 K. The sample cell has the design described by Wagner and Richert and assures a constant sample volume.[48] In order to extract time constants from the dielectric susceptibility data, unless described differently in the text a Kohlrausch stretched exponential was used to fit the α_1-relaxation peaks (on the timescale of PS dynamics), and the mean relaxation time $\tau = \Gamma(1/\beta_K)\ \tau_0/\beta_K$ is discussed. For the α_2-peaks (reflecting faster TPP dynamics) a Havriliak-Negami (HN) function had to be used due to stretching parameters significantly less than unity on the low-frequency side of the peak. In these cases the maximum correlation times given by $\tau_{max} = 1/(2\pi \nu_{max})$ are discussed.

C. Depolarized light scattering

Depolarized dynamic light scattering measurements were performed with a vertically polarized Coherent Verdi-V2 laser at a wavelength of 532 nm and 200 mW optical power in combination with a tandem Fabry-Pérot interferometer (TFPI; JRS Scientific, triple-pass-tandem Etalon) working parallel with a double monochromator (DM; Jobin Yvon, U1000). The TFPI was operated at horizontal polarization in almost

This article is copyrighted as indicated in the article. Reuse of AIP content is subject to the terms at: http://scitation.aip.org/termsconditions. Downloaded to IP: 132.180.21.93 On: Wed, 29 Jan 2014 15:49:49

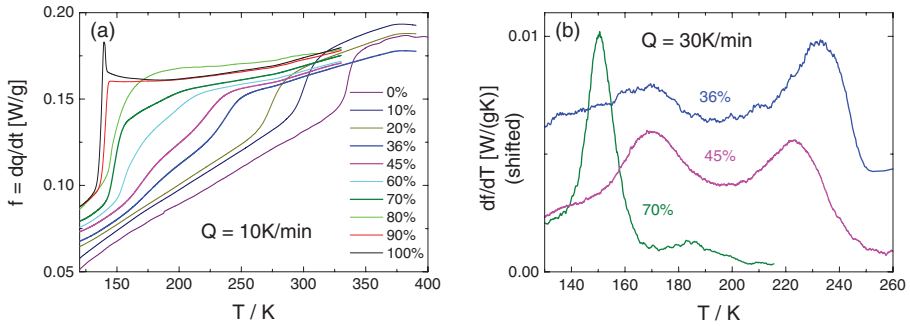

FIG. 1. (a) DSC traces (heat flow per sample mass $f = dq/dt$) for mixtures and neat systems (c_{TPP} = 0%–100%) at the heating rate Q = 10 K/min. (b) Temperature derivative of DSC traces df/dT at heating rate Q = 30 K/min for indicated concentrations.

backscattering geometry, whereas the DM was operated at orthogonal geometry (for details, see Refs. 49 and 50). The TFPI measurements were done with three different free spectral ranges, and the DM measurements with two combinations of slits and frequency intervals. The spectral parts are then adjusted in amplitude to match together and form a smooth spectrum.

D. DSC

DSC experiments were performed with a Q1000 analyzer by TA Instruments. By using a liquid nitrogen cooling system the temperature range T = 120–400 K was covered. Experiments presented were run at heating rates Q = 10–40 K/min. Figure 1(a) displays DSC traces of neat PS and TPP as well as mixtures with c_{TPP} = 10%–90% TPP in PS (nominal concentrations, see Table I), recorded with a heating rate of Q = 10 K/min. For both of the neat samples a distinct glass step is found. For the mixtures a comparably broad glass transition temperature range is observed, consisting of two individual, more or less separated steps. This is best seen in Fig. 1(a) for intermediate concentrations. In order to achieve a better resolution of both contributions the temperature derivative of the DSC traces[13] are considered (Fig. 1(b)). The best results were obtained here by choosing a heating rate of Q = 30 K/min for all samples. Glass temperatures as yielded by DSC experiments were defined as the peak temperatures of the temperature derivatives just described (cf. Fig. 10).

In order to calculate calorimetric time constants the formula,

$$\tau_{cal} \approx \frac{RT_g^2}{\Delta H_{eff}} \cdot \frac{1}{Q}, \tag{1}$$

was used.[17,51] It turns out that for all systems a constant prefactor $\frac{RT_g^2}{\Delta H_{eff}} \approx 1.7$ could be used in good approximation, leading to an error in τ_{DSC} smaller than a factor of two. The extracted time constants are included in Fig. 9.

E. NMR

Regarding the NMR analysis we refer to Paper II.[47] In the present paper we only report some of the NMR results concerning correlation times.

III. RESULTS

A. Neat components – dielectric spectra

The susceptibility spectra of PS (T_g = 335 K) are shown in Fig. 2 and fit well into the collection of dielectric data on polystyrene samples of different molecular weights given in Ref. 52. Above T_g a pronounced peak is visible, which is identified as structural or α-relaxation shifting to high frequencies with increasing temperature. The low amplitude reflects the rather non-polar nature of the PS monomer. Close to T_g, the high-frequency side of the α-peak is made up of a crossover from one power-law behavior to another one, the latter often being called excess wing.[1,7,53] When the sample is cooled below T_g the α-peak moves out of the frequency window and the signal, now consisting only of the excess wing contribution, drops close to the resolution limit of the spectrometer. No indications for a secondary (β) relaxation peak are observed for PS (cf. Ref. 45).

The dielectric spectra of neat TPP (T_g = 135 K) are also displayed in Fig. 2. As in the case of PS, above T_g an α-relaxation peak can be identified, the amplitude of which exceeds the one of PS by a factor of 1000, i.e., the TPP molecule carries a high dipole moment. At frequencies several decades above the maximum position of the α-peak a secondary relaxation is well resolved (type-B glass former). This secondary (β-) peak survives at temperatures below T_g when the α-peak has already left the frequency window. When temperature is increased above, say, T = 150 K, both peaks approach each

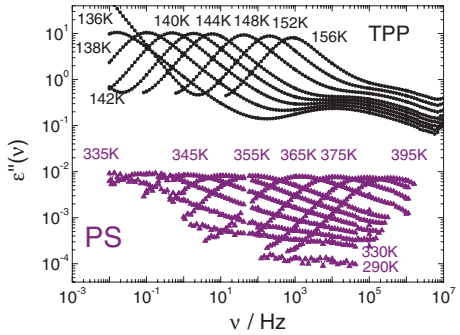

FIG. 2. Susceptibility spectra of neat TPP (top, circles; temperatures indicated). Dielectric spectra of neat PS; T = 290 K and T = 330–355 K in 5 K steps, T = 365–395 K in 10 K steps (bottom, triangles; some temperatures indicated).

This article is copyrighted as indicated in the article. Reuse of AIP content is subject to the terms at: http://scitation.aip.org/termsconditions. Downloaded to IP: 132.180.21.93 On: Wed, 29 Jan 2014 15:49:49

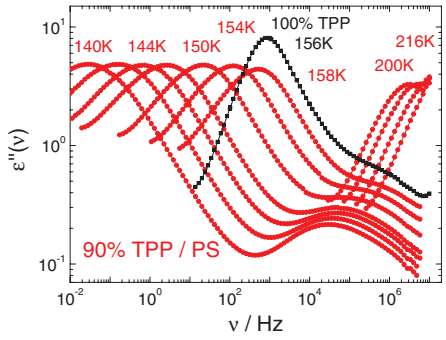

FIG. 3. Susceptibility of the mixture 90% TPP in PS (circles, some temperatures indicated). Data of neat TPP at $T = 156$ K for comparison (squares). Temperature gap is due to crystallization.

other until above $T = 156$ K the measurement of the supercooled liquid cannot be continued due to the crystallization of the sample. Spectra of the β-process have been analyzed in Refs. 45 and 54, and are not considered further here. At the low-frequency side of the α-peak a contribution of ionic conductivity is found which, for the sake of clarity, is only shown for the 152 K data of TPP.

Time constants of TPP and PS, as well as of some mixtures, are shown in Fig. 5. A collection of the time constants of all analyzed systems is given in Fig. 9. Good agreement with NMR measurements on neat PS[55] is observed. We further note that FTS applies for the spectra of the neat systems, i.e., all spectra can be collapsed to a single master curve (cf. Fig. 11). This feature is well known for being characteristic of cooperative dynamics.[2,7]

B. Mixtures

In order to develop a conclusive picture of the relaxation processes over the full concentration range it is useful to start with the dielectric results of the very high and the very low concentrated mixtures, i.e., the limiting cases of the investigated concentration series. Figure 3 shows the susceptibility of 90% TPP/PS, i.e., some small amount of polystyrene has been added to TPP. For comparison one spectrum of neat TPP (not scaled) is included in Fig. 3. Note that due to the low dipole moment of PS exclusively TPP dynamics is monitored. Clearly, the α-peak of the 90% sample is significantly broader, and the maximum value of the peaks is lower than in the case of 100% TPP. In particular, the low-frequency side of the α-peaks follows obviously a power-law with a lower exponent than in the case of neat TPP. In contrast, the high-frequency flanks of the relaxation peaks found for both samples are almost parallel. The peak position of the 158 K data set of the 90% mixture is situated at a lower frequency than the one of the 156 K data set of neat TPP. This slowing down of the TPP dynamics is due to the anti-plasticizer effect caused by the presence of PS. TPP time constants $\tau_{max} = 1/(2\pi\nu_{max})$ provided by DS (full red circles) as well as ^{31}P-NMR (open red circles, cf. Paper II[47]) and DLS (red pentagons) are included in Fig. 5 (nominal concentrations given there, see Table I). Good agreement between all three methods is found.

Figure 4 shows dielectric data of the (a) 10% and (b) 20% TPP/PS mixture. In contrast to the 90% mixture now two relaxation phenomena (grey and black data points) are observed. In Figure 4(b) the onset of the β-relaxation is recognized at high frequencies for the spectra at 169 K and 190 K. Note that for the mixtures the spectra of the β-process below T_g (more precisely below T_{g2}, cf. below) are always omitted (for an analysis of the β-process see Ref. 45). Regarding high temperatures (triangles), the $c_{TPP} = 10\%$ mixture shows relaxation peaks with a low-frequency flank following a Debye behavior, i.e., $\varepsilon'' \sim \nu^1$, and FTS holds in good approximation. At lower temperatures ($c_{TPP} = 10\%$: $T = 163$–281 K; $c_{TPP} = 20\%$: $T = 169$–270 K), when the peaks just discussed have left the accessible frequency range, another relaxation peak (circles) dominates the susceptibility, which exhibits a strong flattening on the low-frequency flank qualitatively similar to what is also observed for TPP in the 90% mixture. Moreover, FTS does not apply. This relaxation is best resolved in the 20% data (Fig. 4(b)).

For the $c_{TPP} = 20\%$ sample time constants of both relaxation peaks are shown in Fig. 5, the time constants for all mixtures are collected in Fig. 9 and will be discussed later. As mentioned in Sec. II B a Kohlrausch function was fitted to the high-temperature peaks (later called α_1-relaxation), and a HN function was fitted to the peak found at lower temperatures (α_2-relaxation, see below). While the high-temperature relaxation shows a strongly non-Arrhenian temperature dependence, which is similar to that of neat PS, yet shifted to somewhat lower temperature, the low-temperature relaxation

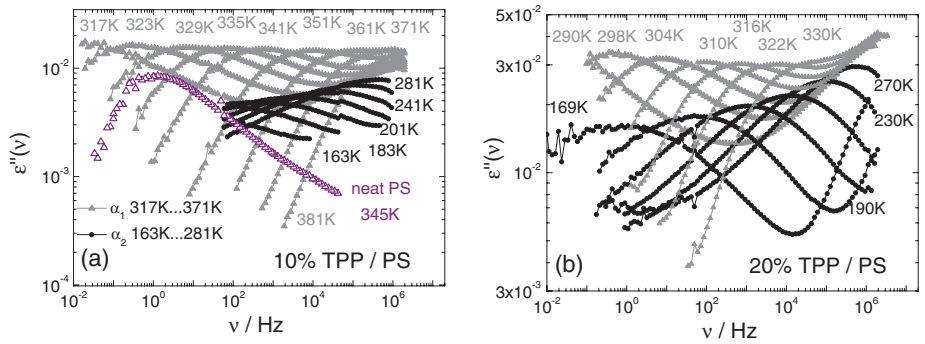

FIG. 4. Dielectric susceptibility of TPP/PS mixtures with low TPP concentration. Triangles, higher temperatures: α_1-relaxation; full circles, lower temperatures: α_2-relaxation. (a) 10% TPP in PS; open triangles: pure PS at 345 K. (b) 20% TPP in PS.

This article is copyrighted as indicated in the article. Reuse of AIP content is subject to the terms at: http://scitation.aip.org/termsconditions. Downloaded to IP: 132.180.21.93 On: Wed, 29 Jan 2014 15:49:49

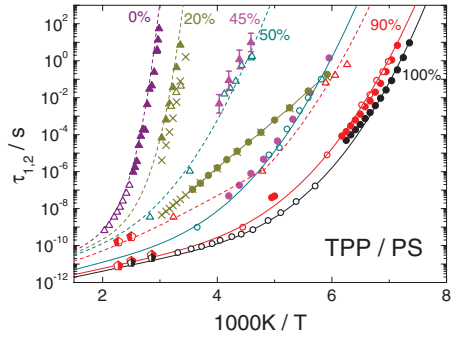

FIG. 5. Time constants for selected mixtures with (nominal) $c_{TPP} = 0\%$, 20%, 45%, 50%, 90%, 100% TPP in PS as obtained by DS (full symbols) and ^{2}H or ^{31}P NMR (open symbols). See Table I for exact concentration values. For $c_{TPP} = 0\%$ NMR data by He *et al.*[55] are included, and for TPP we included ^{31}P NMR results.[46] Triangles: time constants of the α_1-process, circles: α_2-process; Crosses (x): results obtained by the scaling analysis of dielectric data discussed in Appendix A. Pentagons (⬟): light scattering data of α_1-process. Pentagons (◗): DLS data of α_2-process. Lines are guides for the eye; solid lines concern the α_2-relaxation, dashed lines represent the α_1-process. Except the case of $\tau_1(T)$ for $c_{TPP} = 45\%$ error bars are estimated to be smaller than the size of the symbols.

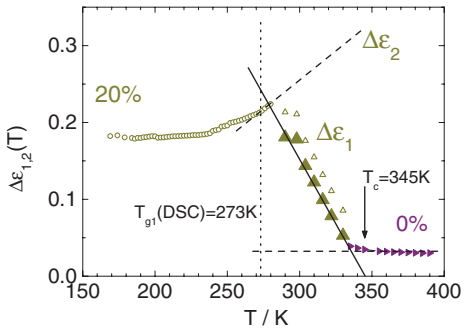

FIG. 6. Relaxation strengths $\Delta\varepsilon_{1,2}(T)$ of the 20% mixture as a function of temperature: $\Delta\varepsilon_2$ of the α_2-process (open circles); obtained from fitting procedure described in Appendix A (cf. Fig. 13). Linear extrapolation of the α_2-relaxation strength indicated as dashed line. Open triangles: $\Delta\varepsilon_1$ of the α_1 process; full triangles (▲):$\Delta\varepsilon_1(T)$ after subtraction of PS contribution. Full triangles (▶): α-process of neat PS. Dashed line: extrapolation of $\Delta\varepsilon(T)$ of neat PS, approximated as constant. Solid line: guide for the eye. Dotted line: Glass temperature T_{g1} (associated with the α_1-process) as obtained by DSC measurements.

follows an Arrhenius law with a rather low activation energy ($E_A(20\%) = 6058$ K $\approx 21T_{g1}$; $E_A(10\%) = 5241$ K $\approx 17T_{g1}$). ^{2}H-NMR experiments probing again the PS dynamics yield correlation times in good agreement with the time constants of the dielectric high-temperature peak (cf. Fig. 5). Comparing the spectral shapes of the relaxations, the high-temperature peak in the 10% mixture is broader and by a factor of about two higher than the α-relaxation of neat PS, in the case of $c_{TPP} = 20\%$ by a factor of four. In other words, the high-temperature peaks are dominated by the TPP signal. Thus we conclude that a fraction of TPP molecules is associated with PS, and therefore part of its α-relaxation. In the following, this relaxation shall be called α_1-process, and the faster relaxation α_2-process. The nature of the latter remains still to be clarified (see below), though, given the two T_g reported in the mixtures, it is natural to assume that it belongs to a second population of TPP molecules reorienting highly decoupled from the PS component. The process may be a liquid-like (isotropic) motion or, given its Arrhenius temperature dependence with rather low-activation energy at low concentrations, a kind of secondary β-process. Clearly, at high TPP concentrations also the α_2-process displays a super-Arrhenius temperature dependence, and for $c_{TPP} \to 1$ it develops continuously into the primary process of neat TPP.

Another phenomenon can be recognized for both data sets in Fig. 4. While the amplitude of the α_1-process decreases, the amplitude of the α_2-process increases with temperature. It appears that, when temperature rises, more and more TPP molecules are freed from being associated with the polymer dynamics. This phenomenon is quantified in Fig. 6, where the relaxation strengths $\Delta\varepsilon_{1,2}(T)$ of both processes are displayed for the case of the 20% mixture. The corresponding fitting strategy is explained in Appendix A. At low temperatures $\Delta\varepsilon_2(T)$ increases only weakly with T while at high temperatures a stronger increase is observed. A complementary decrease is revealed for the relaxation strength $\Delta\varepsilon_1(T)$ of the α_1-relaxation. The rise of $\Delta\varepsilon_2(T)$ around T_g may again remind of the universal behavior of β-processes found in structural as well as orientational glasses.[54,56] In the present case, interpreting the α_2-relaxation again as a population of fast molecules (TPP) in a matrix of slow molecules (PS and TPP), a redistribution of TPP molecules among the two populations takes place, which finally leads to the disappearance of the slowly moving TPP fraction at high temperatures. In other words, when temperature is lowered, more TPP molecules will contribute to the α_1-dynamics dictated by the PS segments instead of performing the α_2-relaxation. After subtraction of the contribution of neat PS (weighted with $c_{PS} = 1 - c_{TPP}$), which is approximated as a constant (dashed line), from the $\Delta\varepsilon_1(T)$ the full triangles in Fig. 6 are obtained. Accepting a linear extrapolation, one finds a temperature $T_c = 345$ K, at which the TPP molecules attached to the slow reorienting PS molecules disappear. Above T_c only fast TPP and slow PS molecules exist.

In Fig. 7 the relaxation strengths $\Delta\varepsilon_1(c_{TPP})$ and $\Delta\varepsilon_2(c_{TPP})$ for the α_1- and α_2-processes of different mixtures are compared. Since at $c_{TPP} > 45\%$ the α_1-relaxation is not discernible in the DS spectra, and at low c_{TPP} both processes are never situated in the accessible frequency range

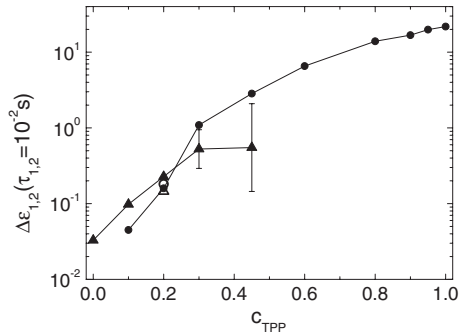

FIG. 7. Relaxation strengths $\Delta\varepsilon_{1,2}$ of α_1- relaxation (▲) and α_2-relaxation (●), respectively, probed at $\tau_{1,2} = 10^{-2}$ s for different concentrations. Results of the fitting procedure explained in Appendix A are included for $c_{TPP} = 20\%$ ($\Delta\varepsilon_1$:Δ, $\Delta\varepsilon_2$: ○). Lines: guides for the eye.

This article is copyrighted as indicated in the article. Reuse of AIP content is subject to the terms at: http://scitation.aip.org/termsconditions. Downloaded to IP: 132.180.21.93 On: Wed, 29 Jan 2014 15:49:49

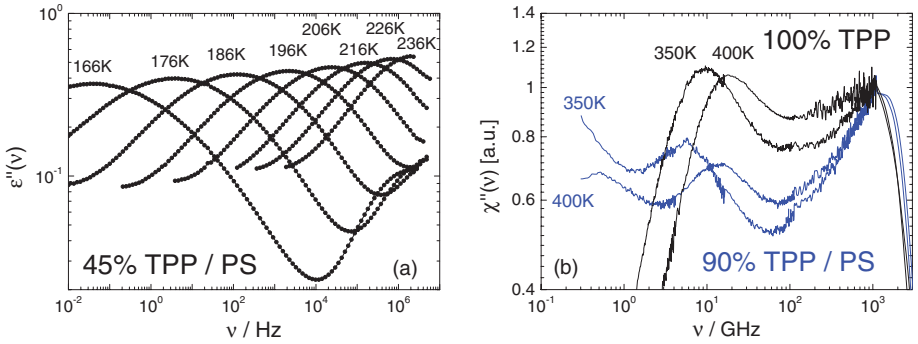

FIG. 8. (a) Dielectric susceptibility of the 45% mixture. (b) Depolarized light scattering spectra of 90% mixture (blue) and neat TPP (black).

simultaneously (at the same temperature), relaxation strengths at identical time constants ($\tau_1 = \tau_2 = 10^{-2}$ s) are used. In spite of the consequence, that spectra of different temperatures are compared, this analysis yields a qualitative estimate of the relative relaxation strengths of the α_1- and α_2-processes at different TPP concentrations. The $\Delta\varepsilon_{1,2}$ were obtained by fitting a Kohlrausch function to the α_1-peak and the HN function to the α_2-peak. The relaxation strengths $\Delta\varepsilon_{1,2}$ of α_1- and α_2-relaxation as yielded by the alternative fitting procedure for $c_{TPP} = 20\%$ described in Appendix A are also included in Fig. 7 as open symbols; similar results are found. For $c_{TPP} = 30\%$ and 45% the α_1-peak had to be revealed by the procedure described in Appendix B. Starting at lowest c_{TPP}, the $\Delta\varepsilon_{1,2}$ of α_1- and α_2-relaxation show similar concentration dependences. At $c_{TPP} \approx 25\%$ both curves intersect. Beyond $c_{TPP} = 30\%$ $\Delta\varepsilon_1(c_{TPP})$ shows indications of a saturation behavior, while $\Delta\varepsilon_2(c_{TPP})$ continues its distinct increase. Note that the data in Fig. 7 are presented on logarithmic scale; in the range of $c_{TPP} = 30\%$–100% $\Delta\varepsilon_2(c_{TPP})$ increases monotonically by a factor of 20.

Figure 8(a) displays the dielectric spectra for $c_{TPP} = 45\%$ TPP in PS (β-relaxation and ionic conductivity omitted). As already pointed out above, only one dielectric relaxation peak is observable as is the case for all mixtures at $c_{TPP} \geq 30\%$. At $c_{TPP} = 30\%$ still clear traces of the α_1-relaxation are observed, yet obscured by the α_2-relaxation peak and the ionic conductivity contribution (cf. Fig. 14(a) in Appendix B). In Appendix B we show how time constant and relaxation strength of the hidden α_1-relaxation can be estimated. The resulting $\tau_1(T)$ are included in Figs. 5 and 9 and fit well into the overall scenario. Dielectric data of further concentrations ($c_{TPP} = 60\%$, 80%, 95%) are collected in Appendix C.

In Fig. 8(b) we show the results from our depolarized light scattering (DLS) experiments, which clearly reveal two separated relaxation peaks up to highest TPP concentrations,

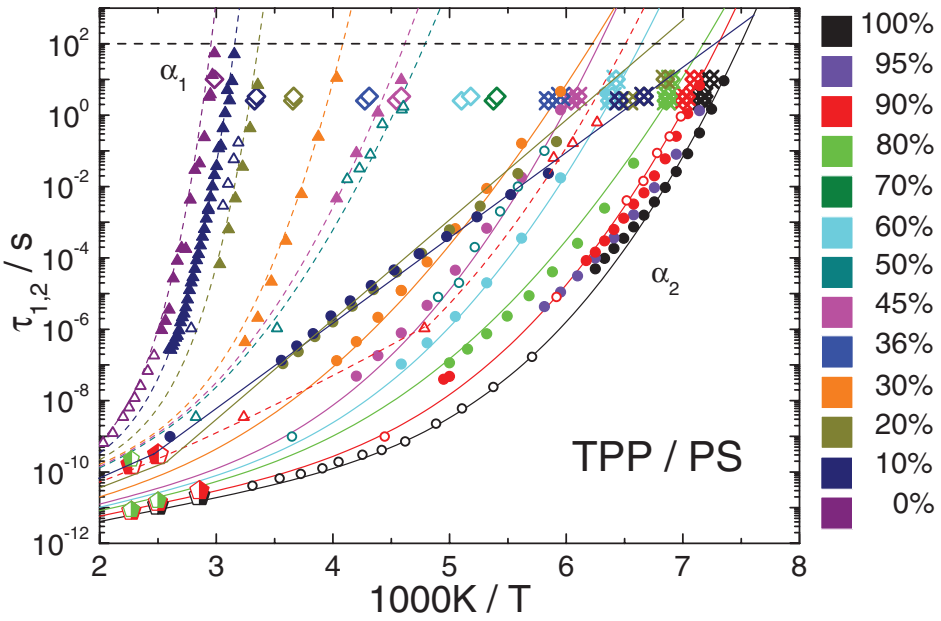

FIG. 9. Time constants from DS (▲: α_1; ●: α_2), NMR (Δ: α_1; ○: α_2), DSC (◊: α_1; ※: α_2) and DLS (◐: α_1; ◑: α_2) for all investigated concentrations (cf. color code). For $c_{TPP} = 0\%$ NMR data by He *et al.*[55] are included, and for TPP we included ^{31}P NMR results.[46] Exact concentrations are given in Table I. Lines are guides for the eye (dashed: α_1-relaxation; solid: α_2-relaxation). Horizontal dashed line marks $\tau_{1,2} = 100$ s (indication of T_g). Error bars in the case of $c_{TPP} = 45\%$ omitted for the sake of clarity; for other concentrations estimated to be smaller than the symbols.

This article is copyrighted as indicated in the article. Reuse of AIP content is subject to the terms at: http://scitation.aip.org/termsconditions. Downloaded to IP: 132.180.21.93 On: Wed, 29 Jan 2014 15:49:49

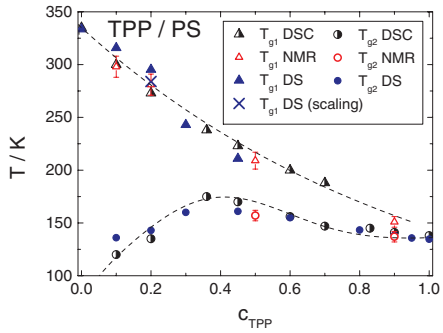

FIG. 10. Glass transition temperatures T_g as a function of TPP concentration as yielded by DSC, NMR, and DS for all investigated mixtures. Dashed lines: guides for the eye.

as demonstrated for $c_{TPP} = 90\%$ in comparison to $c_{TPP} = 100\%$ TPP. The two peaks refer to TPP and PS molecules; TPP molecules attached to PS are probably not present since very high temperatures are investigated. In any case, two time constants can be extracted, which are shown in Figs. 5 and 9. Comparing different concentrations, some weak anti-plasticizer effect is observable in Fig. 8(b) for the high-frequency relaxation reflecting the dynamics of TPP.

In Fig. 9 we collect all the time constants obtained with the help of DS, NMR, DSC, and DLS experiments. Admittedly, the figure is quite "crowded," but it reflects the rather complex dynamics in an asymmetric binary mixture. Again, for the sake of clarity the nominal concentrations are discussed (Table I); the color code defines the concentration, triangles and circles distinguish between α_1- and α_2-process, respectively. Clearly, for the α_2-relaxation one can observe a continuous crossover from super-Arrhenius to thermally activated behavior of the $\tau_2(T)$ when c_{TPP} is reduced.

Given the definition of T_g via $\tau_{1,2}(T_g) = 100$ s we derive two glass transition temperatures T_{g1} (associated with α_1-relaxation) and T_{g2} (associated with α_2-relaxation). The results are displayed in Fig. 10 (triangles: T_{g1}, circles: T_{g2}, cross: T_{g1} as obtained by the scaling procedure presented in Appendix A). While $T_{g1}(c_{TPP})$ decreases steadily from neat PS down to highly diluted PS due to the plasticizer effect, $T_{g2}(c_{TPP})$ is significantly lower and exhibits a maximum around $c_{TPP} = 35\%$. Up to our knowledge such relative maximum in $T_{g2}(c_{TPP})$ has not been reported before; actually it is a natural consequence of the ever-decreasing activation energy displayed by the Arrhenius straight lines in Fig. 9 at low concentrations. In contrast to previous reports[14,17] we do not find any indications that there exists a concentration range in which only a single T_g is observed. The results at $c_{TPP} = 70\%$ still allow to extract two T_g. Moreover, the DLS spectra at $c_{TPP} = 90\%$ show two separate relaxation peaks (Fig. 8(b)). It appears that T_{g2} and T_{g1} approach each other at highest TPP concentrations, but can still be distinguished.

After having discussed the temperature dependence of the two relaxation processes (α_1 and α_2), we inspect in more detail the evolution of the spectral shapes of α_1- and α_2-process at different concentrations. As already mentioned, the spectra of α_1-relaxation of the 10% and 20% mixtures, as well as the spectra of the α-relaxation of neat PS can be collapsed to provide a master curve when scaled to their maximum (Fig. 11(a), solid lines). Clearly, FTS is fulfilled, and each master curve can be interpolated with a Kohlrausch function (dashed lines). Obviously the α_1-peak of the 10% data is more broadened ($\beta_K = 0.27$) than the α-peak of pure PS

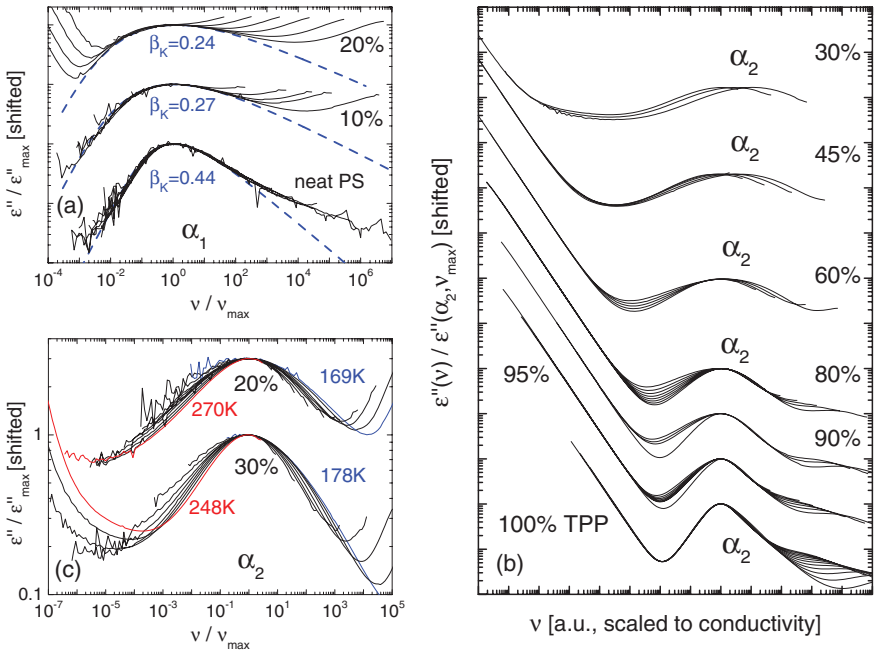

FIG. 11. (a) Master curves for the α_1-relaxation peaks at different temperatures for 20% and 10% TPP in PS, and α-relaxation of neat PS (solid lines). For each system the susceptibility curves are scaled to the maximum; dashed lines: Kohlrausch interpolations with indicated stretching parameters. (b) Susceptibility data representing the α_2-relaxation for mixtures with $c_{TPP} = 30\%$–95% and for neat TPP, scaled to maximum height and conductivity position. (c) α_2-relaxation data of the 20% and 30% TPP/PS mixtures scaled to peak maximum. All panels: Sets of curves representing different concentrations are separated from each other by applying an arbitrary shift factor.

This article is copyrighted as indicated in the article. Reuse of AIP content is subject to the terms at: http://scitation.aip.org/termsconditions. Downloaded to IP: 132.180.21.93 On: Wed, 29 Jan 2014 15:49:49

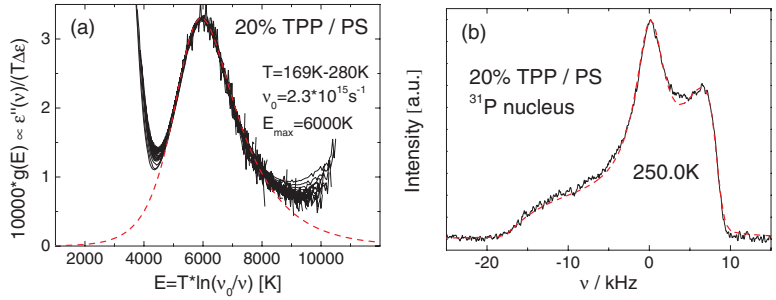

FIG. 12. (a) Results of the $g(E)$-scaling of the α_2-relaxation data for $T = 169$–280 K (solid lines, cf. text). Dashed line: fit to $g(E)$, function given in Ref. 65. (b) Solid line: ^{31}P NMR spectrum of the 20% sample at $T = 250$ K. Dashed line: weighted sum of a powder spectrum and a Lorentzian line, the latter representing isotropic molecular reorientation, fitted to the data.

($\beta_K = 0.44$). The α_1-peak of the 20% data looks similar to the 10% peak, however, the stretching parameter is slightly more reduced ($\beta_K = 0.24$).

The situation is more complicated for the α_2-relaxation. Figure 11(b) displays attempts to get master curves for $c_{TPP} = 30\%$–100%. Here, as a first step, the spectra are scaled vertically to their α_2-maximum values. In a second step the resulting curves are shifted horizontally in order to match best in the region of the conductivity contribution. In the case of neat TPP one sees clearly that this procedure leads, in good approximation, also to a scaling of the complete α-relaxation, which is interfered only by the β-relaxation approaching the high-frequency side of the α-peak. From that we conclude, firstly, that the rotational correlation time is coupled to the time scale of the diffusive process causing ionic conductivity. Secondly, the relaxation peak of neat TPP obeys FTS in good approximation. For concentrations down to 60% a strong broadening of the master curve is observed, in accord with Fig. 3 and Fig. 16 in Appendix C. Additionally, a failure of FTS is recognized, yet at the high-frequency flank the curves still appear to scale. The broadening on the low-frequency side of the main relaxation peak reminds of supercooled liquids in confinement.[57,58] For $c_{TPP} \leq 60\%$ the peak position is fully decoupled from the conductivity time scale. In addition, FTS is hurt at low- as well as high-frequency flank (demonstrated for $c_{TPP} = 30\%$ in more detail in Fig. 11(c)), which is a signature well-known for a β-process.[45,53,54] This is also reflected in the HN parameter $a(T)$ displayed in Fig. 17, Appendix D.

In accord with these findings the temperature dependence of the time constants $\tau_2(T)$ of the α_2-processes show super-Arrhenius behavior at high concentrations and Arrhenius behavior at low concentrations (Figs. 5 and 9), i.e., strong failure of FTS and Arrhenius behavior of the time constants go together. This suggests to apply a scaling procedure, developed in the context of thermally activated dynamics as observed for β-relaxations,[45,54,60–63] to the α_2-relaxation at low concentrations. If thermally activated dynamics are determined by a broad (temperature independent) distribution of activation energies $g(E)$ (see also Ref. 64), the scaling law yields

$$g(E) = g(T \ln(\nu_0/\nu)) = \frac{2}{\pi} \frac{\varepsilon''(\nu)}{T \Delta\varepsilon}. \quad (2)$$

Since a possible distribution of attempt frequencies ν_0 has no strong influence as logarithmic scales are considered, a single ν_0 value (as fit parameter) allows for collapsing all spectra. In Fig. 12(a) the results of the scaling procedure applied to the α_2-relaxation of the 20% TPP/PS mixture are shown. All datasets collapse onto a single master curve, which directly provides the activation energy distribution $g(E)$ of the thermally activated α_2-process. The rescaled peaks can be interpolated by an asymmetric function introduced in Ref. 65 (dashed line in Fig. 12(a)), which finally yields the relaxation strength $\Delta\varepsilon_2(T)$ displayed in Fig. 6.

It appears that the α_2-process at low concentrations shows many features of a β-process which would imply that the reorientational process is not isotropic (as typical of a glass), but rather involves a spatially hindered motion as has been proven for a typical β-process.[66] However, as shown in Figure 12(b), the ^{31}P NMR spectrum of the $c_{TPP} = 20\%$ mixture recorded at $T = 250$ K ($< T_{g1} = 283$ K) shows, besides a solid-state spectrum, a Lorentzian central line originating from TPP molecules reorienting isotropically on a time scale shorter than, say 100 μs. At the same time the PS molecules are immobilized since a temperature below T_{g1} is considered. Thus, the solid-state fraction in the NMR spectrum in Fig. 12(b) contains both slowly but isotropically reorienting TPP molecules involved in the broadly distributed α_2-process, as well as a fraction of immobilized TPP molecules associated with the α_1-process of PS. With the help of two-dimensional ^{31}P NMR it can be shown that essentially all TPP molecules involved in the α_2-process reorient isotropically. Moreover, exchange between fast and slow α_2-molecules is observed as will be discussed in Paper II.[47]

IV. DISCUSSION AND CONCLUSIONS

By combining the results of different methods and covering the full concentration range we reveal the dynamics of both components in an asymmetric binary mixture, which actually discloses a rather complex scenario not fully clarified before. Two glass transition temperatures T_{g1} and T_{g2} are found for all concentrations, a behavior now well established for binary liquids.[20–25] There are no indications that the mixture becomes dynamically homogeneous in the sense that only a single T_g is observed beyond some concentration, a

This article is copyrighted as indicated in the article. Reuse of AIP content is subject to the terms at: http://scitation.aip.org/termsconditions. Downloaded to IP: 132.180.21.93 On: Wed, 29 Jan 2014 15:49:49

scenario suggested previously.[17,28] As demonstrated by light scattering experiments even at 90% TPP in PS two separate relaxation peaks are observed (Fig. 8(b)).

As already reported by Blochowicz and co-workers[13,17] and overlooked in previous reports, in such asymmetric mixtures there exist two relaxation processes of the low-T_g component (α_1 and α_2). They are attributed, in the present case, to two different sub-ensembles of TPP molecules. One is involved in the (slow) dynamics of the high-T_g component PS (α_1-process), another performs faster, highly decoupled dynamics in the more or less immobilized PS matrix (including the α_1 fraction of TPP). ^{31}P NMR demonstrates that the α_2-process involves isotropic reorientations of at least most TPP molecules within a broad distribution $G(\ln\tau)$. At low concentrations $G(\ln\tau)$ of the α_2-process can be mapped to a temperature independent distribution of activation energies $g(E)$, which corresponds to a strong failure of FTS; then its mean correlation time $\tau_2(T)$ displays an Arrhenius temperature dependence. In spite of the isotropic liquid-like nature of the motion, the dynamics shows features which can easily be confused with those of a secondary (β-) process. In particular, its mean activation energy ($E_A(10\%) = 5241$ K $\approx 17T_{g1}$) is typical for β-processes. When concentration is increased, $\tau_2(T)$ of the isotropic motion of the α_2-sub-ensemble displays a monotonic transition from a strong to a fragile temperature dependence.

In accordance with Blochowicz *et al.*[13,17] we take the low-concentration behavior of the TPP molecules contributing to the α_2-process as a signature of intrinsic confinement effects exerted by the rigid PS matrix. NMR[28,30] spectra reported for binary glass formers as well as dielectric[13,17] spectra of their α_2-process resemble those found in neat glass formers confined in porous systems.[33,34,57,59] For example, "lubricated" pores lead to a flattening of the low-frequency part of the α-relaxation,[57,58] similar to what is found for the α_2-relaxation at high TPP concentrations in Fig. 11(b). The spectra typical for confined systems have been explained in accordance with simulation work[58,67] by assuming a spatial gradient of dynamics, i.e., a distribution of T_g or, more precisely, a distribution $G(\ln\tau)$ induced by an interaction of the pore walls with the contained liquid up to a certain penetration length. For many liquids under confinement molecular slowing down is observed at the pore walls, and simulations suggest that the penetration length increases with lowering temperature.[68] In that sense PS could provide a confinement for the TPP molecules which becomes "hard" below T_{g1}. The higher the concentration, the more TPP molecules are beyond the influence of the confinement effect of the PS matrix, and the dynamics becomes similar to that of neat glass formers. In contrast, at low concentrations most TPP molecules are controlled by an immobilized polymer, which causes a broad distribution of activation energies of liquid-like (isotropic) motion. It shall be noted at this point that dynamical exchange is observed within the (broadly distributed) α_2-dynamics. This will be discussed in detail in Paper II.[47]

Regarding the fraction of TPP molecules involved in the dynamics of PS (α_1-process), they become isotropic only when the primary process of the PS matrix sets in. Their relaxation characteristics are similar to those of PS itself, e.g., FTS applies. The α_1-fraction of TPP molecules increases when the overall TPP concentration is reduced. If only few TPP molecules are added to the PS sample ($c_{TPP}\rightarrow 0$), it appears that the molecules preferably become associated to the matrix. Figure 7 suggests that beyond a certain threshold the matrix sites appear to "saturate," i.e., no more additive molecules are incorporated in the α_1-process. One consequence of this interpretation is that the TPP molecules still may act as a probe for the matrix dynamics, but only in the case of low TPP concentrations. When the TPP content is increased beyond a certain level, the overall TPP dynamics become bimodal and highly heterogeneous, and the α_1-relaxation is difficult to identify in the dielectric spectra. The situation is improved when the T_g contrast is high.[17] We note that the existence of two different sub-ensembles of additive molecules may also be related to phenomena observed for gas transport in polymers, for which a dual mode sorption model has been proposed.[69] Above T_{g1} the fraction of the TPP molecules associated with PS decreases with increasing temperature until at some temperature T_c all α_1-TPP molecules have disappeared. Such behavior has been interpreted in the frameworks of MCT.[13] While the high-T_g component undergoes a normal glass transition (type-B scenario), a localization transition (type-A scenario) appears for the low-T_g component at lower temperatures. In the present case, the temperature dependent fraction of TPP molecules associated with the slow dynamics of PS may be taken as a measure of the non-ergodicity parameter, which decreases continuously and finally becomes zero at a critical temperature T_c. It remains an experimental challenge to show that the translational diffusion involved in the α_2-process indeed is sub-diffusive as suggested by simulations[35–37] and MCT.[38–40]

ACKNOWLEDGMENTS

Financial support by Deutsche Forschungsgemeinschaft (DFG) through Project Nos. RO 907/10 and RO 907/11 is acknowledged. The authors thank Ute Kuhn, Lehrstuhl für Polymere Werkstoffe, Universität Bayreuth, for her assistance in performing the DSC measurements.

APPENDIX A: ESTIMATION OF RELAXATION STRENGTHS FOR THE 20% SAMPLE

In the case of the 20% mixture both relaxations (α_1 and α_2) are well resolved and an unusual temperature dependence is observed, which is important to be estimated appropriately. Figure 13 shows again the data of the 20% mixture already displayed in Fig. 4(b), now on linear scale. By using the activation energy scaling results (Fig. 12(a)), i.e., $\Delta\varepsilon_2(T)$ and its extrapolation to higher temperatures (dashed line in Fig. 6), susceptibility curves are calculated from $g(E)$ along Eq. (2) for the α_2-peaks (dashed lines in Fig. 13). Good correspondence with the measured α_2-data is found for $T = 169$–280 K. In the temperature range $T = 290$–330 K the α_1-process is well recognized in the accessible frequency window; still a strong influence of the α_2-contribution is anticipated at high

This article is copyrighted as indicated in the article. Reuse of AIP content is subject to the terms at: http://scitation.aip.org/termsconditions. Downloaded to IP: 132.180.21.93 On: Wed, 29 Jan 2014 15:49:49

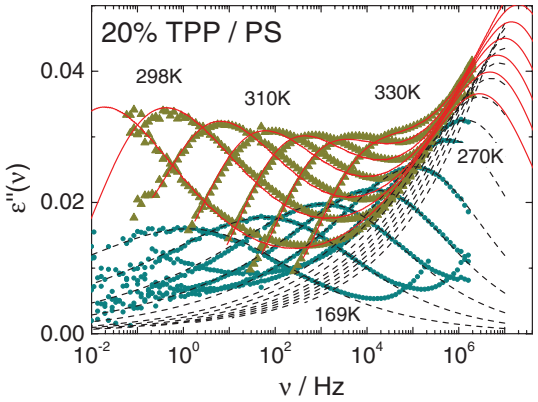

FIG. 13. Data from Fig. 4(b); triangles: α_1-relaxation for $T = 290$–330 K, circles: α_2-relaxation for $T = 169$–280 K. Dashed lines: α_2-contributions calculated from the $g(E)$ scaling result shown in Fig. 12(a) along Eq. (2). Solid lines: fits (cf. text).

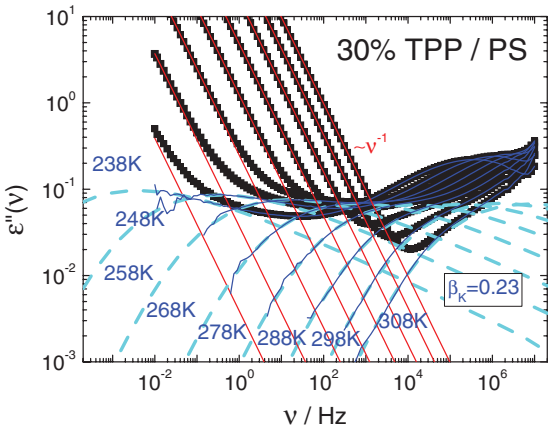

FIG. 15. Susceptibility of the $c_{TPP} = 30\%$ sample (squares). Red lines: conductivity contribution. Blue lines: susceptibility after subtracting conductivity contribution. Dashed lines: Kohlrausch functions with $\beta_K = 0.23$.

frequencies. In this temperature range, each spectrum was fitted with the sum of a Kohlrausch function with $\beta_K(T) = 0.28$–0.38 and the corresponding (fixed) α_2-contribution calculated from the temperature independent $g(E)$. The results (solid red lines in Fig. 13) agree with the data. Resulting time constants τ_1, as well as $\tau_{2,calc} = (1/2\pi\nu_0)\exp(E_{max}/T)$ calculated with $E_{max} = 6000$ K and $\nu_0 = 2.3 \times 10^{15}$ s^{-1} (Fig. 12(a)), are included in Fig. 5 (crosses). Good correspondence with the experimental τ_2, as well as, respectively, the τ_1 yielded by the direct fitting analysis of the α_1-peak (Secs. II B and III B), is observed. The resulting relaxation strengths $\Delta\varepsilon_1(T)$ are included in Fig. 6 (open triangles).

APPENDIX B: REVEALING THE α_1-PROCESS AT INTERMEDIATE CONCENTRATIONS

Figure 14 shows dielectric data for the (a) 30% and (b) 45% TPP/PS mixtures. In contrast to the 10% and 20% data (Fig. 4) only one relaxation peak is explicitly observable. Note that between 30% and 100% TPP only a single peak is observed in the susceptibility (besides the β-process; cf. Appendix C), and with higher concentrations this peak increases further in amplitude and develops continuously into the α-process of neat TPP. In the case of the 30% and 45% mixtures still traces of the α_1-relaxations can be identified.

By plotting the data on linear scale, one can infer from Fig. 14(a) that a very broad minimum is located between conductivity and α_2-peak. When temperature is increased beyond about 272 K up to 346 K the initially broad minimum becomes narrower and decreases its amplitude. A similar, yet weaker effect is observed for $c_{TPP} = 45\%$ between $T = 230$ K and 250 K (Fig. 14(b)). Since in the case of the 10% and 20% mixtures a decrease of $\Delta\varepsilon_1(T)$ with increasing T is observed, we speculate that the decreasing minimum reflects a hidden α_1-relaxation peak.

In order to reveal the α_1-relaxation peak, the conductivity contribution has to be subtracted. This allows for estimating relaxation time and strength. In Fig. 15 this is demonstrated exemplarily for the susceptibility data of the 30% sample; for the 45% data a similar procedure was applied. The resulting $\tau_1(T)$ correspond well with the NMR findings (Fig. 5).

APPENDIX C: FURTHER SUSCEPTIBILITY DATA

Fig. 16 shows further spectra for the mixtures with the TPP concentrations $c_{TPP} = 60\%$, 80%, 95%. At these high concentrations no reasonable estimation of the dielectric time constant τ_1 of the α_1-relaxation is possible any more.

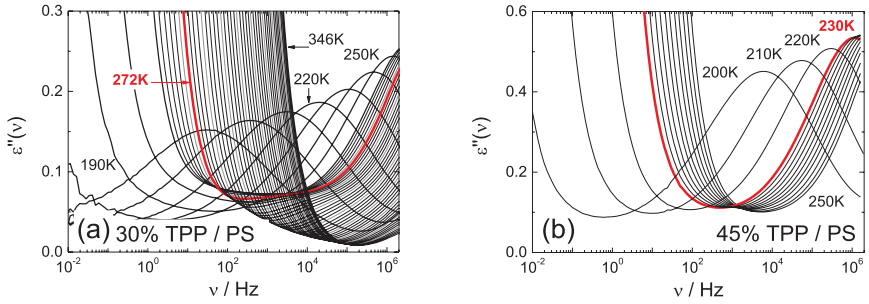

FIG. 14. Dynamic susceptibility data of TPP/PS mixtures. (a) 30% TPP in PS, $T = 190$–260 K in 10 K steps and $T = 262$–346 K in 2 K steps. (b) 45% TPP in PS, $T = 200$–230 K in 10 K steps and $T = 232$–250 K in 2 K steps.

This article is copyrighted as indicated in the article. Reuse of AIP content is subject to the terms at: http://scitation.aip.org/termsconditions. Downloaded to IP: 132.180.21.93 On: Wed, 29 Jan 2014 15:49:49

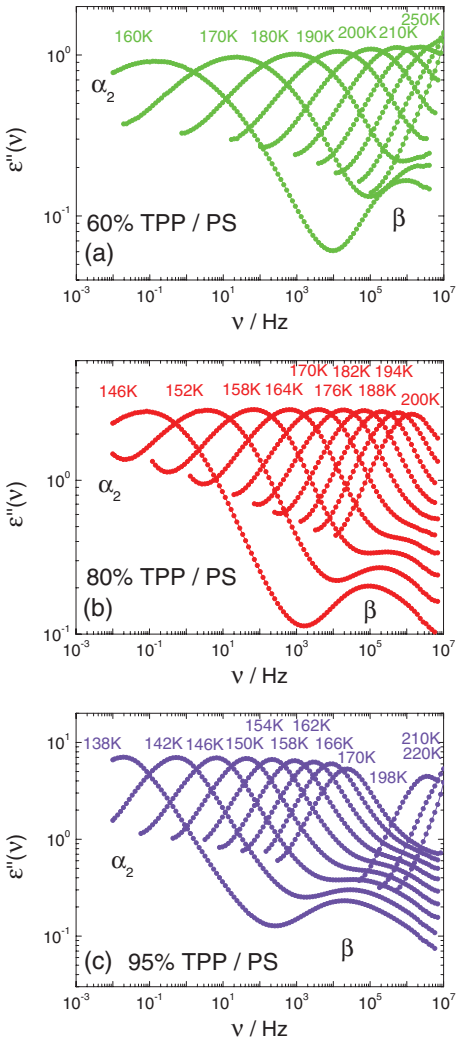

FIG. 16. Susceptibility spectra of mixtures with a TPP concentration of (a) $c_{TPP} = 60\%$, (b) $c_{TPP} = 80\%$, and (c) $c_{TPP} = 95\%$.

APPENDIX D: LINE SHAPE PARAMETERS OF THE α_2-PROCESS AT HIGH CONCENTRATIONS

As is demonstrated in Fig. 11(b), at high TPP concentrations the main temperature effect regarding the shape of the spectra is a broadening on the low-frequency flank of the α_2-relaxation upon cooling. This is also reflected in the shape parameters of the α_2-peak as obtained by fits with the Havriliak-Negami function. In Fig. 17 the temperature dependence of the HN parameter a is displayed for several concentrations. In all cases the strong temperature dependence observed at low temperatures seems to disappear at high temperatures, although a Cole-Davidson behavior with low-frequency exponent 1 cannot be inferred. Yet, one may speculate that the spectral shape does not change any longer at high temperatures, i.e., here FTS applies also for the α_2-process.

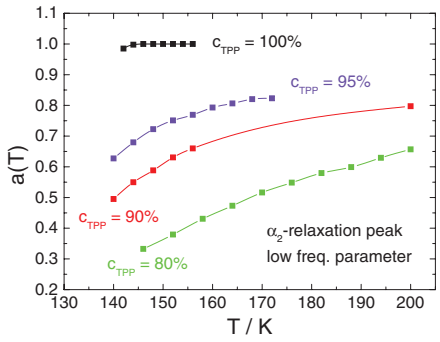

FIG. 17. Havriliak-Negami fit parameter $a(T)$, representing the low frequency exponent of the α_2-relaxation peak, for several concentrations. Lines: guides for the eye.

[1]P. Lunkenheimer, U. Schneider, R. Brand, and A. Loidl, Contemp. Phys. **41**, 15 (2000).
[2]K. Binder and W. Kob, *Glassy Materials and Disordered Solids* (World Scientific, New Jersey, 2005).
[3]A. Brodin, C. Gainaru, V. Porokhonskyy, and E. A. Rössler, J. Phys.: Condens. Matter **19**, 205104 (2007).
[4]L. Berthier and G. Biroli, Rev. Mod. Phys. **83**, 587 (2011).
[5]M. D. Ediger and P. Harrowell, J. Chem. Phys. **137**, 080901 (2012).
[6]R. Richert, in *Structural Glasses and Supercooled Liquids*, edited by P. G. Wolynes and V. Lubchenko (Wiley, Hoboken, 2012), p. 1.
[7]N. Petzold, B. Schmidtke, R. Kahlau, D. Bock, R. Meier, B. Micko, D. Kruk, and E. A. Rössler, J. Chem. Phys. **138**, 12A510 (2013).
[8]P. J. Hains and G. Williams, Polymer **16**, 725 (1975).
[9]M. A. Desando, S. Walker, and W. H. Baarschers, J. Chem. Phys. **73**, 3460 (1980).
[10]M. Scandola, G. Ceccorulli, and M. Pizzoli, Polymer **28**, 2081 (1987).
[11]M. Nakazawa, O. Urakawa, and K. Adachi, Macromolecules **33**, 7898 (2000).
[12]D. Cangialosi, A. Alegría, and J. Colmenero, J. Chem. Phys. **126**, 204904 (2007).
[13]T. Blochowicz, S. Schramm, S. Lusceac, M. Vogel, B. Stühn, P. Gutfreund, and B. Frick, Phys. Rev. Lett. **109**, 035702 (2012).
[14]T. Blochowicz and E. A. Rössler, Phys. Rev. Lett. **92**, 225701 (2004).
[15]K. Kessairi, S. Capaccioli, D. Prevosto, M. Lucchesi, and P. Rolla, J. Chem. Phys. **127**, 174502 (2007).
[16]S. Capaccioli, K. Kessairi, M. Shahin, D. Prevosto, and M. Lucchesi, J. Non-Cryst. Solids **357**, 251 (2011).
[17]T. Blochowicz, S. A. Lusceac, P. Gutfreund, S. Schramm, and B. Stühn, J. Phys. Chem. B **115**, 1623 (2011).
[18]D. Cangialosi, A. Alegría, and J. Colmenero, J. Chem. Phys. **128**, 224508 (2008).
[19]T. P. Lodge, E. R. Wood, and J. C. Haley, J. Polym. Sci., Part B: Polym. Phys. **44**, 756 (2006).
[20]K. Adachi and Y. Ishida, Polym. J. **11**, 233 (1979).
[21]D. A. Savin, A. M. Larson, and T. P. Lodge, J. Polym. Sci., Part B: Polym. Phys. **42**, 1155 (2004).
[22]Y. Miwa, K. Usami, K. Yamamoto, M. Sakaguchi, M. Sakai, and S. Shimada, Macromolecules **38**, 2355 (2005).
[23]J. E. G. Lipson and S. T. Milner, J. Polym. Sci., Part B: Polym. Phys. **44**, 3528 (2006).
[24]A. N. Gaikwad, E. R. Wood, T. Ngai, and T. P. Lodge, Macromolecules **41**, 2502 (2008).
[25]S. Schramm, T. Blochowicz, E. Gouirand, R. Wipf, B. Stühn, and Y. Chushkin, J. Chem. Phys. **132**, 224505 (2010).
[26]H. Sillescu, J. Non-Cryst. Solids **243**, 81 (1999).
[27]M. D. Ediger, Annu. Rev. Phys. Chem. **51**, 99 (2000).
[28]T. Blochowicz, C. Karle, A. Kudlik, P. Medick, I. Roggatz, M. Vogel, C. Tschirwitz, J. Wolber, J. Senker, and E. Rössler, J. Phys. Chem. B **103**, 4032 (1999).
[29]M. Vogel and E. Rössler, J. Phys. Chem. A **102**, 2102 (1998).
[30]D. Bingemann, N. Wirth, J. Gmeiner, and E. A. Rössler, Macromolecules **40**, 5379 (2007).
[31]S. A. Lusceac, C. Koplin, P. Medick, M. Vogel, N. Brodie-Linder, C. LeQuellec, C. Alba-Simionesco, and E. A. Rössler, J. Phys. Chem. B **108**, 16601 (2004).
[32]M. Vogel, P. Medick, and E. A. Rössler, Annu. Rep. NMR Spectrosc. **56**, 231 (2005).
[33]S. Gradmann, P. Medick, and E. A. Rössler, J. Phys. Chem. B **113**, 8443 (2009).
[34]M. Vogel, Eur. Phys. J.: Spec. Top. **189**, 47 (2010).

This article is copyrighted as indicated in the article. Reuse of AIP content is subject to the terms at: http://scitation.aip.org/termsconditions. Downloaded to IP: 132.180.21.93 On: Wed, 29 Jan 2014 15:49:49

[35]T. Voigtmann and J. Horbach, Phys. Rev. Lett. **103**, 205901 (2009).
[36]K. Kim, K. Miyazaki, and S. Saito, Eur. Phys. J.: Spec. Top. **189**, 135 (2010).
[37]J. Kurzidim, D. Coslovich, and G. Kahl, J. Phys.: Condens. Matter **23**, 234122 (2011).
[38]J. Bosse and Y. Kaneko, Phys. Rev. Lett. **74**, 4023 (1995).
[39]V. Krakoviack, Phys. Rev. E **79**, 061501 (2009).
[40]S. Lang, R. Schilling, V. Krakoviack, and T. Franosch, Phys. Rev. E **86**, 021502 (2012).
[41]T. Voigtmann, Euro. Phys. Lett. **96**, 36006 (2011).
[42]R. Kant, S. K. Kumar, and R. H. Colby, Macromolecules **36**, 10087 (2003).
[43]J. Colmenero and A. Arbe, Soft Matter **3**, 1474 (2007).
[44]T. P. Lodge and T. C. B. McLeish, Macromolecules **33**, 5278 (2000).
[45]D. Bock, R. Kahlau, B. Micko, B. Pötzschner, G. J. Schneider, and E. A. Rössler, J. Chem. Phys. **139**, 064508 (2013).
[46]S. Adishchev, D. Bock, C. Gainaru, R. Kahlau, B. Micko, N. Petzold, B. Pötzschner, and E. A. Rössler, Z. Phys. Chem. **226**, 1149 (2012).
[47]D. Bock, R. Kahlau, B. Pötzschner, T. Körber, E. Wagner, and E. A. Rössler, "Dynamics of asymmetric binary glass formers. II. Results from nuclear magnetic resonance spectroscopy," J. Chem. Phys. (submitted).
[48]H. Wagner and R. Richert, J. Phys. Chem. B **103**, 4071 (1999).
[49]J. Wiedersich, N. V. Surovtsev, V. N. Novikov, and E. Rössler, Phys. Rev. B **64**, 064207 (2001).
[50]N. Petzold and E. A. Rössler, J. Chem. Phys. **133**, 124512 (2010).
[51]I. M. Hodge, J. Non-Cryst. Solids **169**, 211 (1994).
[52]J. Hintermeyer, A. Herrmann, R. Kahlau, C. Goiceanu, and E. A. Rössler, Macromolecules **41**, 9335 (2008).
[53]A. Kudlik, S. Benkhof, T. Blochowicz, C. Tschirwitz, and E. Rössler, J. Mol. Struct. **479**, 201 (1999).
[54]R. Kahlau, T. Dörfler, and E. A. Rössler, J. Chem. Phys. **139**, 134504 (2013).
[55]Y. He, T. R. Lutz, M. D. Ediger, C. Ayyagari, D. Bedrov, and G. D. Smith, Macromolecules **37**, 5032 (2004).
[56]C. Tschirwitz, S. Benkhof, T. Blochowicz, and E. Rössler, J. Chem. Phys. **117**, 6281 (2002).
[57]M. Arndt, R. Stannarius, H. Groothues, E. Hempel, and F. Kremer, Phys. Rev. Lett. **79**, 2077 (1997).
[58]P. Scheidler, W. Kob, and K. Binder, Europhys. Lett. **59**, 701 (2002).
[59]G. Dosseh, C. Le Quellec, N. Brodie-Linder, C. Alba-Simionesco, W. Haeussler, and P. Levitz, J. Non-Cryst. Solids **352**, 4964 (2006).
[60]K. S. Gilroy and W. A. Phillips, Philos. Mag. B **43**, 735 (1981).
[61]J. Wiedersich, S. V. Adichtchev, and E. Rössler, Phys. Rev. Lett. **84**, 2718 (2000).
[62]L. Wu and S. R. Nagel, Phys. Rev. B **46**, 11198 (1992).
[63]C. Gainaru, R. Böhmer, R. Kahlau, and E. Rössler, Phys. Rev. B **82**, 104205 (2010).
[64]C. J. F. Böttcher and P. Bordewijk, *Theory of Electric Polarization: Dielectrics in Time-Dependent Fields* (Elsevier, Amsterdam, 1978), Vol. 2.
[65]T. Blochowicz, C. Tschirwitz, S. Benkhof, and E. A. Rössler, J. Chem. Phys. **118**, 7544 (2003).
[66]M. Vogel, C. Tschirwitz, G. Schneider, C. Koplin, P. Medick, and E. Rössler, J. Non-Cryst. Solids **307–310**, 326 (2002).
[67]P. Scheidler, W. Kob, and K. Binder, Europhys. Lett. **52**, 277 (2000).
[68]P. Scheidler, W. Kob, and K. Binder, J. Phys. Chem. B **108**, 6673 (2004).
[69]J. H. Petropoulos, "Mechanisms and theories for sorption and diffusion of gases in polymers," in *Polymeric Gas Separation Membranes*, edited by D. R. Paul and Y. P. Yampol´skii (CRC Press, Boca Raton, FL, 1994).

This article is copyrighted as indicated in the article. Reuse of AIP content is subject to the terms at: http://scitation.aip.org/termsconditions. Downloaded to IP: 132.180.21.93 On: Wed, 29 Jan 2014 15:49:49

Publikation 3

Dynamics of asymmetric binary glass formers. II. Results from nuclear magnetic resonance spectroscopy

D. Bock, R. Kahlau, B. Pötzschner, T. Körber, E. Wagner, and E. A. Rössler
The Journal of Chemical Physics 140, 094505 (2014).

© 2014 AIP Publishing LLC
doi:10.1063/1.4865945

THE JOURNAL OF CHEMICAL PHYSICS **140**, 094505 (2014)

Dynamics of asymmetric binary glass formers. II. Results from nuclear magnetic resonance spectroscopy

D. Bock, R. Kahlau, B. Pötzschner, T. Körber, E. Wagner, and E. A. Rössler[a)]
Experimentalphysik II, Universität Bayreuth, 95440 Bayreuth, Germany

(Received 19 December 2013; accepted 4 February 2014; published online 4 March 2014)

Various ^{2}H and ^{31}P nuclear magnetic resonance (NMR) spectroscopy techniques are applied to probe the component dynamics of the binary glass former tripropyl phosphate (TPP)/polystyrene-d_3 (PS) over the full concentration range. The results are quantitatively compared to those of a dielectric spectroscopy (DS) study on the same system previously published [R. Kahlau, D. Bock, B. Schmidtke, and E. A. Rössler, J. Chem. Phys. **140**, 044509 (2014)]. While the PS dynamics does not significantly change in the mixtures compared to that of neat PS, two fractions of TPP molecules are identified, one joining the glass transition of PS in the mixture (α_1-process), the second reorienting isotropically (α_2-process) even in the rigid matrix of PS, although at low concentration resembling a secondary process regarding its manifestation in the DS spectra. Pronounced dynamical heterogeneities are found for the TPP α_2-process, showing up in extremely stretched, quasi-logarithmic stimulated echo decays. While the time window of NMR is insufficient for recording the full correlation functions, DS results, covering a larger dynamical range, provide a satisfactory interpolation of the NMR data. Two-dimensional ^{31}P NMR spectra prove exchange within the broadly distributed α_2-process. As demonstrated by ^{2}H NMR, the PS matrix reflects the faster α_2-process of TPP by performing a spatially highly hindered motion on the same timescale. © *2014 AIP Publishing LLC*. [http://dx.doi.org/10.1063/1.4865945]

I. INTRODUCTION

Binary glass formers, in contrast to neat systems, are less studied and no broadly accepted picture of the involved relaxation processes has emerged so far. Of special interest are so-called asymmetric glass formers, which are characterized by a large difference of the glass transition temperatures T_g of the components mixed. They are most conveniently prepared by blending a polymer with a low-molecular additive.[1–7] Here it is possible to imagine that the mobile low-T_g component still performs liquid-like dynamics within the matrix of the more or less immobilized high-T_g component. In particular, MD simulations and theoretical works on particles differing significantly in size or exposed to confining geometries discuss this scenario.[8–12]

The present contribution deals with the system tripropyl phosphate (TPP, $T_g = 135$ K)/(deuterated) polystyrene(-d_3) (PS, $M_w \approx 2 \times 10^3$ g/mol, $T_g = 335$ K) which is investigated by means of dielectric spectroscopy (DS), differential scanning calorimetry (DSC) and depolarized light scattering (DLS), and in particular by means of different nuclear magnetic resonance (NMR) techniques. The system is characterized by a large T_g contrast of the pure components ($\Delta T_g \cong 200$ K). In Ref. 13 we have mainly presented the results of our DS study. Two glass transition temperatures (T_{g1} and T_{g2} with $T_{g2} < T_{g1}$) have been identified over the entire concentration range; the lower one displays a maximum as function of concentration, a behavior not reported before but well understood from our findings regarding the corresponding relaxation times. The dielectric spectra, which are actually dominated by the relaxation of the TPP molecules, show two relaxation processes above T_{g2}. One process (α_2) is much faster than that of PS, the corresponding spectra are strongly broadened with respect to the one in neat TPP, and the temperature dependence of the correlation times changes from a super-Arrhenius behavior at high concentrations to an Arrhenius behavior at low concentrations. The spectral broadening at low concentrations is described by a temperature independent distribution of activation energies. Thus, the additive process may be confused with a β-process, and it is up to NMR to prove whether the process is still isotropic (liquid-like) or spatially hindered as is the case for a typical β-process.

Importantly, a second relaxation process (α_1-process) with essentially the same time constant as PS in the mixture is identified in the dielectric spectra reflecting TPP dynamics, as mentioned above. This has been interpreted in terms of TPP molecules being attached to the polymer. This fraction seems to disappear continuously upon increasing temperature, thus suggesting a possible interpretation in terms of a type-A scenario predicted by MCT as already discussed by Blochowicz *et al.*[7] Finally, we note that in Ref. 14 we have thoroughly investigated the β-process which can be identified as a third process in the dielectric and NMR spectra at low temperatures (e.g., $\tau_\beta \approx 10^{-5}$ s at $T = 120$ K, mean activation energy $E = 24\ T_g$) but which is not dealt with here.

In the current contribution we present our results collected by various ^{2}H and ^{31}P NMR experiments. As deuterated PS is investigated, ^{2}H NMR provides information solely on the dynamics of PS which in the mixtures cannot be

a)Author to whom correspondence should be addressed. Electronic mail: ernst.roessler@uni-bayreuth.de.

 © 2014 AIP Publishing LLC

This article is copyrighted as indicated in the article. Reuse of AIP content is subject to the terms at: http://scitation.aip.org/termsconditions. Downloaded to IP: 132.180.10.132 On: Mon, 28 Apr 2014 09:04:16

accessed by dielectric spectroscopy due to the weak dipole moment of the PS monomer (yet by DSC and depolarized light scattering, see Ref. 13). ^{31}P NMR gives insight into the dynamics of the TPP molecules. In particular, two-dimensional (2D) exchange spectra allow addressing the question which kinds of motional processes are reflected by the two relaxation processes identified in the dielectric spectra of the mixture. It is the challenge of the present contribution to understand the NMR and DS phenomena within a common quantitative description. NMR also answers the question whether the dynamic heterogeneities identified are transient or static, i.e., whether exchange processes between slow and fast molecules take place. All in all, by collecting the results from several different spectroscopic probes the two parts of our contribution are meant to suggest a general scenario of the dynamics in asymmetric binary glass formers.

II. NMR BACKGROUND AND EXPERIMENTAL DETAILS

In the solid state, provided that the interaction tensor is axially symmetric, the NMR frequency depends solely on the angle θ between the principal (local) interaction tensor axis and the magnetic field direction. This is the case for ^{2}H as well as ^{31}P NMR in the present study. Thus,

$$\omega_{local}(\theta) = 2\,\pi\,\nu(\theta) = (\pm)(3\cos^2\theta - 1)\cdot 2\pi\delta_{CSA/Q}/2 \quad (1)$$

holds, where ω_{local} is the shift of the angular resonance frequency with respect to the Larmor frequency ω_L. The parameter $\delta_{CSA/Q}$ (in kHz) specifies the anisotropy of the interaction tensor, which in the case of ^{2}H NMR is given by the interaction of the nuclear quadrupolar moment with the electrical field gradient (δ_Q). For PS-d$_3$ the reorientation of the ^{2}H–C bonds on the backbone is probed. Due to spin $I = 1$ two transitions occur in Eq. (1). In the case of ^{31}P NMR (spin $I = 1/2$) the spectrum is determined by the chemical shift anisotropy (CSA), and in Eq. (1) only the negative sign applies together with δ_{CSA}. For an isotropic distribution of tensor orientations (e.g., in glasses) a characteristic powder spectrum is observed, a (symmetric) Pake spectrum in the case of ^{2}H NMR, whereas the CSA spectrum is asymmetric.

Upon heating above T_g, isotropic reorientation gets fast leading to a gradual collapse of the powder spectrum into a central narrow line. In contrast, in the case of a broad distribution of relaxation times $G(\ln\tau)$, as is the case in binary glass formers in particular regarding the low-T_g component (here TPP), a superposition of a Lorentzian central line $S_{Lor}(\nu)$, reflecting fast molecules, and a solid-state powder spectrum $S_{sol}(\nu)$ reflecting slow molecules is observed, often referred to as "two-phase spectra."[15] A temperature dependent weighting factor $W(T)$ specifies the fraction of the Lorentzian line:

$$S(\nu, T) = W(T)S_{Lor}(\nu) + (1 - W(T))S_{sol}(\nu). \quad (2)$$

The quantity $W(T)$ is given as an integral over $G(\ln\tau)$ with an upper bound given by the inverse coupling constant δ, explicitly[16]

$$W(T) \approx \int_{-\infty}^{1/(2\pi\delta)} G(\ln\tau, T)d\ln\tau. \quad (3)$$

The solid-state spectra were collected by applying a Hahn-echo (^{31}P NMR) or a solid-echo sequence (^{2}H NMR) with an inter-pulse delay t_p preceded by a saturation sequence of five $\pi/2$ pulses. The build-up time was chosen to be 2.5 T_1 or 1s at least. ^{1}H decoupling was applied during the Hahn-echo sequence in order to remove the heteronuclear dipolar coupling. Appropriate 8-fold (^{2}H) and 16-fold (^{31}P) phase cycling was chosen.[17] In order to keep spectral changes due to motion during the time t_p small, t_p was chosen short, typically 20 μs.

The decay of the stimulated echo provides quantitative information on the orientational correlation function. A three-pulse sequence, $(\pi/2) - t_p - (\pi/2) - t_m - (\pi/2)$, was applied with a fixed evolution time t_p to monitor the ^{31}P stimulated echo as a function of the mixing time, t_m. With the appropriate phases of the pulses only the sine part of the stimulated echo is observed.[15,18] The echo amplitude reads

$$I(t_p, t_m) \propto \langle \sin(\omega_{local}(0)t_p)\sin(\omega_{local}(t_m)t_p)\rangle \times \exp(-(t_m/T_1)^{\beta_K}). \quad (4)$$

The factor in angular brackets represents the orientational correlation function $F_{tp}{}^{\sin}(t_m)$, and the stretched exponential term is a damping factor caused by NMR relaxation effects. For ^{31}P NMR, the property T_1 is given by the spin-lattice relaxation time (with $\beta_K = 1$), while for the ^{2}H NMR it has to be replaced by the quadrupolar relaxation time constant T_{1Q} (with $\beta_K < 1$).

The normalized correlation function $F_{tp}{}^{\sin}(t_m)$ can be decomposed,[19]

$$F_{tp}{}^{\sin}(t_m) = [1 - F_\infty]\phi_{tp}(t_m) + F_\infty, \quad (5)$$

where $\phi_{tp}(t_m)$ denotes a function describing the loss of correlation caused by the motional process, while $F_\infty = F_\infty(t_p)$ stands for the residual correlation which does not relax. Its value depends on the geometry of the reorientational motion and is well documented for isotropic motion.[15,19] For short delay times t_p, the residual correlation $F_\infty(t_p)$ approaches 0, and the normalized correlation function $\phi_{tp}(t_m)$ approximates the correlation function $\langle\omega(0)\omega(t_m)\rangle$ which is proportional to the orientational correlation function of the second Legendre polynomial $C_2(t_m)$ via Eq. (1); explicitly[15]

$$\lim_{tp\to 0}\phi_{tp}(t_m) \propto \langle\omega_{local}(0)\omega_{local}(t_m)\rangle \propto C_2(t_m). \quad (6)$$

The evolution time t_p was set to 12.5 μs in the case of ^{31}P NMR. Regarding ^{2}H NMR a four-pulse sequence was applied with $t_p = 3$ μs together with appropriate pulse lengths.[18,20]

The spin-lattice relaxation time $T_1(T)$ was measured independently for each temperature and in the case of ^{31}P NMR found to be mono-exponential. The quadrupolar relaxation time $T_{1Q}(T)$ cannot be measured independently. Assuming that at sufficiently low temperatures dynamics is too slow to damp the stimulated echo, the measured decay was attributed to T_{1Q}. Its temperature dependence was assumed to be proportional to that of $T_1(T)$ and the stretching parameter β_K was

This article is copyrighted as indicated in the article. Reuse of AIP content is subject to the terms at: http://scitation.aip.org/termsconditions. Downloaded to IP: 132.180.10.132 On: Mon, 28 Apr 2014 09:04:16

kept fixed as obtained at low temperatures. In the case of ^{31}P NMR, the stimulated echo decays at long times and low temperatures are furthermore affected by spin diffusion (magnetization exchange without molecular dynamics) which exhibits only a weak temperature dependence and thus was measured independently.[6] Here, Kohlrausch decays with $\beta_K = 0.6$ and time constants τ_{SD} between 10 s and 50 s were found. The impact of corrections for spin diffusion on stimulated echo decays can be inferred from Fig. 11.

A 2D NMR spectrum, $S(\omega_1, \omega_2; t_m)$, measures the conditional probability, $P(\omega_2, t_m \mid \omega_1, 0)$, to find a frequency ω_2 at time t_m if it was ω_1 at time $t = 0$.[18] Thus, 2D spectra provide direct visualization of the evolution of the reorientational process. A four-pulse sequence utilizing the TPPI technique[18] was applied to determine the 2D ^{31}P NMR spectra as a function of the mixing time t_m. After data acquisition and complex Fourier transformation, the 2D spectra were symmetrisized and convoluted with a 1 kHz broad Gaussian. In the case of isotropic motion characterized by a broad distribution of correlation times the 2D spectra can be described as a weighted sum of the four sub-spectra (a phenomenon well known from asymmetric binary glass formers, see also Refs. 6, 15, 21–23): $S_{dia}(\omega_1, \omega_2; t_m)$ corresponding to molecules immobile during the mixing time, $S_{reo}(\omega_1, \omega_2; t_m)$ corresponding to molecules showing isotropic reorientation during mixing time, $S_{liq}(\omega_1, \omega_2; t_m)$ reflecting molecules in the fast motion limit, and $S_{ex}(\omega_1, \omega_2; t_m)$ reflecting molecules exchanging their correlation time during t_m from $\tau < 1/(2\pi\delta)$ to $\tau > 1/(2\pi\delta)$ and vice versa. Explicitly,

$$\begin{aligned} \mathrm{S}(\omega_1, \omega_2; t_m) = {} & p^{dia}\mathrm{S}_{\mathrm{dia}}(\omega_1, \omega_2; t_m) + p^{reo}\mathrm{S}_{\mathrm{reo}}(\omega_1, \omega_2; t_m) \\ & + p^{liq}\mathrm{S}_{\mathrm{liq}}(\omega_1, \omega_2; t_m) + p^{ex}\mathrm{S}_{\mathrm{ex}}(\omega_1, \omega_2; t_m) \end{aligned} \tag{7}$$

with $\Sigma p^i = 1$.

Provided that all molecules take part in the exchange, due to statistical independence the long- time limits of the weighting factors become[6,21]

$$\begin{aligned} p^{dia}(t_m \to \infty) &= 0, \\ p^{liq}(t_m \to \infty) &= W^2, \\ p^{ex}(t_m \to \infty) &= 2W(1 - W), \\ p^{reo}(t_m \to \infty) &= (1 - W)^2, \end{aligned} \tag{8}$$

with W being the 1D weighting factor introduced in Eq. (2).

Supposing that no molecules exist in the fast motion limit, p^{liq} as well as p^{ex} are zero and the 2D spectra can be described by a weighted sum of the remaining two sub-spectra, i.e., "two-phase 2D" spectra are observed.[6,24]

The ^{31}P NMR experiments were carried out using a Bruker Avance III console and a Spectrospin 400 MHz cryomagnet with a field strength of 9.4 T corresponding to a Larmor frequency $\omega_L = 2\pi \times 161.98$ MHz. The length of the $\pi/2$–pulse was 2.2 μs. For measurements at temperatures below 300 K a home-built (in cooperation with Bruker Biospin GmbH) double resonance probe was cooled by liquid nitrogen using an Oxford CF1200 cryostat, controlled by an Oxford ITC-503 instrument. Temperature accuracy was ± 2 K, stability was better than ± 0.2 K. At temperatures above 300 K a Bruker wide-bore double resonance probe was used. A Bruker VT 2000 temperature controller heated a flow of cold nitrogen gas to regulate temperature within 1 K. The ^{2}H NMR experiments were carried out on a Bruker Avance DSX spectrometer and an Oxford 300 MHz cryomagnet. A field strength of 7 T corresponds to a ^{2}H Larmor frequency of $\omega_L = 2\pi \times 46.067$ MHz; the length of the $\pi/2$–pulse was 2.8 μs. For measurements at temperatures below 330 K a home-built probe was cooled by liquid nitrogen using a CryoVac Konti cryostat and an Oxford ITC-503 temperature controller. Temperature accuracy was better than ± 1 K, stability was better than ± 0.2 K. At temperatures above 330 K a Bruker wide-bore probe was used. A Bruker VT 2000 temperature controller heated a flow of cold nitrogen gas to regulate the temperature of the sample within 1 K.

Regarding details of the experiments carried out by DS, DSC, and DLS as well as sample preparation the reader is referred to Ref. 13. In the following we describe the NMR results employed to investigate the dynamics of (deuterated) polystyrene ($M_W = 2440$ g/mol, Source: PSS Polymer Standards Service GmbH, Mainz) by applying ^{2}H NMR and of TPP (Source: Sigma Aldrich) by means of ^{31}P NMR.

The studied concentrations c_{TPP} (by mass) are given again in Table I. For reasons of clarity throughout the paper always the nominal concentrations are taken to specify the sample.

III. RESULTS

A. Previous results from dielectric spectroscopy and NMR spectra

In order to provide an overview of the major results reported in our previous publication,[13] Figure 1(a) displays the correlation times $\tau(T)$ for the TPP/PS system for all concentrations c_{TPP} as they have been compiled by DS, DSC, and DLS, in addition some of the ^{2}H NMR results collected in the present contribution are included; they will be

TABLE I. TPP mass concentrations c_{TPP} of mixtures studied by the different methods, including the assumed errors. The samples are named after their nominal concentration.

c_{TPP} [%] nom.	0	10	20	30	36	45	50	60	70	80	90	95	100
DS	0	8 ± 3	18 ± 3	29 ± 2	…	45 ± 1	…	60 ± 1	…	80 ± 1	90 ± 1	95 ± 1	100
DSC	0	10 ± 1	20 ± 1	…	36 ± 1	45 ± 1	…	60 ± 1	70 ± 1	83 ± 1	90 ± 1	…	100
DLS	…	…	…	…	…	…	…	…	…	80 ± 1	90 ± 1	…	100
^{2}H NMR	0	10 ± 1	20 ± 1	…	…	…	50 ± 1	…	…	80 ± 1	90 ± 1	…	…
^{31}P NMR	…	10 ± 1	20 ± 1	…	…	…	50 ± 1	…	…	80 ± 1	90 ± 1	…	100

This article is copyrighted as indicated in the article. Reuse of AIP content is subject to the terms at: http://scitation.aip.org/termsconditions. Downloaded to IP: 132.180.10.132 On: Mon, 28 Apr 2014 09:04:16

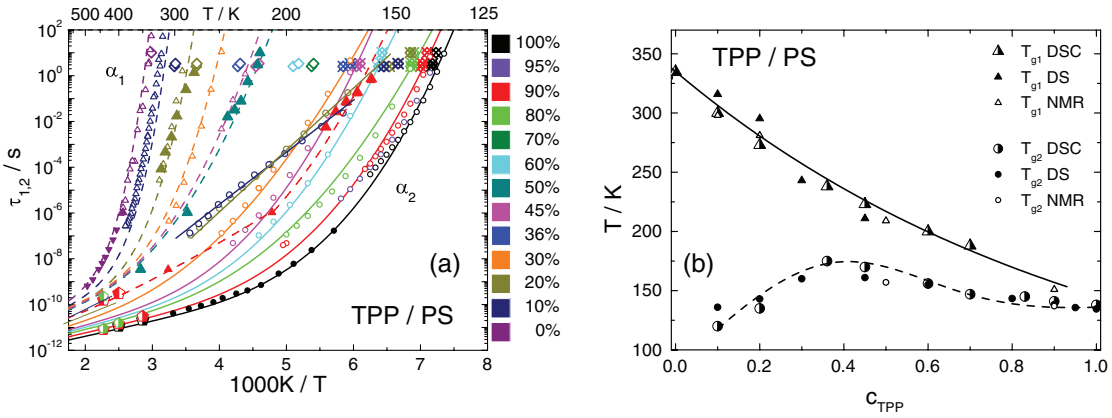

FIG. 1. (a) Time constants from DS (△: α_1; ○: α_2), ^{2}H NMR (▲; ▼: neat PS, Ref. 25), ^{31}P NMR (●: neat TPP, Ref. 26), DSC (◊: α_1; ⊠: α_2), and DLS (◖: α_1; ◗: α_2) for all investigated concentrations (cf. color code). Exact concentrations are given in Table I. Curved lines are guides for the eye (dashed: α_1-relaxation; solid: α_2-relaxation) (adapted from Ref. 13). (b) Glass transition temperatures as revealed by DSC, DS, and NMR (adapted from Ref. 13, lines serve as guides to the eye).

discussed in detail below. The full NMR results are displayed in Fig. 9 where they again are compared to part of the results provided by the other techniques. Concerning the TPP dynamics two relaxational processes have been identified which are attributed to two sub-ensembles of TPP molecules. One (α_1-process) shows frequency-temperature superposition (FTS) and displays time constants identical with those of the slow PS matrix (long time scale) addressed by ^{2}H NMR as will be demonstrated again below. The other reflects fast TPP dynamics (α_2-process; short time scale). Two glass transition temperatures T_{g1} and T_{g2} are identified (cf. Fig. 1(b)). $T_{g1}(c_{TPP})$ decreases steadily from neat PS down to highly diluted PS, $T_{g2}(c_{TPP})$ is significantly lower and exhibits a maximum around $c_{TPP} = 0.35$. The latter is a consequence of the anti-plasticizer effect, raising $T_{g2}(c_{TPP})$ by adding PS, and moreover a decreasing activation energy of the Arrhenius-like α_2-process at lower c_{TPP} (cf. Fig. 1(a)).

Regarding the spectral shape of the α_2-process, FTS does not apply and at low TPP concentration, the spectral evolution is governed by a temperature independent distribution of activation energies $g(E)$, which leads to mean logarithmic correlation times following Arrhenius laws; here, the α_2-relaxation highly resembles a secondary (β-) process.

For a first overview, solid-echo ^{2}H NMR spectra of neat PS ($T_g = 335$ K) as well as for the mixtures studied are shown in Fig. 2(a). In the case of neat PS at temperatures below 375 K the segmental correlation time is long compared to the inverse coupling constant $1/(2\pi\delta_Q)$, and a Pake spectrum typical of a solid with $\delta_Q = 125$ kHz (a fit is shown in Fig. 3(a)) is observed. Upon heating the line shape collapses within a

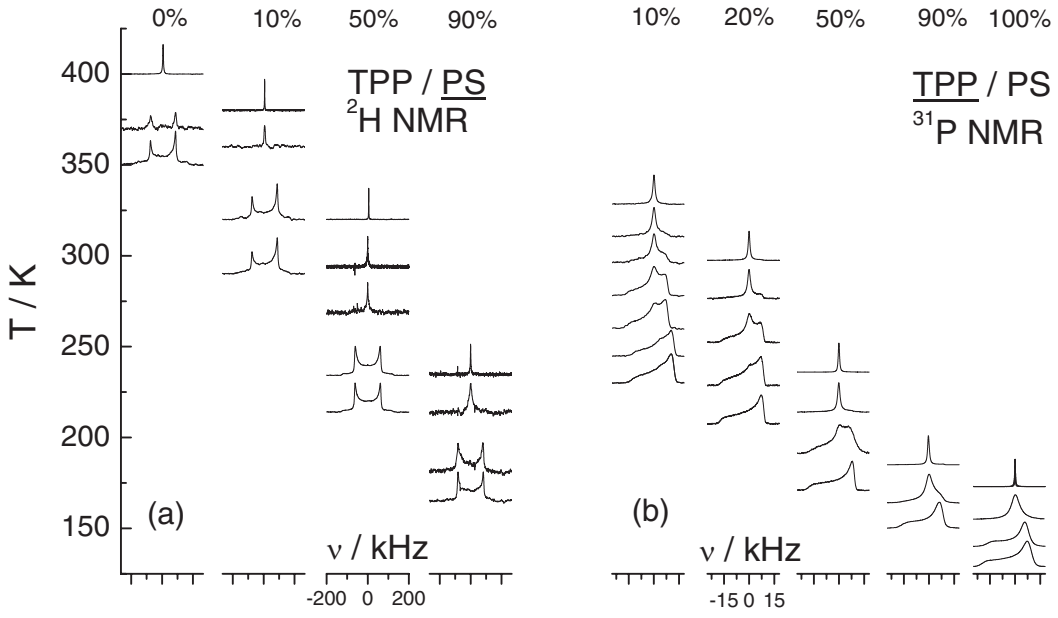

FIG. 2. (a) Selection of ^{2}H NMR solid-echo spectra for neat PS and PS in the mixtures; (b) ^{31}P NMR Hahn-echo spectra of neat TPP and TPP in mixtures. Temperature is given by the baseline of each spectrum.

This article is copyrighted as indicated in the article. Reuse of AIP content is subject to the terms at: http://scitation.aip.org/termsconditions. Downloaded to IP: 132.180.10.132 On: Mon, 28 Apr 2014 09:04:16

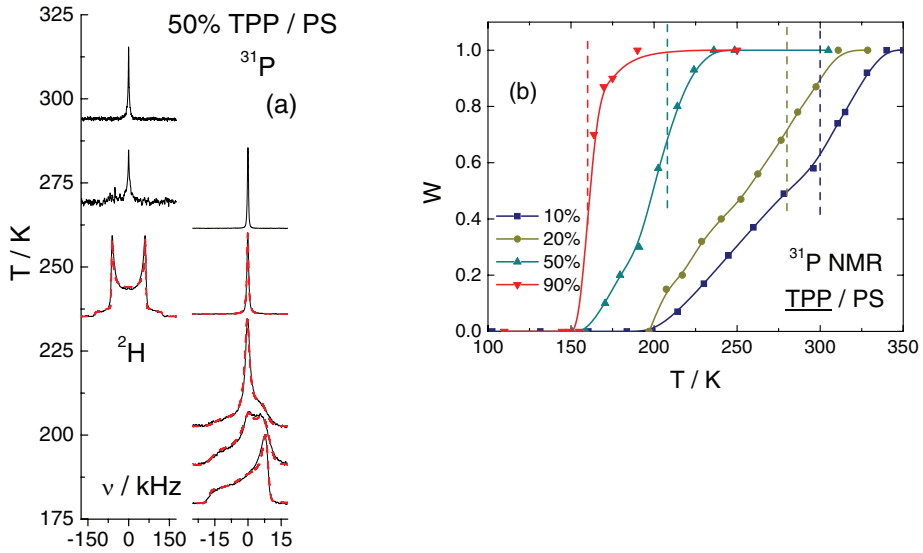

FIG. 3. (a) ^{2}H NMR solid-echo spectra (left column; probing PS) and ^{31}P NMR Hahn-echo spectra (right column; probing TPP), directly compared for c_{TPP} = 50%. Dashed red lines are two-phase spectral fits along Eqs. (1) and (2). (b) Temperature dependency of weighting factor $W(T)$ extracted from the fits of (a). Solid lines are guides for the eye. Vertical dashed lines indicate T_{g1} of the corresponding mixtures.

narrow temperature interval and at 400 K a central Lorentzian line, indicating isotropic reorientation faster than $1/(2\pi\delta_Q)$, is reached. With increasing TPP concentration the spectral collapse of PS is shifted to lower temperatures reflecting accelerated dynamics due to the plasticizer effect. The time constants $\tau(T) = 1/(2\pi\delta_Q) \approx 10^{-6}$ s estimated from the analysis of the line shape collapse are included in Fig. 9 (up triangles) for c_{TPP} = 0%, 10%, 50%, and 90%, where they are compared to the NMR results taken from Ref. 25 (neat PS) as well as results from our DS study;[13] good agreement is found. In the mixtures up to c_{TPP} = 50% the spectra of PS reveal $\tau(T)$ very close to that of the α_1-process probed by DS, while for even higher c_{TPP} values the α_1-process (probing actually the PS dynamics) cannot be resolved by DS because the weak signal is covered by DC conductivity, yet the $\tau(T)$ data fit well into the picture drawn by the other NMR results (cf. below). Besides a temperature shift no qualitative change of the ^{2}H NMR solid-echo spectra is observed, at any concentration the spectral collapse from Pake to the Lorentzian line is completed within a temperature interval of about 30 K. No indication of two-phase spectra is observed, i.e., the distribution of correlation times remains rather narrow as in the case of pure PS.

The corresponding ^{31}P NMR spectra of neat TPP and TPP in the mixtures are depicted in Fig. 2(b); they are dominated by the CSA interaction yielding an asymmetric spectrum at low temperatures. In the case of neat TPP (T_g = 135 K) a gradual collapse of the solid-state spectrum is observed within 20 K, characteristic of a rather narrow distribution $G(ln\,\tau)$ typical of neat glass formers. The spectral changes observed at c_{TPP} = 90% are still similar to that of neat TPP. At lower TPP concentrations, besides a shift of the spectral collapse to higher temperatures, mirroring the antiplasticizer effect, a different spectral quality is recognized as demonstrated in detail for c_{TPP} = 50% in Fig. 3(a). In contrast to the ^{2}H NMR spectra so-called two-phase spectra arise spanning a temperature range of up to 100 K.[6,27] As explained (cf. Sec. II, Eq. (2)) they are described by a weighted sum of a central Lorentzian line (reflecting liquid-like TPP molecules) and a solid-state subspectrum (reflecting slowly reorienting or immobilized molecules). Corresponding fits along Eqs. (1) and (2) are included in Fig. 3(a) yielding δ_{CSA} = 19.8 kHz. As a measure of the spectral change the weighting factor $W(T)$, that is the fraction of the liquid-like spectrum, is reproduced in Fig. 3(b). With decreasing TPP concentration, an increasing temperature interval is covered by $W(T)$.

Comparing the results of ^{31}P and ^{2}H NMR for a given sample, e.g., c_{TPP} = 50% in Fig. 3(a), one clearly recognizes the decoupling of the dynamics of the components, a phenomenon well known from previous NMR studies.[6,22,28] At T = 236 K all PS molecules in the 50% mixture are rigid (slow), however, all TPP molecules show fast isotropic reorientation. At first glance this seems to contradict the finding by DS of a slow TPP sub-ensemble associated with the PS dynamics. Here one has to keep in mind that according to our DS results the fraction $S_{\alpha 1}$ of α_1-molecules is around 0.1 collected for c_{TPP} = 50% at low temperature (see Fig. 5(b)) but strongly decreases upon heating, finally leading to a disappearance of the α_1-subensemble. Thus, the actual value of $S_{\alpha 1}$ at about 240 K is expected to be significantly lower than 0.1 and thus is not expected to be discernible in the ^{31}P spectra. However, a slight bimodality of $W(T)$ could be noticed for the lower concentrations. At any investigated concentration (except c_{TPP} = 90% where dynamic heterogeneities are less pronounced) isotropic reorientation of TPP molecules is probed far below T_{g1} that can only be attributed to the α_2-process and therefore the α_2-process has to be considered as liquid-like motion. However it is *a priori* not clear if it keeps its motional character at even lower temperatures. Given the fact that the process shows features typical of a β-process it could be possible that it involves hindered (spatially restricted) reorientation at low temperatures. 2D NMR, sensitive to slower motions,

This article is copyrighted as indicated in the article. Reuse of AIP content is subject to the terms at: http://scitation.aip.org/termsconditions. Downloaded to IP: 132.180.10.132 On: Mon, 28 Apr 2014 09:04:16

will show that the latter scenario most likely is not the case (cf. below).

While the PS dynamics in the mixtures, apart from the acceleration due to the plasticizer effect, remains similar compared to the neat system, the TPP dynamics becomes qualitatively very different when PS molecules are present. Besides the anti-plasticizer effect we find pronounced dynamic heterogeneities for the TPP molecules. With decreasing TPP concentration, an increasing temperature interval is covered by $W(T)$. This agrees with a broad distribution $G(\ln \tau)$ found by DS for the α_2-process (cf. Fig. 6). However, it cannot be decided from the TPP spectra if the powder sub-spectra are caused by a broadly distributed α_2-process or a α_1-process reflecting more or less immobilized TPP molecules associated with the PS dynamics. This problem is addressed in Sec. III B.

B. ^{2}H and ^{31}P NMR stimulated echo decays

More quantitative results concerning the slow dynamics of PS (probed by ^{2}H NMR) as well as that of TPP (by ^{31}P NMR) are provided by measuring stimulated echo decays. As short t_p values were chosen, the decay represents the reorientational correlation function $C_2(t)$. Regardless of the fact, that the rank-one correlation function $C_1(t)$ of the TPP molecules is probed by DS, we attempt to quantitatively compare both NMR and DS results.

The correlation functions measured by ^{2}H NMR (left column in Fig. 4) all can be interpolated by Kohlrausch decays $C_2(t) = \exp(-(t/\tau_K)^{\beta_K})$ and the time constants $\tau = \tau_K \Gamma(1/\beta_K)/\beta_K$ are included in Figs. 1(a) and Fig. 9. They coincide with those for the α_1-process of TPP compiled from DS. Thus, we once again conclude that a fraction of TPP molecules is associated with the dynamics of PS. The results of NMR, DLS, and DSC agree well. Clearly, the time constants differ strongly from those of the α_2-process reflecting TPP dynamics decoupled from that of the PS matrix. For each concentration time-temperature superposition (TTS) is well obeyed for PS. With rising concentration a weak trend to stronger stretching is observed; the corresponding Kohlrausch parameter β_K is given in Fig. 5(a). A similar trend is found for β_K obtained from the α_1-relaxation measured by DS, yet β_K is somewhat smaller. In the case of neat PS the NMR result for β_K taken from Ref. 25 coincides with the DS finding.

The ^{31}P stimulated echo decays probing the TPP dynamics reveal a more complex behavior (see right column in Fig. 4). A strong stretching is observed becoming extremely wide at low TPP concentration. Here, actually only part of the correlation loss shows up within the NMR time window and the correlation loss becomes similar to a quasi-logarithmic decay;[6,29] in addition, TTS does not apply. The decays have to be compared with the DS spectra shown in Fig. 6(a) displaying the α_2-process with $\nu_{max} \approx 1$ kHz, i.e., basically the Fourier transform of the function $C_1(t)$ probed by DS. The full sets of DS spectra have been reported in Ref. 13. Here, it is of relevance that the α_2-process exhibits a severe broadening, the extent of which is increasing with decreasing c_{TPP}. Explicitly the spectra broaden in particular on the low-frequency flank (cf. Fig. 6). The spectra therefore cannot be reproduced by a Kohlrausch function, yet a Havriliak-Negami (HN) function[30,31] works well for $c_{TPP} > 20\%$. At lower c_{TPP} values a temperature independent distribution of activation energies $g(E)$ is found (see the Appendix, Fig. 16, and Ref. 13). As discussed, DS also probes an α_1-process associated with the PS dynamics. Its relative contribution is only of relevance at low TPP concentrations (see Fig. 5(b)), and it has to be taken into account when comparing DS and NMR results for low concentration (cf. below).

In agreement with the low-frequency broadening of the DS spectra, at $c_{TPP} = 90\%$, the HN function, numerically transformed into the time domain, gives an appropriate interpolation of the stimulated echo (solid lines in Fig. 4, right column), while a Kohlrausch decay (dotted line) fails at long times. For the fitting, the product ab of the HN-parameters, defining the high-frequency flank of the DS peak and found to be independent of temperature, was fixed to $ab = 0.81$ as reported by DS. The fits yield $a(T)$ which coincides with that provided by DS (see Fig. 7(a)), and also the derived time constants agree well (see Fig. 9). Similarly, for $c_{TPP} = 80\%$ agreement is found between $C_2(t)$ and $C_1(t)$. As expected, both techniques probe virtually the same dynamics.

Inspecting the ^{31}P stimulated echo decays for lower TPP concentrations (Fig. 4), as said, they become extremely stretched. Moreover, the NMR time window is too narrow to resolve the initial as well as the long-time decay in most cases. In such cases, the short-time value is actually unknown. Since the fraction $W(T)$ of TPP molecules reorients faster than $1/(2\pi\delta_{CSA}) \approx 10^{-5}$ s and, therefore, does not contribute to the stimulated echo signal, the timescale of Fig. 4 starts at 10^{-5} s and the signal amplitude is normalized to $C_2(t = 10^{-5}\text{ s}, T) = 1 - W(T)$. Assuming again that the same dynamics is probed by DS and ^{31}P NMR, fits of the DS spectra reflecting the α_2-process are extrapolated adequately and Fourier transformed to the time domain (Fig. 4, dashed lines). In the case of $c_{TPP} = 50\%$ corresponding fits for $T = 168.1$ K, 174.6 K, and 198.2 K are included in Fig. 4. They show too fast decays and the long-time tail is underestimated. We attribute this discrepancy to the existence of a sub-ensemble of TPP molecules being essentially immobile, namely, the α_1-process well identified by DS and associated with the PS dynamics. In particular, a clearly bimodal decay is perceived at $c_{TPP} = 50\%$, $T = 198.2$ K (Fig. 4). In order to take this additional process into account a quantity $S_{\alpha 1}$ is introduced, representing the fraction of α_1-molecules which relaxes via a Kohlrausch decay at much longer times with a stretching and $\tau_1(T)$ given by the DS results ($\beta_K = 0.23$, see Fig. 5(a)) while $1 - S_{\alpha 1}$ reflects the fraction relaxing by the α_2-process. Clearly, the shape of the decay curves can be approximated with $S_{\alpha 1} \approx 0.12$ being essentially temperature independent. To exactly match the experimental data, the time constants $\tau_2(T)$ had to be slightly shifted; a direct comparison is given in Fig. 9. Aware of the uncertainties of comparing the results from different techniques and samples and the problem of fixing the absolute amplitude of the stimulated echoes, we think a fair agreement is achieved.

A similar approach was chosen for the mixtures with $c_{TPP} = 20\%$ and 10%. Here, DS revealed a thermally activated process based on a temperature independent distribution of activation energies $g(E)$ (see Fig. 16 and Ref. 13). This result

This article is copyrighted as indicated in the article. Reuse of AIP content is subject to the terms at: http://scitation.aip.org/termsconditions. Downloaded to IP: 132.180.10.132 On: Mon, 28 Apr 2014 09:04:16

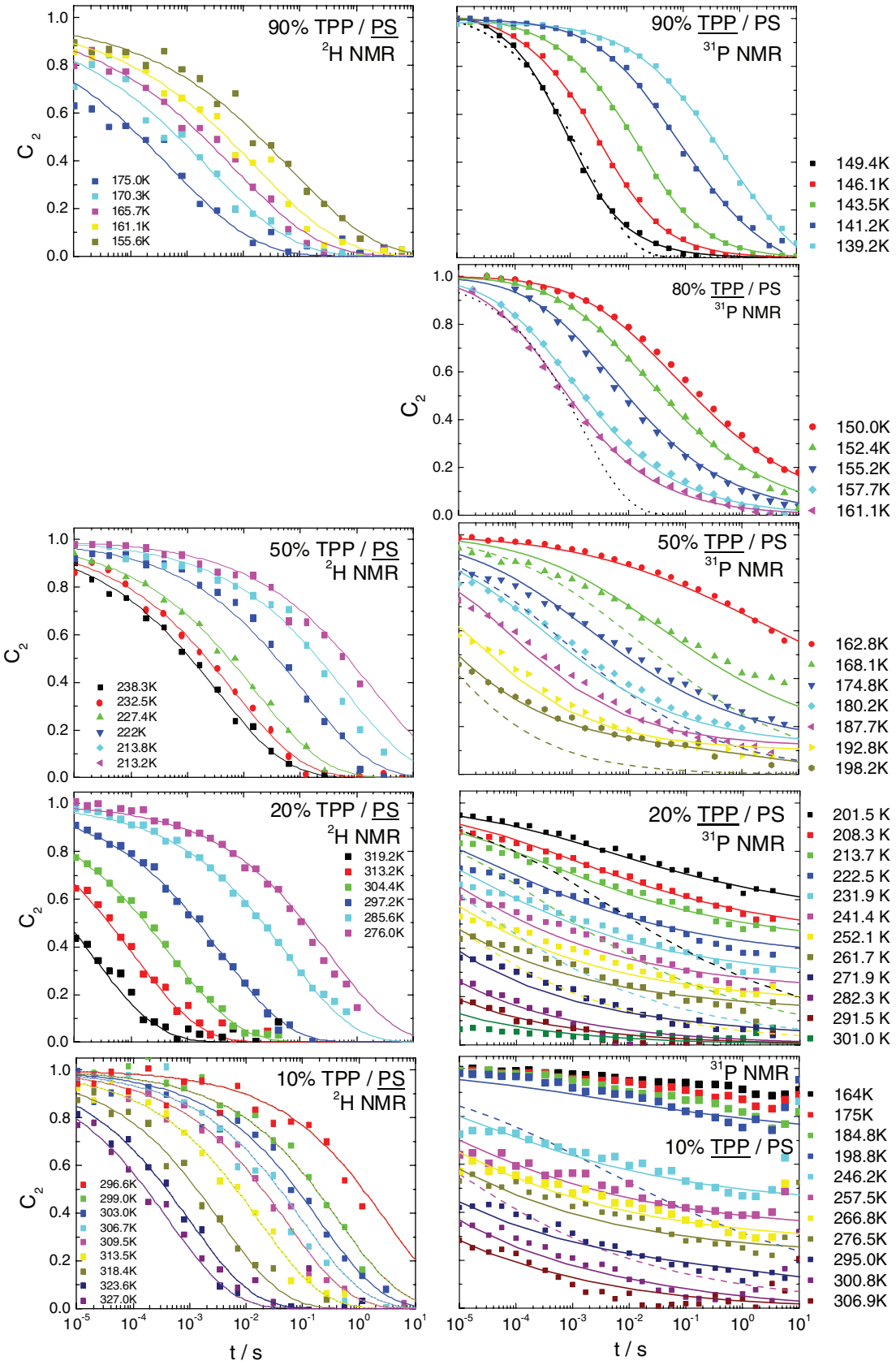

FIG. 4. Reorientational correlation functions $C_2(T)$, measured by the stimulated echo technique (all curves corrected for spin-lattice relaxation). Left column: ^{2}H NMR, solid lines: Kohlrausch fits. Right column: ^{31}P NMR (additionally corrected for spin diffusion), solid lines for $c_{TPP} = 90\%$, 80%: Havriliak-Negami (HN) fits, dotted lines: Kohlrausch fits with $\beta_K = 0.53$. Solid lines for $c_{TPP} \leq 50\%$: interpolation based on DS data, taking also α_1 contribution into account (cf. text); dashed lines: HN-fits accounting solely for the α_2-process.

This article is copyrighted as indicated in the article. Reuse of AIP content is subject to the terms at: http://scitation.aip.org/termsconditions. Downloaded to IP: 132.180.10.132 On: Mon, 28 Apr 2014 09:04:16

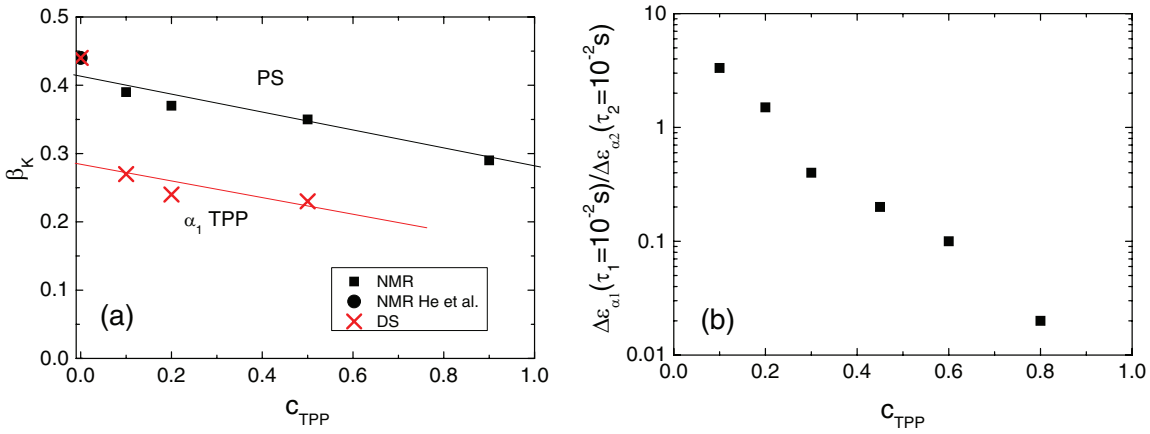

FIG. 5. (a) Kohlrausch stretching parameter β_K for neat PS (NMR taken from Ref. 25, DS taken from Ref. 13), PS in mixture measured by ^{2}H NMR, and polymer-attached TPP measured by DS. (b) Dielectric relaxation strength of α_1-process at $\tau_1 = 10^{-2}$ s relative to α_2-process at $\tau_2 = 10^{-2}$ s (cf. Ref. 13).

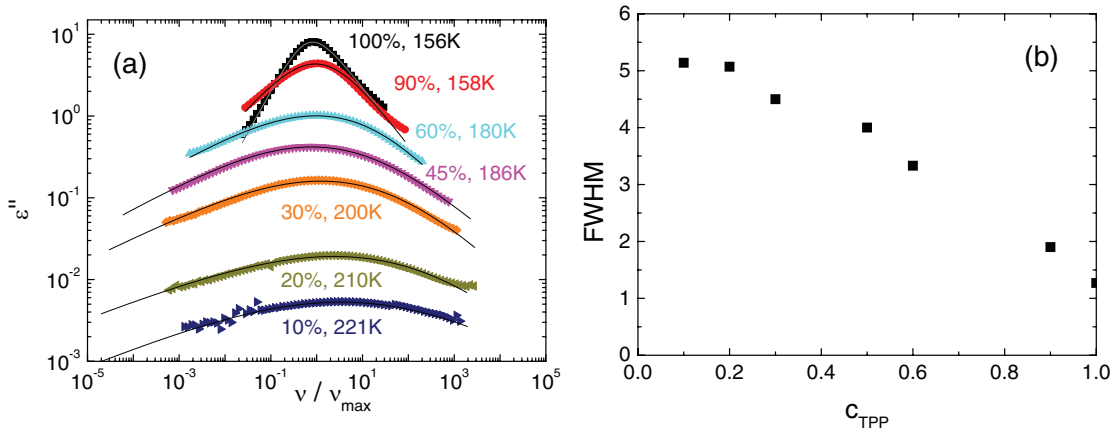

FIG. 6. (a) Dielectric spectra for different TPP concentrations at $\nu_{\max} \approx 1$ kHz. Solid lines: HN-fits, except for $c_{TPP} = 10\%$ and $c_{TPP} = 20\%$ for which interpolation by $g(E)$ is applied (cf. Appendix and Fig. 16). (b) Decadic width of DS α_2-peak shown in (a).

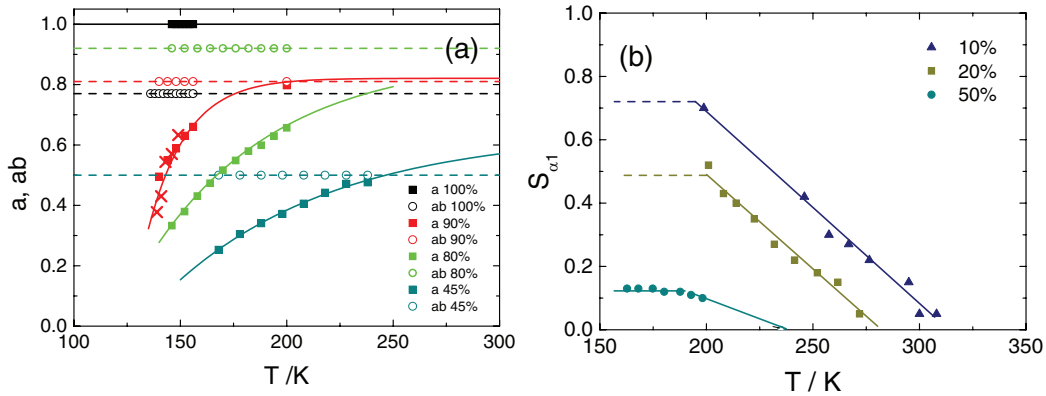

FIG. 7. (a) Temperature dependency of HN parameters a and ab, for various concentrations c_{TPP} as derived from DS data (full squares and open circles) and NMR stimulated echo decays (crosses); extrapolations for a (solid) and ab (dashed). (b) Fraction $S_{\alpha 1}(T)$ of TPP molecules participating in α_1-process, extracted from interpolations of ^{31}P NMR curves (Fig. 4, right column); solid lines serve as guides to the eye, dashed lines: anticipated behavior.

This article is copyrighted as indicated in the article. Reuse of AIP content is subject to the terms at: http://scitation.aip.org/termsconditions. Downloaded to IP: 132.180.10.132 On: Mon, 28 Apr 2014 09:04:16

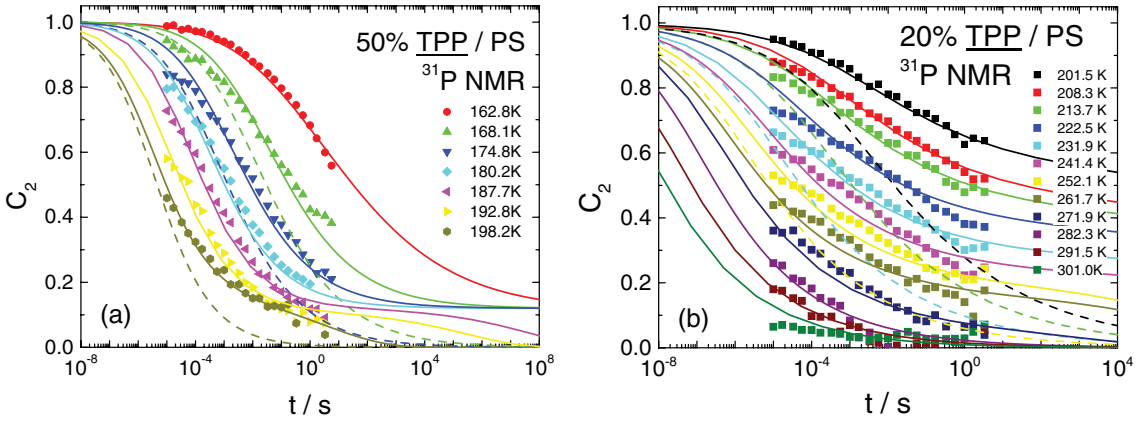

FIG. 8. ^{31}P stimulated echo data from Fig. 4 displayed on the time range provided by the DS results (solid lines), (a) $c_{TPP} = 50\%$. (b) $c_{TPP} = 20\%$. Dashed lines show mere α_2 decays from DS data interpolation.

taken, and again adding a slowly relaxing component caused by the α_1-process, the stimulated echo decays once more can be interpolated rather well. Now, the fraction $S_{\alpha 1}(T)$ exhibits a distinct temperature dependence (Fig. 7(b), see also Fig. 8(b) for $c_{TPP} = 20\%$). It grows upon cooling, a finding in qualitative agreement with DS results. Again, slight differences of $\tau_2(T)$ with respect to that of the DS analysis are recognized in Fig. 9. Remarkably, at $T \geq T_{g1}$ the temperature dependence of τ_2 grows (mind the arrows in Fig. 9), suggesting a transition from Arrhenius to non-Arrhenius behavior. For $c_{TPP} = 10\%$ the situation is similar. $S_{\alpha 1}(T)$ is extrapolated as given in Fig. 7(b) for all c_{TPP}, expecting a saturation behavior at low temperatures, as found in DS for 10% and 20%, and decreases to zero upon heating.

Summarizing, the dynamics of both TPP sub-ensembles identified by DS are re-discovered in the correlation functions $C_2(t)$ probed by the stimulated echo decays. In order to compare DS (including α_1 and α_2) and NMR, some inter-/extrapolations of DS data already shown in Fig. 4 are plotted within a larger time window (Fig. 8). Obviously, the stimulated echo decays cover only a smaller part. Yet, the DS forecasts provide a acceptable interpolation of the curves. The question still has to be answered whether the α_2-process, the appearance of which in the DS spectra highly resembles that of a secondary process, is an isotropic, liquid-like process for all temperatures, i.e., also for temperatures for which a solid-state spectrum is revealed (for example, at $c_{TPP} = 20\%$ and $T = 200$ K in Fig. 2(b)). Here, 2D spectra allow insight into the geometry of motion.

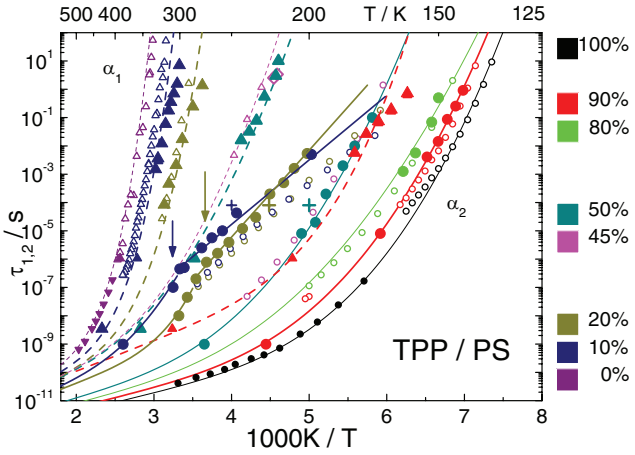

FIG. 9. Time constants from DS (△: α_1; ○: α_2), ^{2}H NMR (▲;▼: neat PS, Ref. 25; +: solid-echo (see Fig. 14)), ^{31}P NMR (●, neat TPP, Ref. 26), for investigated concentrations (cf. color code). Exact concentrations are given in Table I. Lines are guides to the eye (dashed: α_1-relaxation; solid: α_2-relaxation). Arrows indicate T_{g1}.

C. 2D ^{31}P NMR spectra

2D spectra for the sample with $c_{TPP} = 20\%$ at $T = 200$ K and at mixing times $t_m = 0.05$ ms, 500 ms, and 5000 ms are depicted in Fig. 10. No isotropic motion faster than

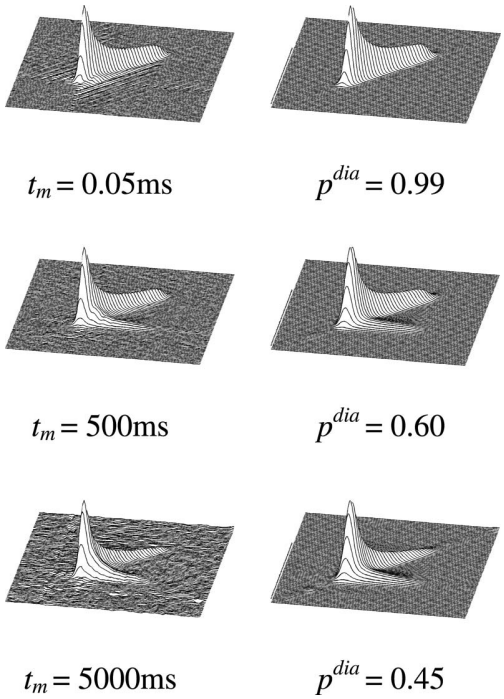

FIG. 10. 2D ^{31}P NMR spectra of TPP, $c_{TPP} = 20\%$, $T = 200$ K; left: experimental spectra with mixing times indicated; right: spectra calculated according to a two-phase model along Eq. (7) ($p^{liq} = p^{ex} = 0$), weighting factor p^{dia} of diagonal spectrum is given.

This article is copyrighted as indicated in the article. Reuse of AIP content is subject to the terms at: http://scitation.aip.org/termsconditions. Downloaded to IP: 132.180.10.132 On: Mon, 28 Apr 2014 09:04:16

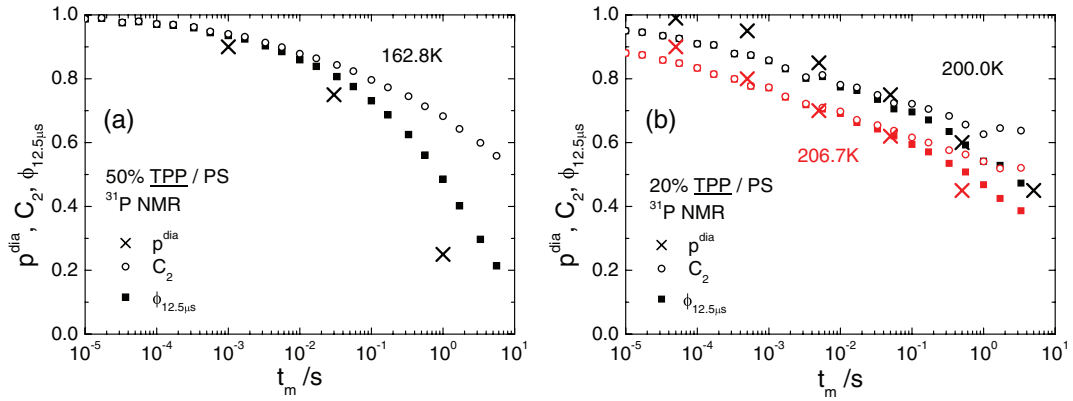

FIG. 11. Squares: Normalized correlation function $\phi_{12.5\mu s}(t_m)$ as function of mixing time (cf. Eq. (5), still affected by spin diffusion) as given by the decay of the stimulated echo; circles: $C_2(t)$ (corrected for spin diffusion); crosses: weighting factor p^{dia} from analysis of the 2D NMR spectra (partly shown in Fig. 10) (a) 50%, (b) 20%.

$1/(2\pi\delta_{CSA})$ is detectable, as no Lorentzian line is visible. For $t_m = 0.05$ ms essentially the entire intensity is found on the diagonal, i.e., no reorientation occurs on this time scale. For $t_m = 500$ ms signal in the plane arises, clearly indicating spatially unrestricted (isotropic) reorientation, and for $t_m = 5000$ ms the signal in the plane further gains intensity while diagonal intensity decreases. For a quantitative analysis the spectra are reproduced by the two-phase model (cf. Sec. II), i.e., a weighted sum of the two sub-spectra S_{dia} and S_{reo}, belonging to not reorienting and fully isotropically reorienting molecules, respectively. The model captures the essential features of the experimental 2D spectra (cf. Fig. 10, right column). As expected in the case of a broad distribution $G(\ln\tau)$ the weighting factor of the diagonal sub-spectra $p^{dia}(t_m)$ coincides fairly well with the stimulated echo decay $\phi_{12.5\mu s}(t_m)$[24] which, however, is damped by spin diffusion (cf. Fig. 11). Yet, even at longest times some intensity along the diagonal is still recognized indicating that not all molecules have moved. Those consist of the slowest molecules involved in the α_2-process, as well as immobilized molecules of the α_1-process. Due to the restricted time window, limited by spin-diffusion, the two α-processes cannot be discriminated. Since all observed motion can be attributed to fully isotropic reorientation, we conclude that there are no indications that the α_2-process changes its nature at low temperatures and becomes spatially restricted upon cooling.

Dynamic heterogeneities in asymmetric binary glass formers have been identified to be of transient nature as previously reported for other systems.[6,18,21] This is also observed in the present work as is demonstrated for $c_{TPP} = 20\%$ and $T = 269.5$ K in Fig. 12 (left). A typical cross-like pattern occurs for long t_m, which indicates that the timescales of fast and slowly reorienting molecules exchange. The spectra can quantitatively be reproduced by a weighted superposition of the four sub-spectra introduced in Sec. II (cf. Fig. 12 (right)). The resulting weighting factors p^i are given in Fig. 13. For short mixing times t_m the spectrum is a superposition of diagonal and Lorentzian sub-spectra, determined by the weighting factor W of the 1D spectrum. For longer t_m values isotropic reorientation and exchange occur both on the same timescale. A detailed analysis reveals some discrepancy between the p^i measured at longest t_m and that expected for the

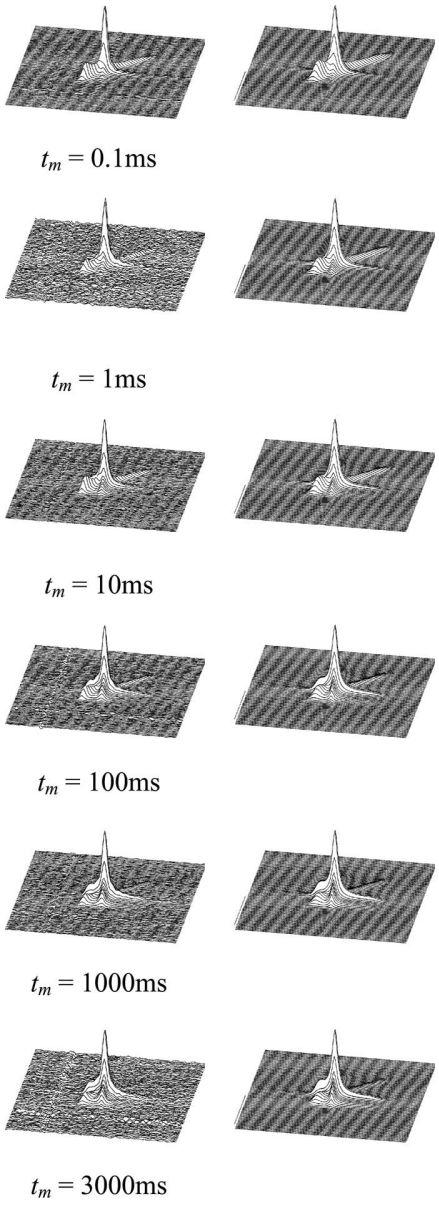

FIG. 12. 2D ^{31}P NMR exchange spectra, $c_{TPP} = 20\%$, $T = 269.5$ K; left: experimental, mixing times indicated; right: spectra calculated according to a four-phase model along Eq. (7).

This article is copyrighted as indicated in the article. Reuse of AIP content is subject to the terms at: http://scitation.aip.org/termsconditions. Downloaded to IP: 132.180.10.132 On: Mon, 28 Apr 2014 09:04:16

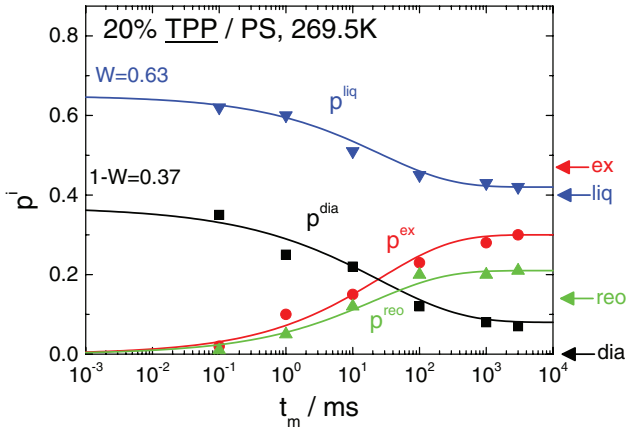

FIG. 13. 2D spectra weighting factors p^i estimated by superimposing four sub-spectra as obtained for the $c_{TPP} = 20\%$ sample shown in Fig. 12. Lines are guides for the eye, long-time limits as expected for full exchange are indicated by arrows (see Sec. II).

long-time limit considering full exchange (cf. Sec. II, Eq. (8)). In particular, a complete decay to zero is not observed for p^{dia} and also $p^{ex}(t_m \rightarrow \infty)$ lags behind the expectation. This discrepancy is explained by assuming a contribution of α_1 molecules which only relax at much longer times, in agreement with the analysis of the stimulated echo decays discussed above. Thus, the α_1-molecules exhibiting much longer correlation times do not take part in the observed exchange.

D. ^{2}H NMR solid echo and spin-lattice relaxation

A remarkable detail is revealed by the analysis of ^{2}H NMR solid-echo spectra, in particular, at temperatures below T_{g1} for which the usual solid-state Pake spectrum of PS-d_3 is observed, i.e., the isotropic PS dynamics is found in the limit of slow motion (cf. Fig. 2(a)). By prolonging the inter-pulse delay t_p of the solid-echo pulse sequence, sensitivity on small angular reorientation is gained, i.e., for long t_p values spatially highly restricted motion is probed, which actually does not affect the NMR spectra measured at short t_p.[32] This feature has been exploited to analyze the β-process in the present TPP/PS mixed glasses ($T < T_{g2}$) as well as in other glasses.[14,32–34] Figure 14(a) displays ^{2}H NMR solid-echo spectra of PS-d_3 at short $t_p = 20\ \mu$s (dashed lines) as well as at long $t_p = 200\ \mu$s, measured for $c_{TPP} = 20\%$ at temperatures well below T_{g1}. While the spectra for short t_p reflect the Pake spectrum, for long t_p and $T = 225$ K one can observe reduced intensity in the center of the spectrum. For quantification of the spectral effect, a parameter $R(T)$, specifying the intensity of the solid-echo spectra at $\nu = 0$ with respect to the intensity of the singularities, has been introduced.[34,35] A spatially restricted relaxation process crossing the time scale of the solid- or Hahn-echo experiment, i.e., $\tau \sim 1/\delta$ (see Ref. 36) leads to a minimum in $R(T)$.[14,32,37] In Fig. 14(b) $R(T)$ measured with long inter-pulse delay $t_p = 200\ \mu$s is depicted for neat PS and PS in mixtures. While neat PS does not show a distinct temperature dependence, a minimum around 120 K is found for the mixtures, which is due to the β-process and was discussed in Ref. 14. Around $T = 225$ K ($c_{TPP} = 20\%$) and $T = 250$ K ($c_{TPP} = 10\%$) a second minimum – corresponding to the spectra plotted in Fig. 14(a) – occurs before at even higher temperatures $R(T)$ decreases to zero due to the spectral collapse caused by the isotropic α-process of PS. The time constants $\tau \approx 1/\delta_Q$ are included in Fig. 9 as crosses and coincide with $\tau_{\alpha 2}$ corresponding to the fast α_2-process of TPP. Unmistakably the α_2-process, being an isotropic process for TPP, influences the PS matrix to perform a spatially highly restricted reorientational motion on the same timescale. In the case of $c_{TPP} = 50\%$ the minimum is not resolved because α_1- and α_2-process are not sufficiently separated.

The conclusion is further supported by measurements of the mean spin-lattice relaxation times $\langle T_1 \rangle$ displayed in Fig. 15 (cf. also Ref. 14). In the case of neat PS ($c_{TPP} = 0\%$), for $T < 320$ K, a weak temperature dependence is observed while for $T > 330$ K a strong decrease is found as the isotropic motion of the PS segments takes over the relaxation. In the case of the mixtures, the relaxation at low temperatures is governed by the β-process involving both TPP and PS (marked by β). Yet, in the case of $c_{TPP} = 50\%$ and 90% traces of a second minimum are seen well separated from

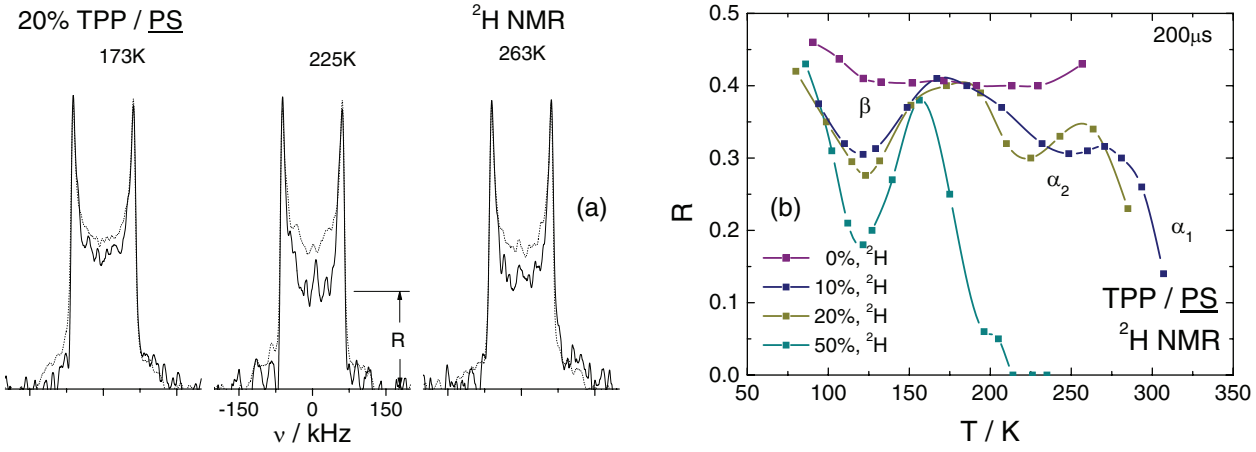

FIG. 14. (a) ^{2}H solid-echo spectra for $c_{TPP} = 20\%$, $t_p = 20\ \mu$s (dotted line) and $t_p = 200\ \mu$s (solid line) measured at indicated temperatures (below T_{g1}) and normalized to singularities. (b) line shape parameter R (see text) of ^{2}H NMR solid-echo spectra measured with $t_p = 200\ \mu$s of neat PS and PS in mixtures.

This article is copyrighted as indicated in the article. Reuse of AIP content is subject to the terms at: http://scitation.aip.org/termsconditions. Downloaded to IP: 132.180.10.132 On: Mon, 28 Apr 2014 09:04:16

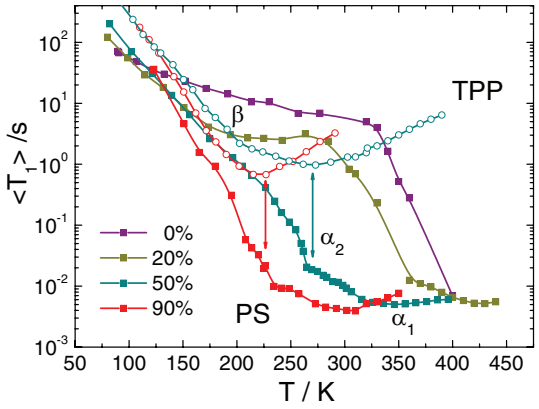

FIG. 15. Mean ^{2}H NMR spin-lattice relaxation times (full squares) for neat PS and PS in mixtures, arrows indicate coincidence with minima of corresponding ^{31}P NMR spin-lattice relaxation times (open circles).

the minimum around 400 K reflecting the α_1-process. The temperature of the second minimum coincides with the minimum in ^{31}P NMR spin-lattice relaxation time (open symbols, arrows), governed by the α_2-process.

IV. CONCLUSIONS

In a series of two papers we have analyzed the dynamics in the asymmetric binary glass former TPP/PS over a broad range of concentrations and temperature by means of DS, DLS, DSC, and NMR. Due to a large T_g contrast of $\Delta T_g \cong 200$ K pronounced dynamic heterogeneities are identified for the low-T_g component TPP while the PS dynamics remains essentially the same as in neat PS. We note that similar two-phase spectra have been reported for polymers plasticized with phosphorus containing low-molecular additives by Jones and coworkers[28,38] as well as for additives in polystyrene and PMMA.[6,24] The TPP dynamics comprises two sub-ensembles of molecules both of which exhibit isotropic liquid-like reorientation, which is also reflected by the fact that two T_g values are found. One sub-ensemble (α_1) is linked to the dynamics of PS, the other (α_2) performs a dynamically decoupled motion in a matrix of essentially immobilized PS and TPP molecules. The $G(\ln\tau)$ corresponding to the α_2-process is extremely broad in particular at low c_{TPP} and FTS does not apply. We note that extremely broadened and strongly temperature dependent correlation time distributions have also been reported for polymer blends.[39] In the time domain the corresponding decay extends over more than 16 decades which actually is too broad to be fully captured by the ^{31}P NMR stimulated echo technique. Yet, transforming the dielectric spectra into the time domain the fundamental features of the stimulated echo decays are reproduced.

Moreover, 2D NMR allows to identify exchange within the distribution occurring on virtually the same time scale as τ_2 as reported before for other systems.[6,21,40] The exchange among fast and slow molecules of the α_2-subensemble occurs even in the rigid PS matrix and we have concluded that the α_1 sub-ensemble is not involved in the exchange process. Regarding the fraction of the α_2-subensemble a strong decrease is observed at high temperatures, which finally leads to a disappearance of this slow sub-ensemble at a certain temperature. At higher temperatures all TPP molecules reorient significantly faster than those of PS, although the separation of the timescales becomes smaller and smaller upon heating, as expected.

The temperature dependence of the fast α_2-process changes from non-Arrhenius behavior at high concentration to Arrhenius behavior at low concentration. The corresponding mean activation energy decreases at even lower concentrations. This explains the maximum in $T_{g2}(c_{TPP})$ (cf. Fig. 1(b)). At low c_{TPP} signatures of a fragile-to-strong transition upon cooling are observed, similar to the results of the study of a polymer blend.[41]

Although the DS spectra of the α_2-process show many features typical of a β-process, NMR identifies the process as an isotropic liquid-like motion, and we reserve the term β-process for a spatially hindered motion persisting also below T_g. The α_2-process of TPP influences the PS matrix in a way to perform a spatially restricted motion on the same time scale, the nature of which still has to be elucidated.

In conclusion, only by combining the strength of the different experimental methods, the rather complex dynamics of asymmetric binary glass formers has been unravelled. In particular, selectivity and sensitivity of NMR allows to clarify the very nature of the different relaxational processes.

ACKNOWLEDGMENTS

The authors acknowledge financial support by Deutsche Forschungsgemeinschaft (DFG) under Grant Nos. RO 907/10 and /11.

APPENDIX: DISTRIBUTION OF ACTIVATION ENERGIES FOR α_2-PROCESS AS REVEALED BY DIELECTRIC SPECTROSCOPY

For $c_{TPP} = 10\%$ and 20% a temperature independent distribution of activation energies $g(E)$ describes the DS spectra of the α_2-process (cf. Ref. 13). The result is shown in Fig. 16. For calculations of NMR observables, namely, $C_2(t)$,

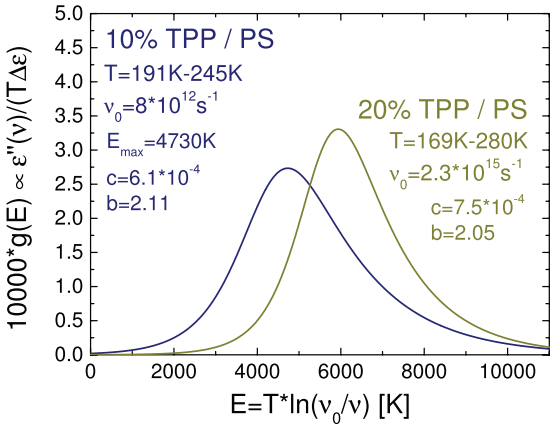

FIG. 16. Distributions of activation energies $g(E)$ according to Eqs. (A1) and (A2) derived from DS data for $c_{TPP} = 10\%$ and $c_{TPP} = 20\%$ as used for interpolations of NMR data.

This article is copyrighted as indicated in the article. Reuse of AIP content is subject to the terms at: http://scitation.aip.org/termsconditions. Downloaded to IP: 132.180.10.132 On: Mon, 28 Apr 2014 09:04:16

the distribution $g(E)$ was interpolated with a phenomenological function (see Ref. 42); explicitly

$$g(E) = N(c, b)\frac{1}{b\exp\left[c\left(E - E_m\right)\right] + \exp\left[-cb\left(E - E_m\right)\right]} \tag{A1}$$

with a normalization factor

$$N(c, b) = \frac{c\left(1 + b\right)}{\pi} b^{b/(1+b)} \sin\left(\frac{\pi b}{1 + b}\right). \tag{A2}$$

The parameters used are given in Fig. 16.

[1] P. J. Hains and G. Williams, Polymer **16**, 725 (1975).
[2] M. A. Desando, S. Walker, and W. H. Baarschers, J. Chem. Phys. **73**, 3460 (1980).
[3] M. Scandola, G. Ceccorulli, and M. Pizzoli, Polymer **28**, 2081 (1987).
[4] M. Nakazawa, O. Urakawa, and K. Adachi, Macromolecules **33**, 7898 (2000).
[5] D. Cangialosi, A. Alegría, and J. Colmenero, J. Chem. Phys. **126**, 204904 (2007).
[6] D. Bingemann, N. Wirth, J. Gmeiner, and E. A. Rössler, Macromolecules **40**, 5379 (2007).
[7] T. Blochowicz, S. Schramm, S. Lusceac, M. Vogel, B. Stühn, P. Gutfreund, and B. Frick, Phys. Rev. Lett. **109**, 035702 (2012).
[8] J. Bosse and Y. Kaneko, Phys. Rev. Lett. **74**, 4023 (1995).
[9] V. Krakoviack, Phys. Rev. E **79**, 061501 (2009).
[10] T. Voigtmann and J. Horbach, Phys. Rev. Lett. **103**, 205901 (2009).
[11] T. Voigtmann, Europhys. Lett. **96**, 36006 (2011).
[12] J. Kurzidim, D. Coslovich, and G. Kahl, J. Phys.: Condens. Matter **23**, 234122 (2011).
[13] R. Kahlau, D. Bock, B. Schmidtke, and E. A. Rössler, J. Chem. Phys. **140**, 044509 (2014).
[14] D. Bock, R. Kahlau, B. Micko, B. Pötzschner, G. J. Schneider, and E. A. Rössler, J. Chem. Phys. **139**, 064508 (2013).
[15] R. Böhmer, G. Diezemann, G. Hinze, and E. A. Rössler, Prog. Nucl. Magn. Reson. Spectrosc. **39**, 191 (2001).
[16] E. Rössler, M. Taupitz, K. Börner, M. Schulz, and H.-M. Vieth, J. Chem. Phys. **92**, 5847 (1990).
[17] D. Schaefer, J. Leisen, and H. W. Spiess, J. Magn. Reson., Ser. A **115**, 60 (1995).
[18] K. Schmidt-Rohr and H. W. Spiess, *Multidimensional Solid-State NMR and Polymers* (Academic Press, New York, 1994).
[19] F. Fujara, S. Wefing, and H. W. Spiess, J. Chem. Phys. **84**, 4579 (1986).
[20] M. Bloom, J. H. Davis, and M. I. Valic, Can. J. Phys. **58**, 1510 (1980).
[21] M. Vogel and E. Rössler, J. Phys. Chem. A **102**, 2102 (1998).
[22] T. Blochowicz, C. Karle, A. Kudlik, P. Medick, I. Roggatz, M. Vogel, C. Tschirwitz, J. Wolber, J. Senker, and E. Rössler, J. Phys. Chem. B **103**, 4032 (1999).
[23] M. Vogel, P. Medick, and E. Rössler, Annu. Rep. NMR Spectrosc. **56**, 231 (2005).
[24] P. Medick, M. Vogel, and E. Rössler, J. Magn. Reson. **159**, 126 (2002).
[25] Y. He, T. R. Lutz, and M. D. Ediger, Macromolecules **37**, 5032 (2004).
[26] S. Adishchev, D. Bock, C. Gainaru, R. Kahlau, B. Micko, N. Petzold, B. Pötzschner, and E. A. Rössler, Z. Phys. Chem. **226**, 1149 (2012).
[27] P. Medick, T. Blochowicz, M. Vogel, and E. Rössler, J. Non-Cryst. Sol. **307–310**, 565 (2002).
[28] R. P. Kambour, J. M. Kelly, B. J. McKinley, B. J. Cauley, P. T. Inglefield, and A. A. Jones, Macromolecules **21**, 2937 (1988).
[29] A. J. Moreno and J. Colmenero, J. Chem. Phys. **124**, 184906 (2006).
[30] S. Havriliak and S. Negami, Polymer **8**, 161 (1967).
[31] R. Zorn, J. Polym. Sci., Part B **37**, 1043 (1999).
[32] M. Vogel and E. Rössler, J. Magn. Reson. **147**, 43 (2000).
[33] M. Vogel and E. Rössler, J. Chem. Phys. **114**, 5802 (2001).
[34] B. Micko, C. Tschirwitz, and E. A. Rössler, J. Chem. Phys. **138**, 154501 (2013).
[35] S. A. Lusceac, C. Gainaru, M. Vogel, C. Koplin, P. Medick, and E. A. Rössler, Macromolecules **38**, 5625 (2005).
[36] In the special case of a β-process RW-simulations showed that the minimum temperature of $R(T)$ slightly depends on t_p and $\tau \approx 1/\delta$ gives an appropriate estimation for $t_p = 200\ \mu$s.
[37] S. A. Lusceac, Ph.D. thesis, Universität Bayreuth, 2005.
[38] P. Bergquist, Y. Zhu, A. A. Jones, and P. T. Inglefield, Macromolecules **32**, 7925 (1999).
[39] M. Wachowicz and J. L. White, Macromolecules **40**, 5433 (2007).
[40] K. Schmidt-Rohr and H. W. Spiess, Phys. Rev. Lett. **66**, 3020 (1991).
[41] C. Lorthioir, A. Alegria, and J. Colmenero, Phys. Rev. E **68**, 031805 (2003).
[42] T. Blochowicz, C. Tschirwitz, S. Benkhof, and E. A. Rössler, J. Chem. Phys. **118**, 7544 (2003).

This article is copyrighted as indicated in the article. Reuse of AIP content is subject to the terms at: http://scitation.aip.org/termsconditions. Downloaded to IP: 132.180.10.132 On: Mon, 28 Apr 2014 09:04:16

Publikation 4

Dynamic heterogeneities in glass-forming systems

D. Bock, N. Petzold, R. Kahlau, S. Gradmann, B. Schmidtke, N. Benoit, and E. A. Rössler

Journal of Non-Crystalline Solids 407, 88 (2015).

© 2014 Published by Elsevier B.V.
doi:10.1016/j.jnoncrysol.2014.09.029

Journal of Non-Crystalline Solids 407 (2015) 88–97

Contents lists available at ScienceDirect

Journal of Non-Crystalline Solids

journal homepage: www.elsevier.com/ locate/ jnoncrysol

Dynamic heterogeneities in glass-forming systems

D. Bock, N. Petzold, R. Kahlau, S. Gradmann, B. Schmidtke, N. Benoit, E.A. Rössler *

Universität Bayreuth, Experimentalphysik II, D-95440 Bayreuth, Germany

ARTICLE INFO

Article history:
Received 26 May 2014
Received in revised form 10 September 2014
Accepted 13 September 2014
Available online 2 October 2014

Keywords:
Binary glass formers;
Confinement effects;
Relaxation;
NMR

ABSTRACT

We discuss the manifestation of dynamic heterogeneities in binary glass formers made of components with strongly different glass transition temperatures as revealed by ^{2}H and ^{31}P nuclear magnetic resonance spectroscopy (NMR) techniques such as line-shape, spin-lattice relaxation, and 2D exchange NMR. Polymer–plasticizer and non-polymeric mixtures are considered. Together with results from dielectric spectroscopy as well as from dynamic light scattering the component dynamics is probed separately. While the high-T_g component shows relaxation features similar to that of neat glass formers, the majority of the low-T_g component displays significantly faster dynamics and shows pronounced dynamic heterogeneities, i.e., an extremely broad distribution of correlation times $G(\ln\tau)$, which may lead to quasi-logarithmic correlation functions and which are reflected in a characteristic NMR phenomenology. Consequently, two glass transition temperatures with non-trivial concentration dependences are identified. The dynamic heterogeneities are transient in nature as proven by 2D exchange NMR. Thus, below the upper T_g liquid-like (isotropic) reorientation as well as exchange within the distribution $G(\ln\tau)$ is observed in an essentially rigid matrix formed by the high-T_g component. Yet, we find indications that a small fraction of the low-T_g component follows the dynamics of the high-T_g component. The results are compared with those collected for glass formers subjected to confining geometries. In both cases, the NMR features are very similar suggesting that also in binary glass formers (intrinsic) confinement effects may control the dynamics.

© 2014 Elsevier B.V. All rights reserved.

1. Introduction

The glass transition is a well studied phenomenon, yet full understanding is still missing [1–12]. Among its prominent features, like super-Arrhenius temperature dependence of the structural relaxation time and relaxation stretching, the presence of dynamic heterogeneities has gained particular interest [11–15]. That is, mobile and less mobile molecules can be distinguished, moreover, according to computer simulations, they are clustered in space and the correlated regions appear to grow in size upon cooling thus reflecting an increasing length scale as a possible cause of the glass transition phenomenon. While actually the extent of dynamic heterogeneities, represented by the measured distribution of correlation times $G(\ln\tau)$, is rather small in pure (viscous) liquids and sophisticated experimental techniques have to be applied to identify them [16–18], pronounced effects are observed in binary systems like polymer–plasticizer systems [19–26] or even in mixtures of simple liquids [27–32]. Regarding polymer blends not being within the scope of this contribution similar features are reported [33–35]. The effects strongly depend on the difference of the glass transition temperature T_g of the pure components, i.e., on the T_g contrast ΔT_g. As many polymers show high T_g, asymmetric binary glass formers are most conveniently prepared by blending a polymer with a low-molecular mass additive. It is well established that such systems may exhibit two glass transition temperatures albeit they are fully miscible [32–37]. The pronounced dynamic heterogeneities in mixed systems are documented in particular by nuclear magnetic resonance spectroscopy (NMR), especially with the help of two-dimensional (2D) exchange spectra which also allow for identifying the transient nature of the dynamic heterogeneities [22,24–26,38,39]. As the distribution $G(\ln\tau)$ in such asymmetric glass formers is much broader than in the case of pure glass formers it is experimentally quite easy to select a subensemble of molecules and monitor its evolution in time — as will also be documented in the present contribution.

Strong dynamic heterogeneities are also observed for glass formers embedded in confining geometries, like liquids in nano-porous systems [40–47]. Here, the NMR phenomenology appears to be rather similar to that of asymmetric binary glass formers. Intrinsic confinement effects may thus also be expected when the more mobile (low-T_g) component still relaxes in a matrix made up by the arrested (high-T_g) component. It is the purpose of the present contribution to demonstrate the high similarity of the phenomena in binary glass formers and glass formers in confining geometries, especially as documented by NMR experiments.

Binary systems of particles differing significantly in size or exposed to confining geometries have also been investigated by molecular dynamic simulations as well as by mode coupling theory (MCT) [48–52]. In contrast to neat systems, for which a type-B glass transition scenario is expected by MCT, which is triggered by cage formation and characterized by a discontinuous change of the non-ergodicity parameter f from zero to $f > 0$ at a critical temperature T_c, the mobile molecules in binary

* Corresponding author.
E-mail address: ernst.roessler@uni-bayreuth.de (E.A. Rössler).

http://dx.doi.org/10.1016/j.jnoncrysol.2014.09.029
0022-3093/© 2014 Elsevier B.V. All rights reserved.

liquids are expected to exhibit a type-A transition, and f should increase continuously from zero upon cooling below T_c. Here, the mobile (small) particles undergo a localization transition, while the less mobile (large) ones are still arrested due to the cage effect. First experimental hints for such type-A transitions in mixed molecular liquids have recently been reported [37,53]. We note that dynamic heterogeneities in mixed systems have also been explained either by concentration fluctuations [54] or self-concentration effects [30,55,56].

It is the aim of the present contribution to dwell on this issue by reporting on the results of recent NMR experiments, including line shape, stimulated echo, 2D, and spin-lattice relaxation experiments. For binary glass formers, NMR allows us to study selectively the dynamics of each component. In all NMR experiments characteristic features are observed which signal the presence of strong dynamic heterogeneities. The paper is meant as a kind of review; part of the results have been published elsewhere [26,37,38,44] while all the T_1 relaxation data as well as the results for a non-polymeric binary mixture are presented for the first time. Concerning details of the NMR methodology the reader may consult Refs. [8,16,57–59]. The results are quantitatively analyzed together with those compiled by dielectric spectroscopy. In addition we collected data from dynamic light scattering including tandem-Fabry–Perot interferometry (TFPI) [60,61] and photon correlation spectroscopy (PCS) [62]. We consider the components tripropyl phosphate (TPP), m-tricresyl phosphate (m-TCP), 2-methyltetrahydrofuran (MTHF), polystyrene (PS) and polymethylmethacrylate (PMMA). They are studied in mixtures in the combinations TPP/PS ($\Delta T_g \cong 200$ K), m-TCP/PMMA ($\Delta T_g \cong 176$ K), and MTHF/m-TCP (a non-polymeric system with $\Delta T_g \cong 109$ K) as well as in confining geometry. Concentrations are given in mass percentage of the low-T_g component.

2. Results

2.1. NMR spectra

The ^{31}P NMR spectra of neat m-TCP and in mixtures with PMMA are shown in Fig. 1(a); they are dominated by the chemical shift anisotropy (CSA) interaction yielding an asymmetric solid-state spectrum at low temperatures, while at high temperatures a Lorentzian central line is observed due to fast isotropic (liquid) dynamics. In the case of neat m-TCP ($T_g = 205$ K) a continuous collapse of the solid-state spectrum is observed within about 20 K, characteristic of a rather narrow distribution of correlation times $G(\ln \tau)$ typical of neat glass formers. While the spectral changes observed at $c_{m\text{-}TCP} = 86\%$ are still similar to that of neat m-TCP, at lower m-TCP concentrations, besides a shift of the spectral collapse to higher temperatures, mirroring the anti-plasticizer effect, a different spectral quality is recognized, namely the occurrence of the so-called two phase spectra [38,58,63] spanning a temperature interval of up to 100 K. They are described by a weighted sum of a central Lorentzian line (reflecting liquid-like molecules) and a solid-state sub-spectra (reflecting slowly reorienting or immobilized molecules). Such two-phase spectra are a finger print of strong dynamical heterogeneities and their explanation is sketched in Fig. 2. Due to a broad distribution $G(\ln \tau)$ only the limiting spectra of fast (isotropic) and slow (isotropic) reorientation are observed; the so-called intermediate spectra as observed in the case of neat glass formers can be ignored, since the fraction of molecules with reciprocal time constants on the order of the NMR coupling constant is small in a broad distribution [38,58,63]. As a measure of the spectral change, the weighting factor $W(T)$, that is the fraction of the liquid-like spectrum, is reproduced in Fig. 3(a) as derived from a fit to the spectra. With decreasing m-TCP concentration, an increasing temperature range is covered by $W(T)$.

Determined by the quadrupolar interaction, the ^{2}H NMR spectra of PS in another system, a 50% mixture of TPP in PS, are shown in Fig. 3(b). Compared to neat PS [38] the spectral collapse of PS is shifted to lower temperatures reflecting accelerated dynamics due to the plasticizer effect. Besides a temperature shift no qualitative change of the ^{2}H spectra is observed: At any concentration the spectral collapse from Pake to the Lorentzian line is finished within a narrow temperature interval. Comparing the ^{31}P and ^{2}H NMR spectra for a given sample (cf. Fig. 3(b)) one clearly recognizes the decoupling of the dynamics of the components. While for PS a broad solid-state spectrum characteristic of slow motion is observed, the ^{31}P spectra of TPP still reflect fast isotropic motion — even below T_{g1}. In addition, in contrast to TPP, the high-T_g component polystyrene in the mixed glass formers does not show strong dynamic heterogeneities as no two-phase spectra are observed.

We also measured binary glass formers made from non-polymeric components which still exhibit a large T_g contrast. In Fig. 4 the NMR spectra of the system MTHF/m-TCP are shown. In the mixture, again, two-phase spectra are recognized for the low-T_g component MTHF while they are not found for the high-T_g component m-TCP. Yet, the temperature interval for which two-phase spectra appear is significantly smaller than in the case of m-TCP/PMMA and, of course, is found at much lower temperature when compared with the polymer–plasticizer system TPP/PS or m-TCP/PMMA. The corresponding weighting factors of the two-phase spectra are included in Fig. 3(b); they cover

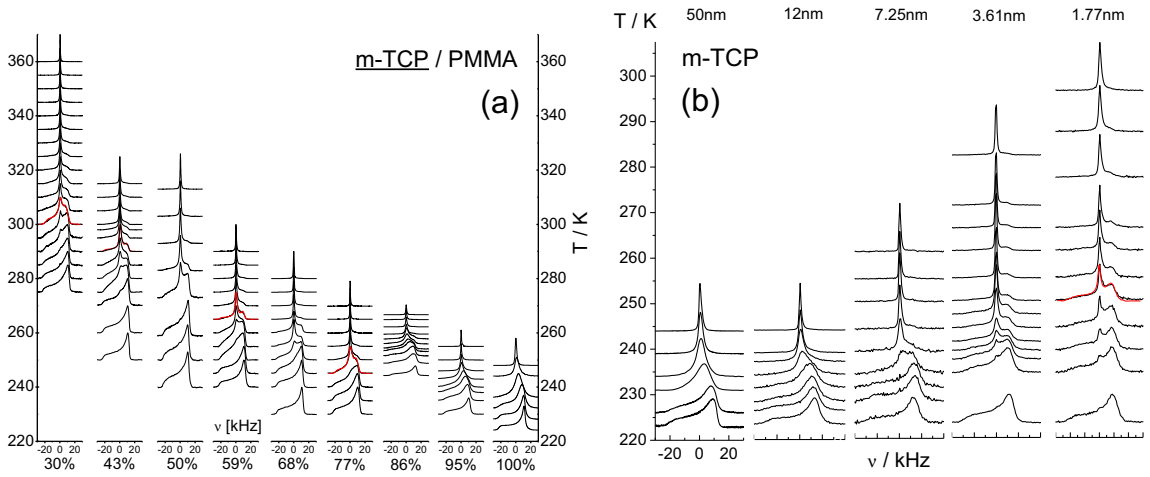

Fig. 1. ^{31}P NMR spectra, baseline of spectra marks temperature on vertical axis. Red lines are spectral fits by the two-phase model. (a) m-TCP in PMMA at different concentrations. (b) m-TCP in porous silica matrices with different pore radii in nm, adapted with permission from Ref. [45]. Copyright (2009) American Chemical Society.

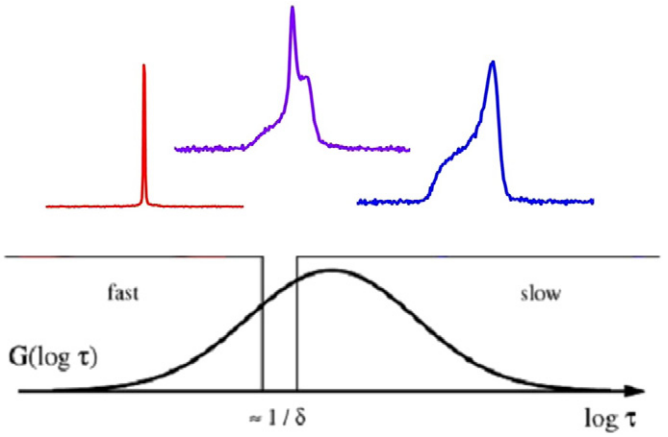

Fig. 2. So-called two-phase ^{31}P NMR spectra, explained by the presence of a broad distribution of correlation times $G(\ln \tau)$. A superposition of a central Lorentzian line (fast isotropic dynamics) and a broad solid-state spectrum (slow motion) is found while the distribution shifts through the NMR time window.

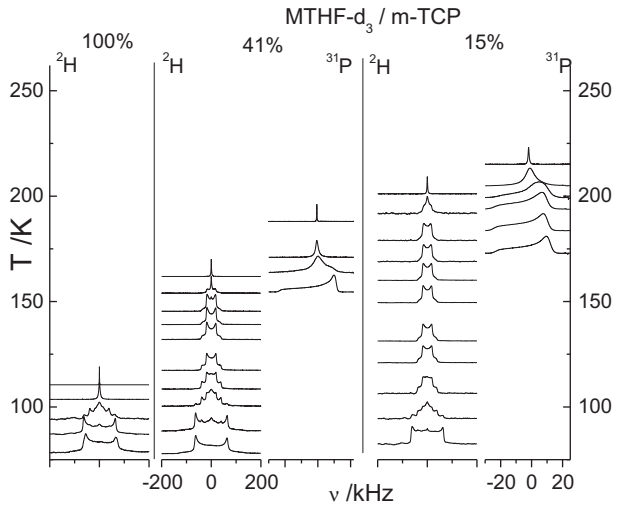

Fig. 4. ^{2}H NMR spectra of neat MTHF (c_{MTHF} = 100%) and in MTHF in mixtures with m-TCP (c_{MTHF} = 41% and 15%), and ^{31}P NMR spectra of m-TCP in mixtures. Baseline of spectra marks temperature on vertical axis.

significantly lower temperatures as for the m-TCP/PMMA mixtures. In the case of MTHF (see Fig. 4), at lowest temperatures the spectra further broaden due to the slowing down of the methyl group reorientation.

Finally, in Fig. 1(b) the ^{31}P NMR spectra of m-TCP in nano-porous silica matrices are displayed for comparison [45]. For a pore radius of r = 50 nm the liquid still shows spectra identical with those of neat m-TCP, however, starting with r = 7.55 nm first indications of two-phase spectra are found and they are most pronounced in the case r = 1.77 nm. Thus, also in confining geometries below a pore radius of, say, 10 nm the dynamics of glass formers is controlled by a broad distribution $G(\ln \tau)$ reflecting dynamic heterogeneities.

2.2. Dielectric spectra

As the dynamics in binary glass-forming liquids appears to be rather complex, dielectric spectra provide additional important information, in particular, they allow for extracting time constants for the various relaxation processes [41] and thereby facilitate the interpretation of the NMR results. Here we again consider the mixed systems TPP/PS and MTHF/m-TCP.

As described previously [37], the dielectric susceptibility spectra of neat PS (M = 2240 g/mol and T_g = 335 K) reflecting the structural or α-relaxation follow frequency–temperature superposition (FTS), i.e., the spectral shape of the susceptibility does not significantly change with temperature. Close to T_g, the high-frequency side of the α-peak is made up of a crossover from one power-law behavior to another one, which constitutes the excess-wing phenomenon [3–5,8,37,64–66], yet, no indications for a secondary (β) relaxation is observed in PS. In the dielectric spectra of neat TPP (T_g = 135 K) in addition to an α-relaxation a β-process is well resolved [37]. The time constants given by $\tau = 1/(2\pi\nu_{max})$ for PS and TPP are included in Fig. 7(a). Importantly, the amplitude of the α-relaxation exceeds the one of PS by a factor of 1000, i.e., in the mixtures the TPP molecules dominate the dielectric response. We note that the β-process in neat TPP as well as in the mixtures with PS has been thoroughly analyzed [64].

Fig. 5(a) shows the spectra of 60% TPP/PS. Data at low frequencies affected by ionic conductivity is omitted. Clearly, the α-peak is significantly broader than in neat glass formers, in particular, a broadening on the low-frequency side is recognized, a feature not found in neat systems

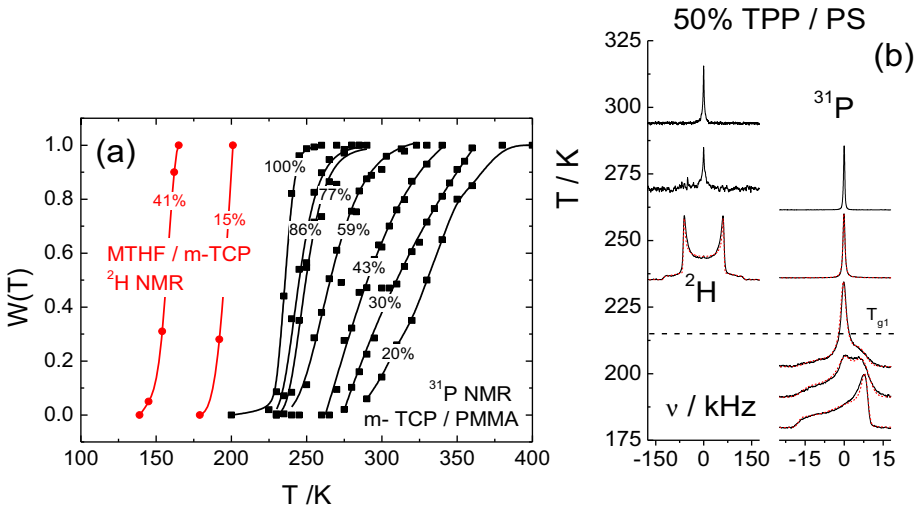

Fig. 3. (a) Weighting factor of the liquid spectrum $W(T)$ of MTHF in m-TCP (^{2}H NMR, red circles) and m-TCP in PMMA (^{31}P NMR, black squares); lines serve as guides to the eye. (b) ^{2}H NMR spectra (left column) and ^{31}P NMR spectra (right column) of 50% TPP in PS. Dashed red lines are two-phase spectral fits; baseline of spectra marks temperature on vertical axis. Dashed horizontal line: T_{g1} = 215 K (T_{g2} = 155 K). Reprinted with permission from Ref. [38]. Copyright 2014, AIP Publishing LLC.

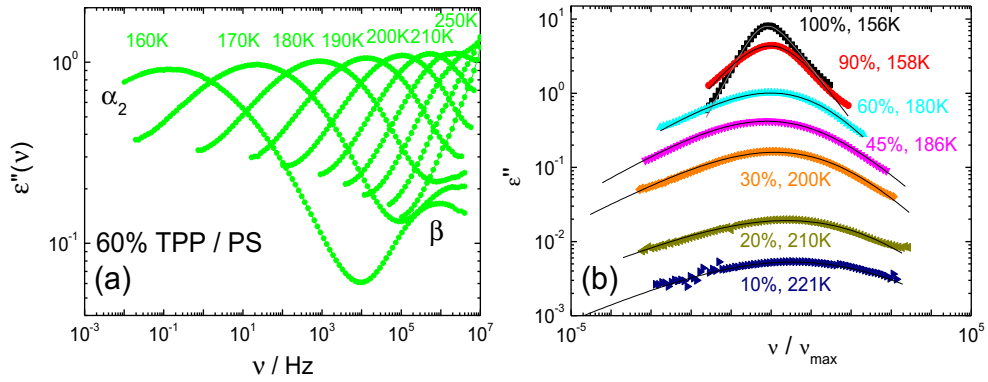

Fig. 5. (a) Dielectric susceptibility spectra of 60% TPP in PS. Reprinted with permission from Ref. [37]. Copyright 2014, AIP Publishing LLC. (b) Dielectric susceptibility spectra of TPP in PS vs. re-scaled frequency for different concentrations of TPP in PS, peak frequency $\nu_{max} \approx 1$ kHz. Solid lines are fits by a Havriliak–Negami function, in the case of $c_{TPP} = 10\%$ and $c_{TPP} = 20\%$ an interpolation by a temperature independent distribution of activation energies is applied. Reprinted with permission from Ref. [38]. Copyright 2014, AIP Publishing LLC.

but it is typical of the low-T_g component in mixed system. For example, in Fig. 5(b) the dielectric loss around 1 kHz is shown for several concentrations. The low-frequency broadening together with an overall broadening is obvious when decreasing the TPP concentration. In the mixture the main relaxation is shifted to lower frequencies compared to that in neat TPP while actually the β-relaxation is not shifted. This slowing down of the TPP dynamics is due to the anti-plasticizer effect caused by the presence of PS.

Fig. 6(a) shows dielectric data for the 20% TPP/PS mixture. In contrast to the 60% mixture now two main relaxation phenomena are observed. Note, only the TPP dynamics is probed by dielectric spectroscopy due to the low dipole moment of PS. The process displayed at high temperatures (open triangles) shows relaxation peaks with a low-frequency flank following a Debye behavior, i.e. $\varepsilon'' \sim \nu^1$, and FTS holds in good approximation. At lower temperatures another relaxation peak (full circles) passes through the DS frequency window, which exhibits a strong overall flattening qualitatively similar to what is observed for TPP in the 60% mixture (cf. Fig. 5(a)). Also, FTS does not apply. A Kohlrausch function was fitted to the high-temperature peak, now called α_1-relaxation, and a Havriliak–Negami (HN) function was applied to the peak found at lower temperatures, now called α_2-relaxation. At lowest TPP concentrations a temperature independent distribution of activation energies $g(E)$ is found for the α_1-relaxation which, when transformed to the distribution $G(\ln \tau)$, reproduces the spectra upon cooling [37]. Important to note is that the relaxation strength of the α_2-process grows with temperature while that of the α_1-process decreases; in addition the fraction of the α_2-process increases strongly with increasing TPP concentration. Actually, the α_1-process is not resolved at high concentrations.

A selection of corresponding correlation times for both components determined by dielectric and NMR (see below) spectroscopy as well as by dynamic light scattering is displayed in Fig. 7(a) [37]. Clearly, well separated time constants are identified for the two components in the mixtures. Most importantly, the time constants of PS collected by ^{2}H NMR (open circles) are identical with those of the α_1-process determined for TPP by DS (open squares, see Fig. 6(a)). This is interpreted in terms of a fraction of TPP molecules (α_1-process) following the dynamics of the high-T_g component PS. At high TPP concentrations the correlation times of the α_1-process exhibit a non-Arrhenius behavior; however, at low concentration (20% sample, dark yellow symbols in Fig. 7(a)) a crossover to an Arrhenius-law is found at low temperatures. Actually, the crossover occurs at T_{g1}, i.e., at T_g of the high-T_g component PS (cf. arrow in Fig. 7(a)). Thus, at low temperatures for which the PS matrix has become essentially rigid, the α_2-process shows high similarity with a β-process, yet, as will be shown below, the NMR spectra clearly reveal isotropic reorientation of the TPP molecules.

Given the time constants for each component one can extract the corresponding glass transition temperatures T_{g1} and T_{g2}. This is shown in Fig. 8, where we also included the results from DSC measurements, which are able to detect two "glass steps" [37]. While $T_{g1}(c_{TPP})$ decreases steadily from neat PS down to highly diluted PS, $T_{g2}(c_{TPP})$ is significantly lower and exhibits a maximum around $c_{TPP} = 0.35$. The latter feature is a consequence of the interplay of the anti-plasticizer effect on the one hand, raising $T_{g2}(c_{TPP})$ by adding PS, and a decreasing activation energy

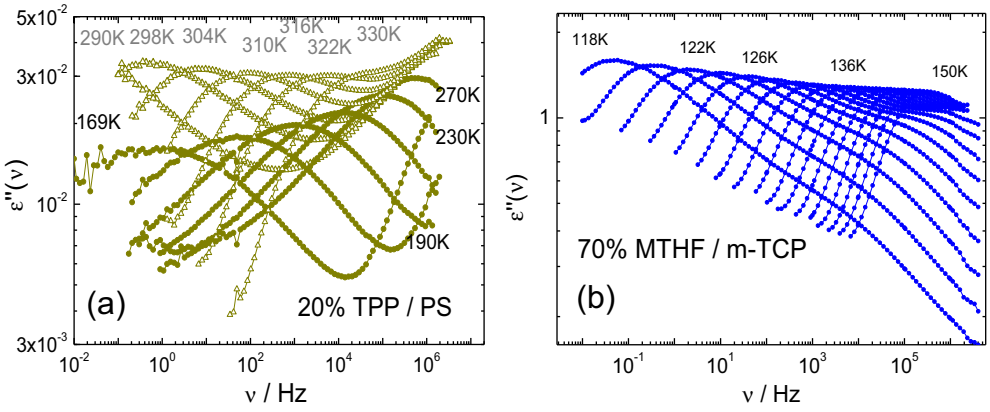

Fig. 6. (a) Dielectric susceptibility of TPP/PS mixture with low TPP concentration ($c_{TPP} = 20\%$). Open triangles, high temperatures: α_1-relaxation; full circles, low temperatures: α_2-relaxation. Reprinted with permission from Ref. [37]. Copyright 2014, AIP Publishing LLC. (b) Dielectric susceptibility of MTHF/m-TCP mixture, $c_{MTHF} = 70\%$.

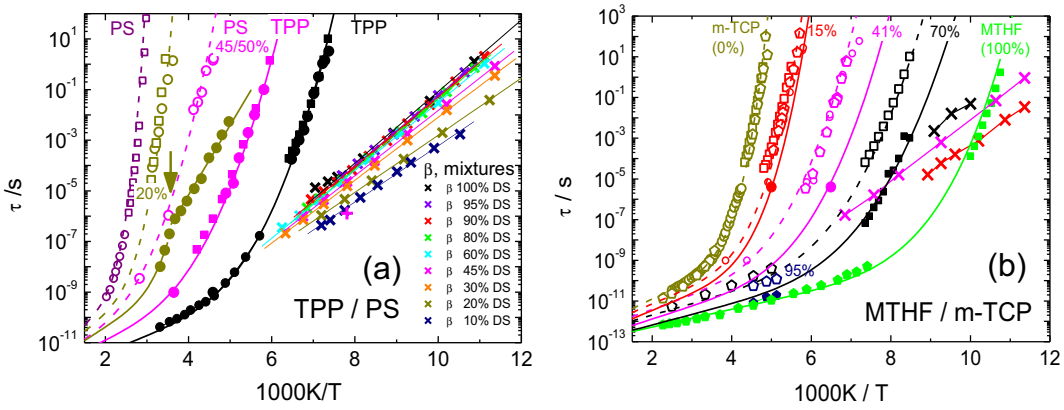

Fig. 7. Time constants of (a) the TPP/PS mixture (cf. also Ref. [37], reprinted with permission from Ref. [38]. Copyright 2014, AIP Publishing LLC.) and (b) MTHF/m-TCP as revealed by DS (squares, crosses), NMR (circles, neat PS taken from Ref. [67]), and dynamic light scattering PCS and TFPI; pentagons. Lines serve as guides-to-the-eye (dashed: α_1-relaxation; solid: α_2-relaxation and β-process in the case of TPP/PS). Color code defines concentration, open symbols show α_1-, full symbols α_2-process and crosses β-process (x: DS, +: NMR). Arrow in (a) marks T_{g1} of 20% sample.

of the Arrhenius-like α_2-process at lower c_{TPP} on the other hand (cf. Fig. 7(a)).

In the case of TPP/PS a β-process is identified and thoroughly investigated by our group [64]. Its time constant shows a typical Arrhenius behavior with a mean activation energy $< E > /k \cong 24\ T_g$, which virtually does not vary upon mixing (cf. Fig. 7(a)). We note, that similar findings of τ_β hardly changing with concentration were reported before [68]. In this context we also mention that in experiments for different combinations of temperature and pressure keeping τ_α constant also τ_β remains unchanged [69]. The β-process is associated with a spatially highly hindered dynamics as found in other glasses [59,70]. In the present context, only a spatially highly restricted process shall be called a β-process. Introduced by TPP, in the mixture TPP as well as PS participate in the β-process. This has been taken as an indication of its cooperative nature [64].

In the case of the non-polymeric system MTHF/m-TCP, regarding the correlation times, a similar scenario is found. Here, we also added the results from a PCS study; the latter essentially probes the m-TCP dynamics (as ^{31}P NMR). Again two time constants characterizing the dynamics of m-TCP (α_1) and MTHF (α_2) are identified. Yet, the decoupling between the dynamics of the components is not as large as in the case of TPP/PS. Here, the two relaxation processes observed in the dielectric spectra (cf. Fig. 6(b)) reflect the dynamics of m-TCP and MTHF, as in this case both components are dielectrically active. Again, a β-process is observed the activation of which essentially does not change in the mixture (cf. Fig. 7(b)). Only a single T_g can be resolved by DSC (cf. Fig. 8).

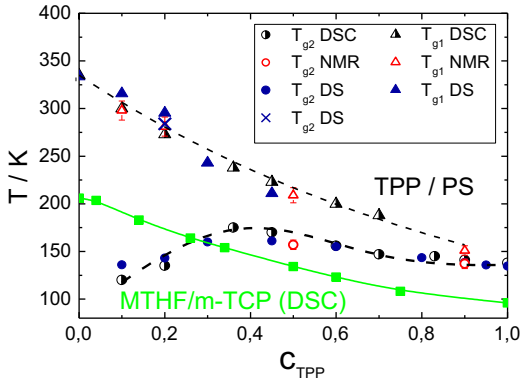

Fig. 8. Glass transition temperatures for the mixture TPP/PS (as revealed by DSC, DS and NMR), and for MTHF/m-TCP (green squares, measured by DSC). Lines serve as guide-for-the-eye.

2.3. Reorientational correlation function probed by stimulated echo experiments

More quantitative results concerning the slow dynamics of PS (probed by ^{2}H NMR) as well as that of m-TCP and TPP (probed by ^{31}P NMR) are provided by measuring stimulated echo decays [8,57–59,71,72]. Basically, a three-pulse sequence is applied in a temperature range where solid-state spectra are observed. The decay directly represents a rank-two reorientational correlation function $C_2(t)$ which is monitored in the range 10 μs–100 s. Regarding DS a rank-one correlation function $C_1(t)$ is probed in the frequency domain, and attempts are made to quantitatively compare both NMR and DS results.

In Fig. 9(a) the ^{31}P stimulated echo decays of m-TCP in the mixture with PMMA is shown for different concentrations. While at high m-TCP concentrations the decay can be described by a stretched exponential typical of neat systems, the decay becomes extremely stretched resembling a quasi-logarithmic curve at lowest m-TCP concentrations. Rather similar decay curves are observed when m-TCP embedded in the abovementioned nano-porous systems is considered (see Fig. 9(b)). Starting at a radius r = 12 nm a long-time tail emerges which for smallest pores yields again a much stretched overall decay, yet some indications of a bimodal relaxation are seen.

Next, we consider the case TPP/PS in some detail in Fig. 10, where the ^{2}H NMR stimulated echo decays (probing PS dynamics) are shown in the left column and the ^{31}P NMR decays (probing TPP dynamics) in the right column. Clearly, significant differences are recognized between the behavior of the high-T_g component PS and the low-T_g component TPP. The correlation functions measured by ^{2}H NMR all can be interpolated by a Kohlrausch decay and the time constants are included in Fig. 7(a). For each concentration time-temperature superposition (TTS) applies. With lowering concentration only a weak trend to stronger stretching is observed. As already mentioned the correlation times of PS coincide with those for the α_1-process of TPP compiled from DS, and thus the conclusion was drawn that a fraction of TPP molecules is associated with the dynamics of PS. Clearly, the time constants differ strongly from those of the α_2-process reflecting TPP dynamics decoupled from that of the PS matrix.

The ^{31}P stimulated echo decays probing the TPP dynamics reveal a quite different behavior. A pronounced stretching is observed becoming extremely large at low TPP concentration. Here, the correlation loss again becomes quasi-logarithmic, and actually only part of the correlation loss shows up within the NMR time window. Clearly, TTS does not apply. Assuming that DS and NMR probe similar dynamics, the NMR decays have to be compared with the Fourier transform of the spectral density measured by DS. As mentioned, the TPP α_2-process probed by the DS spectra exhibits a severe broadening the extent of

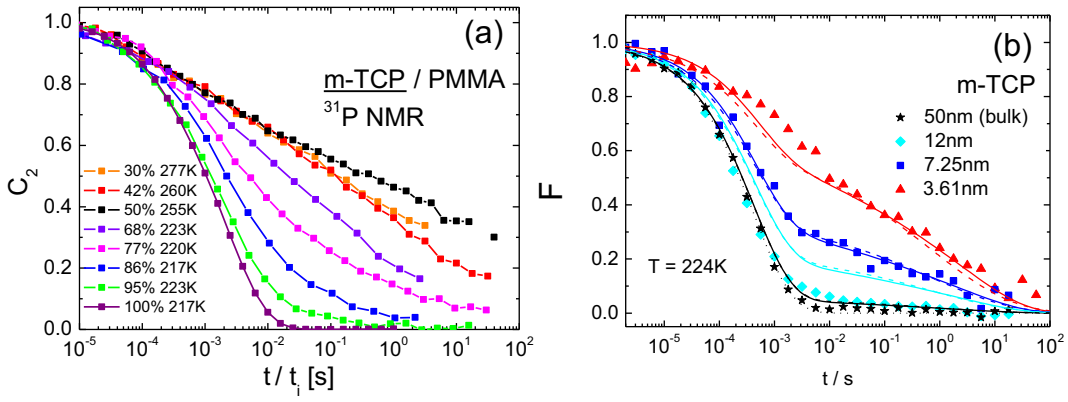

Fig. 9. (a) ^{31}P NMR stimulated echo decays of m-TCP in mixture with PMMA for different concentrations (C_2 or F); a reduced time scale is used to allow direct comparison of the shape of the correlation functions, lines serve as guide-for-the-eye. (b) ^{31}P NMR stimulated echo decays of m-TCP embedded in nano-porous silica matrices with different pore radii; reprinted with permission from Ref. [45]. Copyright (2009) American Chemical Society. Symbols: experimental data; lines: prediction by different models (cf. text).

which increases with decreasing c_{TPP}, explicitly the spectra broaden in particular on the low-frequency flank (cf. Fig. 5(b)). In agreement with the DS spectra at $c_{TPP} = 80\%$ the HN function, Fourier transformed into the time domain, gives an appropriate interpolation (solid lines in Fig. 10) of the stimulated echo while a Kohlrausch decay (dashed line) fails. Indeed, both techniques probe virtually the same dynamics. Inspecting the ^{31}P stimulated echo decays for lower TPP concentrations, as said, they become extremely stretched. Again, interpolations of the DS spectra reflecting the α_2-process are Fourier transformed and displayed as dashed lines for the case of $c_{TPP} = 50\%$ (cf. Fig. 10). They

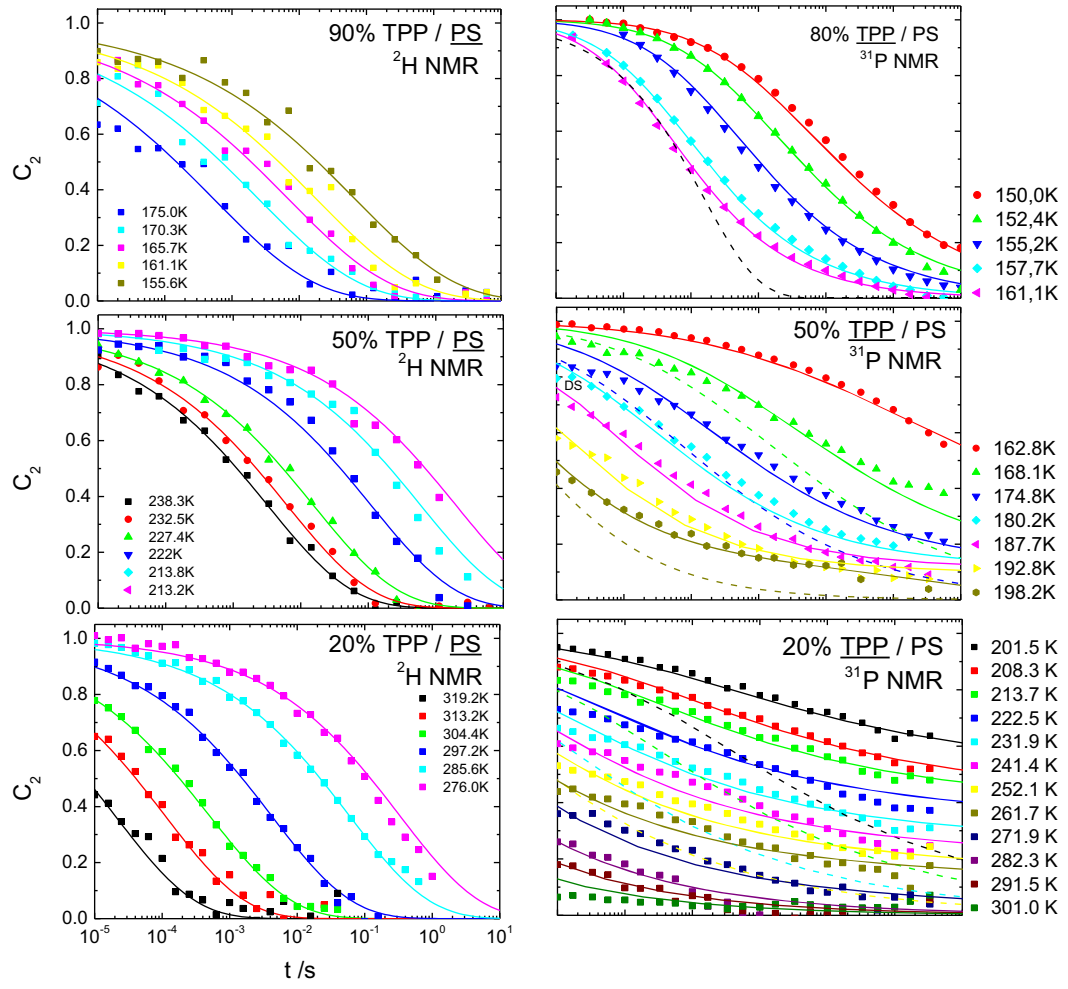

Fig. 10. Reorientational correlation functions measured by the stimulated echo technique: Left column: ^{2}H NMR, solid lines: Kohlrausch fits. Right column: stimulated echo decay probed by ^{31}P NMR for $c_{TPP} = 80\%$, solid lines: Havriliak–Negami (HN) fits, dashed lines: Kohlrausch fits with $\beta = 0.53$. For $c_{TPP} = 50\%$, solid lines: interpolation based on DS data utilizing a superposition of Kohlrausch (α_1) and HN decay (α_2), dashed lines: α_1 contribution omitted. For $c_{TPP} = 20\%$: solid lines: calculation based on DS data utilizing a superposition of Kohlrausch (α_1) and a temperature independent distribution of activation energies $g(E)$ (α_2), dashed lines: α_1 contribution omitted. Reprinted with permission from Ref. [38]. Copyright 2014, AIP Publishing LLC.

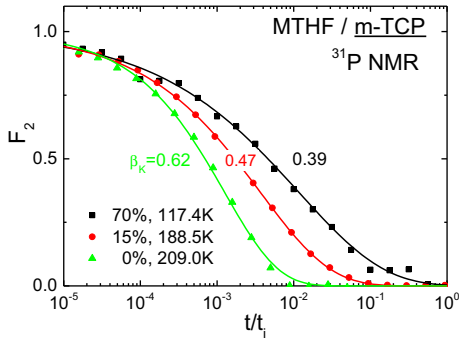

Fig. 11. ^{31}P stimulated echo decays of m-TCP in the mixture MTHF/m-TCP at different MTHF concentrations interpolated by a Kohlrausch function.

show decays too fast and the long-time tails are underestimated. We attribute this discrepancy to the existence of a sub-ensemble of TPP molecules being essentially immobile, namely the α_1-process well identified by DS and associated with TPP molecules following the PS dynamics. Indeed, a bimodal decay is perceived at $T = 198.2$ K (Fig. 10). In order to take this additional process into account a fraction of molecules is introduced which relaxes at much longer times via a Kohlrausch decay. Now, the shape of the decay curves can essentially be reproduced. A similar approach was chosen for the mixtures with $c_{TPP} = 20\%$.

In the case of MTHF/m-TCP ^{2}H stimulated echo decays of the low-T_g component MTHF do not reveal relevant information, since the methyl group reorientation dominates the decays. However, the stimulated echo decays of the high-T_g component display a behavior typical of neat glass formers (as in the case of PS in Fig. 10): The decays are described by a Kohlrausch function and the stretching slightly increases upon adding MTHF (cf. Fig. 11). Again, TTS is fulfilled when different temperatures are considered.

Summarizing, the dynamics of both TPP sub-ensembles identified by DS are re-discovered in the extremely stretched correlation functions $C_2(t)$ probed by the NMR stimulated echo decays. The question still has to be answered whether the α_2-process, the appearance of which in the dielectric spectra highly resembles that of a secondary process, is an isotropic, liquid-like process for all temperatures, i.e., also for temperatures for which a solid-state spectrum is revealed (for example at $c_{TPP} = 20\%$ and $T = 200$ K in Fig. 2(b)). Here, 2D spectra allow insight into the nature of motion.

2.4. Two-dimensional spectra

Two-dimensional (2D) NMR exchange spectra directly visualize the evolution of the reorientational process [8,57–59]. More precisely, a 2D spectrum, $S(\omega_1, \omega_2; t_m)$, measures the conditional probability, $P(\omega_2, t_m|\omega_1, 0)$, to find a frequency ω_2 at time t_m, provided that it was ω_1 at time $t = 0$. Usually, 2D spectra are collected for some fixed values of the mixing time t_m. As the NMR frequency ω is connected to the orientation of the interaction tensor (chemical shift anisotropy for ^{31}P, or quadrupolar interaction for ^{2}H), which is fixed in a molecular frame, the spread of intensity out from the diagonal spectrum into the ω_1–ω_2 plane monitors the progress of the reorientational process. As will be demonstrated, 2D NMR allows for identifying not only the geometry of molecular reorientation but also the exchange processes within the broad distribution $G(\ln \tau)$ [22,24–26,38,57].

The 2D spectra of the TPP/PS sample with $c_{TPP} = 20\%$ and at mixing times $t_m = 0.05$ ms, 500 ms and 5000 ms are depicted in Fig. 12. No fast isotropic motion is detected, as no Lorentzian line is visible. For $t_m = 0.05$ ms, very short exchange times, the entire intensity essentially is found along the diagonal, i.e., no reorientation occurs on this time scale. For $t_m = 500$ ms signal in the plane arises, clearly indicating spatially unrestricted (isotropic) reorientation, and for $t_m = 5000$ ms the

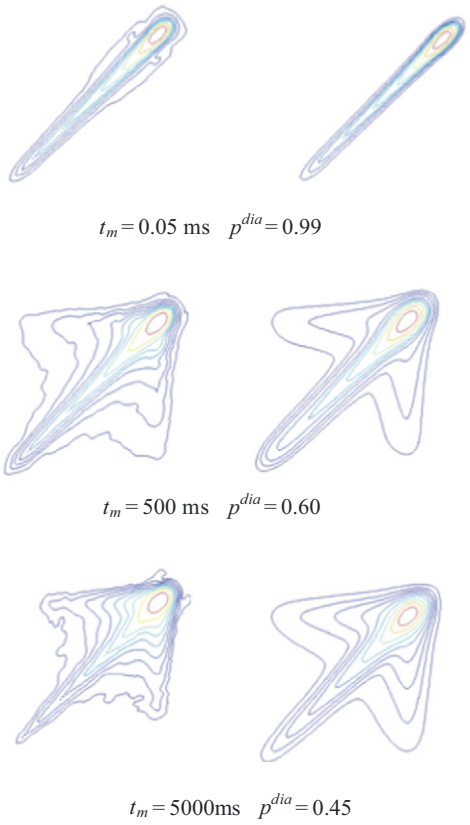

Fig. 12. 2D ^{31}P NMR exchange spectra of TPP, $c_{TPP} = 20\%$, $T = 200$ K; left: experimental spectra with mixing times t_m indicated; right: spectra calculated according to a two-phase model weighting factor p^{dia} of diagonal spectrum is given.

signal in the plane further gains intensity while diagonal intensity decreases. Yet, even at longest times some intensity along the diagonal still remains indicating that some molecules virtually have not yet moved, again demonstrating the extremely wide distribution $G(\ln \tau)$. For a quantitative analysis the spectra are reproduced by a two-phase model, i.e., a weighted sum of the two 2D sub-spectra belonging to not reorienting and fully isotropically reorienting molecules, respectively (right column in Fig. 12). The simple model captures the essential features of the experimental 2D spectra. Once again one benefits from the presence of a broad distribution $G(\ln \tau)$ which leads to "2D two-phase spectra". We conclude that the α_2-process does not change its nature and remains isotropic even at low temperatures, in particular also below T_{g1}.

Dynamic heterogeneities in asymmetric binary glass formers have been identified to be of transient nature [22,24–26,38,57]. This is again observed in Fig. 13 (left) for the $c_{TPP} = 20\%$ sample; here a higher temperature ($T = 296.5$ K) than in Fig. 12 is considered where the two-phase character of the (1D) spectrum with its central Lorentzian line is clearly recognized. A cross-like pattern occurs for long t_m in the 2D spectrum, which indicates that fast molecules and slowly reorienting molecules mutually exchange. Again, the spectra can quantitatively be reproduced (right). Analyzing in detail the weighting factors of the now four sub-spectra, it has been shown that isotropic reorientation and exchange occur both on the same timescale [38]. Thereby, it is assumed that the TPP population responsible for the α_1 process does not take part in the observed exchange.

Very similar 2D exchange patterns are observed in the case of m-TCP embedded in the nano-porous silica matrices, cf. Fig. 14. While at low temperature the 2D spectrum visualizes a broad distribution of isotropic reorientation, at high temperature two-phase spectra with a central Lorentzian line are found in the 1D spectrum leading to features of a cross-like exchange pattern in the 2D spectrum similar to those in

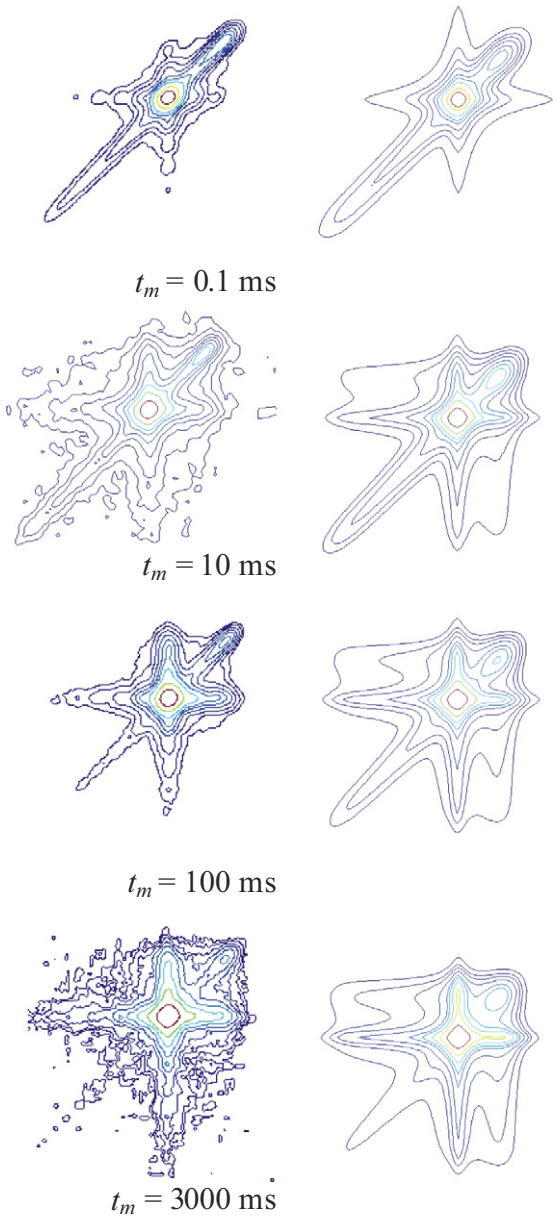

Fig. 13. 2D exchange spectra of TPP/PS at $c_{TPP} = 20\%$ and $T = 269.5$ K demonstrating exchange among liquid-like and solid-like TPP molecules; left: experimental; right: calculated spectra (cf. Ref. [38]).

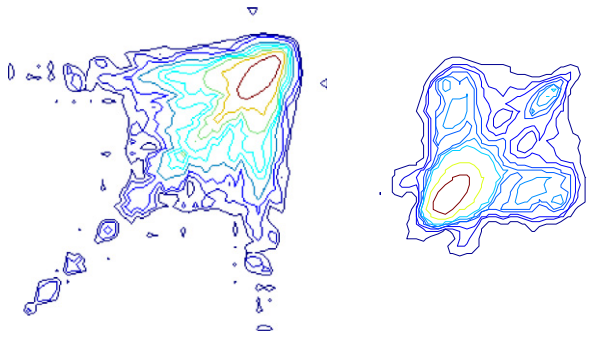

Fig. 14. 2D ^{31}P NMR exchange spectra of m-TCP embedded in a nano-porous silica matrix, $r = 3.61$ nm, for a mixing time of $t_m = 3$ s. Left: $T = 234$ K; right: $T = 241$ K, in the latter case exchange among fast and slow m-TCP molecules is revealed.

Fig. 13. Thus, also here the dynamic heterogeneities are transient in nature.

3. Spin-lattice relaxation

The spin-lattice relaxation of ^{31}P, as the spectra dominated by the CSA interaction, probes the spectral density at a single (Larmor) frequency close to 160 MHz [73], which is larger than the frequencies covered by our DS experiments. Thus, given the described complexity of the dynamics in mixed glass formers, e.g., failure of FTS for the mobile component, a quantitative description is almost impossible. However, qualitative trends can be revealed and they corroborate the results already collected by DS and 2D NMR.

In Fig. 15 the ^{31}P NMR spin-lattice relaxation rate is plotted vs. temperature for the case of m-TCP/PMMA mixtures with different concentrations. While for neat m-TCP a narrow and high relaxation maximum is observed it successively broadens and lowers its amplitude upon adding PMMA. In addition, the maximum shifts to higher temperatures indicating a slowing-down of the dynamics due to the anti-plasticizer effect of adding PMMA. The strong broadening and decreasing of the relaxation curve is a direct consequence of the emergence of the pronounced dynamic heterogeneities in binary glass formers, described by a distribution $G(\ln \tau)$ becoming broader and broader at low m-TCP concentrations. The corresponding relaxation data of TPP/PS displayed in Fig. 15(b) reveal another relaxation scenario. In this case two relaxation maxima appear at high PS concentration. The one at low temperatures has to be attributed to the β-process well identified by DS (cf. Fig. 7(a)). In the case of the mixtures α_2- and β-process become more separated which leads to well resolved relaxation peaks even at high frequencies. In contrast, in neat TPP the two processes have essentially merged at high frequencies/temperatures. Finally, we show in Fig. 16(a) the spin-lattice rate of the high-T_g component m-TCP in the mixture MTHF/m-TCP. No broadening is observed. Actually a slight opposite effect is recognized: The maximum slightly increases with MTHF added, which appears to be at variance with the findings of the stimulated echo decay (cf. Fig. 11) where the relaxation stretching increases somewhat. At the same time, the low-temperature relaxation pattern changes its appearance upon dilution: In neat m-TCP below 250 K the temperature dependence of T_1 weakens, and an analysis applying a Cole–Davidson distribution fails to describe the relaxation data [74,75]. This finding is caused by the excess-wing contribution determining the relaxation close to T_g. In the mixtures, however, no flattening upon cooling is observed and the strong temperature dependence continues to lowest measured temperatures, suggesting even the absence of an excess-wing contribution. In conclusion, it appears that the spectral density becomes less broad explaining the increasing relaxation maximum.

In the case of m-TCP embedded in the porous matrices similar relaxation behavior as for m-TCP in PMMA is found. The distribution $G(\ln \tau)$ becomes broader as the confinement becomes smaller, and the relaxation maximum shifts to higher temperatures indicating that the dynamics becoming slower.

Regarding the α_2-process in the mixtures of TPP/PS, FTS does not hold, consequently the width parameter of $G(\ln \tau)$ is a function of temperature in addition to the time constants. Thus a simple analysis of the spin-lattice relaxation as in the case of neat glass formers, for which a Cole–Davidson susceptibility with temperature-independent stretching parameter suffices to describe the temperature dependence of the relaxation rate [8,74,75], is not possible in the case of mixed systems. Regarding the high-T_g component, in contrast, this approach works as here FTS still applies. We note that the HN susceptibility, frequently applied for the interpolation of dielectric spectra broadened at the low-frequency flank, does not exhibit a well defined time constant (the spectral density at zero frequency $J(0)$ diverges) and therefore is not suited for the analysis of NMR experiments including T_1 and T_2 relaxations. Describing the fast component dynamics in binary systems one may

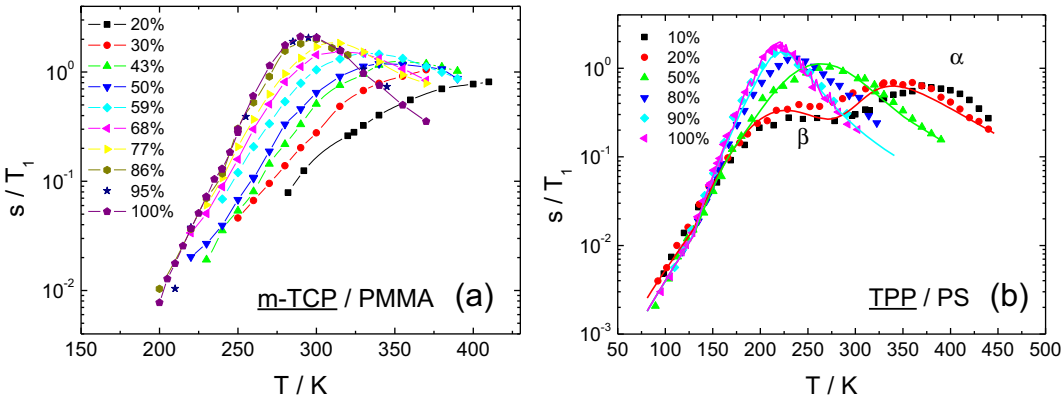

Fig. 15. ^{31}P NMR spin-lattice relaxation rate $1/T_1$ as a function of temperature for different concentrations: (a) m-TCP/PMMA, lines are guides-for-the-eye; and (b) TPP/PS; solid-lines: forecast by extrapolating DS results to high frequencies.

introduce a long-time cut-off in $G(\ln \tau)$ given by the time constant $\tau_{\alpha 1}(T)$ belonging to the slow component. By using this modified HN distribution $T_1(T)$ (and T_2) can be reproduced. In Fig. 15(b) the solid lines represent the forecast by DS which captures the salient features of the relaxation curves. In this case, the DS spectra of TPP in the mixture provide sufficient information to allow for an extrapolation to high frequencies probed by ^{31}P relaxation.

4. Conclusions

The dynamics in asymmetric binary glass formers appears to display a rather complex scenario, and understanding is strongly facilitated when the results from NMR, dielectric spectroscopy as well as dynamic light scattering are combined. In addition, the selectivity of NMR allowing for separately monitoring the dynamics of each component and the power of 2D NMR (stimulated echo decays and 2D spectra) are of great advantage. The results demonstrate that the high-T_g and the low-T_g component show significantly different dynamics. While the high-T_g component essentially behaves like in neat systems, for the low-T_g component pronounced dynamic heterogeneities are identified; the corresponding distribution $G(\ln \tau)$ becomes extremely broad at low concentration and low temperature, in some cases leading to quasi-logarithmic decays. We note that two-phase NMR spectra characteristic of a broad distribution $G(\ln \tau)$ have also been reported for other polymer-plasticizer systems [76]. In the case of TPP/PS presented here as well as MTHF/PS investigated by Blochowicz et al. [32,53] the low-T_g component exhibits two sub-ensembles of molecules both of which exhibit isotropic liquid-like reorientation. One sub-ensemble (α_1) is linked to the dynamics of PS, the other (α_2) performs a dynamically decoupled motion in a matrix of essentially immobilized PS molecules. The fraction of the α_2-sub-ensemble increases with temperature on the expense of the α_1-fraction; the latter appears to disappear at high temperatures. This may be taken as a signature of a type-A glass transition in the frame of MCT [53]. Transforming the dielectric spectra into the time domain essentially reveals agreement with the NMR results. In addition, the 2D NMR spectra allow to identify exchange within the distribution occurring on virtually the same time scale as the isotropic reorientation as reported before for other systems. The exchange among fast and slow molecules of the α_2 sub-ensemble occurs even in the rigid PS matrix.

Pronounced dynamic heterogeneities have also been identified for glass formers in confining geometries by NMR as well as DS [24,41,43–45]. The NMR results have been explained by a topological model for which the broad distribution of correlation times $G(\ln \tau)$ becomes spatially inhomogeneous, i.e., the correlation time becomes a function of the distance from the pore wall, and a penetration depth increasing when temperature is decreased [44]. The use of the model was inspired by molecular dynamic simulations [77]. A similar approach was recently presented for confined polymers [78]. Among the different layers with different dynamics exchange occurs as proven again by 2D NMR. Thus, the heterogeneities exhibit a transient nature. A similar situation might exist in asymmetric binary glass formers. Here, the low-T_g component performs a highly decoupled (isotropic) motion in an essentially immobilized matrix of the high-T_g component. Thus, the low-concentration behavior of the low-T_g component to the α_2-process, showing actually high similarity with a β-process, could be taken as a signature of intrinsic confinement effects exerted by the rigid PS matrix as already suggested by Blochowicz and co-workers [32]. In that sense PS provides a confinement for the TPP molecules which becomes "hard" below T_{g1}. The higher the concentration, the more TPP molecules

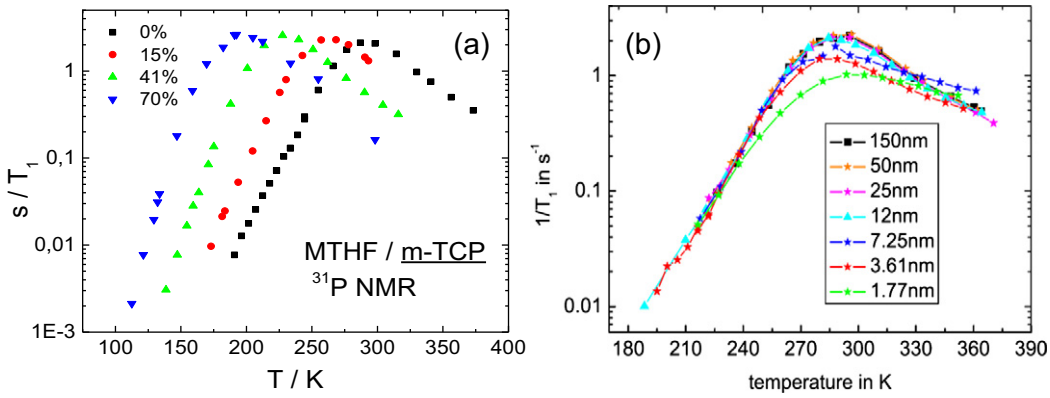

Fig. 16. ^{31}P NMR spin-lattice relaxation rate $1/T_1$ as a function of temperature for m-TCP in the mixture MTHF/m-TCP for different m-TCP concentrations. (b) Relaxation data for m-TCP embedded in nano-porous silica matrices of different pore radius. Lines are guides-for-the-eye.

are beyond the influence of the confinement effect of the PS matrix and the dynamics become similar to that of neat glass formers. In terms of the scenario promoted by MD simulations as well as MCT analyses the dynamics of the low-T_g component might be accompanied by a strong sub-diffusive motion governed by a localization transition [49].

Acknowledgment

Financial support of the Deutsche Forschungsgemeinschaft (DFG) through the projects RO 907/10,11,15 is acknowledged.

References

[1] M.D. Ediger, Annu. Rev. Phys. Chem. 51 (2000) 99.
[2] C.A. Angell, K.L. Ngai, G.B. McKenna, P.F. McMillan, S.W. Martin, J. Appl. Phys. 88 (2000) 3113.
[3] R. Brand, P. Lunkenheimer, U. Schneider, A. Loidl, Phys. Rev. Lett. 82 (1999) 1951.
[4] U. Schneider, P. Lunkenheimer, R. Brand, A. Loidl, Phys. Rev. E. 59 (1999) 6924.
[5] P. Lunkenheimer, U. Schneider, R. Brand, A. Loidl, Contemp. Phys. 41 (2000) 15.
[6] W. Kob, Supercooled liquids, the glass transition, and computer simulations, in: J.-L. Barrat, M.V. Feigelman, J. Kurchan, J. Dalibard (Eds.), Slow Relaxations and Nonequilibrium Dynamics in Condensed Matter, Les Houches, vol. 77, Springer, Berlin, 2003, p. 199.
[7] K. Binder, W. Kob, Glassy Materials and Disordered Solids, World Scientific, New Jersey, 2005.
[8] T. Blochowicz, A. Brodin, E.A. Rössler, Adv. Chem. Phys. 133 (2006) 127.
[9] G. Floudas, M. Paluch, A. Grzybowski, K.L. Ngai, Molecular Dynamics of Glass-forming Systems, Springer, Berlin, 2011.
[10] L. Berthier, G. Biroli, Rev. Mod. Phys. 83 (2011) 587.
[11] Structural Glasses and Supercooled Liquids, in: P.G. Wolynes, V. Lubchenko (Eds.), Wiley, Hoboken, 2012.
[12] N. Petzold, B. Schmidtke, R. Kahlau, D. Bock, R. Meier, B. Micko, D. Kruk, E.A. Rössler, J. Chem. Phys. 138 (2013) 12A510.
[13] H. Sillescu, J. Non-Cryst. Solids 243 (1999) 81.
[14] M.D. Ediger, P. Harrowell, J. Chem. Phys. 137 (2012) 080901.
[15] L. Berthier, G. Biroli, J.-P. Bouchaud, L. Cipelletti, W. Saarloos, Dynamical Heterogeneities in Glasses, Colloids and Granulat Media, Oxford University Press, Oxford, 2011.
[16] K. Schmidt-Rohr, H.W. Spiess, Phys. Rev. Lett. 66 (1991) 3020.
[17] U. Tracht, M. Wilhelm, A. Heuer, H. Feng, K. Schmidt-Rohr, H.W. Spiess, Phys. Rev. Lett. 81 (1998) 2727.
[18] E. Vidal Russel, N.E. Israeloff, Nature 408 (2000) 695.
[19] P.J. Hains, G. Williams, Polymer 16 (1975) 725.
[20] M.A. Desando, S. Walker, W.H. Baarschers, J. Chem. Phys. 73 (1980) 3460.
[21] M. Scandola, G. Ceccorulli, M. Pizzoli, Polymer 28 (1987) 2081.
[22] T. Blochowicz, C. Karle, A. Kudlik, P. Medick, I. Roggatz, M. Vogel, C. Tschirwitz, J. Wolber, J. Senker, E. Rössler, J. Phys. Chem. B 103 (1999) 4032.
[23] M. Nakazawa, O. Urakawa, K. Adachi, Macromolecules 33 (2000) 7898.
[24] M. Vogel, E. Rössler, J. Phys. Chem. A 102 (1998) 2102.
[25] P. Medick, M. Vogel, E. Rössler, J. Magn. Reson. 159 (2002) 126.
[26] D. Bingemann, N. Wirth, J. Gmeiner, E.A. Rössler, Macromolecules 40 (2007) 5379.
[27] D. Cangialosi, A. Alegría, J. Colmenero, J. Chem. Phys. 126 (2007) 204904.
[28] T. Blochowicz, E.A. Rössler, Phys. Rev. Lett. 92 (2004) 225701.
[29] K. Kessairi, S. Capaccioli, D. Prevosto, M. Lucchesi, P. Rolla, J. Chem. Phys. 127 (2007) 174502.
[30] M.D. Ediger, T.R. Lutz, Yiyong He, J. Non-Cryst. Solids 352 (2006) 4718.
[31] S. Capaccioli, K. Kessairi, M. Shahin, D. Prevosto, M. Lucchesi, J. Non-Cryst. Solids 357 (2011) 251.
[32] T. Blochowicz, S.A. Lusceac, P. Gutfreund, S. Schramm, B. Stühn, J. Phys. Chem. B 115 (2011) 1623.
[33] K.L. Ngai, C.M. Roland, Macromolecules 37 (2004) 2817.
[34] M. Wachowicz, J.L. White, Macromolecules 40 (2007) 5433.
[35] K.L. Ngai, S. Capaccioli, J. Chem. Phys. 138 (2013) 054903.
[36] G. Floudas, W. Steffen, E.W. Fischer, J. Chem. Phys. 99 (1992) 695.
[37] R. Kahlau, D. Bock, B. Schmidtke, E.A. Rössler, J. Chem. Phys. 140 (2014) 044509.
[38] D. Bock, R. Kahlau, B. Pötzschner, T. Körber, E. Wagner, E.A. Rössler, J. Chem. Phys. 140 (2014) 094505.
[39] T. Blochowicz, E.A. Rössler, J. Chem. Phys. 122 (2005) 224511.
[40] T.P. Lodge, E.R. Wood, J.C. Haley, J. Polym. Sci. Part B: Polym. Phys. 44 (2006) 756.
[41] F. Kremer, A. Schönhals, Broadband Dielectric Spectroscopy, Springer Verlag, Berlin, 2002.
[42] P. Medick, M. Vogel, E. Rössler, J. Non-Cryst. Solids 307–310 (2002) 565.
[43] S.A. Lusceac, C. Koplin, P. Medick, M. Vogel, N. Brodie-Linder, C. LeQuellec, C. Alba-Simionesco, E.A. Rössler, J. Phys. Chem. B 108 (2004) 16601.
[44] C. Alba-Simionesco, B. Coasne, G. Dosseh, G. Dudziak, K.E. Gubbins, R. Radhakristhan, M. Sliwinska-Bartkowiak, J. Phys. Condens. Matter 18 (2006) R15.
[45] S. Gradmann, P. Medick, E.A. Rössler, J. Phys. Chem. B 113 (2009) 8443.
[46] G. Buntkowsky, H. Breitzke, A. Adamczyk, E. Roelofs, T. Emmler, E. Gedat, B. Grunberg, Y.P. Xu, H.H. Limbach, I. Shenderovich, A. Vyalikh, G. Findenegg, Phys. Chem. Chem. Phys. 9 (2007) 4843.
[47] M. Vogel, Eur. Phys. J. Spec. Top. 189 (2010) 47.
[48] J. Bosse, Y. Kaneko, Phys. Rev. Lett. 74 (1995) 4024.
[49] T. Voigtmann, J. Horbach, Phys. Rev. Lett. 103 (2009) 205901.
[50] V. Krakoviack, Phys. Rev. E. 79 (2009) 061501.
[51] T. Voigtmann, Eur. Phys. Lett. 96 (2011) 360006.
[52] J. Kurzidim, D. Coslovich, G. Kahl, J. Phys. Condens. Matter 23 (2011) 234122.
[53] T. Blochowicz, S. Schramm, S. Lusceac, M. Vogel, B. Stühn, P. Gutfreund, B. Frick, Phys. Rev. Lett. 109 (2012) 035702.
[54] R. Kant, S.K. Kumar, R.H. Colby, Macromolecules 36 (2003) 10087.
[55] J. Colmenero, A. Arbe, Soft Matter 3 (2007) 1474.
[56] T.P. Lodge, T.C.B. McLeish, Macromolecules 33 (2000) 5278.
[57] K. Schmidt-Rohr, H.W. Spiess, Multidimensional Solid State NMR and Polymers, Academic, London, 1997.
[58] R. Böhmer, G. Diezemann, G. Hinze, E.A. Rössler, Prog. Nucl. Magn. Reson. Spectr. 39 (2001) 191.
[59] M. Vogel, P. Medick, E.A. Rössler, Ann. Rep. NMR Spectr. 56 (2005) 231.
[60] H.Z. Cummins, G. Li, Y.H. Hwang, G.Q. Shen, W.M. Du, J. Hernandez, N.J. Tao, Z. Phys. B 103 (1997) 501.
[61] J.A.H. Wiedersich, N.V. Surovtsev, V.N. Novikov, E. Rössler, Phys. Rev. B 64 (2001) 064207.
[62] N. Petzold, E.A. Rössler, J. Chem. Phys. 133 (2010) 124512.
[63] E. Rössler, M. Taupitz, K. Börner, M. Schulz, H.-M. Vieth, J. Chem. Phys. 92 (1990) 5847.
[64] D. Bock, R. Kahlau, B. Micko, B. Pötzschner, G.J. Schneider, E.A. Rössler, J. Chem. Phys. 139 (2013) 064508.
[65] A. Kudlik, S. Benkhof, T. Blochowicz, C. Tschirwitz, E.A. Rössler, J. Mol. Struct. 479 (1999) 201.
[66] T. Blochowicz, C. Gainaru, P. Medick, C. Tschirwitz, E.A. Rössler, J. Chem. Phys. 124 (2006) 134503.
[67] Y. He, T.R. Lutz, M.D. Ediger, C. Ayyagari, D. Bedrov, G.D. Smith, Macromolecules 37 (2004) 5032.
[68] M. Sun, L. Wang, Y. Tian, R. Liu, K.L. Ngai, C. Tan, J. Phys. Chem. B 115 (2011) 8242.
[69] M. Mierzwa, S. Pawlus, M. Paluch, E. Kaminska, K.L. Ngai, J. Chem. Phys. 128 (2008) 044512;
S. Capaccioli, M. Paluch, D. Prevosto, Li-Min Wang, K.L. Ngai, J. Phys. Chem. Lett. 3 (2012) 6.
[70] B. Micko, C. Tschirwitz, E.A. Rössler, J. Chem. Phys. 138 (2013) 154501.
[71] F. Fujara, S. Wefing, H.W. Spiess, J. Chem. Phys. 84 (1986) 4579.
[72] H.W. Spiess, J. Chem. Phys. 72 (1980) 6755.
[73] A. Abragam, The Principles of Nuclear Magnetism, Oxford University Press, Oxford, 1961.
[74] Th. Dries, F. Fujara, M. Kiebel, E. Rössler, H. Sillescu, J. Chem. Phys. 88 (1988) 2139.
[75] E. Rössler, P. Eiermann, J. Chem. Phys. 100 (1994) 5237.
[76] R.P. Kambour, J.M. Kelly, B.J. McKinley, B.J. Cauley, P.T. Inglefield, A.A. Jones, Macromolecules 21 (1988) 2937.
[77] P. Scheidler, W. Kob, K. Binder, Europhys. Lett. 52 (2000) 277.
[78] A. Papon, H. Montes, M. Hanafi, F. Lequeux, L. Guy, K. Saalwächter, Phys. Rev. Lett. 108 (2012) 065702.

Literaturverzeichnis

[1] Rössler, E.: *Persönliche Korrespondenz*

[2] Adishchev, S. ; Bock, D. ; Gainaru, C. ; Kahlau, R. ; Micko, B. ; Petzold, N. ; Pötzschner, B. ; Rössler, E. A.: Reorientational Dynamics of Organophosphate Glass Formers - a joint Study by ^{31}P NMR, Dielectric Spectroscopy and Light Scattering. In: *Z. Phys. Chem.* 226 (2012), S. 1149. http://dx.doi.org/doi:10.1524/zpch.2012.0281

[3] Petzold, N. ; Schmidtke, B. ; Kahlau, R. ; Bock, D. ; Meier, R. ; Micko, B. ; Kruk, D. ; Rössler, E. A.: Evolution of the dynamic susceptibility in molecular glass formers: Results from light scattering, dielectric spectroscopy, and NMR. In: *J. Chem. Phys* 138 (2013), Nr. 12, S. 12A510. http://dx.doi.org/10.1063/1.4770055

[4] Götze, W. ; Sjögren, L.: Relaxation processes in Supercooled Liquids. In: *Rep. Prog. Phys.* 55 (1992), Nr. 3, S. 241–376. http://dx.doi.org/10.1088/0034-4885/55/3/001

[5] Hodge, I. M.: Physical aging in polymer glasses. In: *Science* 267 (1995), Nr. 5206, S. 1945. http://dx.doi.org/10.1126/science.267.5206.1945

[6] Dyre, J. C.: The glass transition and elastic models of glass-forming liquids. In: *Rev. Mod. Phys.* 78 (2006), S. 953–972. http://dx.doi.org/10.1103/RevModPhys.78.953

[7] Sillescu, H.: Heterogeneity at the glass transition: a review. In: *J. Non-Cryst. Solids* 243 (1999), S. 81–108. http://dx.doi.org/10.1016/S0022-3093(98)00831-X

[8] Böhmer, R. ; Chamberlin, R. V. ; Diezemann, G. ; Geil, B. ; Heuer, A. ; Hinze, G. ; Kuebler, S. C. ; Richert, R. ; Schiener, B. ; Sillescu, H. ; Spiess, H. W. ; Tracht, U. ; Wilhelm, M.: Nature of the non-exponential primary relaxation in structural glass-formers probed by dynamically selective experiments. In: *J. Non-Cryst. Solids* 235 (1998), S. 1–9. http://dx.doi.org/10.1016/S0022-3093(98)00581-X

[9] Schmidt-Rohr, K. ; Spiess, H. W.: Nature of nonexponential loss of correlation above the glass transition investigated by multidimensional NMR. In: *Phys. Rev. Lett.* 66 (1991), Nr. 23, S. 3020–3023. http://dx.doi.org/10.1103/PhysRevLett.66.3020

[10] Cicerone, M. T. ; Ediger, M. D.: Relaxation of spatially heterogeneous dynamic domains in supercooled ortho-terphenyl. In: *J. Chem. Phys.* 103 (1995), Nr. 13, S. 5684–5692. http://dx.doi.org/10.1063/1.470551

[11] Schiener, B. ; Böhmer, R. ; Loidl, A. ; Chamberlin, R. V.: Nonresonant spectral hole burning in the slow dielectric response of supercooled liquids. In: *Science* 274 (1996), S. 752. http://dx.doi.org/10.1126/science.274.5288.752

[12] Richert, Ranko: Evidence for dynamic heterogeneity near T_g from the time-resolved inhomogeneous broadening of optical line shapes. In: *J. Phys. Chem. B* 101 (1997), S. 6323–6326. http://dx.doi.org/10.1021/jp9713219

[13] Böhmer, R. ; Diezemann, G. ; Hinze, G. ; Sillescu, H.: A nuclear magnetic resonance study of higher-order correlation functions in supercooled ortho-terphenyl. In: *J. Chem. Phys.* 108 (1998), Nr. 3, S. 890–899. http://dx.doi.org/10.1063/1.475452

[14] Yang, Min ; Richert, Ranko: Observation of heterogeneity in the nanosecond dynamics of a liquid. In: *The Journal of Chemical Physics* 115 (2001), Nr. 6, S. 2676–2680. http://dx.doi.org/10.1063/1.1380206

[15] Blochowicz, T. ; Rössler, E. A.: Non-Resonant Dielectric Hole Burning in Neat and Binary Organic Glass Formers. In: *J. Chem. Phys.* 122 (2005), Nr. 22, S. 224511. http://dx.doi.org/10.1063/1.1931647

[16] Ediger, M. D.: Spatially Heterogeneous Dynamics in Supercooled Liquids. In: *Ann. Rev. Phys. Chem.* 51 (2000), S. 99. http://dx.doi.org/10.1146/annurev.physchem.51.1.99

[17] Böhmer, R. ; Hinze, G. ; Diezemann, G. ; Geil, B. ; Sillescu, H.: Dynamic heterogeneity in supercooled ortho-terphenyl studied by multi-dimensional deuteron NMR. In: *Europhys. Lett.* 36 (1996), S. 55. http://dx.doi.org/10.1209/epl/i1996-00186-5

[18] Heuer, A. ; Wilhelm, M. ; Zimmermann, H. ; Spiess, H. W.: Rate Memory of Structural Relaxation in Glasses and Its Detection by Multidimensional NMR. In: *Phys. Rev. Lett.* 75 (1995), Oct, 2851–2854. http://dx.doi.org/10.1103/PhysRevLett.75.2851

[19] Flenner, Elijah ; Szamel, Grzegorz: Lifetime of dynamic heterogeneities in a binary Lennard-Jones mixture. In: *Phys. Rev. E* 70 (2004), Nov, 052501. http://dx.doi.org/10.1103/PhysRevE.70.052501

[20] Deschenes, Laura A. ; Bout, David A. V.: Single-Molecule Studies of Heterogeneous Dynamics in Polymer Melts Near the Glass Transition. In: *Science* 292 (2001), Nr. 5515, S. 255. http://dx.doi.org/10.1126/science.1056430

[21] Deschenes, Laura A. ; Bout, David A. V.: Molecular Motions in Polymer Films near the Glass Transition: a Single Molecule Study of Rotational Dynamics. In: *J. Phys. Chem. B* 105 (2001), Nr. 48, S. 11978. http://dx.doi.org/10.1021/jp012238v

[22] Deschenes, Laura A. ; Vanden Bout, David A.: Retraction of Deschenes and Vanden Bout, Science 292 (5515) 255-258. In: *Science* 312 (2006), Nr. 5771, S. 195. http://dx.doi.org/10.1126/science.312.5771.195b

[23] Kudlik, Andreas ; Benkhof, Stefan ; Blochowicz, Thomas ; Tschirwitz, Christian ; Rössler, Ernst: The dielectric response of simple organic glass formers. In: *J. Mol. Struct.* 479 (1999), S. 201–218. http://dx.doi.org/10.1016/S0022-2860(98)00871-0

[24] Johari, Gyan P. ; Goldstein, Martin: Viscous liquids and the glass transition II: Secondary relaxations in glasses of rigid molecules. In: *J. Chem. Phys.* 53 (1970), Nr. 6, S. 2372–2388. http://dx.doi.org/10.1063/1.1674335

[25] Johari, Gyan P.: Intrinsic Mobility of Molecular Glasses. In: *J. Chem. Phys.* 58 (1973), Nr. 4, S. 1766. http://dx.doi.org/10.1063/1.1679421

[26] Johari, Gyan P.: Glass Transition and Secondary Relaxations in Molecular Liquids and Crystals. In: *Annals of the N. Y. Acad. Sci.* 279 (1976), S. 117–140. http://dx.doi.org/10.1111/j.1749-6632.1976.tb39701.x

[27] Rösner, P. ; Samwer, K. ; Lunkenheimer, P.: Indications for an excess wing in metallic glasses from the mechanical loss modulus in Zr65Al7.5Cu27.5. In: *Europhys. Lett.* 68 (2004), Nr. 2, S. 226–232. http://dx.doi.org/10.1209/epl/i2004-10193-6

[28] Rivera, Alberto ; Rössler, Ernst A.: Evidence of secondary relaxations in the dielectric spectra of ionic liquids. In: *Phys. Rev. B* 73 (2006), S. 212201. http://dx.doi.org/10.1103/PhysRevB.73.212201

[29] Jarosz, Georgina ; Mierzwa, Michal ; Zioło, Jerzy ; Paluch, Marian ; Shirota, Hideaki ; Ngai, K. L.: Glass Transition Dynamics of Room-Temperature Ionic Liquid 1-Methyl-3-trimethylsilylmethylimidazolium Tetrafluoroborate. In: *J. Phys.l Chem. B* 115 (2011), Nr. 44, S. 12709–12716. http://dx.doi.org/10.1021/jp207291k

[30] Kremer, F. (Hrsg.) ; Schönhals, A. (Hrsg.): *Broadband Dielectric Spectroscopy.* Berlin, Heidelberg, New York : Springer-Verlag, 2003

[31] Kahlau, R. ; Dörfler, T. ; Rössler, E. A.: Secondary relaxations in a series of organic phosphate glasses revealed by dielectric spectroscopy. In: *J. Chem. Phys.* 139 (2013), S. 134504. http://dx.doi.org/10.1063/1.4822002

[32] Kudlik, A. ; Tschirwitz, C. ; Benkhof, S. ; Blochowicz, T. ; Rössler, E.: Slow Secondary Relaxation Processes in Supercooled Liquids. In: *Europhys. Lett.* 40 (1997), Nr. 6, S. 649–654. http://dx.doi.org/10.1209/epl/i1997-00518-y

[33] Wu, L. ; Nagel, S.: Secondary Relaxation in o-Terphenyl Glass. In: *Phys. Rev. B* 46 (1992), Nr. 17, S. 11198–11200. http://dx.doi.org/10.1103/PhysRevB.46.11198

[34] Wiedersich, J. ; Adichtchev, S. ; Rössler, E.: Spectral Shape of Relaxations in Silica Glass. In: *Phys. Rev. Lett.* 84 (2000), Nr. 12, S. 2718–2721. http://dx.doi.org/10.1103/PhysRevLett.84.2718

[35] Gainaru, C. ; Böhmer, R. ; Kahlau, R. ; Rössler, E.: Energy landscape in molecular glasses probed by high-resolution dielectric experiments. In: *Phys. Rev. B* 82 (2010), Nr. 10, S. 104205. http://dx.doi.org/10.1103/PhysRevB.82.104205

[36] Williams, Graham ; Watts, David C.: Analysis of Molecular Motion In the Glassy State - effect of temperature and pressure on dielectric beta relaxation of polyvinyl chloride. In: *Trans. Farad. Soc.* 67 (1971), Nr. 583, S. 1971–1989. http://dx.doi.org/10.1039/tf9716701971

[37] Vogel, M. ; Rössler, E.: On the Nature of Slow β–Process in Simple Glass Formers: A ^{2}H NMR Study. In: *J. Phys. Chem. B* 104 (2000), Nr. 18, S. 4285–4287. http://dx.doi.org/10.1021/jp9942466

[38] Vogel, M. ; Rössler, E.: Effects of Various Types of Molecular Dynamics on 1D and 2D ^{2}H NMR Studied by Random Walk Simulations. In: *J. Magn. Reson.* 147 (2000), Nr. 1, S. 43–58. http://dx.doi.org/10.1006/jmre.2000.2160

[39] Vogel, M. ; Rössler, E.: Slow β-process in simple organic glass formers studied by one- and two-dimensional ^{2}H nuclear magnetic resonance I. In: *J. Chem. Phys.* 114 (2001), Nr. 13, S. 5802–5815. http://dx.doi.org/10.1063/1.1351159

[40] Micko, B. ; Lusceac, S. A. ; Zimmermann, H. ; Rössler, E. A.: Primary and secondary relaxation process in plastically crystalline cyanocyclohexane studied by 2H nuclear magnetic resonance. I. In: *J. Chem. Phys.* 138 (2013), S. 074503. http://dx.doi.org/10.1063/1.4790397

[41] Micko, B. ; Kruk, D. ; Rössler, E. A.: Primary and secondary relaxation process in plastically crystalline cyanocyclohexane studied by 2H nuclear magnetic resonance. II. Quantitative analysis. In: *J. Chem. Phys.* 138 (2013), S. 074504. http://dx.doi.org/10.1063/1.4790398

[42] Rössler, E. ; Sokolov, A. P. ; Eiermann, P. ; Warchewske, U.: Dynamical phase transition in simple supercooled liquids and polymers - an NMR approach. In: *Physica A* 201 (1993), Nr. 1-3, S. 237–256. http://dx.doi.org/10.1016/0378-4371(93)90419-5

[43] Hinze, G. ; Sillescu, H.: ^{2}H nuclear magnetic resonance study of supercooled toluene: Slow and fast processes above and below the glass transition. In: *J. Chem. Phys.* 104 (1996), Nr. 1, S. 314–319. http://dx.doi.org/10.1063/1.470902

[44] Wagner, Hermann ; Richert, Ranko: Spatial Uniformity of the β-Relaxation in D-Sorbitol. In: *J. Non-Cryst. Solids* 242 (1998), Nr. 1, S. 19–24. http://dx.doi.org/10.1016/S0022-3093(98)00777-7

[45] Vogel, M. ; Rössler, E.: Slow β-process in simple organic glass formers studied by one and two-dimensional ^{2}H nuclear magnetic resonance. II. Discussion of motional models. In: *J. Chem. Phys.* 115 (2001), Nr. 23, S. 10883–10891. http://dx.doi.org/10.1063/1.1415495

[46] Micko, B. ; Tschirwitz, C. ; Rössler, E. A.: Secondary relaxation processes in binary glass formers: Emergence of “islands of rigidity”. In: *J. Chem. Phys.* 138 (2013), S. 154501. http://dx.doi.org/10.1063/1.4798655

[47] Vogel, M. ; Medick, P. ; Rössler, E.A.: Secondary Relaxation Processes in Molecular Glasses Studied by Nuclear Magnetic Resonance. In: *Ann. Rep. NMR Spectr.* 56 (2005), S. 231–299. http://dx.doi.org/10.1016/S0066-4103(05)56005-8

[48] Lusceac, S. A. ; Koplin, C. ; Medick, P. ; Vogel, M. ; Brodie-Linder, N. ; LeQuellec, C. ; Alba-Simionesco, C. ; Rössler, E. A.: Type A versus Type B Glass Formers: NMR Relaxation in Bulk and Confining Geometry. In: *J. Phys. Chem. B* 108 (2004), Nr. 43, S. 16601–16605. http://dx.doi.org/10.1021/jp040376p

[49] Vogel, M. ; Tschirwitz, C. ; Schneider, G. ; Koplin, C. ; Medick, P. ; Rössler, E.: A ^{2}H NMR and dielectric spectroscopy study on the slow β-process in organic glass formers. In: *J. Non-Cryst. Solids* 307-310 (2002), Nr. 0, S. 326–335. http://dx.doi.org/10.1016/S0022-3093(02)01492-8

[50] Micko, B.: *Secondary relaxation processes in neat and binary glass formers studied by 2H NMR spectroscopy*, Univ. Bayreuth, Diss., 2012

[51] Gibbs, J. H. ; DiMarzio, E. A.: Nature of the Glass Transition and the Glassy State. In: *J. Chem. Phys.* 28 (1958), Nr. 3, S. 373. http://dx.doi.org/10.1063/1.1744141

[52] Adam, G. ; Gibbs, J. H.: On the Temperature Dependence of Cooparative relaxation properties in Glass-Forming Liquids. In: *J. Chem. Phys.* 43 (1965), Nr. 1, S. 139

[53] Doolittle, A. K.: Studies in Newtonian Flow. II. The Dependence of the Viscosity of Liquids on Free-Space. In: *J. Appl. Phys.* 22 (1951), S. 1471. http://dx.doi.org/10.1063/1.1699894

[54] Cohen, Morrel H. ; Turnbull, David: Molecular Transport in Liquids and Glasses. In: *J. Chem. Phys.* 31 (1959), Nr. 5, S. 1164–1169. http://dx.doi.org/10.1063/1.1730566

[55] Kovacs, A. J.: Transition vitreuse dans les polymères amorphes. Etude phénoménologique. In: *Fortsch. Hochpolym.-Forsch.* 3 (1963), S. 394. http://dx.doi.org/10.1007/BFb0050366

[56] Goldstein, M.: Glass and other relaxations in liquids. In: *Faraday Symp. Chem. Soc.* 6 (1972), S. 7–13. http://dx.doi.org/10.1039/FS9720600007

[57] Diezemann, Gregor: A free-energy landscape model for primary relaxation in glass-forming liquids: Rotations and dynamic heterogeneities. In: *J. Chem. Phys.* 107 (1997), S. 10112. http://dx.doi.org/10.1063/1.474148

[58] Dyre, Jeppe C. ; Olsen, N. B. ; Christensen, T.: Local elastic expansion model for viscous-flow activation energies of glass-forming molecular liquids. In: *Phys. Rev. B* 53 (1996), S. 2171. http://dx.doi.org/http://dx.doi.org/10.1103/PhysRevB.53.2171

[59] Leutheusser, E.: Dynamical model of the liquid-glass transition. In: *Phys. Rev. A* 29 (1984), Nr. 5, S. 2765–2773. http://dx.doi.org/10.1103/PhysRevA.29.2765

[60] Das, Shankar P.: Mode-coupling theory and the glass transition in supercooled liquids. In: *Rev. Mod. Phys.* 76 (2004), S. 785. http://dx.doi.org/10.1103/RevModPhys.76.785

[61] Lubchenko, V. ; Wolynes, P. G.: Theory of Structural Glasses and Supercooled Liquids. In: *Ann. Rev. Phys. Chem.* 58 (2007), S. 235. http://dx.doi.org/10.1146/annurev.physchem.58.032806.104653

[62] Bouchaud, J. P. ; Biroli, G.: On the Adam-Gibbs-Kirkpatrick-Thirumalai-Wolynes scenario for the viscosity increase in glasses. In: *J. Chem. Phys.* 121 (2004), S. 7347. http://dx.doi.org/10.1063/1.1796231

[63] Goldstein, Martin: Viscous Liquids and the Glass Transition: A Potential Energy Barrier Picture. In: *J. Chem. Phys.* 51 (1969), Nr. 9, S. 3728–3739. http://dx.doi.org/10.1063/1.1672587

[64] Debenedetti, Pablo G. ; Stillinger, Frank H.: Supercooled liquids and the glass transition. In: *Nature* 410 (2001), Nr. 6825, S. 259–267. http://dx.doi.org/10.1038/35065704

[65] Tarjus, G. ; Kivelson, S. A. ; Nussinov, Z ; Viot, P.: The frustration-based approach of supercooled liquids and the glass transition: a review and critical assessment. In: *J. Phys.: Condens. Matter* 17 (2005), S. R1143. http://dx.doi.org/10.1088/0953-8984/17/50/R01

[66] Schweizer, K. S. ; Saltzman, E. J.: Activated Hopping, Barrier Fluctuations, and Heterogeneity in Glassy Suspensions and Liquids. In: *J. Phys. Chem. B* 108 (2004), Nr. 51, S. 19729. http://dx.doi.org/10.1021/jp047763j

[67] Garrahan, Juan P. ; Chandler, David: Coarse-grained microscopic model of glass formers. In: *Proc. Natl. Acad. Sci.* 100 (2003), Nr. 17, S. 9710–9714. http://dx.doi.org/10.1073/pnas.1233719100

[68] Kob, Walter ; Andersen, Hans C.: Testing mode-coupling theory for a supercooled binary Lennard-Jones mixture I: The van Hove correlation function. In: *Phys. Rev. E* 51 (1995), May, 4626–4641. http://dx.doi.org/10.1103/PhysRevE.51.4626

[69] Megen, W. van ; Underwood, S. M.: Glass transition in colloidal hard spheres: Mode-coupling theory analysis. In: *Phys. Rev. Lett.* 70 (1993), S. 2766. http://dx.doi.org/10.1103/PhysRevLett.70.2766

[70] Goetze, W.: *Complex Dynamics of Glass-Forming Liquids - A Mode Coupling Theory.* New York : Oxford University Press, 2009

[71] Götze, W.: Recent tests of the mode-coupling theory for glassy dynamics. In: *J. Phys.: Condens. Matter* 11 (1999), Nr. 10A, S. A1–A45. http://dx.doi.org/10.1088/0953-8984/11/10A/002

[72] Ediger, M. D. ; Harrowell, P.: Perspective: Supercooled liquids and glasses. In: *J. Chem. Phys.* 137 (2012), S. 080901. http://dx.doi.org/10.1063/1.4747326

[73] Binder, K. ; Kob, W.: *Glassy Materials and Disordered Solids.* New Jersey : World Scientific, 2005

[74] Kämmerer, Stefan ; Kob, Walter ; Schilling, Rolf: Test of mode coupling theory for a supercooled liquid of diatomic molecules. I. Translational degrees of freedom. In: *Phys. Rev. E* 58 (1998), Nr. 2, S. 2131–2140. http://dx.doi.org/10.1103/PhysRevE.58.2131

[75] Kruk, D. ; Herrmann, A. ; Rössler, E. A.: Field-Cycling NMR relaxometry of viscous liquids and polymers. In: *Prog. Nucl. Magn. Reson. Spectr.* 63 (2012), S. 33. http://dx.doi.org/10.1016/j.pnmrs.2011.08.001

[76] Böhmer, R. ; Diezemann, G. ; Hinze, G. ; Rössler, E.: Dynamics of supercooled liquids and glassy solids. In: *Prog. Nucl. Magn. Reson. Spectr.* 39 (2001), Nr. 3, S. 191–267. http://dx.doi.org/10.1016/S0079-6565(01)00036-X

[77] Lunkenheimer, P. ; Schneider, U. ; Brand, R. ; Loidl, A.: Glassy dynamics. In: *Contemporary Physics* 41 (2000), Nr. 1, S. 15–36. http://dx.doi.org/10.1080/001075100181259

[78] Brodin, A. ; Gainaru, C. ; Porokhonskyy, V. ; Rössler, E. A.: Evolution of the Dynamic Susceptibility in Molecular Glass Formers - A Critical Assessment. In: *J. Phys.: Condens. Matter* 19 (2007), Nr. 20, S. 205104. http://dx.doi.org/10.1088/0953-8984/19/20/205104

[79] Berthier, L. ; Biroli, G.: Theoretical perspective on the glass transition and amorphous materials. In: *Rev. Mod. Phys.* 83 (2011), Nr. 2, S. 587. http://dx.doi.org/10.1103/RevModPhys.83.587

[80] Richert, R. ; Wolynes, P. G. (Hrsg.) ; Lubchenko, V. (Hrsg.): *Structural Glasses and Supercooled Liquids , p. 1.* Hoboken : Wiley, 2012

[81] Chung, G.-C. ; Kornfield, J. A. ; Smith, S. D.: Component Dynamics in Miscible Polymer Blends: A Two-Dimensional Deuteron NMR Investigation. In: *Macromolecules* 27 (1994), Nr. 4, S. 964–973. http://dx.doi.org/10.1021/ma00082a013

[82] Chung, G.-C. ; Kornfield, J. A. ; Smith, S. D.: Compositional Dependence of Segmental Dynamics in a Miscible Polymer Blend. In: *Macromolecules* 27 (1994), Nr. 20, S. 5729–5741. http://dx.doi.org/10.1021/ma00098a030

[83] Adachi, K. ; Fujihara, I. ; Ishida, Y.: Diluent effects on molecular motions and glass transition in polymers. I. Polystyrene-Toluene. In: *J. Polymer Sci.: Polym. Phys. Ed.* 13 (1975), Nr. 11, S. 2155–2171. http://dx.doi.org/10.1002/pol.1975.180131108

[84] Hains, Philip J. ; Williams, Graham: Molecular motion in polystyrene-plasticizer systems as studied by dielectric relaxation. In: *Polymer* 16 (1975), Nr. 10, S. 725–739. http://dx.doi.org/10.1016/0032-3861(75)90188-3

[85] Desando, M.A. ; Walker, S. ; Baarschers, W.H.: Relaxation processes of some aromatic sulfides, sulfoxides, and sulfones in a polystyrene matrix. In: *J. Chem. Phys.* 73 (1980), Nr. 7, S. 3460–3472. http://dx.doi.org/10.1063/1.440497

[86] Scandola, M. ; Ceccorulli, G. ; Pizzoli, M.: Composition dependence of the glass transition of polymer-diluent mixtures: 2. Two concomitant glass transition processes as a general feature of plasticized polymers. In: *Polymer* 28 (1987), Nr. 12, S. 2081–2084. http://dx.doi.org/10.1016/0032-3861(87)90045-0

[87] Floudas, G. ; Steffen, W. ; Fischer, E. W. ; Brown, W.: Solvent and polymer dynamics in concentrated polystyrene/toluene solutions. In: *J. Chem. Phys.* 99 (1993), S. 695–703. http://dx.doi.org/10.1063/1.465742

[88] Nakazawa, M. ; Urakawa, O. ; Adachi, K.: Effect of Local Heterogeneity on Dielectric Relaxation Spectra in Concentrated Solutions of Poly(vinyl acetate) and Poly(vinyl octanoate). In: *Macromolecules* 33 (2000), Nr. 21, S. 7898–7904. http://dx.doi.org/10.1021/ma000102+

[89] Cangialosi, D. ; Alegría, A. ; Colmenero, J.: "Self-concentration" effects on the dynamics of a polychlorinated biphenyl diluted in 1,4-polybutadiene. In: *J. Chem. Phys.* 126 (2007), Nr. 20, S. 204904. http://dx.doi.org/10.1063/1.2740632

[90] Blochowicz, T. ; Schramm, S. ; Lusceac, S. ; Vogel, M. ; Stühn, B. ; Gutfreund, P. ; Frick, B.: Signature of a Type-A Glass Transition and Intrinsic Confinement Effects in a Binary Glass-Forming System. In: *Phys. Rev. Lett.* 109 (2012), Nr. 3, S. 035702. http://dx.doi.org/10.1103/PhysRevLett.109.035702

[91] Blochowicz, T. ; Rössler, E.A.: Beta Relaxation versus High Frequency Wing in the Dielectric Spectra of a Binary Molecular Glass Former. In: *Phys. Rev. Lett.* 92 (2004), Nr. 22, S. 225701. http://dx.doi.org/10.1103/PhysRevLett.92.225701

[92] Kessairi, K. ; Capaccioli, S. ; Prevosto, D. ; Lucchesi, M. ; Rolla, P.: Relaxation dynamics in tert-butylpyridine/tristyrene mixture investigated by broadband dielectric spectroscopy. In: *J. Chem. Phys.* 127 (2007), Nr. 17, S. 174502. http://dx.doi.org/10.1063/1.2784190

[93] Capaccioli, S. ; Kessairi, K. ; Shahin, M. ; Prevosto, D. ; Lucchesi, M.: The Johari–Goldstein β-relaxation of glass-forming binary mixtures. In: *J. Non-Cryst. Solids* 357 (2011), Nr. 2, S. 251–257. http://dx.doi.org/10.1016/j.jnoncrysol.2010.08.007

[94] Blochowicz, T. ; Lusceac, S. A. ; Gutfreund, P. ; Schramm, S. ; Stühn, B.: Two Glass Transitions and Secondary Relaxations of Methyltetrahydrofuran in a Binary Mixture. In: *J. Phys. Chem. B* 115 (2011), Nr. 7, S. 1623–1637. http://dx.doi.org/10.1021/jp110506z

[95] Cangialosi, D. ; Alegría, A. ; Colmenero, J.: Dielectric relaxation of polychlorinated biphenyl/toluene mixtures: Component dynamics. In: *J. Chem. Phys.* 128 (2008), Nr. 22, S. 224508. http://dx.doi.org/10.1063/1.2937449

[96] Blochowicz, Th. ; Karle, C. ; Kudlik, A. ; Medick, P. ; Roggatz, I. ; Vogel, M. ; Tschirwitz, Ch. ; Wolber, J. ; Senker, J. ; Rössler, E.: Molecular Dynamics in Binary Organic Glass Formers. In: *J. Phys. Chem. B* 103 (1999), Nr. 20, S. 4032–4044. http://dx.doi.org/10.1021/jp983754x

[97] Adachi, K. ; Ishida, Y.: Effect of Diluent on Molecular Motion and Glass Transition in Polymers. IV. System Poly(methyl acrylate)—Toluene. In: *Polymer J.* 11 (1979), Nr. 3, S. 233–239. http://dx.doi.org/10.1295/polymj.11.233

[98] Savin, Daniel A. ; Larson, Anne M. ; Lodge, Timothy P.: Effect of Composition on the Width of the Calorimetric Glass Transition in Polymer-Solvent

and Solvent-Solvent Mixtures. In: *J. Polym. Sci.: Part B: Polym. Phys.* 42 (2004), Nr. 7, S. 1155–1163. http://dx.doi.org/10.1002/polb.10776

[99] Miwa, Yohei ; Usami, Kaori ; Yamamoto, Katsuhiro ; Sakaguci, Masato ; Sakai, Masahiro ; Shimada, Shigetaka: Direct Detection of Effective Glass Transitions in Miscible Polymer Blends by Temperature-Modulated Differential Scanning Calorimetry. In: *Macromolecules* 38 (2005), Nr. 6, S. 2355–2361. http://dx.doi.org/10.1021/ma0480401

[100] Lipson, J. E. G. ; Milner, S. T.: Multiple glass transitions and local composition effects on polymer solvent mixtures. In: *J. Polymer Sci.: Part B: Polymer Phys.* 44 (2006), Nr. 24, S. 3528–3545. http://dx.doi.org/10.1002/polb.21023

[101] Gaikwad, A. N. ; Wood, E. R. ; Ngai, T. ; Lodge, T. P.: Two Calorimetric Glass Transitions in Miscible Blends Containing Poly(ethylene oxide). In: *Macromolecules* 41 (2008), Nr. 7, S. 2502–2508. http://dx.doi.org/10.1021/ma702429r

[102] Schramm, S. ; Blochowicz, T. ; Gouirand, E. ; Wipf, R. ; Stühn, B. ; Chushkin, Y.: Concentration fluctuations in a binary glass former investigated by x-ray photon correlation spectroscopy. In: *J. Chem. Phys.* 132 (2010), Nr. 22, S. 224505. http://dx.doi.org/10.1063/1.3431537

[103] Utracki, L. A.: *Polymer alloys and blends: thermodynamics and rheology.* : München, Germany : Hanser Verlag, 1989

[104] Sakaguchi, T. ; Taniguchi, N. ; Urakawa, O. ; Adachi, K.: Calorimetric Study of Dynamical Heterogeneity in Blends of Polyisoprene and Poly(vinylethylene). In: *Macromolecules* 38 (2005), Nr. 2, S. 422–428. http://dx.doi.org/10.1021/ma048280g

[105] Plazek, D. J. ; Riande, E. ; Markovitz, H. ; Raghupathi, N.: Concentration Dependence of the Visoelastic Properties of Polystyrene-Tricresyl Phosphate Solutions. In: *J. Polym. Sci.: Polym. Phys. Ed.* 17 (1979), Nr. 12, S. 2189–2213. http://dx.doi.org/10.1002/pol.1979.180171214

[106] Bingemann, D. ; Wirth, N. ; Gmeiner, J. ; Roessler, E.A.: Decoupled Dynamics and Quasi-Logarithmic Relaxation in the Polymer-Plasticizer System Poly(Methyl Methacrylate)/Tri-m-Cresyl Phosphate Studied with 2D NMR. In: *Macromolecules* 40 (2007), S. 5379–5388. http://dx.doi.org/10.1021/ma070519g

[107] Resing, H. A.: Apparent Phase—Transition Effect in the NMR Spin—Spin Relaxation Time Caused by a Distribution of Correlation Times. In: *J. Chem. Phys.* 43 (1965), S. 669. http://dx.doi.org/10.1063/1.1696791

[108] Zetsche, A. ; Fischer, E. W.: Dielectric studies of the α-relaxation in miscible polymer blends and its relation to concentration fluctuations. In: *Acta Polym.* 45 (1994), Nr. 3, S. 168–175. http://dx.doi.org/10.1002/actp.1994.010450306

[109] Lodge, T. P. ; McLeish, T. C. B.: Self-Concentration and Effective Glass Transition Temperatures in Polymer Blends. In: *Macromolecules* 33 (2000), Nr. 14, S. 5278–5284. http://dx.doi.org/10.1021/ma9921706

[110] Leroy, Eric ; Alegria, Angel ; Colmenero, Juan: Segmental Dynamics in Miscible Polymer Blends: Modeling the Combined Effects of Chain Connectivity and Concentration Fluctuations. In: *Macromolecules* 36 (2003), Nr. 19, S. 7280–7288. http://dx.doi.org/10.1021/ma034144k

[111] Gradmann, S. ; Medick, P. ; Roessler, E.A.: Glassy Dynamics in Nanoconfinement as Revealed by ^{31}P NMR. In: *J. Phys. Chem. B* 113 (2009), Nr. 25, S. 8443–8445. http://dx.doi.org/10.1021/jp9027518

[112] Moreno, Angel J. ; Colmenero, Juan: Logarithmic relaxation in a kinetically constrained model. In: *J. Chem. Phys.* 125 (2006), Nr. 1, 016101. http://dx.doi.org/10.1063/1.2212422

[113] Lorthioir, C. ; Alegría, A. ; Colmenero, J.: Out of equilibrium dynamics of poly(vinyl methyl ether) segments in miscible poly(styrene)-poly(vinyl methyl ether) blends. In: *Phys. Rev. E* 68 (2003), Nr. 3, S. 031805. http://dx.doi.org/10.1103/PhysRevE.68.031805

[114] Genix, A.-C. ; Arbe, A. ; Alvarez, F. ; Colmenero, J. ; Willner, L. ; Richter, D.: Dynamics of poly(ethylene oxide) in a blend with poly(methyl methacrylate): A quasielastic neutron scattering and molecular dynamics simulations study. In: *Phys. Rev. E* 72 (2005), Nr. 3, S. 031808. http://dx.doi.org/10.1103/PhysRevE.72.031808

[115] Kurzidim, Jan ; Coslovich, Daniele ; Kahl, Gerhard: Dynamic arrest of colloids in porous environments: disentangling crowding and confinement. In: *J. Phys.: Condens. Matter* 23 (2011), Nr. 23, S. 234122. http://dx.doi.org/10.1088/0953-8984/23/23/234122

[116] Voigtmann, Th. ; Horbach, J.: Double Transition Scenario for Anomalous Diffusion in Glass-Forming Mixtures. In: *Phys. Rev. Lett.* 103 (2009), Nr. 20, S. 205901. http://dx.doi.org/10.1103/PhysRevLett.103.205901

[117] Sjoegren, L.: Diffusion of impurities in a dense fluid near the glass transition. In: *Phys. Rev. A* 33 (1986), Nr. 2, S. 1254–1260. http://dx.doi.org/10.1103/PhysRevA.33.1254

[118] Kaneko, Y. ; Bosse, J.: Dynamics of Two-Component Liquids near the Glass Transition. In: *J. Mol. Liquids* 65-66 (1995), S. 429–432. http://dx.doi.org/10/fmj9t3

[119] Kaneko, Y. ; Bosse, J.: Dynamics of binary liquids near the glass transition: a mode-coupling theory. In: *J. Non-Cryst. Solids* 205–207, Part 2 (1996), S. 472–475. http://dx.doi.org/10/dw29hn

[120] Lorentz, H. A.: The motion of electrons in metallic bodies. In: *KNAW, Proceedings* 7 (1905), S. 438

[121] Dettmann, Carl P.: Diffusion in the Lorentz gas. In: *Commun. Theor. Phys.* 62 (2014), Nr. 4, S. 521. http://dx.doi.org/10.1088/0253-6102/62/4/10

[122] Höfling, Felix ; Franosch, Thomas ; Frey, Erwin: Localization Transition of the Three-Dimensional Lorentz Model and Continuum Percolation. In: *Phys. Rev. Lett.* 96 (2006), Apr, 165901. http://dx.doi.org/10.1103/PhysRevLett.96.165901

[123] Kurzidim, Jan ; Coslovich, Daniele ; Kahl, Gerhard: Impact of random obstacles on the dynamics of a dense colloidal fluid. In: *Phys. Rev. E* 82 (2010), Oct, 041505. http://dx.doi.org/10.1103/PhysRevE.82.041505

[124] Krakoviack, V.: Liquid-Glass Transition of a Fluid Confined in a Disordered Porous Matrix: A Mode-Coupling Theory. In: *Phys. Rev. Lett.* 94 (2005), Nr. 6, S. 065703. http://dx.doi.org/10.1103/PhysRevLett.94.065703

[125] Chong, S.-H. ; Götze, W. ; Singh, A. P.: Mode-coupling theory for the glassy dynamics of a diatomic probe molecule immersed in a simple liquid. In: *Phys. Rev. E* 63 (2000), Nr. 1, S. 011206. http://dx.doi.org/10.1103/PhysRevE.63.011206

[126] Kim, K. ; Miyazaki, K. ; Saito, S.: Molecular dynamics studies of slow dynamics in random media: Type A-B and reentrant transitions. In: *Eur. Phys. J. Special Topics* 189 (2010), Nr. 1, S. 135–139. http://dx.doi.org/10.1140/epjst/e2010-01315-y

[127] Kahlau, Robert: *Primary and Secondary Relaxations in Neat and Binary Glass Formers Studied by Means of Dielectric Spectroscopy*, Univ. Bayreuth, Diss., 2014

[128] He, Yiyong ; Lutz, T. R. ; Ediger, M. D. ; Ayyagari, Chakravarthy ; Bedrov, Dmitry ; Smith, Grant D.: NMR Experiments and Molecular Dynamics Simulations of the Segmental Dynamics of Polystyrene. In: *Macromolecules* 37 (2004), Nr. 13, S. 5032–5039. http://dx.doi.org/10.1021/ma049843r

[129] Vogel, M. ; Rössler, E.: Exchange Processes in Disordered Systems Studied by Solid-State 2D NMR. In: *J. Phys. Chem. A* 102 (1998), Nr. 12, S. 2102–2108. http://dx.doi.org/10.1021/jp973461o

[130] Schmidtke, Bernd: *From the Boiling Point to the Glass Transition: Reorientational Dynamics as Revealed by Dynamic Light Scattering*, Universität Bayreuth, Diss., 2015

[131] Petzold, Nikolaus: *unveröffentlichte Ergebnisse.* 2013

[132] Capaccioli, S. ; Kessairi, K. ; Prevosto, D. ; Lucchesi, M. ; Ngai, K. L.: Genuine Johari-Goldstein β-relaxations in glass-forming binary mixtures. In: *Journal of Non-Crystalline Solids* 352 (2006), S. 4643–4648. http://dx.doi.org/10.1016/j.jnoncrysol.2006.01.145. – ISSN 0022–3093

[133] Mierzwa, M. ; Pawlus, S. ; Paluch, M. ; Kaminska, E. ; Ngai, K. L.: Correlation between primary and secondary Johari-Goldstein relaxations in supercooled liquids: Invariance to changes in thermodynamic conditions. In: *The Journal of Chemical Physics* 128 (2008), Nr. 4, S. 044512. http://dx.doi.org/10.1063/1.2828496

[134] Kessairi, K. ; Capaccioli, S. ; Prevosto, D. ; Lucchesi, M. ; Sharifi, S. ; Rolla, P. A.: Interdependence of Primary and Johari-Goldstein Secondary Relaxations in Glass-Forming Systems. In: *The Journal of Physical Chemistry B* 112 (2008), Nr. 15, S. 4470–4473. http://dx.doi.org/10.1021/jp800764w. – PMID: 18366219

[135] Thayyil, M. S. ; Ngai, K.L. ; Prevosto, D. ; Capaccioli, S.: Revealing the rich dynamics of glass-forming systems by modification of composition and change of thermodynamic conditions. In: *Journal of Non-Crystalline Solids* 407 (2015), Nr. 0, S. 98–105. http://dx.doi.org/10.1016/j.jnoncrysol.2014.10.025. – ISSN 0022–3093

[136] Starkweather, Howard W.: Noncooperative Relaxations. In: *Macromolecules* 21 (1988), Nr. 6, S. 1798–1802. http://dx.doi.org/10.1021/ma00184a043

[137] Mano, J. F. ; Lanceros-Méndez, S.: Simple versus cooperative relaxations in complex correlated systems. In: *J. Appl. Phys.* 89 (2001), Nr. 3, S. 1844. http://dx.doi.org/10.1063/1.1334937

[138] Cohen, Y. ; Karmakar, S. ; Procaccia, I. ; Samwer, K.: The nature of the beta-peak in the loss modulus of amorphous solids. In: *Eur. Phys. Lett.* 100 (2012), Nr. 3, S. 36003. http://dx.doi.org/10.1209/0295-5075/100/36003

[139] Fragiadakis, D. ; Roland, C. M.: Dynamic correlations and heterogeneity in the primary and secondary relaxations of a model molecular liquid. In: *Phys. Rev. E* 89 (2014), S. 052304. http://dx.doi.org/10.1103/PhysRevE.89.052304

[140] Gainaru, C. ; Lips, O. ; Troshagina, A. ; Kahlau, R. ; Brodin, A. ; Fujara, F. ; Rössler, E. A.: On the nature of the high frequency relaxation in a molecular glass former: A joint study of glycerol by field cycling NMR, dielectric spectroscopy, and light scattering. In: *J. Chem. Phys.* 128 (2008), Nr. 17, S. 174505. http://dx.doi.org/10.1063/l.2906122

[141] Qi, F. ; El Goresy, T. ; Böhmer, R. ; Döss, A. ; Diezemann, G. ; Hinze, G. ; Sillescu, H. ; Blochowicz, T. ; Gainaru, C. ; Rössler, E. A. ; Zimmermann, H.: Nuclear magnetic resonance and dielectric spectroscopy of a simple supercooled liquid: 2-methyl tetrahydrofuran. In: *J. Chem. Phys.* 118 (2003), Nr. 16, S. 7431–7438. http://dx.doi.org/10.1063/1.1563599

[142] Qi, F. ; Hinze, G. ; Böhmer, R. ; Sillescu, H. ; Zimmermann, H.: Slow and fast methyl group rotations in fragile glass-formers studied by NMR. In: *Chem. Phys. Lett.* 328 (2000), Nr. 3, S. 257. http://dx.doi.org/10.1016/S0009-2614(00)00935-0

[143] Havriliak, S. ; Negami, S.: A complex plain analysis of α-dispersions in some polymer systems. In: *Polymer* 8 (1967), S. 161. http://dx.doi.org/10.1016/0032-3861(67)90021-3

[144] Zorn, R.: Applicability of distribution functions for the Havriliak-Negami spectral function. In: *J. Polym. Sci. B Polym. Phys.* 37 (1999), S. 1043–1044. http://dx.doi.org/cdtqcr

[145] Abragam, D.: *Principles of Nuclear Magnetism.* Oxford : Oxford University Press, 1973

[146] Mehring, M.: *Principles of high resolution NMR in solids.* Berlin : Springer-Verlag, 1983

[147] Slichter, Charles P.: *Principles of Magnetic Resonance*. New York : Springer, 1990

[148] Schmidt-Rohr, K. ; Spiess, H. W.: *Multidimensional Solid-State NMR and Polymers*. London : Academic Press, 1994

[149] Hahn, E. L.: Spin Echoes. In: *J. Phys. Rev.* 80 (1950), S. 580–594. http://dx.doi.org/10.1103/PhysRev.80.580

[150] Powles, J. G. ; Strange, J. H.: Zero Time Resolution Nuclear Magnetic Resonance Transient in Solids. In: *Proc. Phys. Soc.* 82 (1963), S. 6. http://dx.doi.org/10.1088/0370-1328/82/1/303

[151] Bloembergen, N. ; Purcell, E. M. ; Pound, R. v.: Relaxation Effects in Nuclear Magnetic Resonance Absorption. In: *Phys. Rev.* 73 (1948), S. 679–712. http://dx.doi.org/10.1103/PhysRev.73.679

[152] Carr, H. Y. ; Purcull, E. M.: Effects of diffusion on free precession in nuclear magnetic resonance experiments. In: *Phys. Rev.* 94 (1954), S. 630–638. http://dx.doi.org/10.1103/PhysRev.94.630

[153] Meiboom, S. ; Gill, D.: Modified spin-echo method for measuring nuclear relaxation times. In: *Rev. Sci. Instrum.* 29 (1958), S. 688. http://dx.doi.org/10.1063/1.1716296

[154] Schaefer, D. ; Leisen, J. ; Spiess, H. W.: Experimental Aspects of Multidimensional Exchange Solid-State NMR. In: *J. Magn. Reson.* 115 (1996), S. 60–79. http://dx.doi.org/10.1006/jmra.1995.1149

[155] Fujara, F. ; Wefing, W. ; Spiess, H. W.: Dynamics of molecular reorientations: Analogies between quasielastic neutron scattering and deuteron NMR spin alignment. In: *J. Chem. Phys.* 84 (1986), Nr. 8, S. 4579–4584. http://dx.doi.org/10.1063/1.450032

Danksagung

Bedanken möchte ich mich an erster Stelle bei Herrn Prof. Dr. Ernst Rößler, der mir ermöglichte als Teil seiner Arbeitsgruppe in diesem interessanten Gebiet der Wissenschaft tätig zu sein und letztlich diese Arbeit zu erstellen. Dabei gewährte er mir die Freiheit selbständig eigene Wege zu gehen, war jedoch jederzeit ansprechbar und stand mir stets mit großer Geduld und kompetentem Rat zur Seite.

Desweiteren danke ich auch allen gegenwärtigen und ehemaligen Mitgliedern unserer Arbeitsgruppe für die allzeit angenehme und freundschaftliche Atmosphäre, unter ihnen Dr. Axel Hermann, Marius Hofmann, Dr. Roman Meier, Dr. Björn Micko, Nikolaus Petzold und Dr. Bernd Schmidtke.

Besonderer Dank geht an Dr. Robert Kahlau. Die Ergebnisse der fruchtbaren Zusammenarbeit mit ihm haben ganz entscheidend zu dieser Arbeit beigetragen.

Björn Pötzschner und Thomas Körber sei ausdrücklich für das Korrekturlesen der Arbeit gedankt.

Herrn Prof. Dr. Michael Vogel danke ich für die Übernahme des Korreferats.

....

(Name, Vorname) (geboren am)

VERSICHERUNG AN EIDES STATT

Ich erkläre, dass

- ich die Dissertation über das Thema *„Molekulare Dynamik in binären Glasbildnern studiert mittels ^{31}P- und ^{2}H-NMR“* selbstständig verfasst habe, keine anderen als die von mir angegebenen Quellen und Hilfsmittel benutzt habe und sämtliche Stellen, die aus dem Schrifttum wörtlich entnommen sind, als solche kenntlich gemacht habe.
- ich keine gewerbliche Promotionsvermittlung bzw. –beratung oder ähnliche Dienstleistungen weder in Anspruch genommen habe noch künftig in Anspruch nehmen werde.
- Von mir keine früheren Promotionsversuche, weder mit dieser noch mit einer anderen Dissertation erfolgt sind.

Ich bestätige die Richtigkeit dieser Erklärung und versichere an Eides Statt, dass ich nach bestem Wissen die reine Wahrheit erklärt und nichts verschwiegen habe.

..... , ...

Ort Datum Unterschrift

Die Informationen zur Bedeutung der eidesstattlichen Versicherung und zu den strafrechtlichen Folgen einer unrichtigen oder unvollständigen eidesstattlichen Versicherung habe ich zur Kenntnis genommen.

..... ,..... .....

Ort Datum Unterschrift